Photodynamic Therapy in Nanomedicine: Synthesis and Multidisciplinary Characterization of Squaraine Sensitizers for Theranostics

Elisabetta Ronchi
M. S. in Materials Science, University of Milano-Bicocca, 2008

A Thesis Submitted to the
Faculty of Mathematical, Physical and Natural Sciences
in Partial Fulfillment of the
Requirements for the degree of

Doctor of Philosophy in Chemistry
XXIV Cycle

Approved by the
Examining Committee:

Thesis Adviser : Giorgio A. Pagani,
Full Professor at the Department of Materials Science, University of Milano-Bicocca
Milano, Italy

Referee: Luisa De Cola,
Full Professor at Physikalisches Institut, Westfälische-Wilhelms-Universität
Münster, Germany

Referee: Manuela Shieck
Assistant Professor at the Mads Clausen Institute, University of Southern Denmark
Sonderborg, Denmark

University of Milano-Bicocca
Milano, Italy
February, 2012

Abstract

The present dissertation deals with the study of 1,3- and 1,2-substituted squaraine dyes and their functionalized derivatives as efficient combined fluorescent markers and photodynamic therapy (PDT) agents. This well-established medical treatment involves the insurgence of citotoxic species in the cellular environment following up the irradiation of a suitable photosensitizer with visible light in the presence of molecular oxygen.

Squaraine dyes (1,3-dicondensation products of squaric acid and electron-rich molecules) have been successfully employed for their unique optical properties. These cyanine-like chromophores are indeed characterized by an intense absorption and emission band localized in the transparency window of biological tissue (600–900 nm). Furthermore, squaraines are largely stable and non-toxic in the dark, but after irradiation they promote a strong dose-dependent phototoxic effect due to the formation of radical species.

By an accurate choice of the reactants and of the synthesis conditions it has been possible to control the regiochemistry of substitution on the squaric acid core in order to selectively obtain the most common 1,3-regioisomers or the seldom mentioned 1,2-regioisomers. The photophysical and electrochemical behavior of 1,2-squaraines and their higher responsiveness to the chemical environment associates these chromophores to merocyanines.

A challenge that occurs when dealing with photosensitizers is the way they are solubilized and specifically delivered to the biological target. This issue can be addressed by taking advantage of the high flexibility of the squaraine structure, which provides a powerful tool aimed at the improvement of bioavailability. In particular, different functional groups can be incorporated in the squaraine structure without alteration of the photophysical properties, obtaining a library of post-functionalizable squaraines. As representative examples, it is herein reported the study on the conjugation with biologically relevant groups (i.e. choline and galactose) and with zeolite nanocrystals. A promising third generation PDT photosensitizer has been thus obtained, which conjugates diagnostic imaging and therapy into a single integrated nanovector.

Moreover, a fullero-squaraine dyad has been designed in order to combine the photophysical properties of the two portions, so that the conjugate unites the characteristic absorption of squaraine dyes and the high singlet oxygen generation of fullerene *via* intra-molecular energy transfer processes.

For Pat

Acknowkledgements

This dissertation would not have been possible without the expert guidance of my esteemed advisers, Professor Giorgio A. Pagani and Luca Beverina. I deeply appreciate both the scientific and emotional encouragement I have received from them over the past years.

My thanks go to Professor Luisa De Cola, Seda Kehr, Cristian Strassert, Andreas Steffen, André Devaux and all the people in CeNTech and ICB in Münster for having welcomed so warmly in their group in Germany and for having taught me complex photophysics and inorganic synthesis and purification. I would also thank Jehad El-Gindi for the current investigation of the biological aspects of this project, I am sure that the results he will achieve will be as promising as the preliminary data he has already obtained.

I have to thank Patrizio Salice for the important contribution to this project and for everything he taught me, I wouldn't have arrived so far without the constant confrontation with him. All the other people I have shared the lab with in Milan don't deserve to be mentioned here. I would like to thank the NMR technician at the University of Milano-Bicocca, Giorgio "Cioccio" Patriarca, for having always found time to acquire my sometimes difficult spectra and the group of Professor Claudio Maria Mari and Riccardo Ruffo for the electrochemical characterization of some of my squaraines and for having lent me some Argon gas for my syntheses.

I would also like to extend my appreciation to the members of my reading committee, Professor Luisa De Cola at Physikalisches Institut, Westfälische-Wilhelms-Universität, Münster, Germany and Manuela Shieck at the Mads Clausen Institute, University of Southern Denmark, Sonderborg, Denmark for reading and approving my PhD thesis.

A special thought to the few friends that worth a mention: Ferro, Nic, Carla, Brodo, Glauco, Claudia.

My sincere gratitude goes to my parents Luisa and Silvano, my sister Susi, my grandmothers, my parents-in-law Lorenza and Meo, my sister-in-law Greta, my brother-in-law Cassi , my niece Emily, Shika and Yugo and all the relatives that have granted me their love, support, and patience over the last years.

My deepest gratitude goes to Patrizio for having always given me the right reasons to keep me going on. My words fail to describe the way his constant presence has and is currently sustaining me.

Elisabetta Ronchi

February 2012

Author's declaration

I declare that the work in this dissertation was carried out in accordance with the Regulations of the University of Milano-Bicocca.

The work is original except where indicated by special reference in the text and no part has been submitted previously for any other degree. To the best of my knowledge and belief, this thesis contains no material previously published or written by another person, except where due reference has been made.

Any views expressed in the dissertation are those of the author and in no way represent those of the University of Milano-Bicocca. The dissertation has not been presented to any other University for examination either in Italy or abroad.

Table of contents

List of abbreviations

ALA	δ-aminolaevulinic acid
AlPcS	aluminum phthalocyanin sulfonates
DCC	*N,N'*-dicyclohexylcarbodiimide
DCM	dichloromethane
DDQ	2,3-dichloro-5,6-dicyano-*p*-quinone
EPR	enhanced permeation and retention
FD	fluorescence diagnosis
GC-MS	Gas chromatography-mass spectroscopy
GPC	gel permeation chromatography
HpD	haematoporphyrin derivative
HPLC	high pressure liquid chromatography
HPPH	2-[1-hexyloxyethyl]-2-devinyl pyropheophorbide-*a*
ICG	indocyanine green
IR	infrared
*m*THPC	tetra(*m*-hydroxyphenyl)chlorin
NHS	*N*-hydroxysuccinimide
NIR	near infrared
PBS	phosphate buffer solution
PMMA	poly(methyl methacrylate)
PDT	photodynamic therapy
PpIX	protoporphyrin IX
PS	photosensitizer
p-THPP	*meso*-tetra(*p*-hydroxyphenyl)porphyrin
ROS	reactive oxygen species
THF	tetrahydrofuran
THPBC	5,10,15,20-tetra(hydroxyphenyl)bacteriochlorin

THPC	5,10,15,20-tetra(hydroxyphenyl)chlorin
THPP	5,10,15,20-tetra(hydroxyphenyl)porphyrin
TPP	5,10,15,20-tetraphenylporphyrin
TPPS	tetraphenyl porphine sulfonate
UV	ultraviolet
ZnOPPc	Zinc(II) octapentyl phthalocyanine
ZnPc	Zinc(II) phthalocyanine
3-HBT	3-hexylbenzo[d]thiazol-2(3*H*)-one
ε_{max}	maximum molar extinction coefficient
Φ_{Δ}	quantum yield of $O_2(^1\Delta_g)$ formation

List of figures

List of tables

1 Introduction

Current cancer therapy usually involves intrusive processes including application of catheters to allow chemotherapy, initial chemotherapy to shrink any cancer present, surgery to then remove the tumor(s) if possible, followed by more chemotherapy and radiation. The purpose of the chemotherapy and radiation is to kill the tumor cells as these cells are more susceptible to the actions of these drugs and methods because of their growth at a much faster rate than healthy cells, at least in adults. Research efforts to improve chemotherapy over the past 25 years have led to an improvement in patient survival but there is still a need for improvement. Current research areas include development of carriers to allow alternative dosing routes, new therapeutic targets such as blood vessels fueling tumor growth and targeted therapeutics that are more specific in their activity. Clinical trials have shown that patients are open to new therapeutic options and the goal of these new chemotherapeutics is to increase survival time and the quality of life for cancer patients.

In all cases, the effectiveness of the treatment is directly related to the treatment's ability to target and to kill the cancer cells while affecting as few healthy cells as possible. The degree of change in the patient's quality of life and eventual life expectancy is directly related to this targeting ability of the treatment. Most current cancer patients' only selectivity in their treatment is related to the inherent nature of the chemotherapeutic drugs to work on a particular type of cancer cell more intensely than on healthy cells. However, by administering bolus doses of these intense drugs systematically some side effects will always occur and sometimes are so intense that the patient must discontinue therapy before the drugs have a chance to eradicate the cancer. Unfortunately, not all treatments, even if carried through to the oncologists specifications, are effective in killing the cancer before the cancer kills the patient. The advances in treatment of cancer are progressing quickly both in terms of new agents against cancer and new ways of delivering both old and new agents. Hopefully this progress can move us away from near-toxic doses of non-specific agents. This review will primarily address new methods for delivering therapies, both old and new, with a focus on nanoparticle formulations and ones that specifically target tumors.

A single cancerous cell surrounded by healthy tissue will replicate at a rate higher than the other cells, placing a strain on the nutrient supply and elimination of metabolic waste products. Once a small tumor mass has formed, the healthy tissue will not be able to compete with the cancer cells for the inadequate supply of nutrients from the blood stream. Tumor cells will displace healthy cells until the tumor reaches a diffusion-limited maximal size. While tumor cells will typically not initiate apoptosis in a low nutrient

environment, they do require the normal building blocks of cell function like oxygen, glucose and amino acids. The vasculature was designed to supply the now extinct healthy tissue that did not place as high a demand for nutrients due to its slower growth rate.

Tumor cells will therefore continue dividing because they do so without regard to nutrient supply but also many tumor cells will perish because the amount of nutrients is insufficient. The tumor cells at the outer edge of a mass have the best access to nutrients while cells on the inside die creating a necrotic core within tumors that rely on diffusion to deliver nutrients and eliminate waste products. In essence, a steady state tumor size forms, as the rate of proliferation is equal to the rate of cell death until a better connection with the circulatory system is created. This diffusion-limited maximal size of most tumors is around 2 mm. To grow beyond this size, the tumor must recruit the formation of blood vessels to provide the nutrients necessary to fuel its continued expansion. An illustration of tumor development from a single cell to a diffusion-limited tumor is shown in Figure 1–1.

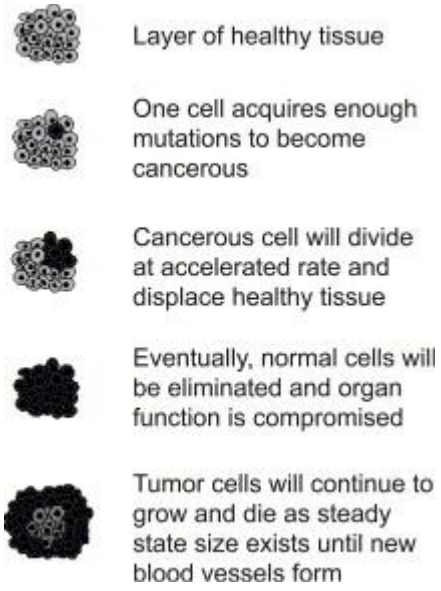

Figure 1–1 Tumor development from initial carcinogenesis to diffusion-limited maximal size.

It is thought that there could be numerous tumors at this diffusion-limited maximal size throughout the body. Until the tumor can gain that access to the circulation it will remain at this size and the process can take years. The exact molecular mechanisms that initiate angiogenesis at a tumor site are not known and could be unique to site of origin but more information about what factors play a role in this process is being discovered. As more is known about the molecular mechanisms that stimulate angiogenesis, the factors involved present new therapeutic targets to prevent tumor development.

1.1 Photodynamic therapy

The photodynamic effect falls into the group of photochemical processes which lack macroscopic order and which involve a variety of reactive biomolecules and more than a single chemical pathway as shown in Figure 1–2.

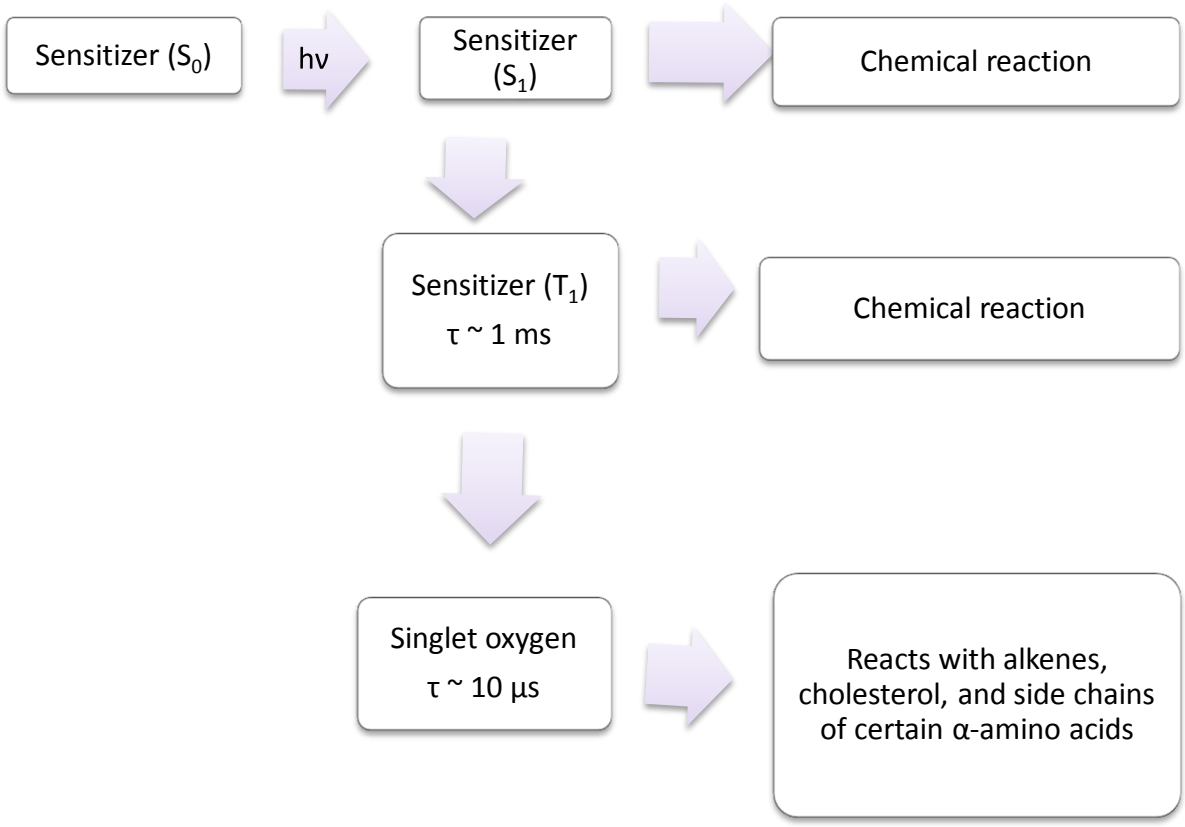

Figure 1–2 Possible multipathway photobiological process. T_1 refers to the first excited triplet state, and τ to the lifetime of the species.

Photodynamic therapy (PDT) is a well-established treatment that involves the insurgence of citotoxic species in the cellular environment after irradiation of a dye with visible light. The presence of molecular oxygen is usually required to induce the generation of highly citotoxic agents like reactive oxygen species (ROS) and/or singlet oxygen ($O_2(^1\Delta_g)$). The ability of clinician to administrate locally and systematically light and/or sensitizers into the human tissues permit to cause cellular damage in a very selective and specific way. Therefore PDT is considered a minimally invasive therapeutic modality and nowadays it has application in cancer treatment, dermatology, age-related macular degeneration treatment, …

Since the first modern clinical trial of PDT by Dougherty et al. was reported in 1978, PDT has been used in people with cancer to help them live longer and improve their

quality of life. Although PDT works and causes no long-term problems, it is not widely used to treat cancer today. Still, it is offered in some treatment centers, and is being studied in many clinical trials, becoming more widely recognized as a valuable treatment option for localized cancers (cancers that have not spread far from where they started). The three drugs currently approved by the United States Food and Drug Administration (FDA) for cancer treatment are: porfimer sodium (Photofrin), aminolevulinic acid (ALA or Levulan®) and the methyl ester of ALA (Metvixia Cream). They are used in the therapy of solid tumors localized into the esophagus, of a type of non-small cell lung cancer, of certain skin cancers, such as basal cell carcinoma and squamous cell carcinoma, of Bowen disease and nevoid basal cell carcinoma syndrome and of some tumors of the vagina, vulva, and cervix that can be reached by the activating light.

Nevertheless, in order to enhance the efficacy of PDT and extend its applications, a variety of second and third generation photosensitizers are now being assessed for their efficacy in cancer therapy. An example of one of these new drugs, Photochlor, is now being used in clinical trials. Photochlor or HPPH (2-[1-hexyloxyethyl]-2-devinyl pyropheophorbide-a) is a second-generation photosensitizer. It is being studied in the treatment of tumors that block the esophagus, early stage esophageal cancer, lung cancer, skin cancer, mouth and throat cancer, and locally recurring breast cancer on the chest wall after mastectomy. So far, studies have shown that photosensitivity lasts a much shorter time, and the drug is removed from the body much faster than Photofrin.

Photosensitizers for PDT should meet several criteria: (1) chemical stability, (2) water-solubility, (3) high quantum yield of $^1O_2$ generation (Φ_Δ), (4) no cytotoxicity in the dark, (5) tumor selectivity, (6) rapid accumulation in target tumor tissues (7) rapid clearance from patients and (8) a high molar absorption coefficient (ε) in the long wavelength (600–800 nm) that can penetrate deeper tissues.

1.2 Drug delivery

Encapsulation of versatile photoactive species such as dyes, drugs, heterogeneous catalysts, and metal nanoparticles in nanoengineered carriers is becoming increasingly important for a wide variety of applications ranging from drug delivery to biomedicine and biotechnology. Among these photoactive ingredients, photosensitized drugs or photosensitizers (PSs) capable of yielding cytotoxic singlet oxygen have been widely explored in cell biology, photodynamic therapy, and blood sterilization. However, many identified PS drugs and other photoactive small molecules used against cancer are poorly water soluble, and hence the PS efficacy is greatly reduced due to the aggregation of PS molecules in aqueous media. To overcome this issue, diverse hydrophilic delivery vehicles

such as gels, liposomes, and colloids were introduced to deliver encapsulated PSs at affected locations and thus enhance their photodynamic effects.

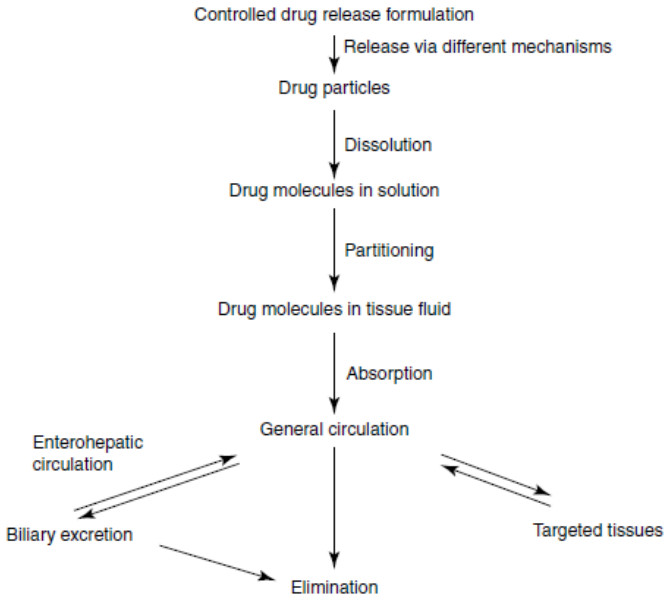

Figure 1–3 Fate of drug in controlled release formulation.

More recently, targeting strategies have been shown to increase the affinity of the photosensitizer for tumour tissue. There have also been reports of selectively targeting subcellular compartments, including the mitochondria. The biochemical usage of conjugated phosensitizers with appropriate targeting approaches have led to third-generation photosensitizers and some of the most promising results to date. Conjugation in this sense may be defined as the covalent attachment of the principal molecular backbone to a second molecular moiety which confers beneficial property on the molecular ensemble. Other examples comprise the pegylation of *m*-THPC by the attachment of polyethylene glycol residues to the four phenolic functions to improve water solubility, the functionalization of chlorins with estradiol to improve selectivity against breast carcinoma cells overexpressing the estrogen receptors by Montforts, and the functionalization of chlorins with oligonucleotides which form specific complexes with suitable single-stranded and double-stranded polynucleotides, and site-direct photodamage to nucleic acid. This work is also relevant to the current search for system with photovirucidal activity

Technology	Technology name (drug)	Application	Company
liposome-based formulations	Evacet (Doxorubicin)	breast cancer and other cancers	Elan with acquisition of Liposome, Inc.
one-yearly drug implant	Viadur (Leuprolide)	prostate cancer	ALZA/J&J
biodegradable implants	Gliadel (BCNU[a])	treatment of brain cancer	Guilford Pharmaceuticals, Inc.
biodegradable microsphere for sustained-release for peptides/proteins	ProLease	delivery of peptides and small molecules	Alkermes, Inc.
time release oral drug release	Pulsincap	drug release at predetermined time or location in the GI-tract	RP Scherer Corp.
oral controlled release system to control the release of a specific drug	Geomatrix	predetermined therapeutic objective for a drug	SkyePharma

[a] *N,N*-bis(2-chloroethyl)-*N*-nitrosourea.

Figure 1–4 Examples of controlled release products in the market.

2 Research background

The term “photodynamische Wirkung” (“photodynamic action”) was introduced in 1904 by one of the pioneers of photobiology: Professor Hermann von Tappeiner,[1] director of the Pharmacological Institute of the Ludwig-Maximilians University in Munich.

The term indicated the damage or destruction of living tissue by visible light in the presence of a sensitizer, emphasizing the requirement of oxygen for the process. It is not clear why he called the process “dynamic”; it might have been to distinguish this biological phenomenon from the reactions taking place in the photographic process that had been discovered a few years earlier. Actually, von Tappeiner was not fully satisfied with this term, as he wrote later: *“*Whether or not the name is to be used further or dropped, must be left to the discretion of my colleagues”.[2]

The term “photochemotherapy” (PCT) has been introduced in recent times[3] as a more correct and descriptive term than “photodynamic therapy” without great success. However, the name “photochemotherapy” would have paved the way for clinical applications better than the name “photodynamic therapy” since all oncologists are familiar with chemotherapy, while “photodynamic” may give associations to “biodynamic” which, at the best, is regarded as a quasi-scientific term.

The photodynamic effect mainly results from energy and/or electron transfer of the lowest excited triplet state T_1 of the photosensitizer to an organic substrate or molecular oxygen. Quenching mechanisms can be distinguished in type I and type II reactions.

In the type I mechanism the photosensitizer excited state generates a radical species, for example by electron transfer from (or to) a substrate, or by hydrogen atom abstraction from a substrate. In type II mechanism an energy transfer occurs from the excited photosensitizer to molecular oxygen, to give the sensitizer in its ground state and singlet oxygen.

2.1 Mechanism of photodynamic action

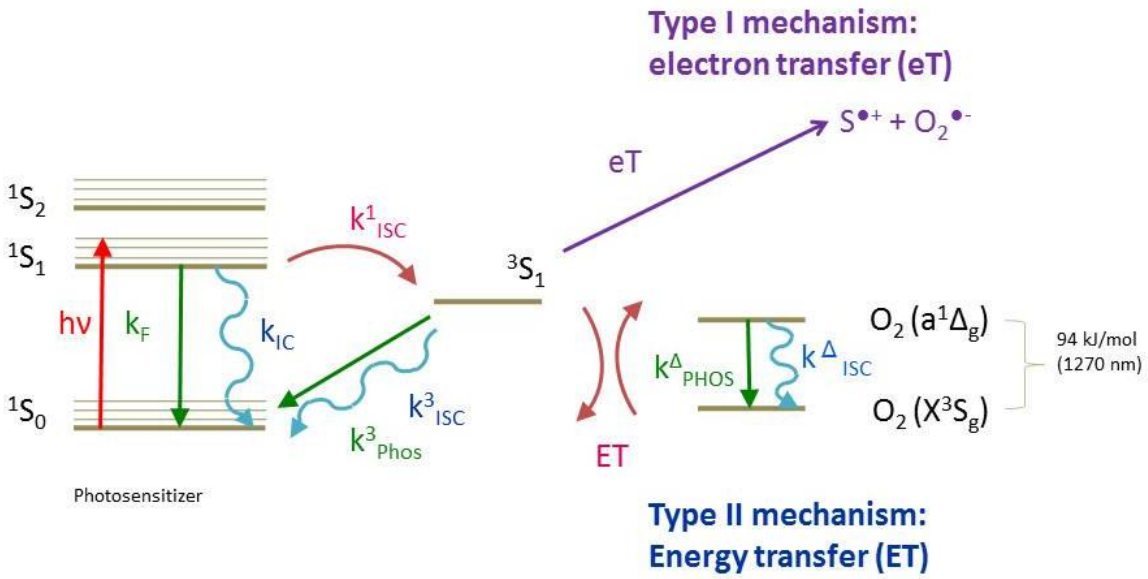

2–1 Modified Jablonski diagram to show type I and type II photooxygenation processes

2.1.1 *The type I mechanism – electron transfer (eT)*

In this mechanism the sensitizer excited state generates a radical species, for example by electron transfer (eT) from (or to) a substrate, or by hydrogen atom abstraction from a substrate. The radical species then reacts with ground state oxygen so that the overall reaction is a photochemically initiated autoxidation:

$$Sens \xrightarrow{h\nu} Sens^*$$

$$Sens^* + A \xrightarrow{eT} Sens^{+\bullet} + A^{-\bullet}$$

$$Sens^* + AH_2 \xrightarrow{H\ atom\ transfer} SensH^\bullet + AH^\bullet$$

$$AH^\bullet + {}^3O_2 \longrightarrow AH - OO^\bullet \longrightarrow products$$

Sens=sensitizer; *=excited state; A=biomolecule; •=radical species; $^3O_2$=triplet ground state molecular oxygen

A propagation sequence in the dark follows the photochemical free radical initiation step, terminating by a quenching of radicals.

A biological process which can proceed by a radical pathway is lipid peroxidation. In the first step a photochemically generated species $R^\bullet$ abstracts a hydrogen atom from an allylic position of an unsaturated lipid. The allylic radical then reacts with triplet oxygen to give a mixture of hydroperoxides and their decomposition products, to give a product mixture more complex than the one obtained for a singlet oxygen reaction.

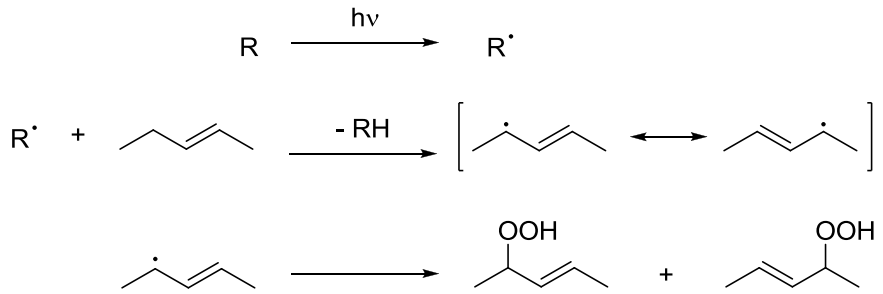

The electron transfer to molecular oxygen gives the superoxide radical anion $O_2^{-\bullet}$:

$$Sens \xrightarrow{h\nu} Sens^* \xrightarrow{^3O_2,\ eT} Sens^{+\bullet} + O_2^{-\bullet}$$

$$Sens(T_1) + A \longrightarrow Sens^{-\bullet} + A^{+\bullet} \xrightarrow{^3O_2} Sens(S_0) + O_2^{-\bullet}$$

Superoxide is not very reactive and it is rapidly oxidized back to molecular oxygen. The protonated form $HOO^{\bullet}$ (hydroperoxil radical) undergoes a dismutation which occurs spontaneously but is also catalyzed by superoxide dismutase enzymes to give oxygen and hydrogen peroxide.

$$O_2^{-\bullet} \xleftrightarrow{H^+} HOO^{\bullet} \xrightarrow{2\times} H_2O_2 + O_2$$

Hydrogen peroxide, which is toxic for the organism, is enzymatically converted to water by catalases or glutathione peroxidases enzymes. However, when hydrogen peroxide is generated in a photochemical process *in vivo* in a situation where peroxidases are ineffective or absent and traces of transition metals or ions are present, the hydroxyl radical $HO^{\bullet}$ is generated. This radical is more reactive than the above-mentioned ones and il promotes radical reactions, including autoxidation processes:

$$H_2O_2 + Fe(II) \xrightarrow{Fenton\ reaction} HO^{\bullet} + OH^- + Fe(III)$$

$$AH + HO^{\bullet} \longrightarrow A^{\bullet} + H_2O \xrightarrow{^3O_2} A - OO^- \longrightarrow products$$

2.1.2 *The type II mechanism – energy transfer (ET)*

In this mechanism electronic excitation energy is transferred from the excited triplet T_1 of the sensitizer (generated by intersystem crossing isc from the ecited singlet S_1) to triplet molecular oxygen, to give the sensitizer in its ground state S_0 and singlet oxygen $^1O_2$:

$$Sens(S_0) \xrightarrow{h\nu} Sens(S_1) \xrightarrow{isc} Sens(T_1)$$

$$Sens(T_1) + {}^3O_2 \longrightarrow Sens(S_0) + {}^1O_2$$

$$A + {}^1O_2 \longrightarrow products$$

2.2 Photosensitizers

Photodynamic activity is not limited to any structural photosensitizer. However, some characteristics are required:

The toxicity in the absence of light should be zero or very low. This means that tumor damage can be controlled by the light dose for a given drug dose;

The composition should be constant, and preferably a single substance without chiral centers;

The synthesis should be as straightforward and as high-yielding as possible;

Amphiphilic photosensitizers show a higher selectivity for tumor and faster clearance after phototherapy. Hydroxy, sulphonic acid, and quaternary ammonium groups are the most used to increase the hydrophilicity of the lipophilic macrocyclic nuclei (porphyrins, phthalocyanines etc.) on which many of the photosensitizers are based.

A delivery system is usually required since many photosensitizers are solid and not water-soluble. Water-miscible solvents (ethanol or polyethyleneglycol-400), surfactant micelles, liposomes, inclusion complexes, lipoproteins, microparticulates are some examples of the delivery strategies that can be used.

A chromophore must be present with absorption in the visible or near-visible region. The maximum absorption should be preferably in the organic tissue transparency window (between 650 and 800 nm). At the blue end of the visible region the absorption (by haemoglobin, melanin, etc) and scattering are greatest, while at longer wavelengths the IR absorption of water is present;

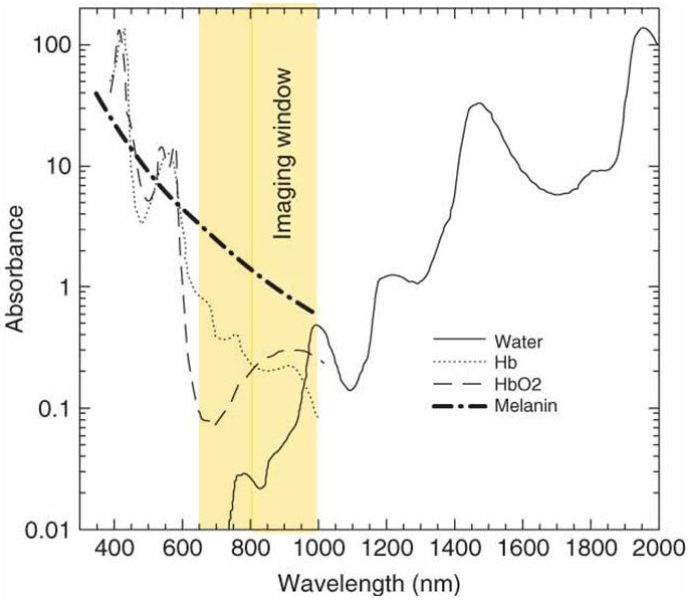

Figure 2–2 Near infrared absorption spectrum of water and main tissue-absorbing components, oxy- and deoxyhemoglobin (Hb and HbO2 respectively). The highest optical transmission window, between 650 and 1000 nm, is highlighted.[4]

The triplet energy E_T should be slightly greater than the energy of singlet oxygen above the ground state (94 kJ mol^{-1}), the triplet state should be generated in high quantum yield Φ_T and its lifetime should be long enough so that the energy transfer Sens $T_1 \rightarrow {}^3O_2$ can occur efficiently. Chromophores with absorption in the UV may not be efficient because E_T is too large and therefore the energy transfer is not efficient, while if the lowest absorption band in the IR ($\lambda_{max,abs}$>900 nm, that is the singlet energy is less than ~130 kJ mol^{-1}) are likely to have a triplet energy lower than singlet oxygen;

If singlet oxygen is involved, the quantum yield of its formation Φ_Δ should be > 0.3 to observe an appreciable photodynamic effect.

2.2.1 Phototherapy: endogenous sensitizers

Phototherapy is the use of visible or near-visible light alone in the treatment of disease. The photodynamic effect is due to light absorption by endogenous sensitizers already present in the organism.

The benefits of sunlight have been known for thousands of years,[5] and medicinal effects (heliotherapy) are indicated by ancient authors, among which Herodotus (VI century BC) and Hippocrates (460-375 BC).

In the XVIII century the effect of sunlight on rickets was known, and Huldschinsky performed convincing observations on phototherapy in 1919 Light in the UV region, indeed, stimulates the production of vitamin D, whose deficiency is responsible of this disease.

The father of modern phototherapy is the Danish physician Niels Ryberg Finsen (1860-1904), who studied with scientific method the effects of light of different wavelengths on animals. Finsen demonstrated that the ultraviolet radiation from the sun ("chemical rays") or from an electric arc may have a stimulating effect on the tissues.[6] If the irradiation is too strong, however, it might give rise to tissue damage. In particular, UV radiation with reduced IR component ("heat rays") was used in the treatment of *lupus vulgaris*, a tubercular condition of the skin which is prevalent in Nordic countries. A Medical Light Institute named after him was erected in Copenhagen as early as 1896, and in the following period of considerable enthusiasm for phototherapy the use of Finsen Light was introduced to Britain at the London Hospital in 1899, where a Light Department was founded. Finsen was awarded the Nobel Prize for Physiology-Medicine in 1903.

Probably the only contribution to medicine which has survived this period is the germicidal effect of UV light, which still finds everyday application.

In the 1950s Richard Cremer in Essex, England, after listening to an observant nurse, introduced phototherapy as a treatment of jaundice in newly-born infants.[7] Jaundice is caused by the accumulation of bilirubin, due to the uridine diphosphoglucuronyl transferase enzyme impairment in infants. UV light allows photochemical isomerization of bilirubin, which is thus rendered water soluble and is excreted in the bile. The phototherapy of neonatal hyperbilirubinemia with white light or blue-enriched white light is today a standard procedure in maternity and pediatric hospitals worldwide.

2.2.2 *The early days of photodynamic therapy*

The toxic effect caused by the combined action of a sensitizer and light was discovered by Oscar Raab in 1897 at the University of Munich, where he was a medical student in Professor von Tappeiner's laboratories. Raab observed that, using low concentrations of acridine, paramecia were killed in the presence of light, but they survived in the dark.[8]

After the publication of the results in 1900, his mentor Professor Hermann von Tappeiner, one of the pioneers of photobiology, started proposing different photosensitizers, among which eosin Y, fluorescein, sodium dichloroanthracene disulfonate and Grubler's Magdalene red, which were tested on a variety of living systems. The dyes were in most cases topically applied, but intratumoral injections were also attempted.[9]

The first photobiological experiments with haematoporphyrin were carried out on paramecia, erythrocytes, mice,[10] guinea pigs[11] and humans[12] in the period between 1908 and 1913. In particular, the Austrian physician Friedrich Meyer-Betz, carried out an experiment on himself.[12] His coworker Hans Fischer, who was awarded the Nobel Prize in 1930 for his work on porphyrins was familiar with the phototoxicity of haematoporphyrin in mice In 1912 Meyer-Betz injected himself intravenously 200 mg of haematoporphyrin; on the following sunny day the photosensitized reaction caused him erythema and oedema on the regions of the body exposed to sunlight, and remained extremely photosensitive for several weeks (Figure 2–3).

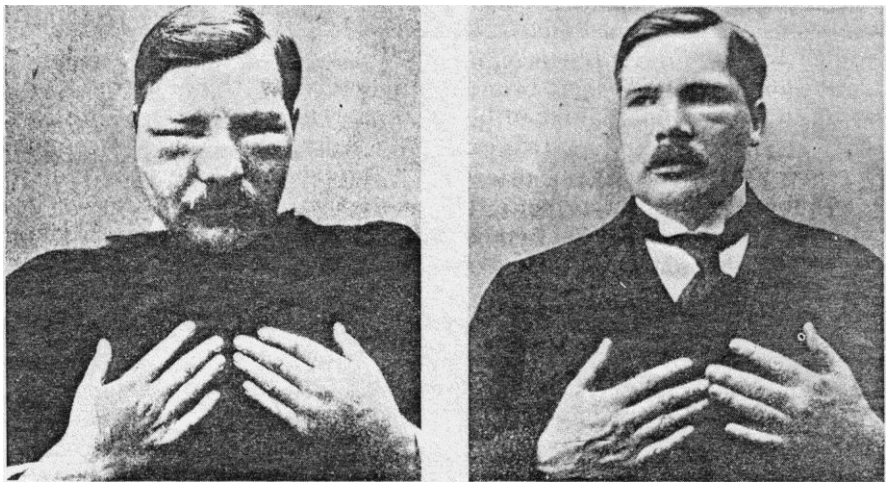

Figure 2–3 The Meyer-Betz self-photosensitization experiment. (Left) three days after the injection, the right side has been most exposed to sunlight. (Right) five days after the injection: the oedema is reducing, but lesions on hands and face are present.

The first observation of porphyrin fluorescence from tumors was published by Policard in 1924[13]. The red fluorescence from endogenously produced porphyrins in experimental rat sarcomas was erroneously attributed to bacteria infecting the tumors. Actually, this was the first reported example of preferential accumulation of porphyrin and porphyrin precursors in neoplastic tissue, as was stated later on by further studies.[14-17]

Dr. Samuel Schwartz, who studied porphyrins from the point of view of radiosensitization at the Mayo Clinic during in the 1960s, tried to purify commercial samples of haematoporphyrins, which contained up to 15 components.[18] Surprisingly, he found that pure haematoporphyrin was a poor tumor-localizer, while treatment with acetic acid-sulfuric acid mixture gave some components with better localization. These haematoporphyrin derivatives, or HPD, were tested for diagnostic and therapeutic purposes in numerous clinical investigations by Lipson and co-workers.[19]

Since HpD was a mixture of a number of porphyrins with widely different properties, the search for pure substances started, leading to the study of the so-called second generation photosensizisers. Winkelman introduced tetraphenyl porphine sulfonate (TPPS) and claimed that it had a better tumor-localizing ability than HpD.[20, 21] Ben-Hur and co-workers introduced phthalocyanines[22] as PDT sensitizers, which present the advantage of a string absorption in the near-IR region, where strong dye lasers are available and biological tissue is more transparent.

The meso-substituted porphyrin, tetra(meta-hydroxyphenyl)porphyrin (*m*-THPP) was introduced by Berenbaum and co-workers[23] and is being used in clinical trials. Recently, some other new photosensitizers have also been introduced for clinical trials.[24]

The use of endogenous protoporphyrin IX (PpIX) induced by exogenous 5-aminolevulinic acid (ALA) is a novel concept of clinical PDT and photodetection,[25] which was experimentally introduced by Malik et al. in 1987 in the treatment of erythroleukemic cells in vitro.[26] In the meantime, based upon their own data on ALA-mediated PpIX production in the normal skin of mice,[27] Kennedy and Pottier successfully treated human skin tumors with topically ALA-based PDT.[28]

2.2.3 First generation photosensitizers: haematoporphyrin derivative (HpD)

Haematoporphyrin possesses two benzylic-type alcohol functions at C-3 and C-8, with resulting diastereoisomerism. Moreover, due to the benzylic reactivity, naturally-derived samples contain up to 15 components.

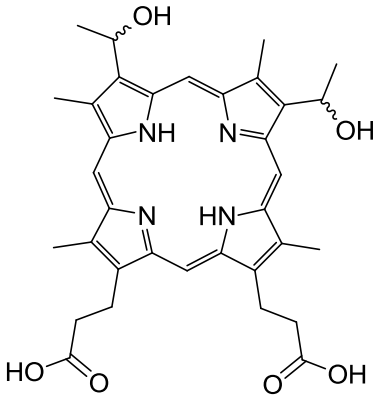

Haematoporphyrin

Haematoporphyrin is obtained in crude form from slaughterhouse blood. Treatment with mineral acid followed by hydrolytic workup removes the protein and the iron to give haematoporphyrin, generally isolated as dihydrochloride.

In the early 1960s Lipson isolated a preparation called Haematoporphyrin Derivative, HpD, which was found to be a powerful photosensitizer and preferentially localized in tumors.[19] Haematoporphyrin dichloride was first treated with sulfuric acid in acetic acid for 15 minutes at room temperature and precipitated with aqueous sodium acetate (HpD stage I), then treated with alkali and neutralized to pH 7.4 for injection (HpD stage II).

HpD stage I contains about 10 components, deriving from esterification and elimination reactions.[29]

HpD stage II contains monomeric hydrolysis and elimination products and higher molecular weight material which is responsible for the biological activity, in particular:[30]

monomers (haematoporphyrin stereoisomers, haematoporphyrin vinyl deuteroporphyrin isomers and protoporphyrin) with a high fluorescence quantum yield but with a poor tumor uptake;

dimers with a lower fluorescence quantum yield but with a higher tumor uptake;

non-fluorescent aggregates with the best tumor-localizing properties.

Photofrin® is a commercial preparation based on the high molecular fractions of HpD. It was originally developed by Dougherty n the 1970s at the Roswell Park Memorial Cancer Institute in Buffalo.[31]

The high molecular weight fraction of HpD increases with an HPLC or GPC separation, though some monomers are still present. The ratio of monomer:dimer:oligomer increases from 22:23:55 (HpD stage II) to 14:19:67 (Photofrin®).[32] In dimers and oligomers the porphyrin units are linked by ether, ester and C–C bonds. The total number of components is about 60.

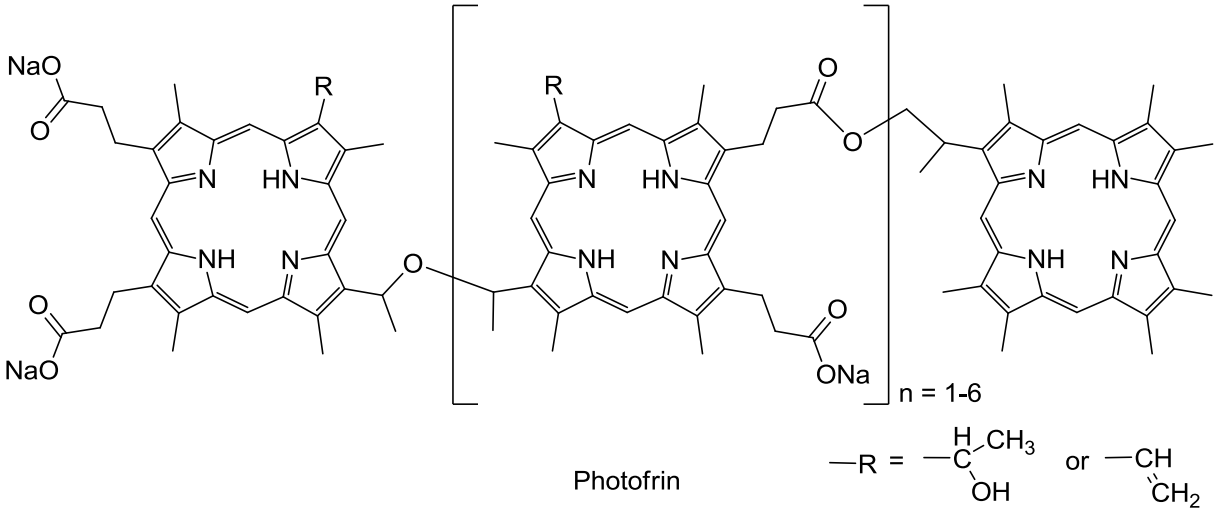

Photofrin

Photofrin® has a Q1 band at 630 nm (ε = 3.0 10^3 mol^{-1} cm^{-1}) in phosphate buffered saline (PBS). The singlet oxygen quantum yield is quite low, at approximately 0.01 in PBS.

In typical PDT treatment, Photofrin® is administrated via intravenous injection (drug dose 2-5 mg/kg) followed by irradiation with light at 630 nm (light dose 100-200 J cm^{-2}) at 24-48 h after injection. Photofrin® requires a long clearance time of 4-8 weeks after injection to avoid skin photosensitization.

Photofrin® has been approved worldwide for clinical use against early- and late-stage lung cancer, esophageal cancer, bladder cancer and malignant, nonmalignant and early-stage cervical cancer.

In conclusion, first generation photosensitizers, that is HpD and its derivatives, present the following advantages:

simple preparation from readily available starting material;
extensive clinical experience recorded in the literature;
it was the first substance to receive regulatory approval (Canada, 1993), and now has approvals in several other countries.

However, several disadvantages have to be considered:

very complex mixture in terms of isomerism, stereoisomerism and oligomeric composition, which is therefore difficult to reproduce;
modest activity in cancer PDT;
low selectivity for cancer tissue, causing sensitization of normal tissue (especially skin) for weeks;
the irradiation excites the Q band I ($\lambda_{max,abs}$ ~630 nm), which has the weakest absorption, therefore higher photosensitizer or light doses are needed to generate a sufficient photodynamic effect.

2.2.4 Porphyrin derivatives

Porphyrins are a class of aromatic macrocycles containing a 18π electron system. Porphyrin itself is planar, but increased substitution at the periphery may cause deformation from planarity. The central cavity may complex a wide variety of metal ions and some metalloids (e.g. silicon).

The absorption spectrum of porphyrins shows an intense band ($\varepsilon \sim 2 \bullet 10^5$ L cm^{-1} mol^{-1}) at about 400 nm, called the Soret or B band, and usually four distinct bands between 500 and 600 nm, called Q bands, denoted by Roman numerals from the low energy side.

Porphyrins can be obtained from three main sources: extracted from haemoglobin, prepared by total synthesis in the laboratory, or generated by manipulation of the biosynthetic pathway to protohaem.

In the first case, haemoglobin is isolated from blood from slaughterhouse by treatment with heparin to prevent coagulation, haemolysis and centrifugation to eliminate the erythrocyte ghosts, then crystallized. In alternative, the chloroiron (III) complex protoporphyrin, (also called protohaemin), can be obtained by treatment with acetic acid and sodium chloride.

Demetallation of protohaemin gives protoporphyrin. Treatment of protohaemin with molten resorcinol and subsequent demetallation in acidic conditions gives deuteroporphyrin.

Haematoporphyrin is prepared by treatment with concentrated hydrobromic acid and acetic acid, which demetallates protohaemin. Subsequent work-up hydrolizes the benzylic bromide functions obtained by addition of HBr to the vinyl groups. The two diastereoisomers can be separated by reverse phase HPLC.

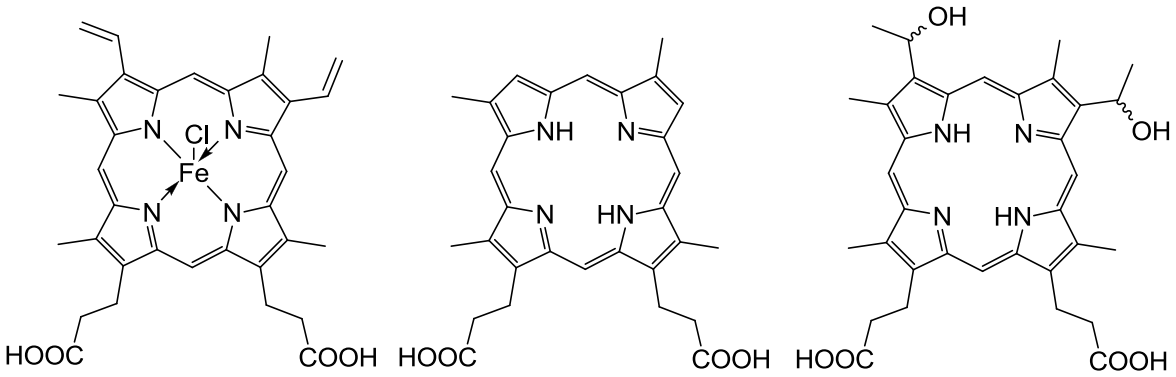

Protoaemin Deuteroporphyrin Haematoporphyrin

Deuteroporphyrin, protoporphyrin and haematoporphyrin are the most common starting materials for the synthesis of PDT sensitizers originating from haemoglobin. For example, the more soluble dimethyl esters obtained from protoporphyrin have been employed in the synthesis of cationic derivatives and chlorins.

The total synthesis of porphyrins can be divided into three main synthetic approaches: class A and B are stepwise processes which allows a substitution pattern with low symmetry, while class C are one-pot reactions which are economically advantageous for symmetrical substitution pattern derivatives.

A common feature is the formation of the *meso* bridges, which can be formed either via the pyrromethene, formed by the electrophilic attack of an α-pyrrole carboxyaldehyde on an α-free pyrrole, or via the dipyrrylmethane, formed by nucleophilic displacement on a substituted α-methyl function with a good leaving group. The macrocycle is initially formed in a reduced state in the *meso* positions, which are readily oxidized either with oxygen in the air or with an added oxidant, to give the aromatic system.

Two notable examples of class A approach are Johnson's biladiene-ac synthesis[33] (Scheme 2–1) and Woodward's chlorophyll synthesis[34] (Scheme 2–2):

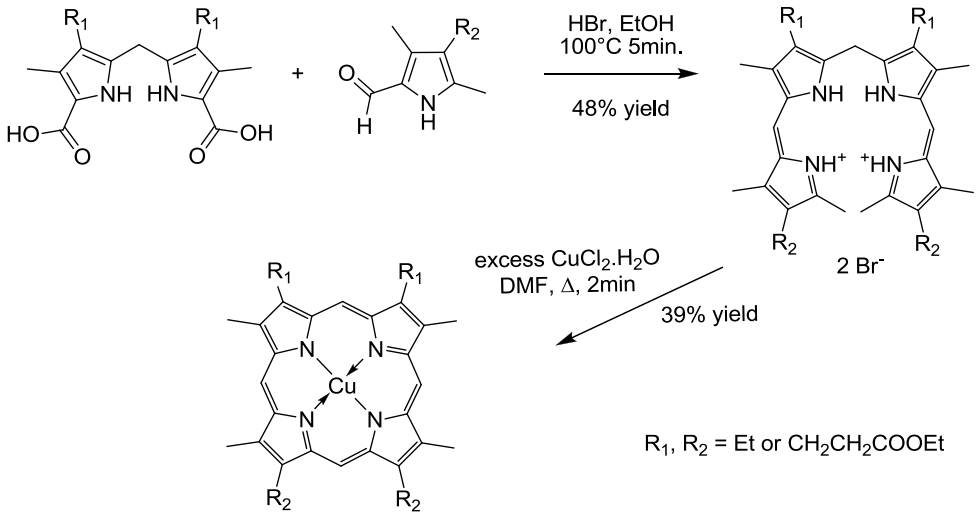

Scheme 2–1 Johnson's biladiene-ac synthesis

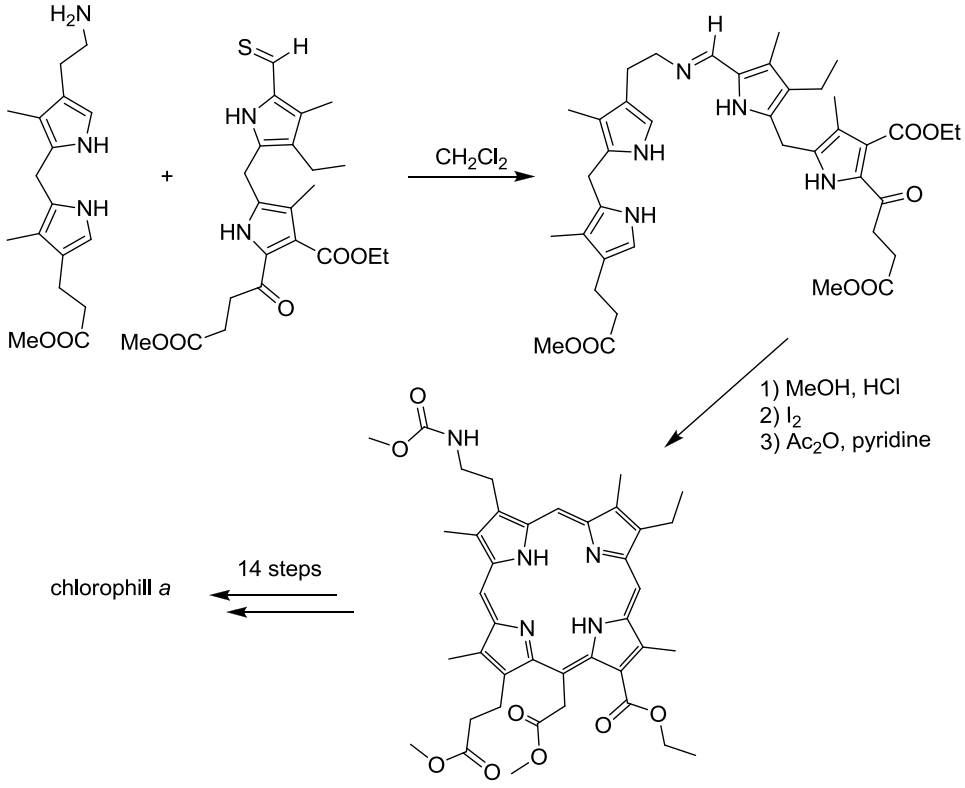

Scheme 2–2 Woodward's chlorophyll synthesis

An example of class B approach is MacDonald's synthesis of uroporphyrin III octametyl ester[35] (Scheme 2–3):

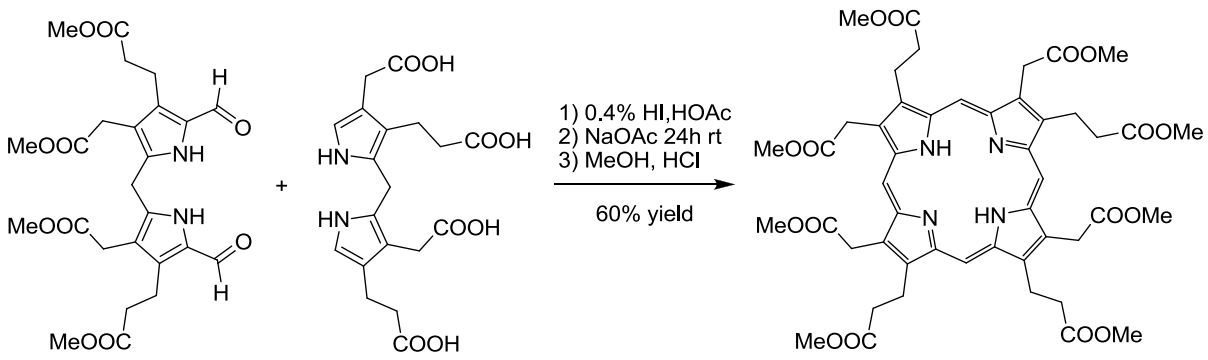

Scheme 2–3 MacDonald's synthesis of uroporphyrin III octamethyl ester

The most common porphyrin synthesis carried out in the laboratory is a class C approach: Rothemund-Adler reaction,[36] which gives meso-substituted products, like 5,10,15,20-tetraphenylporphyrin (TPP) (Scheme 2–4). The product crystallizes directly from the reaction mixture on cooling, and the corresponding chlorin can be removed by treatment with 2,3-dichloro-5,6-dicyano-p-quinone (DDQ).

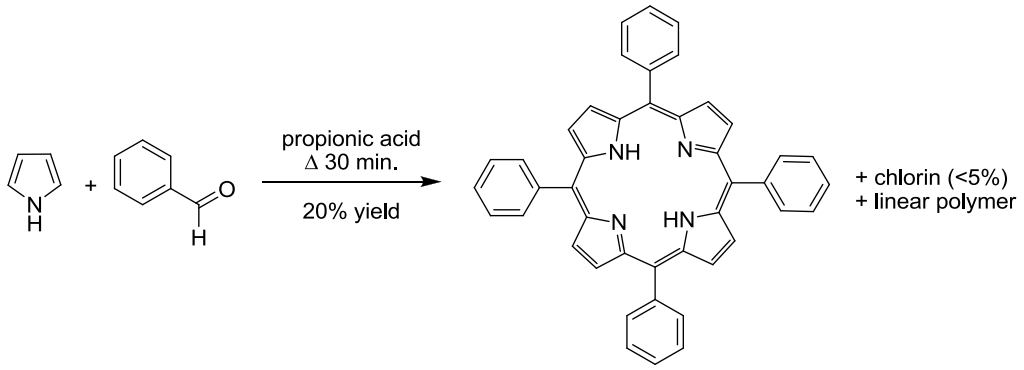

Scheme 2–4 Rotemund-Adler reaction

When two different reactant aldehydes are used, a mixture of products is obtained, which is usually chromatograpically separated.

In Lindsey's modification[37] pyrrole and benzaldehyde react reversibly in dilute solution (10^{-2} M) at room temperature to form an equilibrium distribution of porphyrinogen (reduced in the *meso* positions) and linear polypyrrylmethanes. The addition of an oxidant such as DDQ irreversibly converts porphyrinogen to the aromatic porphyrin. The overall yield can be further increased by adding a dehydrating agent such as triethyl orthoacetate. Due to the mild conditions this method is well suited for compounds with reactive substituents and for *meso*-tetraalkylporphyrins.

The use of surfactant micelles has been proposed by Bonar-Law:[38] the anionic surfactant sodium dodecyl sulfate is presumed to stabilized the cationic intermediate.

This procedure is particularly useful for porphyrins with polar functions, where the Lindsey method is not feasible due to solubility problems.

Sulfonation of TPP gives a mixture of mono, di, tri and tetra sulphonic acids, predominantly at the *para* position, which have been subject of PDT studies. The tetrasulphonic acid derivative shows some neurotoxicity in the rat, while the less substituted derivatives show distinct intracellular localizations and photocytotoxicities.[39]

Meso-tetra(hydroxyphenyl)porphyrins (THPP) are prepared by the Rothemund-Adler route, usually with protection of the phenolic function. From *in vivo* bioassays on tumor implant in the mouse, the orto- meta- and para- isomers were all found to be efficient photosensitizers,[23] although the o-TPP showed severe skin photosensitization.

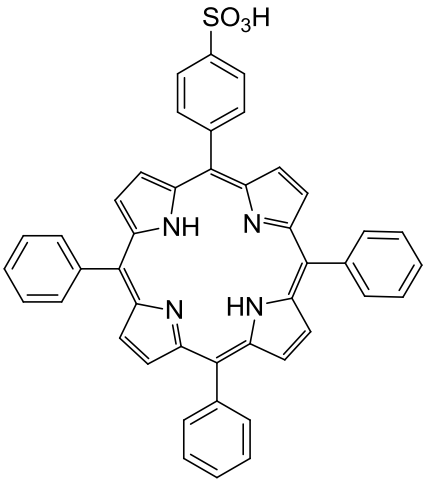

$TPPS_1$

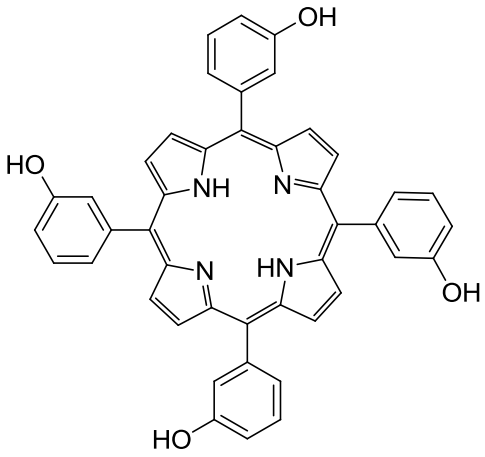

m-THPP

Porphyrins bearing a six-membered anhydride, imide, or isoimide ring fused across a *meso*-position and a neighboring β-position are characterized by a retro-etio spectrum, in which the most intense Q-band is band I.

These derivatives, such as mesoverdin, can be prepared from readily available porphyrin esters via intramolecular Friedel-Crafts reaction, but both the 13,15 and 15,17 regioisomers are formed, which therefore have to be separated by chromatography and fractional crystallization. More common and convenient starting materials are chlorophyll *a* and bacteriochlorophyll, which are oxidized with DDQ to give the corresponding anhydride-fused porphyrins (such as purpuroporphyrin 18 methyl ester), currently being examined as PDT sensitizers.[40, 41]

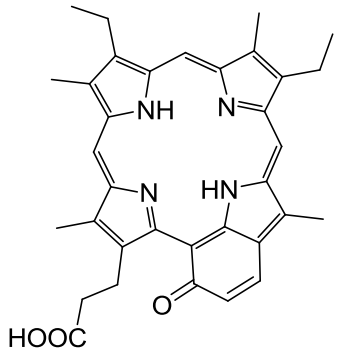

Mesoverdin
(13,15 isomer)

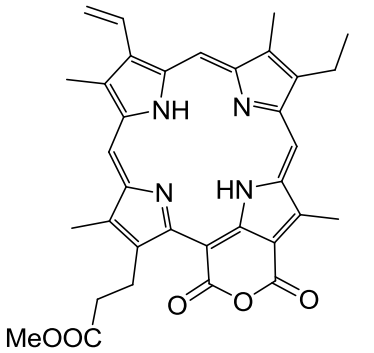

Purpuroporphyrin 18 methy ester

2.2.5 *Endogenous porphyrin: δ-aminolevulinic acid (ALA) as a pro-drug*

The third route to the synthesis of porphyrin derivatives for sensitization is the endogenous generation of protoporphyrin, by making use of the body's enzymatic pathway to produce the porphyrin naturally. In this new approach to PDT a non-phototoxic pro-drug, δ-aminolevulinic acid (ALA) is administered, resulting in the endogenous synthesis of the photosensitizer, protoporphyrin IX (PpIX).

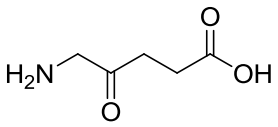

δ-aminolevulinic acid (ALA)

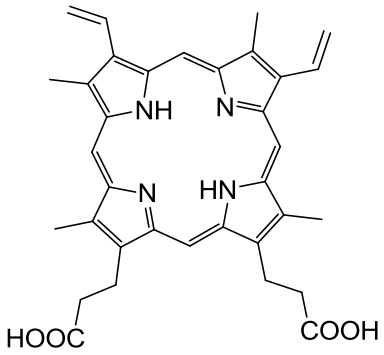

Protoporphyrin IX (PpIX)

ALA is involved in the biosynthesis of heme (Figure 2–4). In the first step of porphyrin-heme synthesis, ALA is formed in mitochondria from succinyl-CoA and glycine by ALA synthase. The four following enzyme-catalyzed steps steps take place in the cytoplasm. The condensation of two ALA molecules gives porphobilinogen (PBG); the head to tail condensation of four PBG molecules gives the linear hydroxylmethylbilane, which rearranges to uroporphyrinogen III and is converted to coproporphyrinogen by removal of CO_2. The last three steps of porphyrin-heme biosynthesis return to the mitochondria. Coproporphyrinogen III is oxidized first to protoporphyrinogen, then to PpIX. Finally, heme is obtained via the chelation addition of a ferrous ion.

This eight stepped pathway is controlled by the intracellular concentration of free heme, which acts as a negative feedback mechanism on the enzyme ALA synthase, thus

regulating ALA production. Exogenous ALA bypasses this normal feedback control point, and the abundant PpIX produced cannot be readily chelated with Fe(II) and therefore remains available as a sensitizer for a limited time. Moreover, the ferrochelatase enzyme shows a decreased activity in tumor cells compared to normal cells, thus the differential higher accumulation of PpIX in tumor cells is observed.

The fluorescence of porphyrins accumulated in cancer tissue after ALA administration enables the visualization of the neoplastic regions. This technique, generally termed fluorescence diagnosis (FD) has been clinically applied in detecting neoplasms in the brain, esophagus, bladder, uterus, and skin. and aids in estimating preoperative states or postoperative residual tumor, and it is also employed for fluorescence-guided resection.[42]

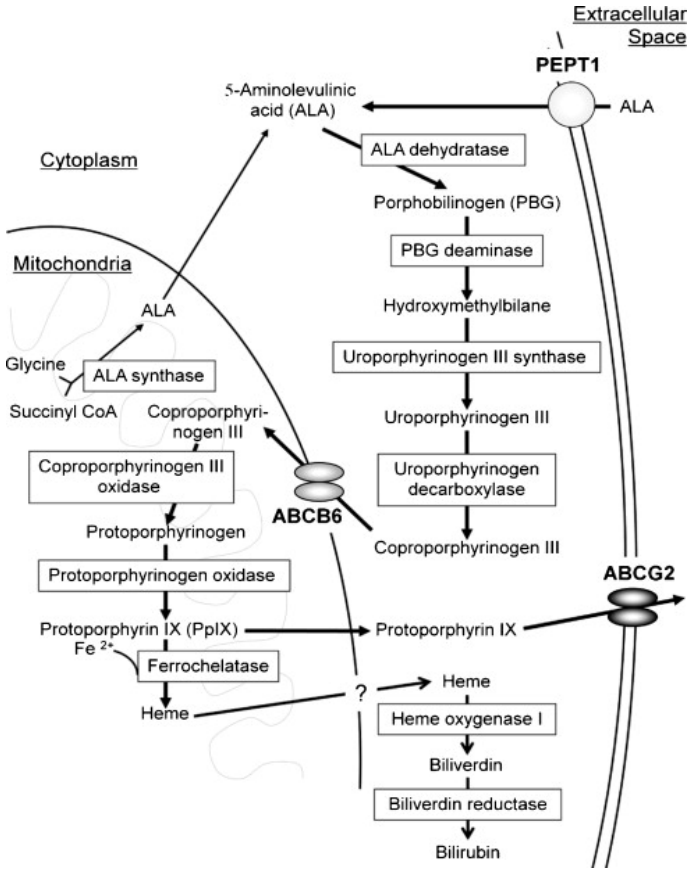

Figure 2–4 Schematic illustration for the transporter-mediated PpIX accumulation in cancer cells after administration of ALA. Rectangles indicate the enzymes involved in heme metabolism.

When tested using an in vivo bioassay with a tumor implant, exogenous PpIX shows little photodynamic activity with respect to ALA-induced PpIX.[43] The difference is mainly due to PpIX localization sites in cellular compartment of HeLa cells: selective accumulation of ALA-induced PpIX in mitochondria was observed whereas exogenous PpIX was accumulated mainly in the plasma membrane, where it is less efficient.

ALA-PDT finds application in the treatment of pre-malignant or malignant lesions in the clinical fields of dermatology, urology, neurosurgery, otorhinolaryngology, gynecology and gastroenterology and in the treatment of bacterial, fungal, viral and parasitic superficial infections.[44] Today, The U.S. Food and Drug Administration (FDA) approved a 20% solution of ALA (Levulan®, DUSA Pharma) for the treatment of actinic keratosis, a pre-cancerous stage of skin cancer, with a blue light source.[45] The European Medicines Agency (EMEA) in Europe and the U.S. FDA have also approved an ALA hexyl ester derivative (Hexvix®, Photocure) for the detection of papillary bladder cancer using fluorescence cystoscopy.

ALA-PDT effectiveness has been demonstrated, nevertheless some drawbacks have to be mentioned:

PpIX tends to be rapidly photobleached when generated *in situ* in this way;
The procedure is suitable only for superficial neoplasms;
The effectiveness of this treatment cannot be increased since it is regulated by a specific enzyme sequence.

2.2.6 *Chlorins and bacteriochlorins*

Chlorins and bacteriochlorins are β-dihydroporphyrins and β-tetrahydroporphyrins, respectively. Two types of β-tetrahydroporphyrins are present: adjacent (isobacteriochlorin) and opposite (bacteriochlorin). β-hexahydroporphyrin is also known.

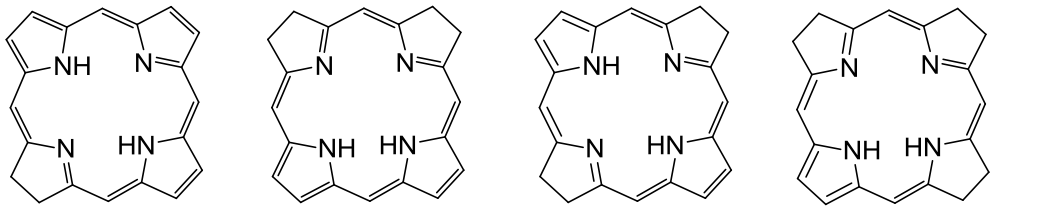

Chlorin Isobacteriochlorin Bacteriochlorin β-hexahydroxyporphyrin

All these hydroporphyrins can be dehydrogenated to the more stable porphyrins, but in case of β,β-disubstitution. The reaction occurs slowly in solution by autoxidation, but is usually rapid and quantitative in the presence of a high potential quinine such as DDQ.

These hydroporphyrins have an 18-π electron aromatic system, while other hydroporphyrins (*meso*- or N-hydro derivatives such as phlorins and porphyrinogens) present an interrupted conjugation, with reduced or absent visible absorption.

These macrocycles have essential function in living organisms. For example, the commonest example of chlorin is the chromophore of chlorophyll *a* and chlorophyll *b*;

bacteriochlorin is the chromophore of the bacterial photosynthetic pigment, bacteriochlorophyll *a*, while isobacteriochlorin occurs in an intermediate stage in the biosynthesis of vitamin B_{12}.

The absorption bands of the chlorins differ in relative intensities from the porphyrin ones. In particular, the Q band I is more intense, thus the characteristic green color of these systems. Due to this characteristic feature, chlorin and bacteriochlorin derivatives have been proposed as PDT sensitizers, since band I lies in the biological tissue transparency window.

These hydroporphyrins can be isolated from natural products or can be fully synthesized.

Concerning the natural source, the common chlorophylls and bacteriochlorophylls have to be chemically modified to be suitable for administration.

In higher plants, photosynthesis is based on a 3:1 mixture of chlorophyll *a* and *b* (7-formyl-7-demethyl derivative). Since the mixture is difficult to separate, a more suitable source is the alga *spirulina maxima*, which essentially contains only chlorophyll *a*. Bacteriochlorophylls are less conveniently available and must be isolated from photosynthetic bacteria specially grown in deep culture for the purpose.

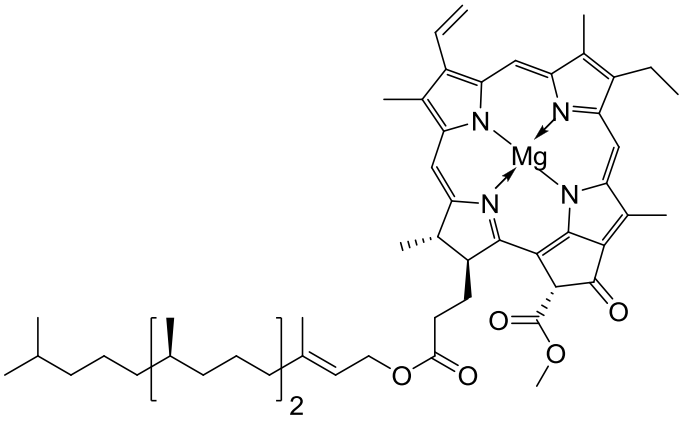

Chlorophyll *a*

The two main reactive functionalities of chlorophyll *a* are the vinyl group at C-3, which can be reduced to ethyl, giving the meso series compounds, and the β-ketoester function in ring E, which is subject to autoxidation and thermal demethoxycarbonylation.

Some chlorophyll-derived photosensitizers worth mentioning are:

Chlorin e_6, studied by Gurinovich's group in Minsk;[46]

Chlorin polyols, studied by Vallés,[47] obtained from the reduction of methyl mesopyropheophorbide *a* and methy mesopheophorbide *a* with lithium

aluminium hydride. *In vitro* assays show increased activity in the series mono-ol<diol<triol.

Chlorin p_6 derivatives: the 3-formyl-3devinyl derivative has been indicated as the most active from Mironov's group,[48] while Smith and Kessel reported numerous bioconjugates,[49] for example the C13 lysyl derivative has proven to be more selective and fast-acting in *in vivo* assays.

Bacteriopurpurin derivatives: Smith[40, 50] and Mironov[51, 52] have studied these analogues of purpurin 18 in the bacteriochlorophyll series, preparing the imide and isoimide analogues. These highly stable compounds show absorption max at λ_{max}>800 nm and are currently tested *in vivo*.

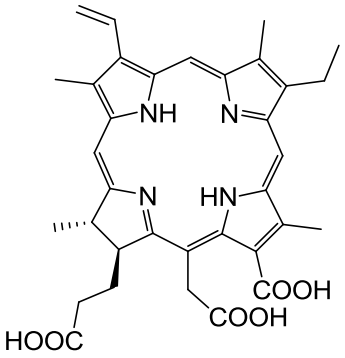

Chlorin e_6

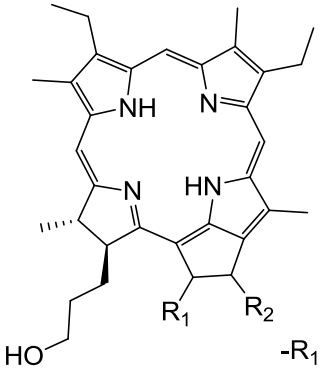

Chloryn polyols

$-R_1 = -R_2 = -H$
$-R_1 = -H, -R_2 = -CH_2CH_2OH$
$-R_1 = -CH_2OH, -R_2 = -OH$

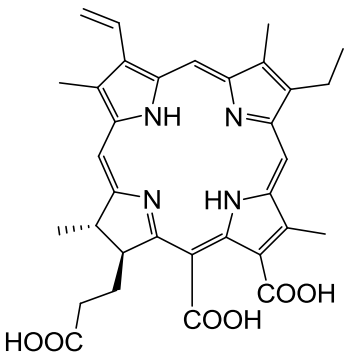

Chlorin p_6

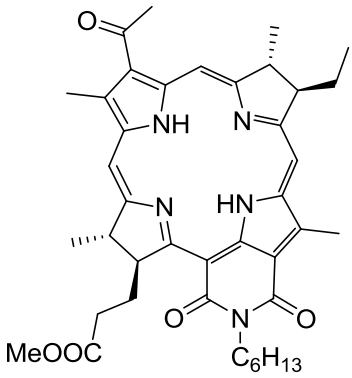

Bacteriopurpurin derivative (imide)

Mono-L-aspartylchlorin-e_6 (MACE, Laserphyrin®) is one of the earliest chlorophyll-derived chlorins with proven PDT application. It is water-soluble, so can be administered in PBS, has a short tumor-accumulation time, thus a short drug-light interval, and rapid clearance thus residual skin photosensitivity is brief.[53] Laserphyrin is prepared from chlorin-e_6 tricarboxylic acid by DCC coupling with di-*t*-butyl aspartate. The clinical similar procedure to that for Photofrin-mediated PDT, but a lower drug dose (0.5-3.5 mg/kg) and

a lower light dose (150 J cm^{-2}) are used. The primary mechanism of Laserphyrin-mediated PDT is cell death triggered by vascular stasis and direct tumor cytotoxicity.[54] Laserphyrin has been approved for clinical use in Japan in 2003 under the acronym NPe6 against early-stage lung cancer, and phase III studies are underway for liver cancer and recurrent neck cancer and head cancer.[55]

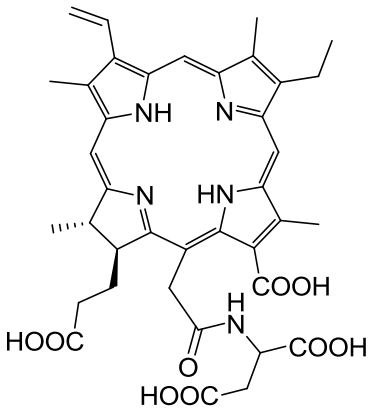

Laserphyrin

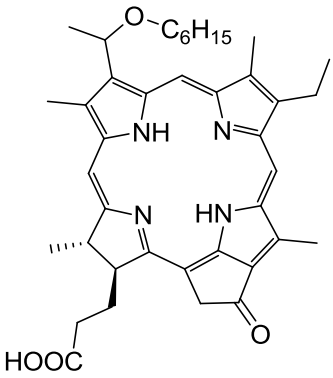

Photochlor

Another chlorophyll-derived photosensitizer is Photochlor® 3-(1-Hexyloxyethyl)-3-devinylpyropheophorbide *a,*[56] with high lipophilicity for enhanced cellular membrane penetration. Photochlor has a higher level of tumor-accumulation than either Photofrin or Foscan, and is removed from human plasma and excreted slowly from the body.[57] Photochlor is prepared as a pure form from methyl pheophorbide *a*, extracted from *spirulina*.[58] Photochlor has been investigated in phase I/II clinical trials against Barrett's esophagus (BE), esophageal cancer, non-small cell lung cancer, basal cell carcinoma and early- and late-stage lung cancer (Roswell Park Cancer Institute, Buffalo). Recently, Photochlor derivatives have been applied as cancer diagnostic drugs owing to their high tumor-accumulation properties.

Chlorins can also be derived from the heme of haemoglobin, with deuteroporphyrin[59] or PpIX[60] as starting materials.

Chlorins by total synthesis can be prepared by reduction of the corresponding porphyrin either by metal-acid reduction, or by treatment with diimide generated from *p*-tosyl hydrazide and potassium carbonate in pyridine.[61] Further reduction may occur to give bacteriochlorins and isobacteriochlorins: these compounds may be either dehydrogenated to the chlorin or they may be isolated by acid-fractionation and chromatography.

Thus, diimide reduction of the m-THPP, a photosensitizer of demonstrated potency in PDT, gives the corresponding chlorin m-THPC and bacteriochlorin, m-THPBC (Scheme 2–5).

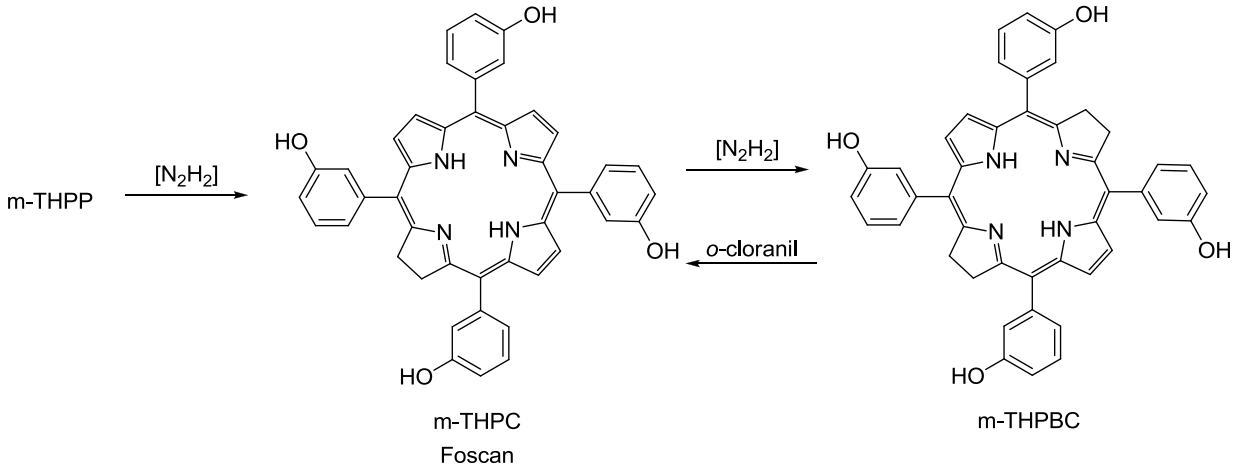

Scheme 2–5 Reduction of m-THPP

The intensities and the λ_{max} values of band I increase on reduction, while triplet quantum yields and Φ_{Δ} do not alter much. However, the photodynamic effect increases with each reduction step proportionally to ε_{max} of band I, at which irradiation occurs. Because of the greater ease of dehydrogenation and greater difficulty in the manufacture of the bacteriochlorin, the main emphasis has been on m-THPC, or Temoporfin, commercially available with the name Foscan®, which is one of the most potent photosensitizers in commercial development.

The typical PDT with Foscan is conducted by intravenous injection of the photosensitizer in water:PEG 400:ethanol = 5:3:2 mixture (drug dose 0.15 mg/kg) followed by irradiation with light at 652 nm (light dose 5-20 J cm^{-2}) at 24-96 hours after the injection. The PDT efficacy of Foscan is approximately 100 times greater than that of Photofrin at the same photodynamic dose, allowing the use of a lower drug dose and a shorter illumination time to achieve similar results.[62] To avoid skin photosensitization, however, Foscan requires a long clearance time of 4–6 weeks from human plasma after injection, which is almost same as that of Photofrin.[63] Foscan has been investigated for use against esophageal cancer, lung cancer, gastric cancer, prostate cancer and skin cancer and has been approved for clinical use against had head cancer and neck cancer. In addition, this photosensitizer has been investigated in phase II clinical trials against head cancer, neck cancer,[64] nasopharyngeal carcinoma and bile duct carcinoma in Europe, the USA and Canada.

Two related photosensitizers which are under commercial development are pegylated m-THPC, which requires a large mass dose but which is more selective, and m-THBC, which is more active but photobleaches quickly.

Formilation of nichel(II) etioporphyrin under Vilsmeier-Haack conditions gives the *meso*-formyl compound, which on Wittig reaction and demetallation gives the *meso*-acrylic ester. Under mild acidic conditions such *meso*-acrylic systems undergo a reversible thermal cyclization to the neighboring β-positions (Scheme 2–6). The resulting product possessing an electron-withdrawing function at the *meso* position adjacent to the reduced ring falls into the purpurin class. A photosensitizer with such structure is Purlytin® (Tin etiopurpurin).[65] The heavy atom present in the structure gives a low fluorescence quantum yield, on the other hand the singlet oxygen quantum yield is substantial (Φ_Δ = 0.7).[66] Purlytin has been investigated in phase II/III clinical trials against metastatic breast adenocarcinoma, basal cell carcinoma (BCC) and Kaposi's sarcoma in patients with AIDS.

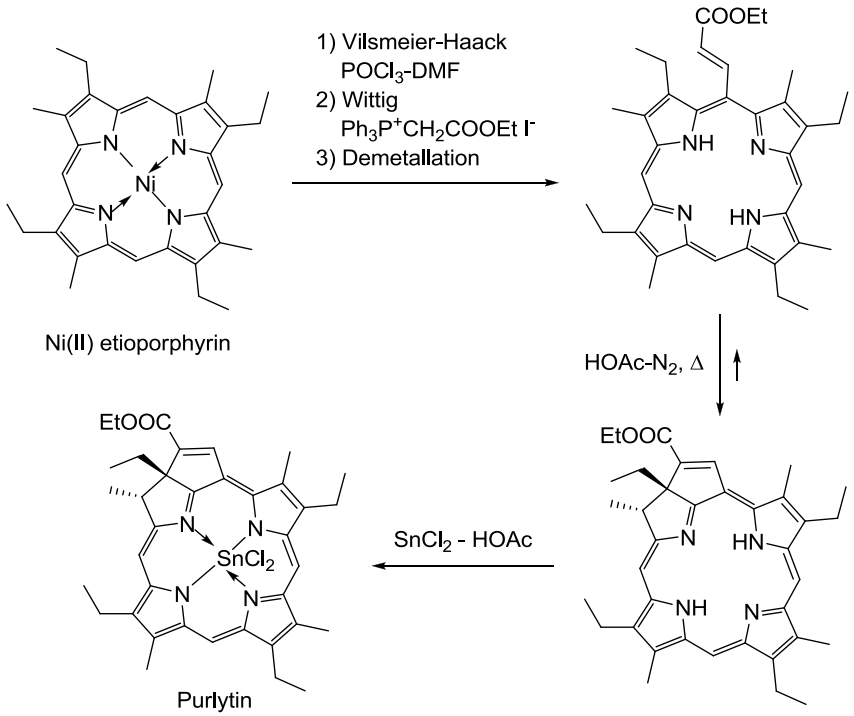

Scheme 2–6 Synthesis of Purlytin

2.2.7 Phthalocyanines and naphthalocyanines

Substitution of nitrogen for a *meso* carbon bridge in a porphyrin gives an azaporphyrin, replacement of all four meso carbon bridges by nitrogens gives a porphyrazine.

The benzocondensate derivatives to the β,β'-bonds of a porphyrin are benzoporphyrins. Replacement of all four *meso* carbon bridges of tetrabenzoporphyrin gives phthalocyanine (Pc).

These macrocycles give more stable metal complexes and become less basic with increasing meso-nitrogen substitution and fusion of benzene rings. The electronic spectrum of phthalocyanines changes dramatically, so that the Q band of phthalocyanines is the strongest band of the spectrum ($\varepsilon \sim 1\text{-}4\cdot10^5$ mol L^{-1} cm^{-1}) and appears in the 670-700 nm region. The metal-free phthalocyanines have two strong bands in this region (Q_x and Q_y), whereas the metallated phthalocyanines usually have only one.

Various elaborations of the phthalocyanine system are known, for example with heteroaromatic rings instead of benzenoid rings, and with more extensive aromatic systems. As the aromatic system becomes larger, the Q band shift in the red, ending up in the NIR region. At the same time the oxidation potential decrease, therefore the compounds beyond naphthalocyanine are poor PDT sensitizers. An important structural consideration is that phthalocyanines and the extended aromatic analogues are flat molecules, a geometry which is very unlike that of most of the chemical constituents of living things. For example, the phthalocyanine nucleus is a disc about 14 Å in diameter.

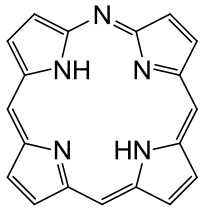

5-Azaporphyrin

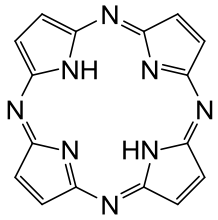

Porphyrazine

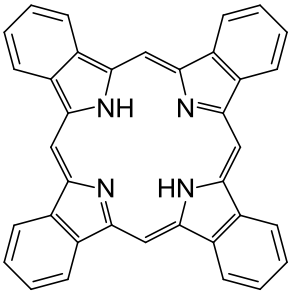

Tetrabenzoporphyrin

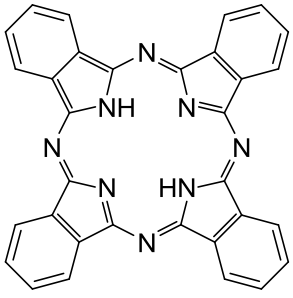

Phthalocyanine

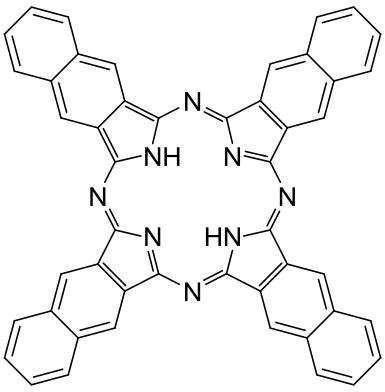

Naphthalocyanine

Some 5-azaporphyrins and benzoporphyrins have been proposed as PDT sensitizers,[67, 68] although phthalocyanines have been studied more estensively than these two less common systems.

The phthalocyanines are produced commercially in tonnage amounts and find application as blue-green pigments (insoluble stable colorants of symmetrical planar structure, used as a solid or slurry) and dyes (less symmetrical derivatives with solubilizing substituents).

Copper (II) phthalocyanine is the typical blue pigment, known as CuPc or Monastral Blue, is produced in amounts of 50000 tons/year and finds application in printing ink (cyan toner) and packaging industry. Aromatic chlorination gives the green pigment Phthalocyanine Green G ($CuPcCl_x$, where x=13-16), which finds application in acrylic paints, coatings and plastics. Nucleophilic substitution of the halogen with an aromatic thiolate gives $CuPc(SAr)_{16}$ which is nearly colorless ($\lambda_{max,abs}$ 800 nm) and thus is the basis of security applications (e.g. invisible barcoding). Water-soluble dyes (e.g. CI Direct Blue) are achieved by sulphonation of CuPc. Reactive dyes have also been produced ("Procion" from Zeneca, "Cibacron" from Ciba), which undergo nucleophilic substitution of the remaining halogen by hydroxy groups in cellulose (cotton), leading to covalent attachment of the dye to the fabric. Patent activity is optical data storage is vigorous, especially from Japanese electronic companies, since the information in compact discs is stored by laser ablation on a phthalocyanine layer which is expected to be as long-lived as possible.

Nearly all the syntheses of phthalocyanines are of the 4x1 type, putting severe symmetry restrictions on the products which can be obtained. Reliable stepwise synthesis strategies have not emerged yet because of the poor stability of the *meso*-nitrogen bridge in two ring and three ring intermediates. Some strategies have been proposed for circumventing the inflexibility of 4x1 synthesis, such as the cross-condensation of two different monomers in suitable molar ratio.[69]

Iron phthalocyanine was serendipitously discovered in 1928 during the course of the industrial production of phthalimide at Scottish Dyes. The process consisted in passing ammonia into molten phthalic anhydride in iron vessels and it was found that during certain preparations traces of a dark blue substance were formed in the molten imide. This material was stable, crystalline, and contained iron which was not eliminated by treatment with concentrated sulfuric acid.[70] Linstead laid the foundation to the chemistry of these compounds and formulated the correct structure in 1934[71, 72] which was confirmed by X-ray analysis by Robertson the next year.[73]

The syntheses which emerged from these and derived studies are summarized in Scheme 2–7. The industrial large-scale synthesis employs phthalic acid or anhydride on cost grounds, while phthalonitrile or diiminoisoindoline are preferable in the laboratory in order to obtain purer products. The *o*-dinitriles may be prepared by dehydration of the corresponding diamides, by nucleophilic substitution or by Diels-Alder reaction, and subsequent nucleophilic cyclization gives the corresponding diiminoisoindolines.

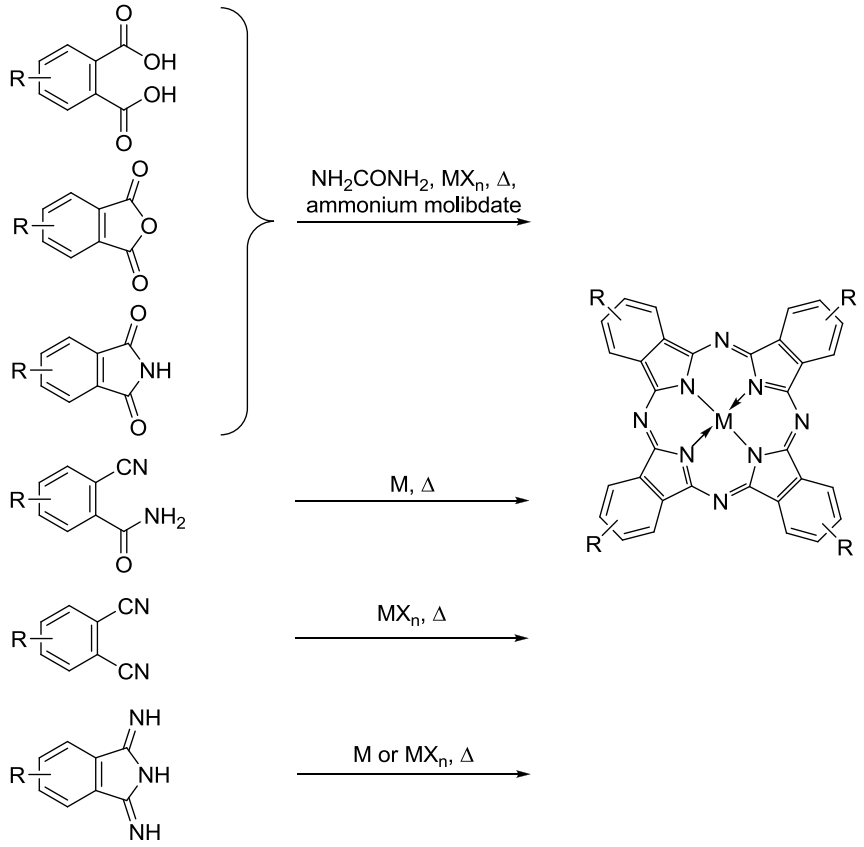

Scheme 2–7 Synthetic routes to metallophthalocyanines

Metal-free phthalocyanines are conveniently obtained using sodium or lithium isopentoxide in the macrocyclization step, since Na or Li are readily removed. Alternative routes to the metal-free compound are the treatment of phthalonitrile with ammonia gas in 2(N,N-dimethylamino)ethanol or the refluxing of diiminoisoindole in this solvent.

The following general points apply to phthalocyanine synthesis:

The reactions are carried out in a melt or a high boiling point solvent. Recently, however, Leznoff as described a general room temperature procedure, with a higher alcohol as a solvent and long reaction time (7-10 days);[74]

Alkyl substitution renders the products soluble in organic solvents, allowing chromatographic purification. In the absence of substituents, the phthalocyanines

and their metal complexes are usually insoluble, thus they can be purified either by washing out the impurities, or by sublimation;

The reaction is a reductive cyclotetramerization. The two electrons required for the dianion of the product are provided by the metal, the metal ion, the solvent or the catalyst;

Yields are very variable, but copper(II) complexes are generally formed in good yields. The reaction can also be extended to aromatic and heteroaromatic 1,2 dinitriles in general;

If the monomer is unsymmetrically substituted four Type isomers will be formed in statistical distribution, provided that steric interactions between the substituents do not intervene.

Zinc(II) phthalocyanine (ZnPC) has proven to be an effective photosensitizer. Due to the poor solubility in water and organic solvents, this compound usually administered with a vehiculating agent. For example, Shopova and Jori administred ZnPc in a liposomal preparation on induced or transplanted rhabdomyosarcoma in harmsters with good results of selective accumulation and photodynamic activity.[75, 76]

The more soluble octalkyl derivatives can be readily prepared from 3,6-dialkylphthalonytriles. Zinc(II) octapentyl phthalocyanine (ZnOPPC), administered as an emulsion, is more effective and more selective than ZnPC in *in vivo* bioassay.[77, 78]

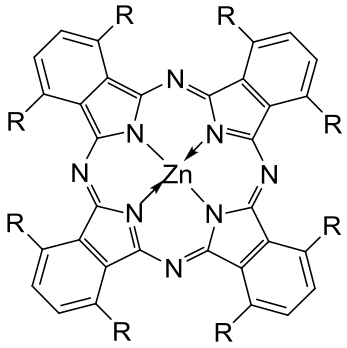

-R = -H ZnPC
-R = -C_5H_{11} ZnOPPc

Water solubility may be achieved by functionalization with polar substituents to give neutral (sulphonic acid, polyethylene glycol), anionic (carboxylic acid, phosphonic acid) and cationic (pyridinium quaternary salts) derivatives.

The direct sulphonation of aluminium and gallium phthalocyanines by electrophilic substitution with H_2SO_6-SO_3 or $ClSO_3H$ occurs at both *endo* and *exo* positions, the distribution of positional isomers depending on the substrate. The sulphonation only in the *exo* position is achieved by ring synthesis starting from 4-sulphophthalic acid, giving a

statistical mixture of Type isomers, while mixed synthesis (4-sulphophthalic acid and 4-phthalic acid) gives a mixture of lower sulphonic acids which may be separated with reverse phase chromatography.

Photosens® is a mixture of di- and trisulphonated aluminium phthalocyanine. The Q1 absorption band at 675 nm has the largest molar absorption coefficient ($\varepsilon = 2 \cdot 10^5$ M^{-1} cm^{-1}) of the second-generation photosensitizers. In a typical Photosens-mediated PDT the drug dose is 0.5-0.8 mg/kg and light (150 J cm^{-2} at 672 nm) is applied at 24-72 h after injection. Photosens has been investigated in phase III clinical trials against squamous cell skin cancer, breast cancer, oropharyngeal cancer, lung cancer and larynx cancers.[79, 80] Residual photosensitivity is a significant problem of this drug, which is not easily photobleached.

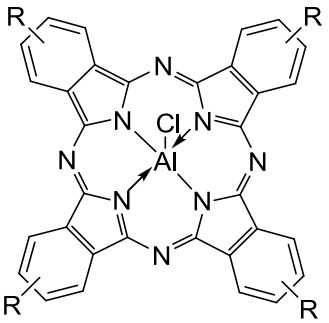

-R = -SO_3H or -H

Photosens

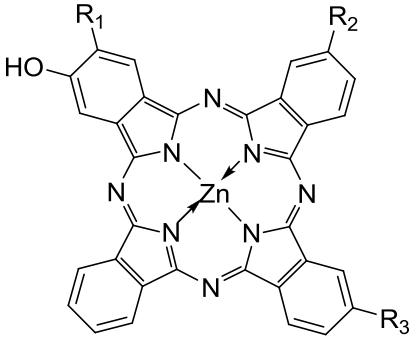

-R_1 = -R_2 = -R_3 = -H	2-Hydroxy ZnPC
-R_1 = -OH, -R_2 = -R_3 = -H	2,3-Diidroxy ZnPC
-R_2 = -OH, -R_1 = -R_3 = -H	2,9-Diidroxy ZnPC
-R_1 = -H, -R_2 = -R_3 = -OH	2,9,16-Trihydroxy ZnPC

Hydroxilated phthalocyanines have also been prepared in order to study whether the PDT efficacy increased like in the case of porphyrins. Tetrahydroxylated derivatives are made in the usual way (Scheme 2–7), while mono-, di-, and trihydroxy compounds are prepared by mixed synthesis or via half-phthalocyanine methods using ether protection in all cases. For biological assay the compounds were emulsified with Chremophor Evaluation *in vitro* against the EMT-6 mammary tumor cell lone showed that the monohydroxy compound was the most active in the series. However, *in vivo* the zinc(II) 2,9-dihydroxyphthalocyanine proved to be the most effective in causing complete tumor regression, being more potent than Photofrin, but less potent than ZnPC.[69]

The hydrophobicity of phthalocyanines can be adjusted for the purpose of improving biological interactions by varying the axial ligands. Thus the silicon phthalocyanine with a quaternary salt side chain is poorly taken up by V79 cells in culture, whereas the corresponding tertiary amine shows high uptake and photoinactivation.[81] Axial ligand

changes may improve solubility, however the possibility of ligand exchange in the inoculums or in the biological system needs to be kept in mind.

Naphthalocyanines are synthesized with a 4x1 approach from naphthalene-1,2-dinitrile or naphthalene-2,3-dinitrile,[82] and it is the latter that have been extensively studied in the PDT area. As with phthalocyanines, naphthalocyanines are poorly soluble compounds, but solubility in organic solvents may be enhanced by bulky alkyl substituents.

Initial results of PDT studies with naphthalocyanines were not encouraging. For example, silicon(IV) naphthalocyanine with hydrophilic axial ligands (polyethylene glycol) were water soluble, and accumulated in fibrosarcoma in mice, but showed little photodynamic activity. Studies with mixture of sulphonated naphthalocyanines made by direct sulphonation showed them to be less potent PDT sensitizers than the corresponding phthalocyanines, and to be susceptible to photodegradation.

More recently these compounds have begun to look more promising in the treatment of melanoma, because the screening absorption of melanin, strong throughout the visible, begins to decrease significantly in the NIR region, where naphthalocyanines have an intense absorption maximum (770-800 nm). Shopova and Wöhrle have demonstrated that zinc(II) naphthalocyanine localizes in and photoinactivates pigmented melanoma cells.[83] Jori, Kreimer-Birnbaum, Kenney and Rodgers have studied the effect of silicon(IV) naphthalocyanines substituted with trialkylsiloxy ligands on melanotic and amelanotic melanoma cells,[84] suggesting that cell death was caused by damage to the lysosomes and the cytoplasmatic membrane.

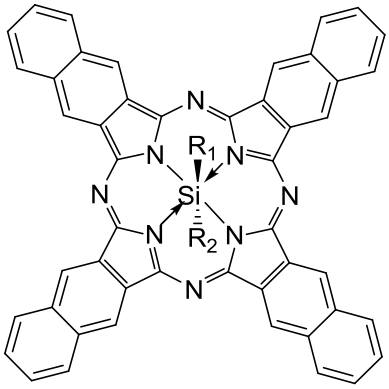

$-R_1 = -OSi(CH_3)_2CH_2CH_2CH_2N(CH_3)_2$
$-R_2 = -OSi(C_{10}H_{21})_3$

$-R_1 = -R_2 = -OSi(C_{18}H_{37})(CH_2CH(CH_3)_2)_2$

2.2.8 *Non-porphyrinoid photosensitizers*

Major emphasis has been placed on porphyrin-related PDT photosensitizers in the previous sections because these compounds offer three main advantages: intense absorption in the visible, aromatic stability and a generally low cytotoxicity in the dark.

However, the reasons that led the first PDT clinicians to choice porphyrins and related compounds are not overwhelming, and certainly do not prevent consideration of photosensitizers based on other chromophoric systems. It has to be said that in many cases the proposed PDT sensitizers have simply been selected from what was available on the shelf and have not been subjected to thoughtful structural variation and bioassay to sort out the best therapeutic candidate.

2.2.8.1 Cyanine dyes

Polymethines are compounds made up from an odd number of methine groups (-CH-) bound together by alternating single and double bonds.[85] Among this class of compounds, cyanine dyes are among the oldest and most investigated family of synthetic pigments.

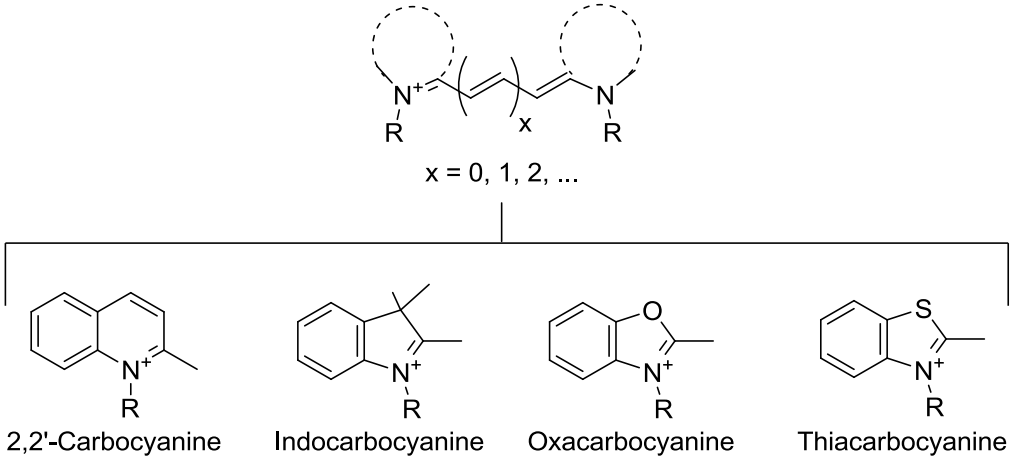

Scheme 2–8 Generic structure of a polymethine cyanine dye-containing alkylic substituents at both nitrogen atoms. The dotted line represents two heterocyclic moieties, the most common ones are depicted below.

Polymethine cyanine dyes are extensively used as photosensitizers in silver halide photography,[86] as mode-locking compounds in laser technology,[87] and in photovoltaic and solar cells.[88] Cyanines have also been broadly used in the life sciences and other biologically related disciplines as optical probes of membrane potential,[89] organelle stains[90] and as probes for membrane structure and dynamics.[91]

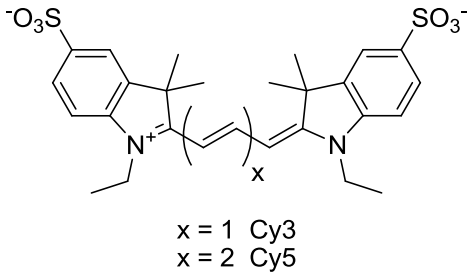

The indocarbocyanines commonly known as Cy3 and Cy5 are the first two compounds of this class which found application in imaging primarily due to their remarkable photostability, large absorption cross sections and fluorescence efficiencies, compatibility with common lasers and single-photon counting detectors, and commercial availability as derivatives for covalent labeling of proteins and nucleic acids.[92]

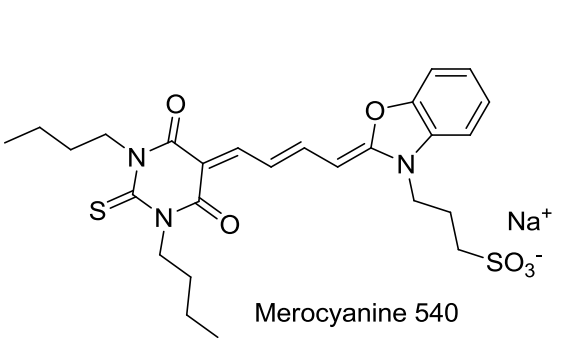

Merocyanine 540

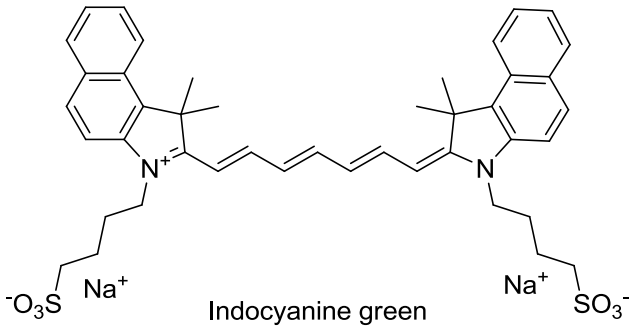

Indocyanine green

Merocyanine 540 has been widely used for imaging applications[93] and has been recently advanced as a phototherapeutic agent in the in the photodynamic inactivation of *Staphylococcus aureus* biofilms[94, 95] and as a photosensitizer in leukemia.[96, 97] Comparative studies in two murine myeloid leukemia cell lines have revealed that m-THPC is significantly more potent and more selective than merocyanine 540, and that both photosensitizers induce cell death *via* apoptosis.[98]

Indocyanine green (ICG) was developed in the Second World War as a coloring agent in photography and tested in 1957 at the Mayo Clinic for use in human medicine and was granted United States Food and Drug Administration (FDA) approval in 1959. ICG finds clinical use in hepatic function diagnostics,[99] in cardiology for the determination of cardiac output and blood volume,[100] and in ophthalmologic fluorescent angiography.[101] The large clinical history means that, if ICG were found to be a useful PDT sensitizer, the route to regulatory approval would be much easier because of existing clinical experience. Indeed, the PDT effect on keratinocytes in cell culture has been investigated[102] and the encouraging results have led to a pilot study of ICG laser therapy of acne vulgaris.[103]

Squaraine dyes represent another class of polymethine compounds, obtained from the condensation of electron-rich substrates and squaric acid or its derivatives.[104-106] these quadrupolar dyes possess a sharp and intense absorption band in the visible and NIR region,[107, 108] good photostability and high photoconductivity.[109] Squaraines have been extensively investigated since the mid-1960s for a large number of technological applications including xerography,[110] data storage,[111] light emitting field-effect transistors,[112] solar cells[113, 114] and nonlinear optics.[115] It has been recently shown that squaraines can also behave as very efficient two-photon absorbers[116] and fluorescent

histological probes.[117] Due to their remarkable properties, squaraines have also been suggested as second generation sensitizers for PDT.[118-122] Since their relevance in this thesis work, squaraine dyes and their biological applications will be discussed in greater detail later on.

2.2.8.2 Hypericin

Hypericin is an extended anthraquinone derivative which is one of the principal active constituents of *Hypericum*. In ethanol the absorption maximum is at λ = 590 nm (ε = 41600 L mol^{-1} cm^{-1}) and the singlet oxygen quantum yield is Φ_Δ = 0.36. In aqueous media Φ_Δ falls to 0.02, possibily due to aggregation.

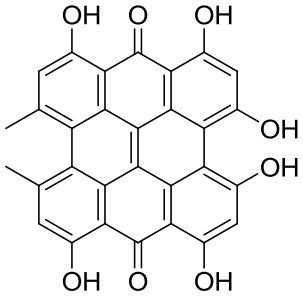

Hypericin

From the observation of the photosensitization effects in livestock grazing on *Hypericum*, which is a worldwide diffused weed,[123] hypericin has been proposed as a PDT agent against viruses[124] and cancer cells.[125, 126] In particular, PDT activity has been shown against human pancreatic cancer *in vitro* and *in vivo*.[127] Since hypericin accumulates preferentially in cancerous tissues, it has also been proposed as a cancerous cells marker.[128]

2.2.8.3 Phenothiazines

Many of the phenothiazine dyes, such as methylene blue, toluidine blue and Nile blue A are commercially available and there is considerable literature on the use of these dyes as biological stains. In particular, toluidine blue has been employed to visualize cancerous lesions *in vivo* as an aid in diagnosis.[129, 130]

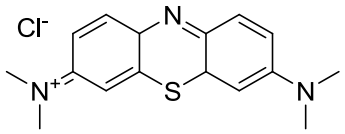

Methylene blue

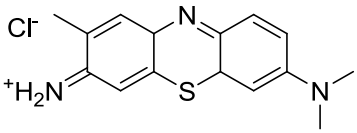

Toluidine blue

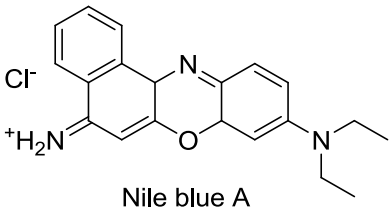

Nile blue A

These well-known cationic dyes show photomicrobicidal properties and have activity as PDT agents in *in vitro* experiments with cancer cell lines.

Since methylene blue is an effective photosensitizer in vitro, but exerts no PDT effect in vivo when it is administrated intravenously due to its high hydrophilicity, Mellish et al. systematically synthesized methylene blue analogues bearing various alkyl chains at the amino groups instead of methyl groups to reduce the hydrophilicity. The photodynamic effect of the derivative with a *n*-propyl chain, had an LD_{50} value, approximately 130 times lower than that of methylene blue (R = Me). Even though the dark cytotoxicity also increased, the ratio of photocytotoxicity over dark cytotoxicity was improved approximately 20 times in comparison with that of methylene blue.

2.2.8.4 BODIPY derivatives and their analogues

Boron dipyrromethene (BODIPY) is a useful fluorescent dye because of its relatively sharp absorption band with a high molar absorption coefficient, its high quantum yield of fluorescence and its acceptable photostability. To use BODIPY and its analogues as photosensitizers, several research groups have attempted to enhance the quantum yield for their triplet excited states by an adding heavy atom, such as a halogen, into the chromophore. As a pioneering work, O'Shea et al. reported the synthesis of halogenated BODIPY analogues, boron azadipyrromethenes, which possess a higher singlet oxygen quantum yield. These derivatives have also shown effective phototoxicity in *in vitro* experiments in two cell lines.

2.3 Squaraine dyes as PDT sensitizers

Squaraine dyes are ideal candidates for fluorescence detection in biomedical applications. They possess a sharp and intense absorption, with molar extinction coefficient up to 3 10^5 L mol^{-1} cm^{-1}, and an emission band in the near-IR region, where the autofluorescence from biological samples is minimal. Squaraines are characterized by a very small Stokes shift as expected from polymethine molecules. Their peculiar quadrupolar structure with an electronpoor central moiety ensure greater photostability and lower photobleaching rates with respect to open-chain cationic cyanines.

Squaraines have been extensively used as the signaling units in chemosensors and chemodosimeters because of their absorbance and fluorescence spectra and fluorescence quantum yields which get perturbed with the polarity of the medium, temperature, pH, and other additives. Indeed, the intense absorption and the emission arising from charge transfer transitions during electronic excitation are highly environmentally sensitive.[131] Therefore, squaraine dyes can signal the binding event in the form of measurable changes in their optical properties. For example, sulphonated indolenine-based squaraines to respond to the alterations in the hydrophobicity of bilayer membranes by a significant increase of their fluorescence intensity and red-shift of emission maximum on going from aqueous to lipidic environment.[132]

Squaraine dyes also show potential as molecular probes in fluorescence lifetime (FLT) based applications.[133] Terpetschnig reported the spectroscopic properties of the water-soluble indolenine-based squaraines before and after conjugation with bovine serum albumin (BSA).[134] These dyes exhibit an enhanced fluorescence quantum yield and a longer fluorescence lifetime when covalently linked to BSA. These properties make them suitable labels for fluorescence binding assays where the binding event is detected by either a change of the fluorescence lifetime or the intensity. For example, Ajayaghosh et al have reported a method for the detection of low molecular weight amino thiols in human blood plasma (HBP).[135] based on the reactivity of the electrophilic core of the aniline-based squaraines towards this nucleophiles, leading to color bleaching and fluorescence quenching.

The ease of chemical modification of the squaraine backbone allows the ready incorporation of different reactive functionalities in order to study their interaction with biological targets and the tuning of optical properties.[136] For this reason, squaraine dyes have been widely used as fluorescent protein labels.[137] The excellent results reported have led to the development of Seta dyes, a group of commercially available dyes based on squaraines. Among these, two succinimidyl esters Square-670-NHS and Seta-635-NHS were conjugated to lysozyme (Lz) to explore protein-lipid interactions.[138] Symmetric and

unsymmetrical squarylium dyes show enhancement of fluorescence intensity also upon noncovalent interactions with proteins such as HSA, β-lactoglobulin A and trypsinogen.

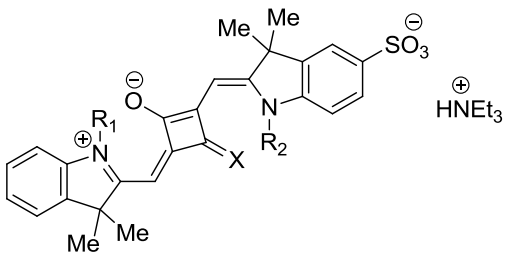

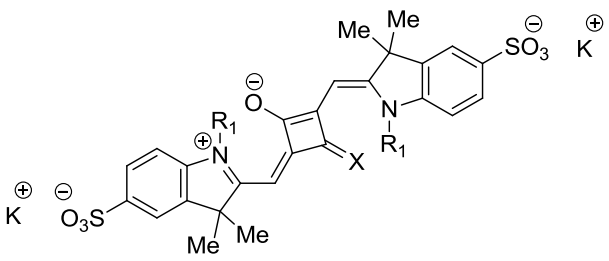

X=O	R_1=Me	R_2=$(CH_2)_5$COOH
X=C(CN)$_2$	R_1=Me	R_2=$(CH_2)_5$COOH
X=S	R_1=Me	R_2=$(CH_2)_5$COOH
X=C(CN)$_2$	R_1=$(CH_2)_3$COOH	R_2=Et
X=O	R_1=Me	R_2=$(CH_2)_5$COOSu
X=C(CN)$_2$	R_1=Me	R_2=$(CH_2)_5$COOSu
X=S	R_1=Me	R_2=$(CH_2)_5$COOSu
X=C(CN)$_2$	R_1=$(CH_2)_3$COOSu	R_2=Et

X=O	R_1=$(CH_2)_3$COOH
X=C(CN)$_2$	R_1=$(CH_2)_3$COOH
X=S	R_1=$(CH_2)_3$COOH
X=O	R_1=$(CH_2)_3$COOSu
X=C(CN)$_2$	R_1=$(CH_2)_3$COOSu
X=S	R_1=$(CH_2)_3$COOSu

Scheme 2–9

Squaraine dyes have also been successfully employed as second generation photosensitizers for photodynamic therapy (PDT). This well-established medical treatment involves the insurgence of cytotoxic species in the cellular environment following irradiation of a suitable dye with visible light in the presence of molecular oxygen. Due to their intense absorption and emission properties in the transparency window of biological tissue (600-900 nm), many squaraine families have been look for potential applications in PDT. Among these squaraines deriving from heteoaryl anhydrobases,[120, 139, 140] aniline,[141] pyrrole,[142, 143] indolizine,[143] quinoline,[144] and trihydroxybenzene[145, 146] derivatives have been reported. Despite the huge effort in the synthesis, few of these dyes have been further investigated in cell lines and animal bearing tumors. Ramaiah et al.[145, 147] have reported that the halogenation of trihydroxy-based squaraines is essential to exploit the PDT efficacy in AS52 Chinese hamster ovary cells.

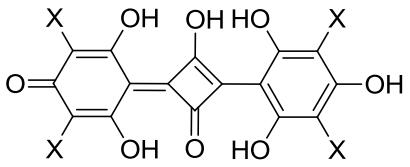

X=H
X=I
X=Br

Scheme 2–10

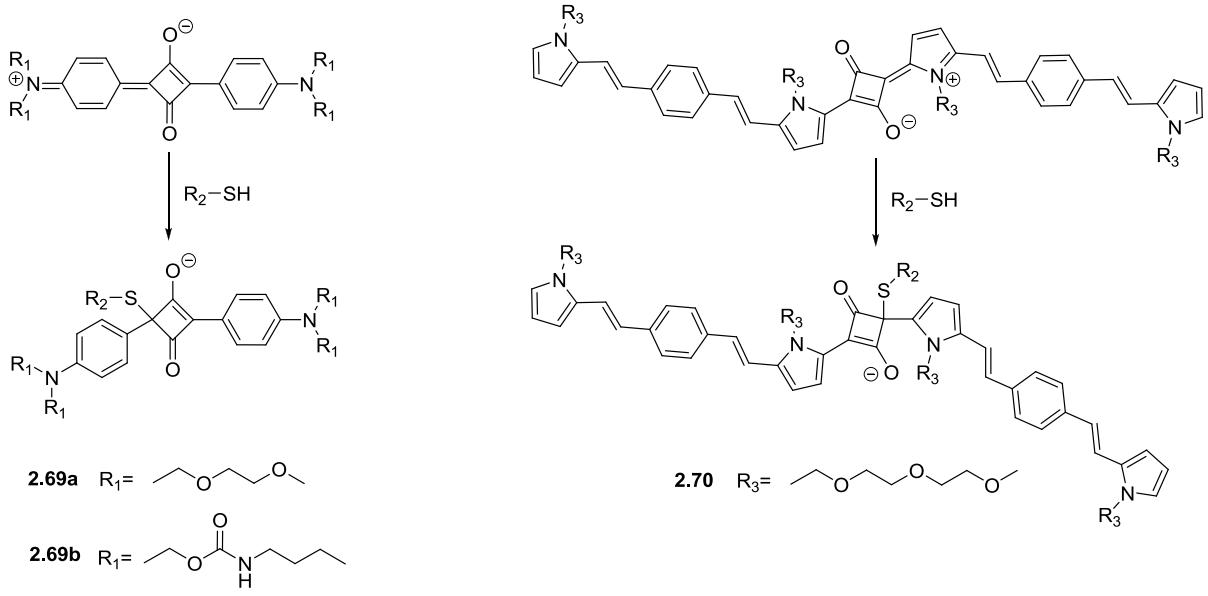

Scheme 2–11

Moreover, Pagani et al. tested the photosensitizing properties of benzothiaziole-based mono- and bis-squaraines in four different cancer cell lines.[148] In the dark these squaraines are largely nontoxic, but when they are irradiated with white light at a fluence of 15 J/cm^2, they promote a strong photodynamic effect that causes cell death in all tested cells. Since the transport of the sensitizer through cell membrane is critical to its effectiveness, different strategies have been studied in this regard. Good water solubility and resistance to the formation of ground state interactions are indeed desirable properties for biological fluorescent labels and PDT sensitizers. Though, squaraine dyes are generally not soluble in water. Their solubility have been increased by the introduction of polar functional groups, such as the sulfonate group,[134, 149] carbohydrates,[144] quaternary ammonium groups,[133] the carboxyl group,[133] polyethylene glycol residues,[143, 150, 151] hydroxyl groups,[152] and phosphonic group.[153] Other strategies take advantage of the strong affinity of some squaraines (i.e, trihydroxybenzene-based squaraines) with BSA[152] and of the synthesis of cholesterol conjugated dyes[144] to enhance cell permeability and perform their photodynamic effect. The low solubility of squaraines afflict also their propensity to aggregate, which reduces the amount of reactive oxygen species generated. The sterically protected squaraine-rotaxanes are indeed more resistant to aggregation, photooxidation, and chemical bleaching by biological nucleophiles, while retaining their photophysical behavior.[141]

2.4 Nanoparticles and targeting

Nanoparticles will usually be taken up by the liver, spleen and other parts of the reticuloendothelial system (RES) depending on their surface characteristics. Particles with more hydrophobic surfaces will preferentially be taken up by the liver, followed by the spleen and lungs. Hydrophilic nanoparticles (35 nm diameter), such as those prepared from poly(vinyl pyrrolidone), show less than 1% uptake by the spleen and liver and 8 h after injection show 5-10% still circulating in the bloodstream. However, nanoparticles prepared of 50% PNVP and 50% N-isopropylacrylamide (45 or 126 nm diameter) instead showed preferential uptake by the liver.

Particles with longer circulation times, and hence greater ability to target to the site of interest, should be 100 nm or less in diameter and have a hydrophilic surface in order to reduce clearance by macrophages. Coatings of hydrophilic polymers can create a cloud of chains at the particle surface which will repel plasma proteins and work in this area began by adsorbing surfactants to the nanoparticles surface. Other routes include forming the particles from branched or block copolymers with hydrophilic and hydrophobic domains.

The heterogeneity of blood flow in non-necrotic regions of tumors is emphasized and the addition of even slower and unpredictable blood flow in necrotic and semi-necrotic regions only adds to the challenge of physically delivering treatment to cancerous tissues.

A critical advantage in treating cancer with advanced, non-solution based therapies is the inherent leaky vasculature present serving cancerous tissues. The defective vascular architecture, created due to the rapid vascularization necessary to serve fast-growing cancers, coupled with poor lymphatic drainage allows an enhanced permeation and retention effect (EPR effect). The ability to target treatment to very specific cancer cells also uses a cancer's own structure in that many cancers overexpress particular antigens, even on their surface. This makes them ideal targets for drug delivery as long as the targets for a particular cancer cell type can be identified with confidence and are not expressed in significant quantities anywhere else in the body.

Tumor-activated prodrug therapy uses the approach that a drug conjugated to a tumor-specific molecule will remain inactive until it reaches the tumor. These systems would ideally be dependent on interactions with cells found specifically on the surface of cancerous cells and not the surface of healthy cells. Most linkers are usually peptidase-cleavable or acid labile but may not be stable enough in vivo to give desirable clinical outcomes. Limitations also exist due to the lower potency of some drugs after being linked to targeting moieties when the targeting portion is not cleaved correctly or at all. Recent research on an adriamycin-conjugated poly(ethylene glycol) linker with

enzymatically cleavable peptide sequences (alanyl-valine, alanyl-proline, and glycyl-proline) has shown a greater selectivity to cleavage at tumor cells.

One such type of target is monoclonal antibodies which were first shown to be able to bind to specific tumor antigens in 1975 but development of these antibodies into tools for cancer treatment took another 20 years. The ideal antigen should be expressed on all tumor cells but not expressed on critical host cells. There should be no mutation or variation and it should be required for cell survival or for a critical cellular function. A number of targeted cancer treatments using antibodies for specific cancer types have been approved by the FDA. While these antibodies can prove to be therapeutic agents of their own, they also have the ability to serve as carriers for drug delivery systems for even more effective and less intrusive cancer therapy.

These strategies both exploit the differences between a malignant cell and a normal cell. Some critical features include uncontrolled proliferation, insensitivity to negative growth regulation, angiogenesis, tissue invasion and metastasis, evasion of apoptosis (programmed cell death) and insensitivity to anti-growth signals.

Angiogenesis is a process vital to the continued development of a tumor mass. This process has been the subject of intense research due to its role in cancer development and has proven to be the result of numerous interactions between regulators, mediators and stimulatory molecules. These molecules regulate the proliferative and invasive activity of the endothelial cells that line blood vessels. Some of the most prominent angiogenesis stimulatory molecules include vascular endothelial growth factor (VEGF), basic fibroblast growth factor, platelet-derived growth factor and certain matrix metalloproteinases. Some endogenous angiogenesis inhibitors are the interferon family (α, β and γ), thrombospondin-1 and -2, certain tissue inhibitors of matrix metalloproteinases and protein fragments such as angiostatin and endostatin. The formation of a new vessel from the pre-existing vasculature is characterized by a number of sequential events. The cellular events are virtually identical whether the stimulus results from the periodic neovascularization of the normal ovarian follicle or from a mass of tumor cells. Prior to neovascularization, endothelial cells exist in a near quiescent state with only about 1 in every 10,000 (0.01%) undergoing division at a given time. The turnover rate of endothelial cells increases up to 50-fold during the formation of a new vascular sprout. These events require the re-modeling of the extracellular matrix, which can also promote angiogenesis by unmasking angiostimulatory molecules. The extracellular matrix surrounds the vessels and contains motility-stimulating fragments and growth factors that combine to promote endothelial cell migration towards the tumor mass or other source of stimulus. These leading edge endothelial cells provide the

framework for the new vessels. Endothelial cell sprouts organize into tubular structures and connect to the vascular network.

Formation of new vessels during physiological angiogenesis is self-limited due to the production and release of angioinhibitory molecules. The equilibrium that normally exists between stimuli and inhibitors for angiogenesis is thought to be unbalanced during neovascularization initiated by tumor cells. Tumor cells are capable of secreting molecules that initiate the angiogenic process. The new vessels will allow the tumor to grow beyond the diffusion-limited maximal size. Some tumor masses never grow beyond this point, as they are incapable of recruiting new vessels. Acquisition of the angiostimulatory phenotype, also called the "angiogenic switch", is thought to result from a local imbalance between positive and negative regulators of angiogenesis.

The inability of the body to halt tumor-induced angiogenesis can have a number of explanations. Tumor cells in some cases no longer express angiogenesis inhibitors that would stop the process. Tumor cells and the surrounding stromal cells can be induced to express angiogenesis promoters at accelerated rates. As the blood vessels begin to form, immune cells that can secrete angiogenesis stimulators gain access to the tumor cells to continue to promote neovascularization. As the tumor cells are in closer proximity to blood vessels, tumor cells may disseminate from the tumor into the circulation. Upon finding a suitable environment, like a distant capillary bed or nearby lymph node, these cells can become metastatic foci of the primary tumor. The end result of a tumor that makes the angiogenic switch is a tumor capable of increased growth, fuelled by both paracrine and autocrine factors, with access to the blood stream to create additional tumors in other organs. Since a vascularized tumor is capable of increased growth and is more readily able to metastasize, increasing amounts of research are focused on developing treatments to slow angiogenesis and limit tumor growth and dissemination. Because so many different molecules are involved in angiogenesis there are many potential targets for therapy. Some examples of therapeutic strategies include limiting endothelial proliferation and motility, increased expression of angiogenesis inhibitors and use of molecules such as soluble VEGF receptor to try and decrease the amount of angiogenesis stimulatory factors at the tumor site.

Targeting the tumor vasculature is a strategy that can allow targeted delivery to a wide range of tumor types. The opportunities for this type of treatment were first discussed by Judah Folkman in 1989. The first vascular targeting was approved by the FDA in 1999 for treatment of age-related macular degeneration. In 2003, clinical trials with the antiangiogenic drug Avastin® (Genentech) showed that its use can prolong survival in patients with metastatic colorectal cancer. Avastin targets vascular endothelial growth factor (VEGF) which is a powerful angiogenesis stimulating protein that also causes tumor

blood vessels to become more permeable. This permeability leads to swelling of the tumor and stops the ability of cancer cells to recruit a blood supply through the process of angiogenesis. VEGF has been shown to be expressed in many solid tumors including those of the lung, kidney, breast, ovary and gastro-intestinal tract. Recent work in gene therapy has also worked to utilize VEGF and targets for the angiogenic inhibitors angiostatin and endostatin including delivery with liposomes and poly(N-vinyl-2-pyrrolidone).

Recent work has also shown that gene delivery may also be targeted to neovasculature by coupling lipid-based cationic nanoparticles to an integrin αvβ-targeting ligand in tumor-bearing mice. This study delivered a mutant Raf gene which blocks endothelial signaling and angiogenesis in response to multiple growth factors. This study compared, among other results, the gene expression in the tumor, lung, liver and heart for non-targeted particles, targeted particles and targeted particles injected with excess soluble targeting ligand. For non-targeted particles, limited expression (<0.5 ng/g tissue) was found in the tumor, lung and heart. For targeted particles significant expression was found in the tumor (4 ng/g tissue) and no expression in the lung, liver or heart. Perhaps most significantly, no gene expression was detected for targeted particles injected with an excess of soluble ligand which leads to the conclusion that the ligand was selectively bound to the tumor over the ligand-nanoparticle combination and fully blocked the particles from reaching the tumor. The tumor size was also noted with treatment begun at day 9 of tumor growth. All mice treated with PBS control, empty targeting nanoparticles or loaded targeting nanoparticles injected with an excess of targeting ligand showed no signs of a slowing of tumor growth and had to be killed by day 25 because of the growth in size of the tumor. However, those mice injected with the gene-loaded targeting nanoparticles showed a significant regression in tumor size, with four of the six mice showing no tumor and the others with >95% reduction in tumor mass and >75% suppression in blood vessel density. This tumor regression was sustained for >250 days.

One of the greatest challenges is defining the optimal targeting agent or agents to selectively and successfully transport nanoparticle systems to cancerous tissue. These strategies also then rely on the targeting agents' or ligands' capability to bind to the tumor cell surface in an appropriate manner to trigger receptor endocytosis. The therapeutic agents will thereby be delivered to the interior of the cancer cell.

An example of the type of work which can be done to identify the ideal ligands for targeting of breast cancer is the development of a strategy to select internalizing antibodies from phage libraries. This technique was used to identify two antibodies (F5 and C1) to the breast tumor cell line SK-BR-3 that bind to ErbB2, a growth factor that is overexpressed in 20–30% of human breastcarcinomas and also in other adenocarcinomas. A research study used Doxil (commercial liposomal doxorubicin

formulation from Alza) with which a modified PEG conjugated to antibody F5 had been incubated to form a coupled liposome system. Comparison in vivo in mice treated with Doxil or F5-coupled Doxil showed a faster and greater regression in tumor volume for F5-containing Doxil over unmodified Doxil.

A promising receptor for liver targeting is the asialoglycoprotein receptor (ASGP-R, galactose receptor). Work by Kim et al. describes nanoparticles that use the galactose moiety from lactobionic acid, biotin and diamine-terminated poly(ethylene glycol) which exhibit in vitro release of A11-trans-retinoic acid (a model cancer drug) at a fairly constant rate over 1 month.

The cell surface receptor for folic acid (folate receptor) is inaccessible from the circulation to healthy cells but is expressed on the surface of cancer cells making it a possible target for a number of types of cancer. These therapies include targeting of immunotherapies using folic acid-derived antibodies or Fab/scFv fragments to the T cell receptor. Some researchers have also studied preparing cancer vaccines to treat folate-receptor positive tumors by developing a vaccine against the folate receptor. This approach in treating folate receptor-positivelung metastases in mice has produced cures in up to 56% of tumor-bearing mice.

Many of the same techniques used to target delivery of drugs to cancerous tissues may also be used to target imaging agents. In fact, as targeted delivery systems approach the stage where they can be used clinically, primary assessment of the utility of a particular formulation in a particular patient may be made with imaging agents to verify that the delivery system goes primarily to the cancerous tissues before any drug regimen is begun.

Studies using vasoactive intestinal peptide (VIP), whose receptors are five times more numerous in breast cancer cells than normal breast cells, as a targeting agent for sterically stabilized liposomes have shown that both passive and active targeting to breast cancer cells will occur in vivo in rats. Specifically, for liposomes of ~110 nm diameter with or without 10 μg/μmol VIP, the amount of the encapsulated radionucleotide Tc99 m-HMPAO the uptake of non-targeted liposomes in breast cancer tissue was three times that of normalbreast tissue and targeted liposomes accumulated at a rate of about six times that in normal breast tissue, all measured 27 h post-injection.

Research activity aimed towards achieving specific and targeted delivery of anti-cancer agents has expanded tremendously in the last 10 years with new avenues of directing drugs to tumors as well as new types of drugs. The first of these creative treatment methods have made it to the clinic and hopefully are well on their way to improving the length and quality of life for cancer patients. However, there is a great deal more that can

be done to treat and perhaps prevent advanced cancer by treating it in as early a stage as possible.

2.5 References

1. Tappeiner, H. v.; Jodlbauer, A., Über die wirkung der photodynamischen (fluorescierenden) stoffe auf protozoen und enzyme. *Deutsches Archiv für klinische Medizin* **1904,** 80, 427-487.
2. Tappeiner, H.; Jodlbauer, A., *Die Sensibilisierende Wirkung Fluorescierender Substanzen: Gesammelte Untersuchungen Über Die Photodynamische Erscheinung*. Vogel: Leipzig, 1907.
3. Moan, J.; Berg, K., Photochemotherapy of cancer: experimental research. *Photochemistry and Photobiology* **1992,** 55, (6), 931-948.
4. Altınoğlu, E. İ.; Adair, J. H., Near infrared imaging with nanoparticles. *Wiley Interdisciplinary Reviews: Nanomedicine and Nanobiotechnology* **2010,** 2, (5), 461-477.
5. Bonnett, R., *Chemical aspects of photodynamic therapy*. Gordon and Breach Science Publishers: Amsterdam, 2000.
6. Finsen, N. R., *Phototherapy*. Arnold: London, 1901.
7. Cremer, R. J.; Perryman, P. W.; Richards, D. H., Influence of light on the hyperbilirubinæmia of infants. *The Lancet* **1958,** 271, (7030), 1094-1097.
8. Raab, O., Uber die Wirkung fluoreszierender Stoffe auf Infusorien. *Z. Biol.* **1900,** 39, 524–546.
9. A. Jesionek, H. v. T., Zur behandlung der Hautcarcinome mit fluorescierenden Stoffen. *Arch. Klin. Med.* **1905,** 82, 223.
10. Hausmann, W., Die sensibilisierende Wirkung des hamatoporphyrins. *Biochem. Z.* **1911,** 30, 276-316.
11. Pfeifer, H., Der Nachweis photodynamischer Wirkungen fluorescierenden Stoffe am lebenden Warmbluter. In *Handbuch der Biochemischen Arbeitsmethoden*, Abderhaldan, E., Ed. Berlin, 1911; pp 563-571.
12. Meyer-Betz, F., Untersuchungen uber die Biologische (photodynamische) Wirkung des hamatoporphyrins und anderer Derivative des Blut-und Gallenfarbstoffs. *Dtsch. Arch. Klin. Med.* **1913,** 112, 476-503.
13. Policard, A., Etude sur les aspects offerts par des tumeurs experimentales examinees a la lumière de Wood. *C. R. Soc. Biol.* **1924,** 91, 1423-1428.
14. Figge, F. H. J. In *The relationship of pyrrol compounds to carcinogenesis*, AAAR Research Conference on Cancer, Washington D.C., 1945; Science Press: Washington D.C., 1945; p 147.
15. Zawirska, B., Comparative porphyrin content in tumors with contiguous nonneoplastic tissues. *Neoplasms* **1979,** 26, 223-229.
16. H. Auler, G. B., Untersuchungen ueber die Rolle der Porphyrine bei geschwulstkranken Menschen und Tieren. *Z. Krebsforsch.* **1942,** 53, 65-68.
17. D.S. Rasmussen-Taxdal, G. E. W., F.H. Figge, Fluorescence of human lymphatic and cancer tissues following high doses of intravenous hematoporphyrin. *Cancer* **1955,** 8, 78-81.
18. S. Schwartz, K. A., H. Vermund, Some relationship of porphyrins, X-rays and tumors. *Univ. Minn. Med. Bull.* **1955,** 27, (Oct. 15), 1-37.

19. Baldes, R. L. L. E. J., The Photodynamic Properties of a Particular Hematoporphyrin Derivative. *Arch Dermatol* **1960,** 82, (4), 508-516.
20. Winkelman, J., Intracellular localization of 'hematoporphyrin' in a transplanted tumor. *J. Natl. Cancer Inst.* **1961,** 27, 1369-1377.
21. Winkelman, J., The Distribution of Tetraphenylporphinesulfonate in the Tumor-bearing Rat. *Cancer Research* **1962,** 22, (5 Part 1), 589-596.
22. E. Ben-Hur, I. R., Photosensitized inactivation of Chinese hamster cells by phthalocyanines. *Photochem. Photobiol.* **1985,** 42, 129-133.
23. Berenbaum, M. C.; Akande, S. L.; Bonnett, R.; Kaur, H.; Ioannou, S.; White, R. D.; Winfield, U. J., Meso-Tetra(hydroxyphenyl)porphyrins, a new class of potent tumour photosensitisers with favourable selectivity. *Br J Cancer* **1986,** 54, (5), 717-725.
24. Dougherty, H., Thomas J., Barbara W.; Gomer, C. J.; Jori, G.; Kessel, D.; Korbelik, M.; Moan, J.; Peng, Q., Photodynamic Therapy. *Journal of the National Cancer Institute* **1998,** 90, (12), 889-905.
25. Peng, Q.; Warloe, T.; Berg, K.; Moan, J.; Kongshaug, M.; Giercksky, K.-E.; Nesland, J. M., 5-Aminolevulinic acid-based photodynamic therapy. *Cancer* **1997,** 79, (12), 2282-2308.
26. Malik, Z.; Lugaci, H., Destruction of erythroleukaemic cells by photoactivation of endogenous porphyrins. *Br J Cancer* **1987,** 56, (5), 589-595.
27. Pottier, R. H.; Chow, Y. F. A.; LaPlante, J. P.; Truscott, T. G.; Kennedy, J. C.; Beiner, L. A., Non-invasive technique for obtaining fluorescence excitation and emission spectra in vivo. *Photochemistry and Photobiology* **1986,** 44, (5), 679-687.
28. Kennedy, J. C.; Pottier, R. H.; Pross, D. C., Photodynamic therapy with endogenous protoporphyrin: IX: Basic principles and present clinical experience. *Journal of Photochemistry and Photobiology B: Biology* **1990,** 6, (1-2), 143-148.
29. Bonnett, R.; Ridge, R. J.; Scourides, P. A.; Berenbaum, M. C., On the nature of 'haematoporphyrin derivative'. *Journal of the Chemical Society, Perkin Transactions 1* **1981**, 3135-3140.
30. Moan, J.; Christensen, T.; Sommer, S., The main photosensitizing components of hematoporphyrin derivative. *Cancer Letters* **1982,** 15, (2), 161-166.
31. Dougherty, T. J., A Brief History of Clinical Photodynamic Therapy Development at Roswell Park Cancer Institute. *Journal of Clinical Laser Medicine & Surgery* **1996,** 14, (5), 219-221.
32. Byrne, C. J.; Marshallsay, L. V.; Ward, A. D., The composition of Photofrin II. *Journal of Photochemistry and Photobiology B: Biology* **1990,** 6, (1-2), 13-27.
33. Grigg, R.; Johnson, A. W.; Kenyon, R.; Math, V. B.; Richardson, K., The cyclisation of 1-bromo-19-methyl- and 1,19-dimethyl-1,19-dideoxybiladiene-ac dihydrobromides. *Journal of the Chemical Society C: Organic* **1969**, (2), 176-182.
34. Woodward, R. B.; Ayer, W. A.; Beaton, J. M.; Bickelhaupt, F.; Bonnett, R.; Buchschacher, P.; Closs, G. L.; Dutler, H.; Hannah, J.; Hauck, F. P.; Itŏ, S.; Langemann, A.; Le Goff, E.; Leimgruber, W.; Lwowski, W.; Sauer, J.; Valenta, Z.; Volz, H., The total synthesis of chlorophyll a. *Tetrahedron* **1990,** 46, (22), 7599-7659.
35. Tarlton, E. J.; MacDonald, S. F.; Baltazzi, E., Uroporphyrin 3. *Journal of the American Chemical Society* **1960,** 82, (16), 4389-4395.

36. Adler, A. D.; Longo, F. R.; Finarelli, J. D.; Goldmacher, J.; Assour, J.; Korsakoff, L., A simplified synthesis for meso-tetraphenylporphine. *The Journal of Organic Chemistry* **1967,** 32, (2), 476-476.
37. Lindsey, J. S.; Schreiman, I. C.; Hsu, H. C.; Kearney, P. C.; Marguerettaz, A. M., Rothemund and Adler-Longo reactions revisited: synthesis of tetraphenylporphyrins under equilibrium conditions. *The Journal of Organic Chemistry* **1987,** 52, (5), 827-836.
38. Bonar-Law, R. P., Porphyrin Synthesis in Surfactant Solution: Multicomponent Assembly in Micelles. *The Journal of Organic Chemistry* **1996,** 61, (11), 3623-3634.
39. Berg, K.; Bommer, J. C.; Winkelman, J. W.; Moan, J., Cellular uptake and relative efficiency in cell inactivation by photo activated sulfonated meso-tetraphenylporphines. *Photochemistry and Photobiology* **1990,** 52, (4), 775-781.
40. Kozyrev, A. N.; Zheng, G.; Lazarou, E.; Dougherty, T. J.; Smith, K. M.; Pandey, R. K., Syntheses of emeraldin and purpurin-18 analogs as target-specific photosensitizers for photodynamic therapy. *Tetrahedron Letters* **1997,** 38, (19), 3335-3338.
41. F. Mironov, A.; V. Efremov, A.; A. Efremova, O.; Bonnett, R.; Martinez, G., Chlorins with an exocyclic δ-lactone ring and their derivatives. *Journal of the Chemical Society, Perkin Transactions 1* **1998**, (21), 3601-3608.
42. Stummer, W.; Pichlmeier, U.; Meinel, T.; Wiestler, O. D.; Zanella, F.; Reulen, H.-J., Fluorescence-guided surgery with 5-aminolevulinic acid for resection of malignant glioma: a randomised controlled multicentre phase III trial. *The Lancet Oncology* **2006,** 7, (5), 392-401.
43. Tabata, K.; Ogura, S.-i.; Okura, I., Photodynamic Efficiency of Protoporphyrin IX: Comparison of Endogenous Protoporphyrin IX Induced by 5-Aminolevulinic Acid and Exogenous Porphyrin IX. *Photochemistry and Photobiology* **1997,** 66, (6), 842-846.
44. Krammer, B.; Plaetzer, K., ALA and its clinical impact, from bench to bedside. *Photochemical & Photobiological Sciences* **2008,** 7, (3), 283-289.
45. Blume, J. E.; Oseroff, A. R., Aminolevulinic Acid Photodynamic Therapy for Skin Cancers. *Dermatologic clinics* **2007,** 25, (1), 5-14.
46. Gurinovich, G. P.; Zorina, T. E.; Melnov, S. B.; Melnova, N. I.; Gurinovich, I. F.; Grubina, L. A.; Sarzhevskaya, M. V.; Cherenkevich, S. N., Photodynamic activity of chlorin e6 and chlorin e6 ethylenediamide in vitro and in vivo. *Journal of Photochemistry and Photobiology B: Biology* **1992,** 13, (1), 51-57.
47. Adams, K. R.; Berenbaum, M. C.; Bonnett, R.; Nizhnik, A. N.; Salgado, A.; Valles, M. A., Second generation tumour photosensitisers: the synthesis and biological activity of octaalkyl chlorins and bacteriochlorins with graded amphiphilic character. *Journal of the Chemical Society, Perkin Transactions 1* **1992**, (12), 1465-1470.
48. Zenkevich, E.; Sagun, E.; Knyukshto, V.; Shulga, A.; Mironov, A.; Efremova, O.; Bonnett, R.; Songca, S. P.; Kassem, M., Photophysical and photochemical properties of potential porphyrin and chlorin photosensitizers for PDT. *Journal of Photochemistry and Photobiology B: Biology* **1996,** 33, (2), 171-180.
49. Kessel, D.; Woodburn, K.; Gomer, C. J.; Jagerovic, N.; Smith, K. M., Photosensitization with derivatives of chlorin p6. *Journal of Photochemistry and Photobiology B: Biology* **1995,** 28, (1), 13-18.

50. Lee, S.-J. H.; Jagerovic, N.; Smith, K. M., Use of the chlorophyll derivative, purpurin-18, for syntheses of sensitizers for use in photodynamic therapy. *Journal of the Chemical Society, Perkin Transactions 1* **1993**, (19), 2369-2377.
51. Mironov, A. F.; Efremov, A. V.; Efremova, O. g. A.; Bonnett, R., Novel Chlorins with a δ-Lactone Ring fused at Ring D. *Tetrahedron Letters* **1997,** 38, (38), 6775-6778.
52. Mironov, A. F.; Lebedeva, V. S., Cyclic N-hydroxyimides in a series of chlorins and porphyrins. *Tetrahedron Letters* **1998,** 39, (8), 905-908.
53. Nelson, J. S.; Roberts, W. G.; Berns, M. W., In Vivo Studies on the Utilization of Mono-l-aspartyl Chlorin (NPe6) for Photodynamic Therapy. *Cancer Research* **1987,** 47, (17), 4681-4685.
54. Spikes, J. D.; Bommer, J. C., Photosensitizing properties of mono-l-aspartyl chlorin e6 (NPe6): A candidate sensitizer for the photodynamic therapy of tumors. *Journal of Photochemistry and Photobiology B: Biology* **1993,** 17, (2), 135-143.
55. Yano, S.; Hirohara, S.; Obata, M.; Hagiya, Y.; Ogura, S.; Ikeda, A.; Kataoka, H.; Tanaka, M.; Joh, T., Current states and future views in photodynamic therapy. *J. Photochem. Photobiol. C-Photochem. Rev.* **2011,** 12, (1), 46-67.
56. Pandey, R. K.; Bellnier, D. A.; Smith, K. M.; Dougherty, T. J., Chlorin and porphyrin derivatives as potential photosensitizers in photodynamic therapy. *Photochemistry and Photobiology* **1991,** 53, (1), 65-72.
57. Bellnier, D.; Greco, W.; Nava, H.; Loewen, G.; Oseroff, A.; Dougherty, T., Mild skin photosensitivity in cancer patients following injection of Photochlor (2-[1-hexyloxyethyl]-2-devinyl pyropheophorbide-a; HPPH) for photodynamic therapy. *Cancer Chemotherapy and Pharmacology* **2006,** 57, (1), 40-45.
58. Pandey, R. K.; Sumlin, A. B.; Constantine, S.; Aoudia, M.; Potter, W. R.; Bellnier, D. A.; Henderson, B. W.; Rodgers, M. A.; Smith, K. M.; Dougherty, T. J., Alkyl Ether Analogs of Chlorophyll-a Derivatives: Part 1. Synthesis, Photophysical Properties and Photodynamic Efficacy. *Photochemistry and Photobiology* **1996,** 64, (1), 194-204.
59. Kusch, D.; Meier, A.; Montforts, F.-P., Synthesis and characterization of amphiphilic chlorins for photodynamic tumor therapy (PDT). *Liebigs Annalen* **1995,** 1995, (6), 1027-1032.
60. Sternberg, E. D.; Dolphin, D.; Brückner, C., Porphyrin-based photosensitizers for use in photodynamic therapy. *Tetrahedron* **1998,** 54, (17), 4151-4202.
61. Bonnett, R.; White, R. D.; Winfield, U. J.; Berenbaum, M. C., Hydroporphyrins of the meso-tetra(hydroxyphenyl)porphyrin series as tumour photosensitizers. *Biochem. J.* **1989,** 261, (1), 277-280.
62. Ball, D. J.; Vernon, D. I.; Brown, S. B., Research Note: The High Photoactivity of m-THPC in Photodynamic Therapy. Unusually Strong Retention of m-THPC by RIF-1 Cells in Culture. *Photochemistry and Photobiology* **1999,** 69, (3), 360-363.
63. Ronn, A.; Nouri, M.; Lofgren, L.; Steinberg, B.; Westerborn, A.; Windahl, T.; Shikowitz, M.; Abramson, A., Human tissue levels and plasma pharmacokinetics of temoporfin (Foscan, mTHPC). *Lasers in Medical Science* **1996,** 11, (4), 267-272.
64. Dilkes, M.; DeJode, M.; Rowntree-Taylor, A.; McGilligan, J.; Kenyon, G.; McKelvie, P., m-THPC photodynamic therapy for head and neck cancer. *Lasers in Medical Science* **1996,** 11, (1), 23-29.

65. Morgan, A. R.; Tertel, N. C., Observations on the synthesis and spectroscopic characteristics of purpurins. *The Journal of Organic Chemistry* **1986,** 51, (8), 1347-1350.
66. Pogue, B. W.; Redmond, R. W.; Trivedi, N.; Hasan, T., Photophysical Properties of Tin Ethyl Etiopurpurin I (SnET2) and Tin Octaethylbenzochlorin (SnOEBC) in Solution and Bound to Albumin. *Photochemistry and Photobiology* **1998,** 68, (6), 809-815.
67. Schiwon, K.; Brauer, H. D.; Gerlach, B.; Müller, C. M.; Montforts, F. P., Potential photosensitizers for photodynamic therapy: IV. Photophysical and photochemical properties of azaporphyrin and azachlorin derivatives. *Journal of Photochemistry and Photobiology B: Biology* **1994,** 23, (2-3), 239-243.
68. Busetti, A.; Soncin, M.; Jori, G.; Rodgers, M. A. J., High efficiency of benzoporphyrin derivative in the photodynamic therapy of pigmented malignant melanoma. *Br J Cancer* **1999,** 79, (5-6), 821-824.
69. Hu, M.; Brasseur, N.; Yildiz, S. Z.; van Lier, J. E.; Leznoff, C. C., Hydroxyphthalocyanines as Potential Photodynamic Agents for Cancer Therapy. *Journal of Medicinal Chemistry* **1998,** 41, (11), 1789-1802.
70. Linstead, R. P., 212. Phthalocyanines. Part I. A new type of synthetic colouring matters. *Journal of the Chemical Society (Resumed)* **1934**, 1016-1017.
71. Byrne, G. T.; Linstead, R. P.; Lowe, A. R., 213. Phthalocyanines. Part II. The preparation of phthalocyanine and some metallic derivatives from o-cyanobenzamide and phthalimide. *Journal of the Chemical Society (Resumed)* **1934**, 1017-1022.
72. Dent, C. E.; Linstead, R. P.; Lowe, A. R., 217. Phthalocyanines. Part VI. The structure of the phthalocyanines. *Journal of the Chemical Society (Resumed)* **1934**, 1033-1039.
73. Robertson, J. M., 136. An X-ray study of the structure of the phthalocyanines. Part I. The metal-free, nickel, copper, and platinum compounds. *Journal of the Chemical Society (Resumed)* **1935**, 615-621.
74. Leznoff, C. C.; Hu, M.; Nolan, K. J. M., The synthesis of phthalocyanines at room temperature. *Chemical Communications* **1996**, (10), 1245-1246.
75. Shopova, M.; Mantareva, V.; Krastev, K.; Hadjiolov, D.; Milev, A.; Spirov, K.; Jori, G.; Ricchelli, F., Comparative pharmacokinetic and photodynamic studies with zinc(II) phthalocyanine in hamsters bearing an induced or transplanted rhabdomyosarcoma. *Journal of Photochemistry and Photobiology B: Biology* **1992,** 16, (1), 83-89.
76. Magaraggia, M.; Visonà, A.; Furlan, A.; Pagnan, A.; Miotto, G.; Tognon, G.; Jori, G., Inactivation of vascular smooth muscle cells photosensitised by liposome-delivered Zn(II)–phthalocyanine. *Journal of Photochemistry and Photobiology B: Biology* **2006,** 82, (1), 53-58.
77. Fabric, C.; Ometto, C.; Milanesi, C.; Jori, G.; Cook, M. J.; Russell, D. A., Tumour-localizing and tumour-photosensitizing properties of zinc (II)-octapentyl-phthalocyanine. *Journal of Photochemistry and Photobiology B: Biology* **1997,** 39, (3), 279-284.
78. Jori, G.; Fabris, C., Relative contributions of apoptosis and random necrosis in tumour response to photodynamic therapy: effect of the chemical structure of Zn(II)-phthalocyanines. *Journal of Photochemistry and Photobiology B: Biology* **1998,** 43, (3), 181-185.

79. Sokolov, S., Zharkova, Iakubovskaia, Filonenko, Astrakhankina, The photodynamic therapy of malignant tumors in basic sites with the preparations photohem and photosens (the results of 3 years of observations). *Vopr Onkol.* **1995,** 41, (2), 134-138.
80. Vakoulovskaya, E., Photodynamic therapy and fluorescence diagnostics of breast cancer metastases with photosense and alasense. *Proc. SPIE* **2002,** 4612, (1), 174.
81. Zaidi, S. I. A.; Agarwal, R.; Eichler, G.; Rihter, B. D.; Kenney, M. E.; Mukhtar, H., Photodynamic effects of new silicon phthalocyanines: in vitro studies utilizing rat hepatic microsomes and human erythrocyte ghosts as model membrane sources. *Photochemistry and Photobiology* **1993,** 58, (2), 204-210.
82. Kovshev, E. I. P., V. A.; Luk'yanets, *J. Org. Chem. USSR* **1971,** 7, 364.
83. Shopova, M., Naphthalocyanine Complexes as Potential Photosensitizers for Photodynamic Therapy of Tumors. *J. Biomed. Opt.* **1999,** 4, (3), 276.
84. Biolo, R.; Jori, G.; Soncin, M.; Pratesi, R.; Vanni, U.; Rihter, B.; Kenney, M. E.; Rodgers, M. A. J., Photodynamic therapy of B16 pigmented melanoma with liposome-delivered Si(IV)-naphthalocyanine. *Photochemistry and Photobiology* **1994,** 59, (3), 362-365.
85. Kachkovski, A. D.; Dekhtyar, M. L., Electronic properties of polymethine compounds: 2. Electron Donor Ability and Relative Stability. *Dyes and Pigments* **1993,** 22, (2), 83-97.
86. Sahyun, M. R. V., Sharma, D.K. & Serpone, N., Mechanisms of spectral sensitization of silver-halides – role of sensitizing dye complexation. *Journal of Imaging Science and Technology* **1995,** 39, 377–385.
87. Ishchenko, A. A., Laser media based on polymethine dyes. *Kvantovaya Elektronika* **1994,** 21, 513-534.
88. Ma, X.; Hua, J.; Wu, W.; Jin, Y.; Meng, F.; Zhan, W.; Tian, H., A high-efficiency cyanine dye for dye-sensitized solar cells. *Tetrahedron* **2008,** 64, (2), 345-350.
89. Waggoner, A., Optical probes of membrane potential. *Journal of Membrane Biology* **1976,** 27, (1), 317-334.
90. Koning, A. J.; Lum, P. Y.; Williams, J. M.; Wright, R., DiOC6 staining reveals organelle structure and dynamics in living yeast cells. *Cell Motility and the Cytoskeleton* **1993,** 25, (2), 111-128.
91. Greenberg, M.; Axelrod, D., Anomalously slow mobility of fluorescent lipid probes in the plasma membrane of the yeast<i>Saccharomyces cerevisiae</i&gt. *Journal of Membrane Biology* **1993,** 131, (2), 115-127.
92. Roy, R.; Hohng, S.; Ha, T., A practical guide to single-molecule FRET. *Nat Meth* **2008,** 5, (6), 507-516.
93. Sieber, F., Merocyanine 540. *Photochemistry and Photobiology* **1987,** 46, (6), 1035-1042.
94. Lin, H.-Y.; Chen, C.-T.; Huang, C.-T., Use of merocyanine 540 for photodynamic inactivation of Staphylococcus aureus planktonic and biofilm cells. *Appl. Environ. Microbiol.* **2004,** 70, (Copyright (C) 2011 American Chemical Society (ACS). All Rights Reserved.), 6453-6458.

95. Sbarra, M. S.; Di, P. A.; Arciola, C. R.; Saino, E.; Sharma, M.; Bragheri, F.; Cristiani, I.; Speziale, P.; Visai, L., Photodynamic action of merocyanine 540 on Staphylococcus epidermidis biofilms. *Int J Artif Organs* **2008,** 31, 848-57.
96. Atzpodien, J.; Gulati, S. C.; Clarkson, B. D., Comparison of the Cytotoxic Effects of Merocyanine-540 on Leukemic Cells and Normal Human Bone Marrow. *Cancer Research* **1986,** 46, (10), 4892-4895.
97. O'Brien, J. M.; Singh, R. J.; Feix, J. B.; Kalyanaraman, B.; Sieber, F., Action spectra of the antileukemic and antiviral activities of merocyanine 540. *Photochemistry and Photobiology* **1991,** 54, (5), 851-854.
98. Chen, J. Y.; Mak, N. K.; Wen, J. M.; Leung, W. N.; Chen, S. C.; Fung, M. C.; Cheung, N. H., A Comparison of the Photodynamic Effects of Temoporfin (mTHPC) and MC540 on Leukemia Cells: Efficacy and Apoptosis. *Photochemistry and Photobiology* **1998,** 68, (4), 545-554.
99. Cherrick, G. S., S.; Leevy, C.; Davidson, C., Indocyanine green: observations on its physical properties, plasma decay, and hepatic extraction. *Journal of Clinical Investigation* **1960,** 39, (4), 592.
100. Bradley, E. C. B., J. W., Determination of blood volume using indocyanine green (Cardio-Green®) dye. *Life Sciences* **1968,** 7, (17), 1001-1007.
101. Kulvin, S. S., L.; Kogure, K.; David, N., Fundus Angiography in Man by Intracarotid Administration of Dye. *Southern Medical Journal* **1970,** 63, (9), 998.
102. Fickweiler, S. S., R.-M.; Bäumler, W.; Steinbach, P.; Karrer, S.; Goetz, A. E.; Abels, C.; Hofstädter, F., Indocyanine green: Intracellular uptake and phototherapeutic effects in vitro. *Journal of Photochemistry and Photobiology B:Biology* **1997,** 38, (2-3), 178-183.
103. Tuchin, V. V.; Genina, E. A.; Bashkatov, A. N.; Simonenko, G. V.; Odoevskaya, O. D.; Altshuler, G. B., A pilot study of ICG laser therapy of acne vulgaris: Photodynamic and photothermolysis treatment. *Lasers in Surgery and Medicine* **2003,** 33, (5), 296-310.
104. Treibs, A.; Jacob, K., Cyclotrimethine Dyes Derived from Squaric Acid. *Angewandte Chemie International Edition in English* **1965,** 4, (8), 694-694.
105. Sprenger, H. E.; Ziegenbein, W., Cyclobutenediylium Dyes. *Angewandte Chemie International Edition in English* **1968,** 7, (7), 530-535.
106. Schmidt, A. H., Reaktionen von Quadratsäure und Quadratsäure-Derivaten. *Synthesis* **1980,** 1980, (12), 961-994.
107. Law, K.-Y., Squaraine Chemistry. Absorption, Fluorescence Emission, and Photophysics of Unsymmetrical Squaraines. *J. Phys. Chem.* **1995,** 99, 9818-24.
108. Law, K.-Y., Absorption, fluorescence emission, and photophysics of squaraines. *Mol. Supramol. Photochem.* **1997,** 1, 519-584.
109. Beverina, L.; Salice, P., Squaraine Compounds: Tailored Design and Synthesis towards a Variety of Material Science Applications. *European Journal of Organic Chemistry* **2010,** 2010, (7), 1207-1225.
110. Law, K. Y.; Bailey, F. C., Squaraine chemistry: effect of synthesis on the morphological and xerographic properties of photoconductive squaraines. *J. Imaging Sci.* **1987,** 31, 172-7.
111. Emmelius, M.; Pawlowski, G.; Vollmann, H. W., Materials for optical data storage. *Spec. Publ. - R. Soc. Chem.* **1991,** 88, 183-200.

112. Smits, E. C. P.; Setayesh, S.; Anthopoulos, T. D.; Buechel, M.; Nijssen, W.; Coehoorn, R.; Blom, P. W. M.; de Boer, B.; de Leeuw, D. M., Near-Infrared Light-Emitting Ambipolar Organic Field-Effect Transistors. *Advanced Materials* **2007,** 19, (5), 734-738.
113. Yum, J.-H.; Walter, P.; Huber, S.; Rentsch, D.; Geiger, T.; Nüesch, F.; De Angelis, F.; Grätzel, M.; Nazeeruddin, M. K., Efficient Far Red Sensitization of Nanocrystalline TiO2 Films by an Unsymmetrical Squaraine Dye. *Journal of the American Chemical Society* **2007,** 129, (34), 10320-10321.
114. Silvestri, F.; Irwin, M. D.; Beverina, L.; Facchetti, A.; Pagani, G. A.; Marks, T. J., Efficient Squaraine-Based Solution Processable Bulk-Heterojunction Solar Cells. *Journal of the American Chemical Society* **2008,** 130, (52), 17640-17641.
115. Chen, C.-T.; Marder, S. R.; Cheng, L.-T., Syntheses and Linear and Nonlinear Optical Properties of Unsymmetrical Squaraines with Extended Conjugation. *Journal of the American Chemical Society* **1994,** 116, (7), 3117-3118.
116. Scherer, D.; Dörfler, R.; Feldner, A.; Vogtmann, T.; Schwoerer, M.; Lawrentz, U.; Grahn, W.; Lambert, C., Two-photon states in squaraine monomers and oligomers. *Chemical Physics* **2002,** 279, (2-3), 179-207.
117. Xiang, Z.; Nesterov, E. E.; Skoch, J.; Lin, T.; Hyman, B. T.; Swager, T. M.; Bacskai, B. J.; Reeves, S. A., Detection of Myelination Using a Novel Histological Probe. *Journal of Histochemistry & Cytochemistry* **2005,** 53, (12), 1511-1516.
118. Ramaiah, D.; Joy, A.; Chandrasekhar, N.; Eldho, N. V.; Das, S.; George, M. V., Halogenated Squaraine Dyes as Potential Photochemotherapeutic Agents. Synthesis and Study of Photophysical Properties and Quantum Efficiencies of Singlet Oxygen Generation. *Photochemistry and Photobiology* **1997,** 65, (5), 783-790.
119. Ramaiah, D.; Eckert, I.; Arun, K. T.; Weidenfeller, L.; Epe, B., Squaraine Dyes for Photodynamic Therapy: Study of Their Cytotoxicity and Genotoxicity in Bacteria and Mammalian Cells. *Photochemistry and Photobiology* **2002,** 76, (6), 672-677.
120. Santos, P. F.; Reis, L. V.; Almeida, P.; Oliveira, A. S.; Vieira Ferreira, L. F., Singlet oxygen generation ability of squarylium cyanine dyes. *Journal of Photochemistry and Photobiology A: Chemistry* **2003,** 160, (3), 159-161.
121. Santos, P. F.; Reis, L. V.; Duarte, I.; Serrano, J. P.; Almeida, P.; Oliveira, A. S.; Ferreira, L. F. V., Synthesis and Photochemical Evaluation of Iodinated Squarylium Cyanine Dyes. *Helvetica Chimica Acta* **2005,** 88, (5), 1135-1143.
122. Beverina, L.; Crippa, M.; Landenna, M.; Ruffo, R.; Salice, P.; Silvestri, F.; Versari, S.; Villa, A.; Ciaffoni, L.; Collini, E.; Ferrante, C.; Bradamante, S.; Mari, C. M.; Bozio, R.; Pagani, G. A., Assessment of Water-Soluble π-Extended Squaraines as One- and Two-Photon Singlet Oxygen Photosensitizers: Design, Synthesis, and Characterization. *Journal of the American Chemical Society* **2008,** 130, (6), 1894-1902.
123. Southwell, I. A.; Campbell, M. H., Hypericin content variation in Hypericum perforatum in Australia. *Phytochemistry* **1991,** 30, (2), 475-478.
124. Lopez-Bazzocchi, I.; Hudson, J. B.; Towers, G. H. N., Antiviral activity of the photoactive plant pigment hypericin. *Photochemistry and Photobiology* **1991,** 54, (1), 95-98.

125. Agostinis, P.; Vantieghem, A.; Merlevede, W.; de Witte, P. A. M., Hypericin in cancer treatment: more light on the way. *The International Journal of Biochemistry & Cell Biology* **2002,** 34, (3), 221-241.
126. VanderWerf, Q. M.; Saxton, R. E.; Chang, A.; Horton, D.; Paiva, M. B.; Anderson, J.; Foote, C.; Soudant, J.; Mathey, A.; Castro, D. J., Hypericin: A New Laser Phototargeting Agent for Human Cancer Cells. *The Laryngoscope* **1996,** 106, (4), 479-483.
127. Liu, C. D.; Kwan, D.; Saxton, R. E.; McFadden, D. W., Hypericin and Photodynamic Therapy Decreases Human Pancreatic Cancer in Vitro and in Vivo. *Journal of Surgical Research* **2000,** 93, (1), 137-143.
128. Miskovsky, P.; Sureau, F.; Chinsky, L.; Turpin, P.-Y., Subcellular distribution of hypericin in human cancer cells. *Photochemistry and Photobiology* **1995,** 62, (3), 546-549.
129. Silverman Jr, S.; Migliorati, C.; Barbosa, J., Toluidine blue staining in the detection of oral precancerous and malignant lesions. *Oral Surgery, Oral Medicine, Oral Pathology* **1984,** 57, (4), 379-382.
130. Warnakulasuriya, K. A. A. S.; Johnson, N. W., Sensitivity and specificity of OraScan® toluidine blue mouthrinse in the detection of oral cancer and precancer. *Journal of Oral Pathology & Medicine* **1996,** 25, (3), 97-103.
131. Bigelow, R.; Freund, H., An MNDO and CNDO/S (S+ DES CI) study on the structural and electronic properties of a model squaraine dye and related cyanine. *Chem. Phys* **1986,** 107, (2-3), 159–174.
132. Ioffe, V.; Gorbenko, G.; Domanov, Y.; Tatarets, A.; Patsenker, L.; Terpetsching, E.; Dyubko, T., A new fluorescent squaraine probe for the measurement of membrane polarity. *Journal of Fluorescence* **2006,** 16, (1), 47-52.
133. Chen, H.; Farahat, M.; Law, K.; Whitten, D., Aggregation of surfactant squaraine dyes in aqueous solution and microheterogeneous media: Correlation of aggregation behavior with molecular structure. *J. Am. Chem. SOC* **1996,** 118, (11), 2584-2594.
134. Tatarets, A. L.; Fedyunyayeva, I. A.; Dyubko, T. S.; Povrozin, Y. A.; Doroshenko, A. O.; Terpetschnig, E. A.; Patsenker, L. D., Synthesis of water-soluble, ring-substituted squaraine dyes and their evaluation as fluorescent probes and labels. *Analytica Chimica Acta* **2006,** 570, (2), 214-223.
135. Sreejith, S.; Divya, K.; Ajayaghosh, A., A near-infrared squaraine dye as a latent ratiometric fluorophore for the detection of aminothiol content in blood plasma. *Angewandte Chemie (International ed. in English)* **2008,** 47, (41), 7883.
136. Terpetschnig, E.; Szmacinski, H.; Ozinskas, A.; Lakowicz, J. R., Synthesis of Squaraine-N-Hydroxysuccinimide Esters and Their Biological Application as Long-Wavelength Fluorescent Labels. *Analytical Biochemistry* **1994,** 217, (2), 197-204.
137. Patonay, G.; Salon, J.; Sowell, J.; Strekowski, L., Noncovalent labeling of biomolecules with red and near-infrared dyes. *Molecules* **2004,** 9, (3), 40–49.
138. Ioffe, V.; Gorbenko, G.; Kinnunen, P.; Tatarets, A.; Kolosova, O.; Patsenker, L.; Terpetschnig, E., Tracing Lysozyme-Lipid Interactions with Long-Wavelength Squaraine Dyes. *Journal of Fluorescence* **2007,** 17, (1), 65-72.
139. Santos, P. F.; Reis, L. V.; Almeida, P.; Serrano, J. P.; Oliveira, A. S.; Vieira Ferreira, L. F., Efficiency of singlet oxygen generation of aminosquarylium cyanines. *Journal of Photochemistry and Photobiology A: Chemistry* **2004,** 163, (1-2), 267-269.

140. Santos, P. F.; Reis, L. V.; Duarte, I.; Serrano, J. P.; Almeida, P.; Oliveira, A. S.; Vieira Ferreira, L. F., Synthesis and Photochemical Evaluation of Iodinated Squarylium Cyanine Dyes. *Helvetica Chimica Acta* **2005,** 88, (5), 1135-1143.
141. Arunkumar, E.; Sudeep, P.; Kamat, P.; Noll, B.; Smith, B., Singlet oxygen generation using iodinated squaraine and squaraine-rotaxane dyes. *New Journal of Chemistry* **2007,** 31, (5), 677-683.
142. Bonnett, R.; Motevalli, M.; Siu, J., Squaraines based on 2-arylpyrroles. *Tetrahedron* **2004,** 60, (40), 8913-8918.
143. Beverina, L.; Crippa, M.; Landenna, M.; Ruffo, R.; Salice, P.; Silvestri, F.; Versari, S.; Villa, A.; Ciaffoni, L.; Collini, E.; Ferrante, C.; Bradamante, S.; Mari, C. M.; Bozio, R.; Pagani, G. A., Assessment of Water-Soluble π-Extended Squaraines as One- and Two-Photon Singlet Oxygen Photosensitizers: Design, Synthesis, and Characterization. *Journal of the American Chemical Society* **2008,** 130, (6), 1894-1902.
144. Jyothish, K.; Avirah, R. R.; Ramaiah, D., Synthesis of New Cholesterol- and Sugar-Anchored Squaraine Dyes: Further Evidence of How Electronic Factors Influence Dye Formation. *Organic Letters* **2005,** 8, (1), 111-114.
145. Ramaiah, D.; Eckert, I.; Arun, K.; Weidenfeller, L.; Epe, B., Squaraine dyes for photodynamic therapy: study of their cytotoxicity and genotoxicity in bacteria and mammalian cells. *Photochemistry and Photobiology* **2002,** 76, (6), 672-677.
146. Ramaiah, D.; Eckert, I.; Arun, K.; Weidenfeller, L.; Epe, B., Squaraine Dyes for Photodynamic Therapy: Mechanism of Cytotoxicity and DNA Damage Induced by Halogenated Squaraine Dyes Plus Light (> 600 nm)¶. *Photochemistry and Photobiology* **2004,** 79, (1), 99-104.
147. Gayathri Devi, D.; Cibin, T. R.; Ramaiah, D.; Abraham, A., Bis(3,5-diiodo-2,4,6-trihydroxyphenyl)squaraine: A novel candidate in photodynamic therapy for skin cancer models in vivo. *Journal of Photochemistry and Photobiology B: Biology* **2008,** 92, (3), 153-159.
148. Rapozzi, V.; Beverina, L.; Salice, P.; Pagani, G. A.; Camerin, M.; Xodo, L. E., Photooxidation and Phototoxicity of π-Extended Squaraines. *Journal of Medicinal Chemistry* **2010,** 53, (5), 2188-2196.
149. Volkova, K. D.; Kovalska, V. B.; Tatarets, A. L.; Patsenker, L. D.; Kryvorotenko, D. V.; Yarmoluk, S. M., Spectroscopic study of squaraines as protein-sensitive fluorescent dyes. *Dyes and Pigments* **2007,** 72, (3), 285-292.
150. Chenthamarakshan, C. R.; Eldo, J.; Ajayaghosh, A., Squaraine Dye Based Molecular Wires Containing Flexible Oxyethylene Chains as Sensors. Enhanced Fluorescence Response on Li+ Recognitionâ€ *Macromolecules* **1999,** 32, (18), 5846-5851.
151. Chenthamarakshan, C. R.; Ajayaghosh, A., Enhanced sensitivity and selectivity in lithium ion recognition property of an oligomeric squaraine dye based fluorescent sensor. *Tetrahedron Letters* **1998,** 39, (13), 1795-1798.
152. Jisha, V. S.; Arun, K. T.; Hariharan, M.; Ramaiah, D., Site-Selective Binding and Dual Mode Recognition of Serum Albumin by a Squaraine Dye. *Journal of the American Chemical Society* **2006,** 128, (18), 6024-6025.

153. Reddington, M. V., Synthesis and Properties of Phosphonic Acid Containing Cyanine and Squaraine Dyes for Use as Fluorescent Labels. *Bioconjugate Chemistry* **2007,** 18, (6), 2178-2190.

3 Philosophy of approach

New photosensitizing drugs should have advantages over the ones now being used. An accurately designed photosensitizer should possess an intense absorption band in the tissue transparency window in the NIR region allowing the treatment of deep tumors, should be more selective for cancer cells as opposed to normal cells and tissues, should be more easily removed from the body, thus reducing photosensitivity reactions, and should have low intrinsic dark cytotoxicity.

Squaraine dyes are promising PDT sensitizers since they offer several advantages. First of all, these dyes possess a strong and sharp absorption NIR region[1]. Second, squaraines are also fairly fluorescent in the same region, thus these compounds are valid theranostic agents. Furthermore, squaraines possess a strong two photon absorption[2] enabling for their use at the wavelengths relevant for clinical applications (644 nm and 806 nm).

Squaraine dyes accumulate in cells and localize in the organelles in the cytoplasm, with low toxicity in the dark and a strong photodynamic effect *via* ROS production when irradiated at the suitable wavelength.[3, 4]

Squaraine dyes have proven to be effective photosensitizers in *in vitro* studies on cancer cells and bacteria[3, 5] and in few *in vivo* studies on skin cancer models in mice, where the PDT treatment selectivity was achieved by a selective irradiation of the superficial tumor.[6]

Preliminary *in vivo* studies on deep tissue tumors in mice have been performed in collaboration with Professor Jori's group at Padova University (Italy). The squaraine dye administered in free form or into liposomes, however, was very rapidly cleared from the body and was found in traces in kidneys and liver after few hours, thus no photodynamic effect was observed.

The challenge that occurs in order to successfully employ this class of versatile compounds as effective PDT sensitizers for deep tissue theranostics is thus to improve the solubility and the delivery to the biological target. The wide flexibility of the squaraine structure provides a powerful tool aimed at the improvement of bioavailability.

The specific tissue localization may be achieved by covalent or non-covalent conjugation of the photosensitizer to nanoparticles, so that the nanocarriers obtained accumulate in tumor tissue through the EPR effect (passive targeting). The cellular and sub-cellular localization may be achieved by covalent conjugation of the photosensitizer or the nanocarrier to a biological ligand such as a protein or an antibody whose specific

receptor is overexpressed in tumor cells (active targeting, third generation photosensitizers).

The first part of my PhD project consists in the incorporation in the squaraine structure of different functional groups such as a halogen atom, a carboxylic acid or a terminal alkine in order to obtain a library of post-fuctionalizable squaraines for both passive and active targeting.

The second part of the project consists in the covalent conjugation of post-functionalizable squaraine dyes to biologically relevant groups and to nanoparticles. Choline and galactose have been chosen as representative examples for active targeting, while zeolite nanocrystals of the appropriate size and shape have been chosen as a model nanocarrier.

Finally, the functionalized squaraines and the squaraine-functionalized nanocarriers will be fully characterized. The photophysical and photochemical characterization will be performed to verify that the functionalization introduced doesn't alter the spectroscopic and ROS-generating ability of the photosensitizer. The subsequent *in vitro* photocitotoxicity tests with normal cells and cancer cells (either in different cultures or in co-culture) will be performed in order to evaluate the selective accumulation of the functionalized squaraines for active targeting and the activity of the nanocarriers.

3.1 References

1. Beverina, L.; Salice, P., Squaraine Compounds: Tailored Design and Synthesis towards a Variety of Material Science Applications. *European Journal of Organic Chemistry* **2010,** 2010, (7), 1207-1225.
2. Beverina, L.; Crippa, M.; Landenna, M.; Ruffo, R.; Salice, P.; Silvestri, F.; Versari, S.; Villa, A.; Ciaffoni, L.; Collini, E.; Ferrante, C.; Bradamante, S.; Mari, C. M.; Bozio, R.; Pagani, G. A., Assessment of Water-Soluble π-Extended Squaraines as One- and Two-Photon Singlet Oxygen Photosensitizers: Design, Synthesis, and Characterization. *Journal of the American Chemical Society* **2008,** 130, (6), 1894-1902.
3. Rapozzi, V.; Beverina, L.; Salice, P.; Pagani, G. A.; Camerin, M.; Xodo, L. E., Photooxidation and Phototoxicity of π-Extended Squaraines. *Journal of Medicinal Chemistry* **2010,** 53, (5), 2188-2196.
4. Salice, P.; Arnbjerg, J.; Pedersen, B. W.; Toftegaard, R.; Beverina, L.; Pagani, G. A.; Ogilby, P. R., Photophysics of Squaraine Dyes: Role of Charge-Transfer in Singlet Oxygen Production and Removal. *The Journal of Physical Chemistry A* **2010,** 114, (7), 2518-2525.
5. Ramaiah, D.; Eckert, I.; Arun, K. T.; Weidenfeller, L.; Epe, B., Squaraine Dyes for Photodynamic Therapy: Study of Their Cytotoxicity and Genotoxicity in Bacteria and Mammalian Cells¶‡. *Photochemistry and Photobiology* **2002,** 76, (6), 672-677.
6. Gayathri Devi, D.; Cibin, T. R.; Ramaiah, D.; Abraham, A., Bis(3,5-diiodo-2,4,6-trihydroxyphenyl)squaraine: A novel candidate in photodynamic therapy for skin cancer

models in vivo. *Journal of Photochemistry and Photobiology B: Biology* **2008,** 92, (3), 153-159.

4 Analysis, design, interpretations of results

4.1 Molecular engineering of squaraine functionalities: post-functionalizable squaraines

The synthesis of squarylium dyes, or squaraines, involves the condensation of a nucleophile with squaric acid or its derivatives to yield a conjugated quadrupolar dye constituted by two electron rich terminals and an electron poor core.[1-5] Some of the electron rich substrates which react with squaric acid and its derivatives are electronrich benzene (e.g., 1,3,5-trihydroxybenzene, aromatic amines), heteroaryl anhydrobases derived from indoleninium, benzothiazolium, benzofuranium salts, and derivatives of pyrrole, aniline and thiophene.

The condensation reactions are usually performed in a mixture of a protic solvent such as acetic acid or alcohols (e.g., buthanol or 2-propanol) with an aromatic hydrocarbon (e.g., benzene or toluene) for the azeotropic removal the condensation water. An external drying agent in the reaction mixture such as tributyl orthoformate (TBOF) has also been employed in an alternative synthesis strategy.[6]

The synthesis of symmetric squaraine requires two equivalents of the nucleophile and one of squaric acid. The first condensation gives an emisquaraine intermediate which undergoes a second condensation to give the 1,3-substituted symmetric squaraine. Depending from the reaction conditions the 1,2-isomer may be also obtained in traces amount.

Unsymmetrical squaraines substituted with two different terminal groups have also received a special interest.[6, 7] A stepwise synthetic pathway is necessary, since the simultaneous condensation of squaric acid with two different nucleophiles gives a distribution of all the possible symmetrically and unsymmetrically substituted products and their separation requires a high expense on time and materials. Moreover, in the reaction between squaric acid and a nucleophile in 1:1 ratio the dicondensation product 1,3 squaraine is always obtained rather than the emisquaraine monocondensation product. The most useful method for preparing emisquaraines consists in the reaction of an ester of squaric acid (e.g., ethyl[8] or butyl[9] squarate) or of the acyl chloride of squaric acid with a nucleophile.[10, 11] The alkyl emisquarates and the squaryl emichlorides obtained can be hydrolyzed to the corresponding emisquaraines in acid or basic conditions. The reaction of the emisquaraine with an equivalent of a different nucleophile yields the desired unsymmetrical squaraine.

A major synthetic issue is the regiochemical control during the preparation of symmetric and unsymmetrical squaraines, but also during the preparation of the intermediates, which will be extensively discussed in Section 0.

Another synthetic issue worth mention is the production of singlet oxygen and ROS by the already formed sensitizer into the reaction mixture, which is responsible for the partial the degradation of both reagents and product. This may be overcome with some expedients:

- The condensation reactions are performed in dark brown glassware and under nitrogen atmosphere;
- The reaction time may be reduced from 18-24 hours with conventional heating (i.e., an oil bath) to 2-6 h with microwave-assisted heating, which improves the azeotropic distillation rate;
- In alternative, the condensation reactions with anhydrobases formed *in situ* from the corresponding indoleninium and benzothiazolium salts may be performed in pyridine, which acts both as solvent and base.

The versatility of squaraine synthesis allows the condensation of a variety of electron rich substrates with different substitution patterns, allowing the fine tuning of the squaraine properties:

- The electronic properties can be controlled by choosing the appropriate heterocycle moieties;
- The solubility can be tuned and specific functionalities can be inserted without affecting the overall electronic properties;
- Concerning the specific topic of the present dissertation, biological agents or nanoformulates can be conjugated to the dye improving the bioavailability and targeting without affecting the photosensitizing activity.

The present dissertation will concentrate on the molecular engineering of benzothiazole and indolenine anhydrobase-derived squaraines, in order to tune the biodistribution of the benchmark symmetric squaraine **4.1**.

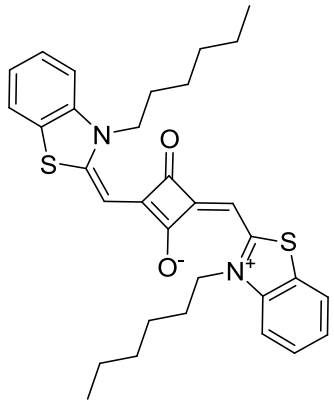

4.1

In order to compare the effect of the functionalities inserted, squaraine **4.1** has been synthesized in refluxing pyridine in the dark from squaric acid and 3-hexyl-2-methylbenzo[*d*]thiazol-3-ium iodide.

The functionalities on the squaraine backbone may be inserted in two different positions, as depicted in Scheme 4–1. The functionalization on the benzene ring of the anhydrobase (**4.2**) allows the introduction of bulky substituents without distortion from planarity, but it may alter the electronic properties in case of electron-withdrawing or electron-donating substituents. On the contrary, the functionalization on the alkyl chain on nitrogen (**4.3**) requires fewer synthetic steps and the electronic properties are less affected since the substituent is not in conjugation with the π system, but bulky functionalities may alter the backbone planarity.

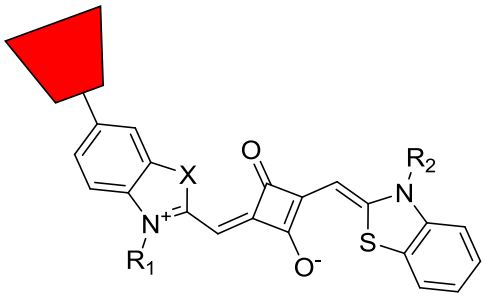

X = S, $C(CH_3)_2$
R_1, R_2 = alkyl chain

4.2

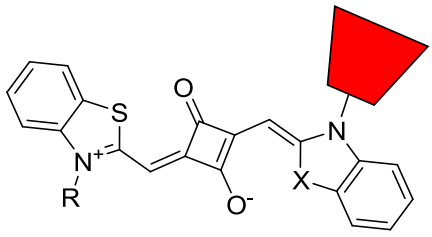

X = S, $C(CH_3)_2$
R = alkyl chain

4.3

Scheme 4–1

The functionality in the squaraines with generic structure **4.2** is inserted on the benzothiazole or indolenine precursor.

2,3,3-trimethyl-3*H*-indol-5-ol **4.5** is prepared following the methods described by Moore (Scheme 4–2).[12]

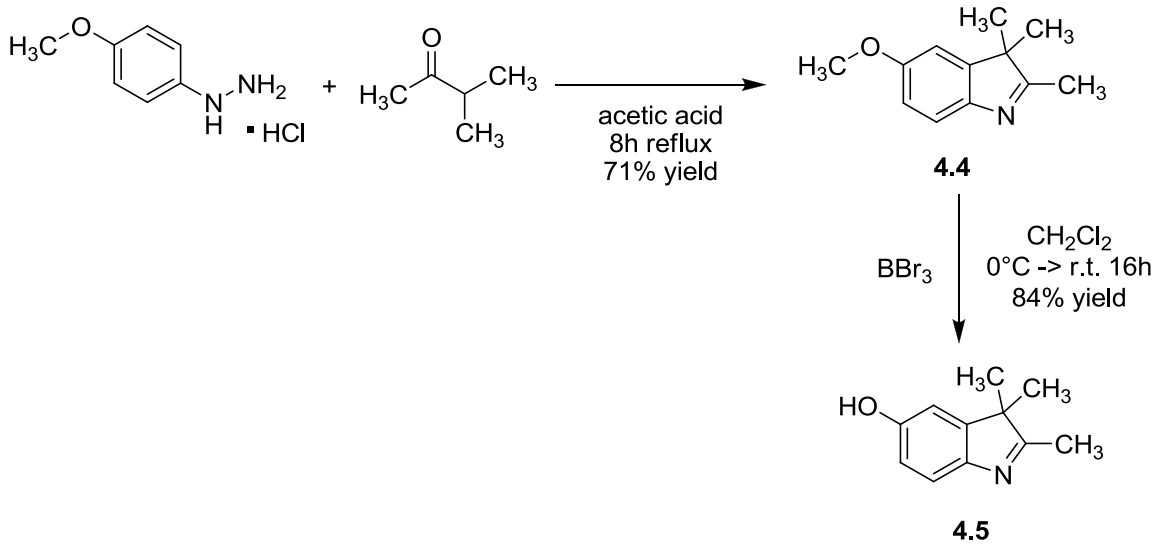

Scheme 4–2

5-bromo-2,3,3-trimethyl-3*H*-indole is prepared in analogous way through Fischer indole synthesis with 4-bromplhenylhydrazine hydrochloride as a precursor (Scheme 4–3).

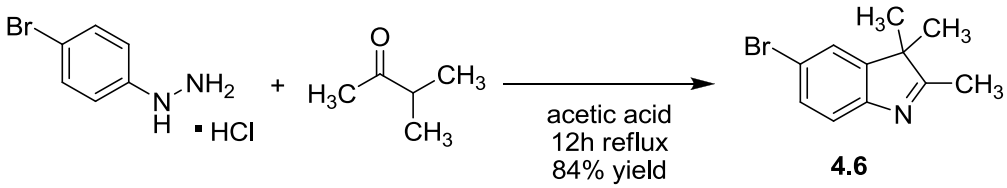

Scheme 4–3

Other functionalities are inserted through the formation of an ether bridge on 2,3,3-trimethyl-3*H*-indol-5-ol **4.5** or 2-methylbenzo[*d*]thiazol-5-ol **4.7**, as shown in Scheme 4–4.

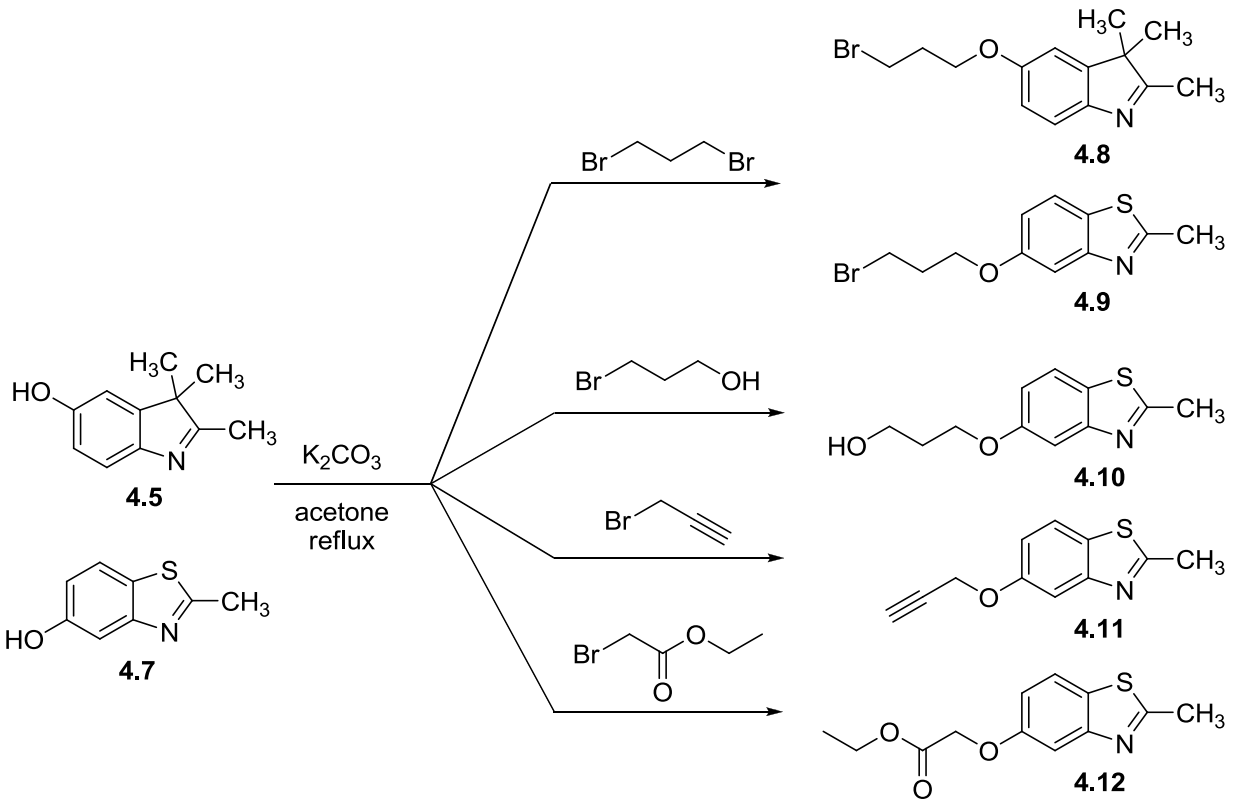

Scheme 4–4

The corresponding functionalized benzothiazolium and indoleninium salts are formed through alkylation with methyl trifluoromethanesulfonate.

The condensation with a benzothiazole or indolenine emisquaraine to give the quasi-symmetric and the unsymmetrical squaraines is performed either by refluxing in pyridine or with a base in 2-propanol:toluene 4:1 mixture for the azeotropic distillation of the water formed (Scheme 4–5).

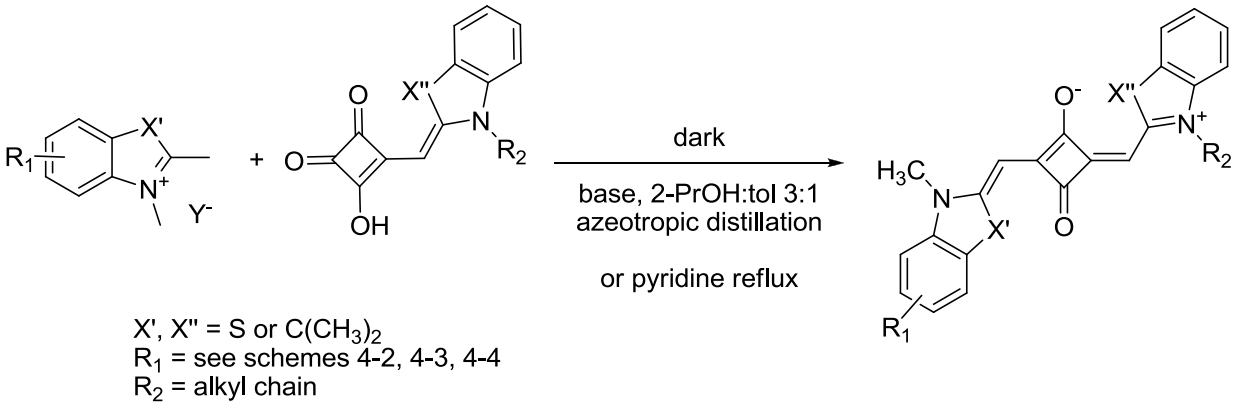

Scheme 4–5

Some representative functionalized squaraines are depicted in Scheme 4–6.

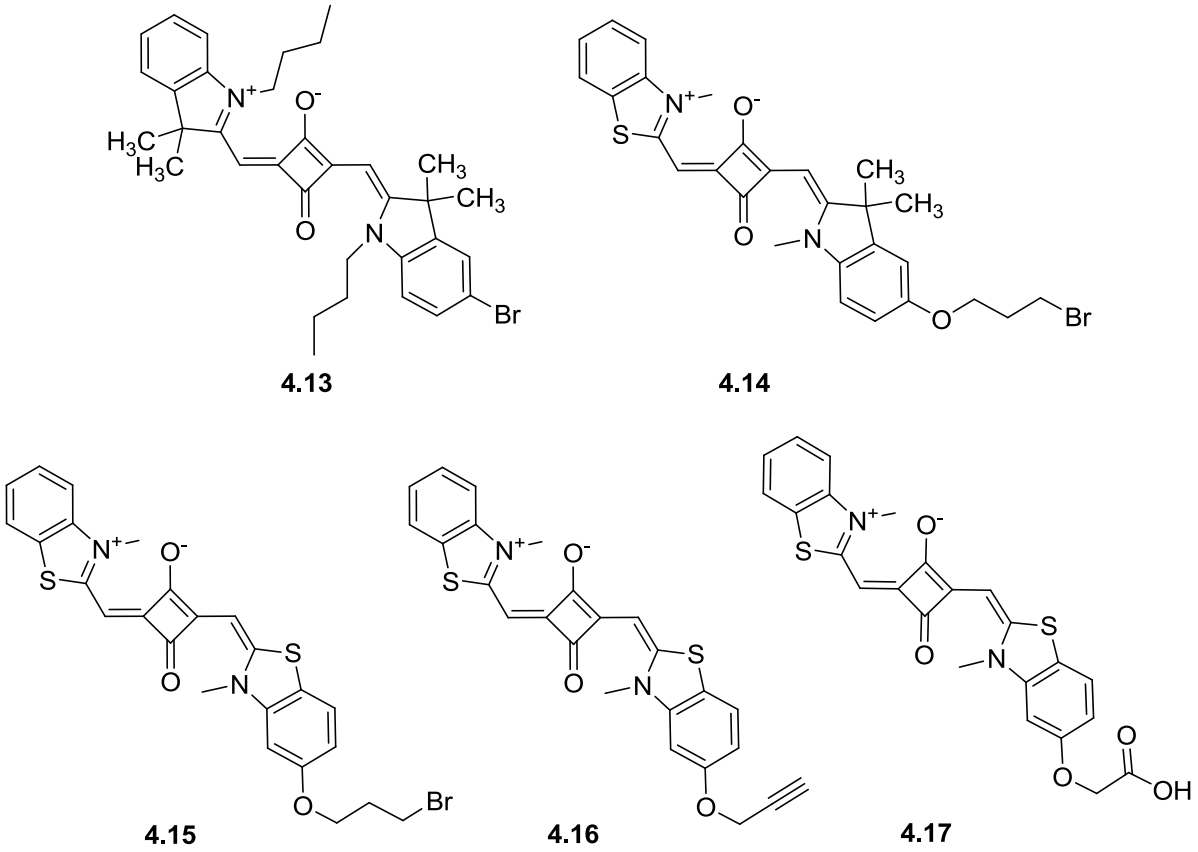

Scheme 4–6

Squaraines **4.14** and **4.15** have been prepared in azeotropic conditions using a non-nucleophile base such as quinaldine to generate the anhydrobase *in situ*, because both the most common bases pyridine and imidazole would react with the aliphatic bromine and the quaternary salt would be obtained. These two derivatives may be converted to the less stable corresponding azide for post-functionalization *via* Huisgen cycloaddition.

In alternative, the squaraine **4.16** with a terminal alkyne has also been prepared for click chemistry post-functionalization.

Squaraine **4.17** has been prepared through the basic hydrolysis of the product obtained from the condensation of the salt from **4.12** and benzothiazole emisquaraine. The carboxylic acid functionality, indeed, is not compatible with the ether bond formation (Scheme 4–4) because the carboxylic acid is deprotonated more effectively than the aromatic hydroxyl group, generating a salt from the alkylating agent, which precipitates in the reaction mixture and does not react further.

The functionality in the squaraines with generic structure **4.3** is inserted on the by choosing the suitable alkylating agent for the synthesis of the benzothiazole or indolenine salt (Scheme 4–7).

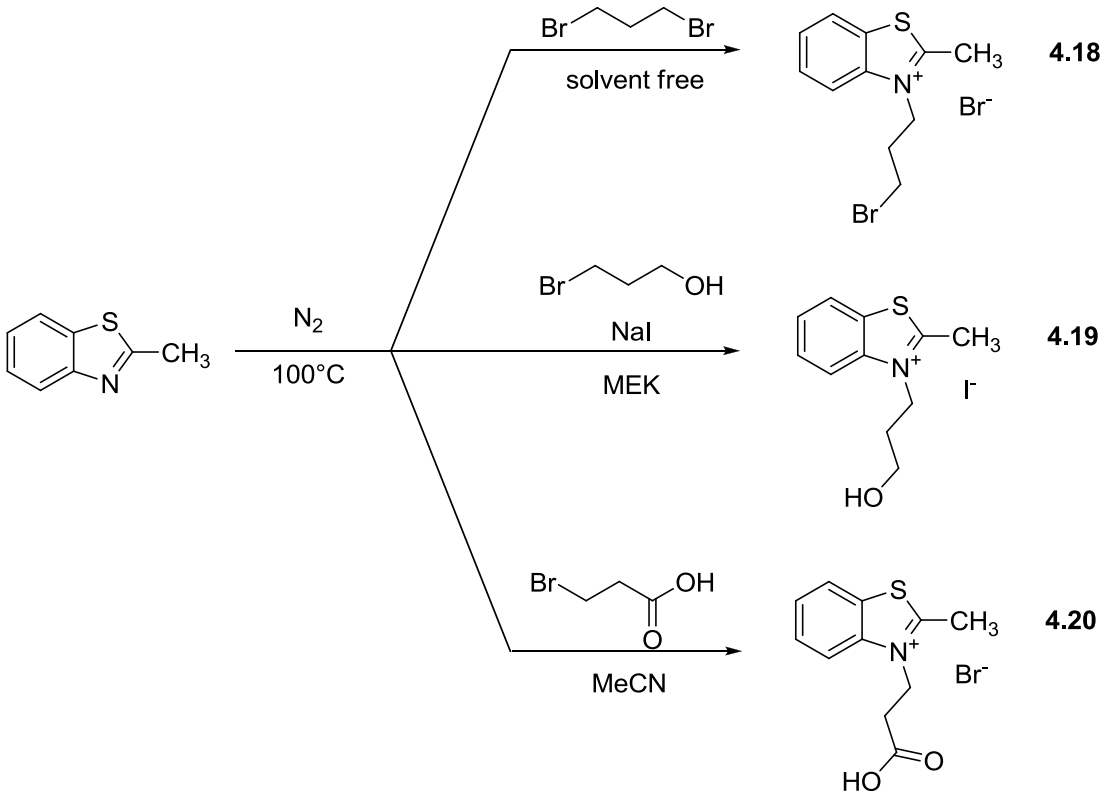

Scheme 4–7

The alkylations are performed under nitrogen atmosphere using an excess alkylating agent as a solvent and adding a polar solvent to improve stirring when the product formed precipitates. The benzothiazolium salt **4.19** has been synthesized in the presence of sodium iodide to generate *in situ* a more effective alkylating agent *via* Finkelstein Reaction.

The condensation with squaric acid or a benzothiazole emisquaraine to give the symmetric and the quasi-symmetric squaraines is performed either by refluxing in pyridine or with a base in 2-propanol:toluene 4:1 mixture for the azeotropic distillation of the water formed (Scheme 4–8).

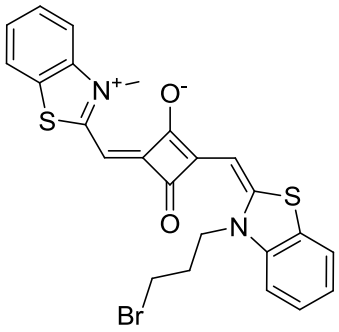

4.21

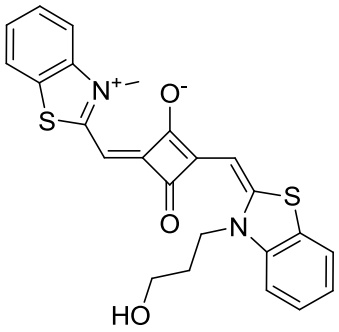

4.22

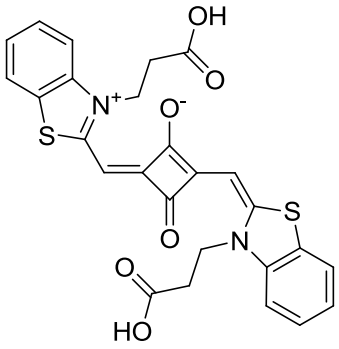

4.23

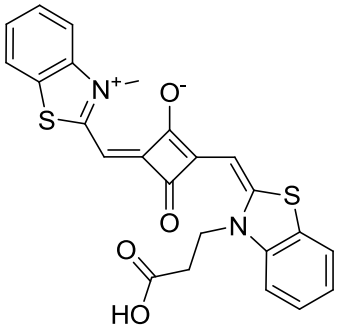

4.24

Scheme 4–8

The photophysics of the quasi-symmetric squaraine **4.15** has been studied in detail and compared with the benchmark symmetric squaraine **4.1** in order to investigate the effect of the substituents. The absorption, emission and excitation spectra of the two squaraines are shown in Figure 4–1.

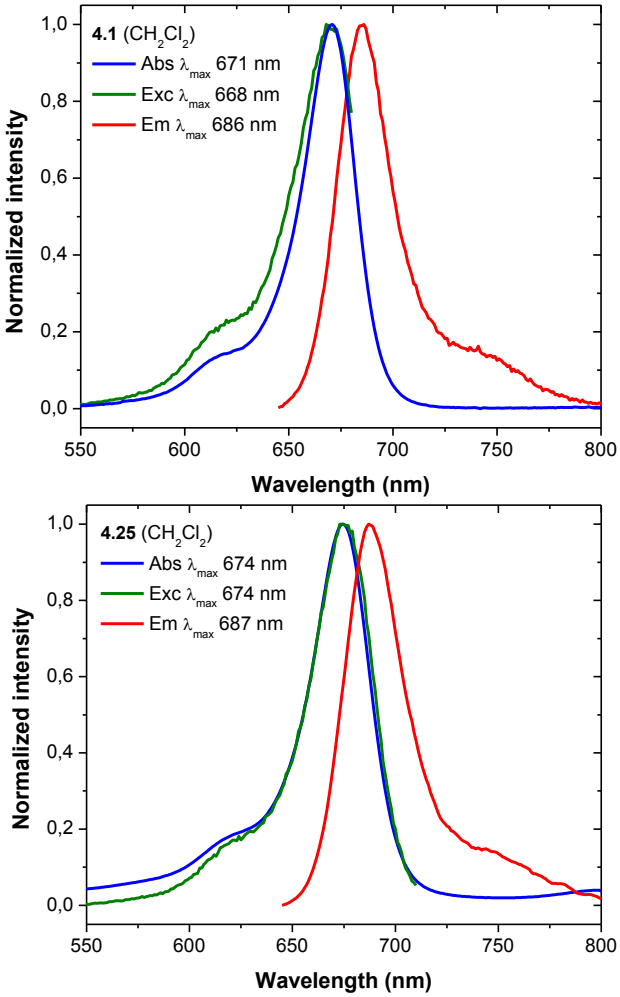

Figure 4–1 Normalized absorption, excitation and emission spectra of 4.1 (left) and 4.15 (right) in DCM.

In a more polar solvent such as acetonitrile the emission bands of both dyes are slightly blue-shifted and the fluorescence lifetimes decrease, as well as the fluorescence quantum yields, while in 2-methyl-tetrahydrofuran glass at 77 K[13] the bands are narrower and the vibronic replica is more defined (Figure 4–2).

The fluorescence quantum yields and lifetimes measured in absence of oxygen increase of 5-10% for both dyes, showing that the excited state is partially deactivated *via* the squaraine-oxygen encounter complex and little singlet oxygen production[14]. The fluorescence lifetime in a rigid environment such as 2-methyl-tetrahydrofuran glass at 77 K is longer, due to the reduced vibrational relaxation and oxygen diffusion (Figure 4–3).

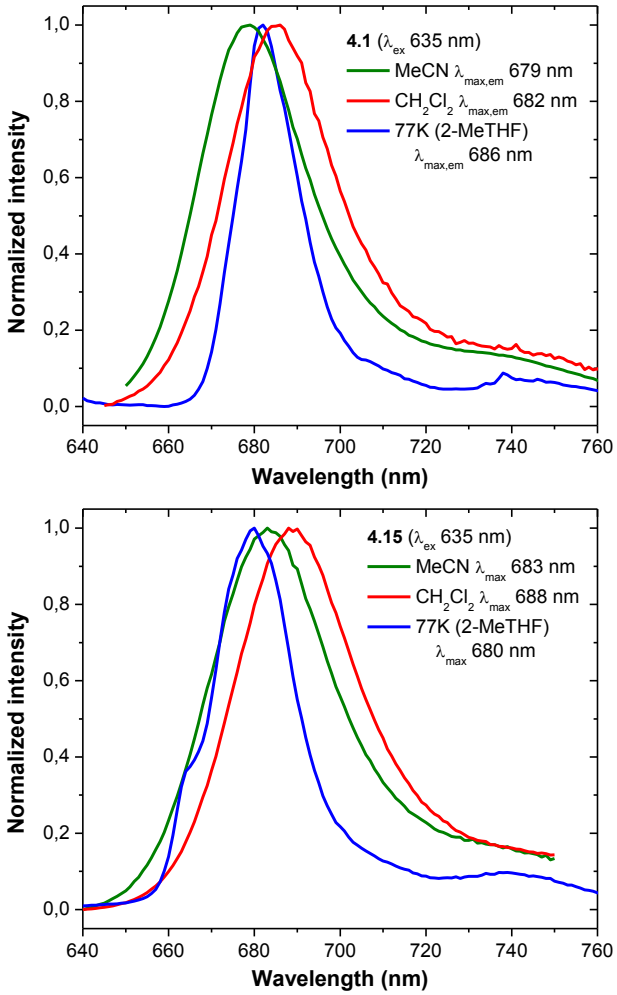

Figure 4–2 Normalized emission spectra of 4.1 (left) and 4.15 (right) in different solvents.

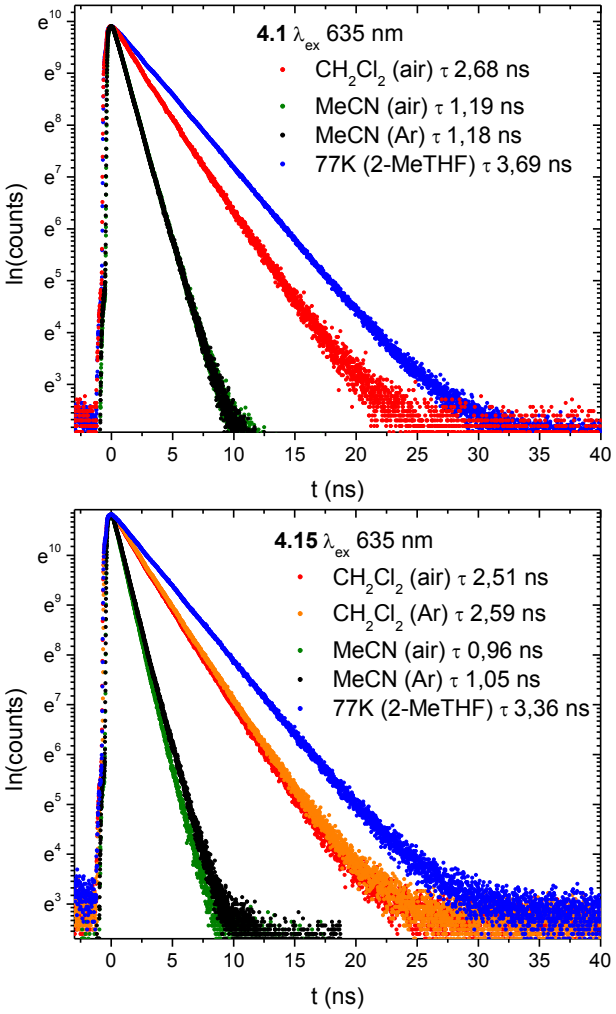

Figure 4–3 Logarithmic scale time-resolved decay of the fluorescence emission intensity of 4.1 (left) and 4.15 (right) recorded at the maximum emission wavelength

The spectroscopic data for **4.15** are summarized in Table 4–2. The values found are very close to the ones measured for **4.1** (Table 4–1), implying that the functionalization of one of the aromatic rings of benzothiazole has minimal influence on the photophysics. It is then expected that also the post-functionalization will not alter the peculiar spectroscopic characteristics of the squaraine dye.

4.1	$\lambda_{abs,max}$[a] /nm (ε[b])	$\lambda_{exc,max}$[c] /nm	$\lambda_{em,max}$[d]/nm (FWHM/nm)	Stokes shift[e] /nm (/cm^{-1})	τ_F/ns	Φ_F[f]
CH_2Cl_2	671 ()	668	686 (31)	15 (326)	2.69 (air)	
MeCN	663 ()	665	679 (31)	16 (355)	1.19 (air) 1.18 (Ar)	0.21 (air)

2-MeTHF glass	683 (17)	3.69

[a] Wavelength of absorption band maximum. Error of ±0.5 nm. [b] Molar extinction coefficient, × 10^5 L mol^{-1} cm^{-1}, estimated error ±10%. [c] Wavelength of excitation band maximum. Error of ±0.5 nm. [d] Wavelength of emission band maximum. Error of ±0.5 nm. [e] Stokes shift in both nm and cm^{-1}. Fluorescence quantum yield in air-equilibrated solvent, measured with relative method using Zinc 2,9,16,23-tetra-tert-butyl-29*H*,31*H*-phthalocyanine in toluene as a standard (ΦF 0.30), irradiation at 630 nm.[15]

Table 4–1 Spectroscopic data for 4.1.

4.15	$\lambda_{abs,max}$[a] /nm (ε[b])	$\lambda_{exc,max}$[c] /nm	$\lambda_{em,max}$[d]/nm (FWHM/nm)	Stokes shift[e] /nm (/cm^{-1})	τ_F/ns	Φ_F[f]
CH_2Cl_2	674 (0.86)	674	688 (35)	14 (302)	2.51	0.86
MeCN	668	669	683 (35)	15 (329)	0.96 (air) 1.05 (Ar)	0.38 (air) 0.42 (Ar)
2-MeTHF glass			683 (22)		3.36	

[a] Wavelength of absorption band maximum. Error of ±0.5 nm. [b] Molar extinction coefficient, × 10^5 L mol^{-1} cm^{-1}, estimated error ±10%. [c] Wavelength of excitation band maximum. Error of ±0.5 nm. [d] Wavelength of emission band maximum. Error of ±0.5 nm. [e] Stokes shift in both nm and cm^{-1}. Fluorescence quantum yield in air-equilibrated solvent, measured with relative method using Zinc 2,9,16,23-tetra-tert-butyl-29*H*,31*H*-phthalocyanine in toluene as a standard (ΦF 0.30), irradiation at 630 nm.[15]

Table 4–2 Spectroscopic data for 4.15.

4.2 Regiochemistry control: 1, 3- and 1, 2-substituted squarylium dyes

The condensation reaction for the synthesis of squaraines is in most cases regioselective, and the major product corresponds to the 1,3-isomer.

From the electronic point of view 1,3-squaraines are cyanines and the most relevant photophysical properties are a sharp and intense absorption band, NIR fluorescence and nonlinear optical behavior.[16]

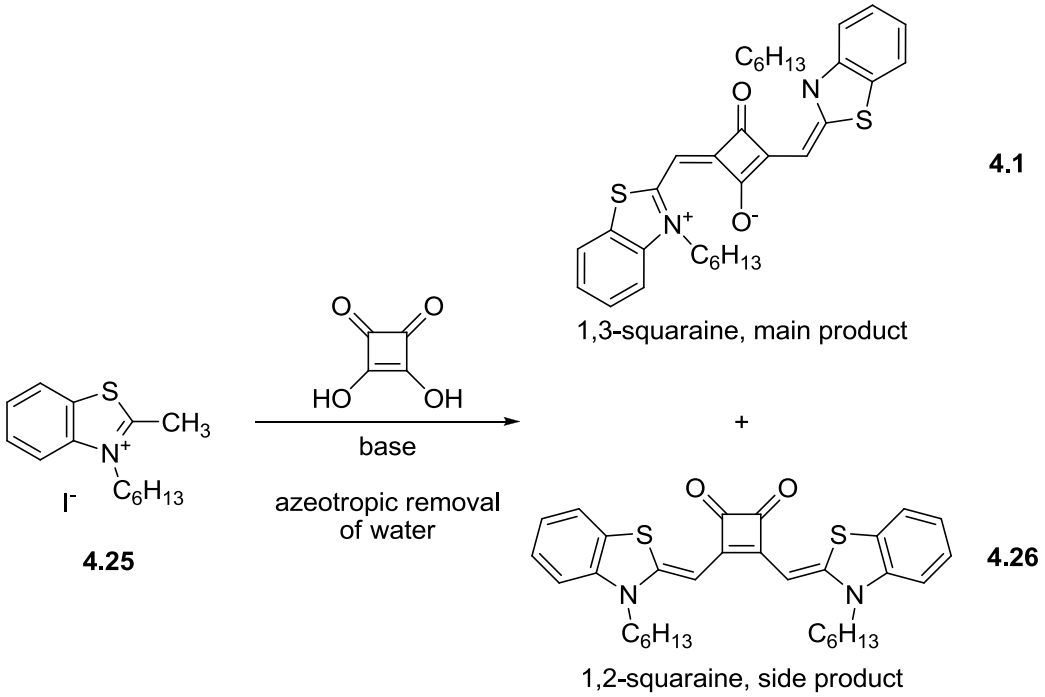

Scheme 4–9

Scheme 4–9 shows, as a representative example, the condensation of two equivalents of the anhydrobase generated *in situ* by reaction of **4.25** with a suitable base (quinoline, imidazole, triethylamine) with squaric acid to give the 1,3-squaraine **4.26**[17] (the major product) and the corresponding 1,2-regioisomer **4.27** (the side product).

The first 1,2-squaraine **4.30** was prepared by acid hydrolysis of 1,2-diphenyl-3,3,4,4-tetrafluorocyclobutene by Blomquist[18] (Scheme 4–10).

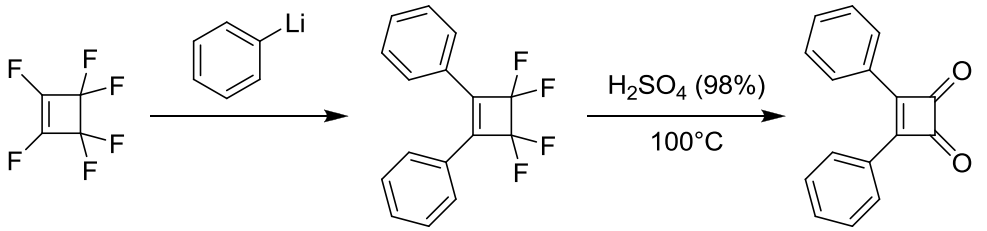

4.27 **4.28** **4.29**

Scheme 4–10

Symmetric diarylcyclobutenediones (1,2-squaraines) have been selectively prepared by the Friedel-Crafts reaction of squaryl chloride and two equivalents of a suitable arene such as fluorene (Scheme 4–11).[19]

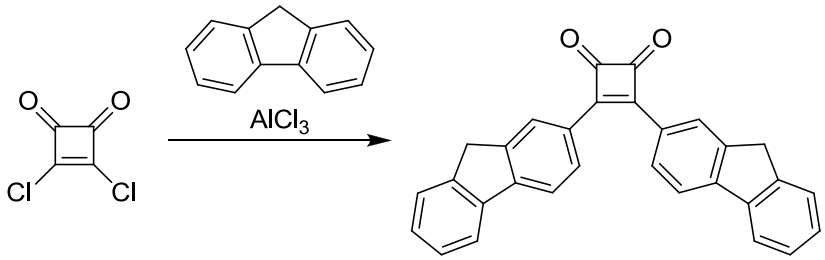

4.30 **4.31**

Scheme 4–11

Unsymmetrical derivatives can be prepared by the sequential Stille−Liebeskind/Srogl reactions of 3-chloro-4-arylthiocyclobutene with suitable precursors.[20]

The direct reaction of an activated arene (dimethylaniline) and butyl squarate in humid BuOH gives the 1,2-squaraines only in traces amount.[9] Treibs and Jacobs obtained 1,2-squaraines by reaction of 2-methyl pyrrole and squaric acid in acetic anhydride.[21] In this case the squaric acid is converted in the corresponding acetate **4.33**, which behaves like squaryl chloride (Scheme 4–12).

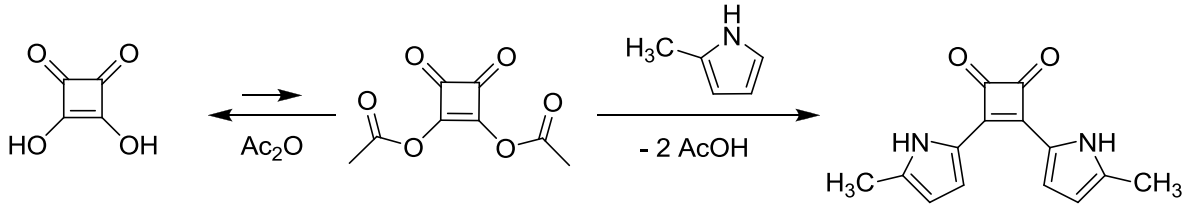

4.32 **4.33**

Scheme 4–12

The literature does not report any useful direct synthesis of 1,2-squaraines from squaric acid or esters. Moreover no detailed characterization of their properties with respect to the most common 1,3-derivatives is available.

The lack of complete condensation regioselectivity in the reaction between an electron rich molecule and squaric acid has important consequences also in the synthesis of polysquaraines.[22] The formation of the 1,2-regioisomer corresponds in this case to the formation of 1,2-diketonic defects that are incorporated in the growing polymer chain.[23] A better understanding of the factors influencing the 1,2- versus 1,3- condensation pathways could provide guidelines for the synthesis of fully regioregular polysquaraines.

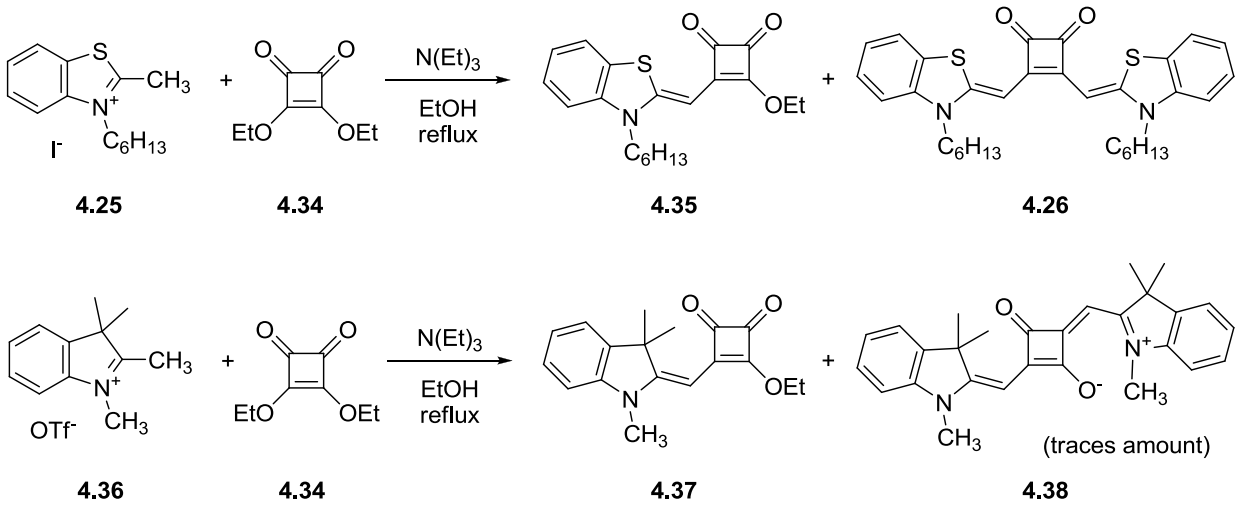

4.25 **4.34** **4.35** **4.26**

4.36 **4.34** **4.37** **4.38**

Scheme 4–13

To explore the potentially appealing chemical and photophysical properties of 1,2-squaraines, I repeated the only literature procedure describing (but without a complete characterization) the direct formation of **4.26** as a byproduct in the synthesis of the benzothiazole emisquarate **4.35**.[24] The reaction of the benzothiazolium salt **4.25** and ethyl squarate **4.34** was performed in refluxing ethanol in the presence of a stoichiometric amount of triethylamine (Scheme 4–13). The reaction gave **4.35**, along with a strongly red colored byproduct which was isolated by chromatography and crystallized by the orthogonal solvents method to obtain single crystals. The diffraction analysis confirmed the proposed structure for derivative **4.26**.

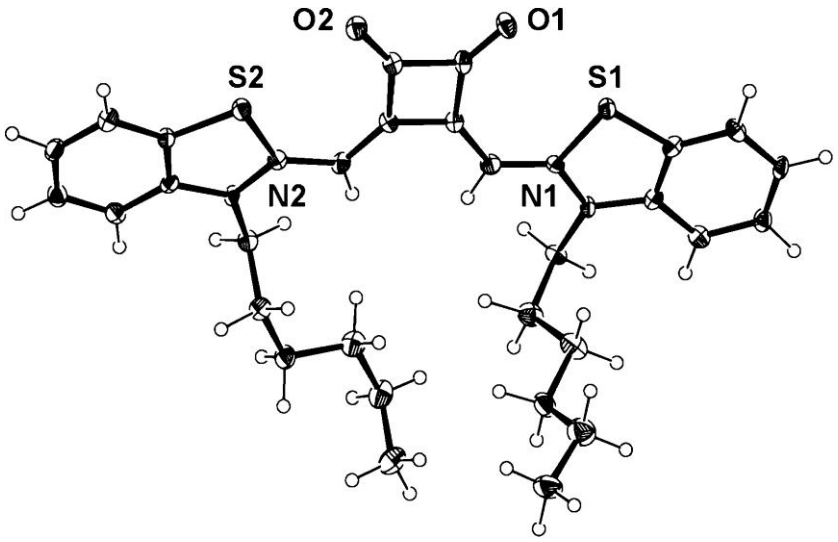

Figure 4–4 A view of the ORTEP diagram of structure of 4.26 (disordered THF solvent molecules have been omitted for clarity). Thermal ellipsoids are drawn at 50% probability.

This first experiment shows that 1,2-squaraines share with their 1,3-regioisomers a strong coloration. They also possess a very remarkable stability and complete redox reversibility. All these properties make them suitable as sensitizers in organic photovoltaic and photodetecting devices.[25] In particular, 1,2-squaraines could be highly interesting for green-operating photodetectors as they show a strong absorption close to the technologically relevant wavelength of 550 nm.[26] The 1,3-squaraines do not efficiently absorb in this region.

During the thesis I have focused my attention on the development of a regioselective synthesis of 1,2-squaraines. As a representative case, the synthesis conditions of the benzothiazole and indolenine symmetric squaraines **4.1** and **4.38** along with their 1,2-regioisomers were studied (Scheme 4–14).

An important observation is that, as previously mentioned, the symmetric benzothiazole 1,2-squaraine **4.26** was obtained for the first time in this thesis work during the preparation of the benzothiazole emisquarate **4.35** as a precursor for unsymmetrical 1,3 squaraines(Scheme 4–13). On the contrary, only traces amount of the 1,3-substituted isomer **4.38** was formed during the preparation of the indolenine emisquarate **4.37**.

The 1,2-squaraine **4.26** could be formed by the reaction of a second equivalent of the benzothiazolium salt **4.25** either with the emisquarate **4.35** or with the corresponding emisquaraine obtained by *in situ* hydrolysis of **4.35**.

The two possible reaction pathways were tested by reacting **4.25** independently with **4.35** in anhydrous ethanol and in inert atmosphere to exclude any possible hydrolysis and with the corresponding emisquaraine in absolute ethanol. In the first case (Scheme 4–

14a) the 1,2-regioisomer **4.26** was the only product obtained. In the second case (Scheme 4–14b) the main product obtained was the 1,3-regioisomer **4.1** with traces amount of **4.26**.

The anhydrobase of **4.25** is thus able to react directly with emisquarate **4.35** and this reaction is exclusively regioselective to give the 1,2 isomer. Conversely, the reaction with the emisquaraine follows a 1,3-condensation pathway. The presence of traces amount of **4.1** can be ascribed to the reaction of the anhydrobase of **4.25** with the little **4.35** formed by *in situ* esterification of the emisquaraine with the solvent of the reaction.

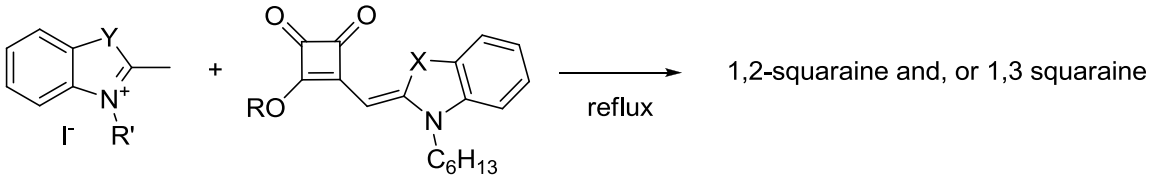

		Y	R’		R	X	Products
a	**4.25**	S	n-C_6H_{13}	**4.35**	Et	S	1,2-sq
b	**4.25**	S	n-C_6H_{13}	**4.40**	H	S	1,3-sq+ 1,2-sq (traces)
c	**4.25**	S	n-C_6H_{13}	**4.35**	Et	S	1,2-sq+ 1,3-sq[a]
d	**4.25**	S	n-C_6H_{13}	**4.37**	Et	$C(CH_3)_2$	1,2-sq
e	**4.36**	$C(CH_3)_2$	n-C_6H_{13}	**4.35**	Et	S	no reaction
f		$C(CH_3)_2$	CH_3	**4.37**	Et	$C(CH_3)_2$	1,3-sq[b]

[a]Refluxing pyridine as the solvent. [b]Microwave heating (100°c, 3 bar), the anhydrobase was generated *ex situ*.

Scheme 4–14

On going from the very reactive benzothiazole anhydrobases to the corresponding more stable indolenine derivatives (Scheme 4–14e, f), a different behavior was observed. The reaction of one equivalent of indolenine anhydrobase from **4.36** with ethyl squarate mainly gave the corresponding emisquarate **4.37** along with little 1,3-squaraine **4.38**, exactly the opposite from the benzothiazole derivatives.

Scheme 4–15 shows the tentative mechanism for the 1,2 and 1,3 condensation pathways. When the anhydrobase **4.39** reacts with the emisquarate **4.35**, the first step involves a 1,4-conjugated addition at the squarate double bond. It follows a 1,5-proton shift between the benzothiazole methylene and the enolate. Finally a thermally promoted elimination of ethanol gives exclusively the 1,2-squaraine **4.25**. The attack involves the

carbonyl α to the benzothiazole methylene because the other carbonyl is in direct conjugation with benzothiazole and thus more electron-rich (and less electrophilic).

Conversely, when the anhydrobase **4.39** reacts with the emisquaraine **4.40**, the nucleophilic attack involves the carbonyl β to the benzothiazole methylene. We speculate that this is the consequence of the high acidity of squaric acid and emisquaraines.[27] **4.40** is partially dissociated in alcoholic solution. The carbonyl in the α position is conjugated with the enolate and thus electron-rich. Conversely, the catalytic protonation of the carbonyl in the β position makes the nucleophilic attack on **4.35** particularly easy. Thermally driven elimination of water gives exclusively the 1,3-squaraine **4.1**. This mechanism is also supported by Law's observation that the reaction of dimethylindolenine with butyl squarate is efficiently catalyzed by sulfuric acid.[9]

Therefore, the formation of a 1,2-squaraine requires a very reactive electron rich precursor, as in this case there is no need of catalytic protonation to enhance the reaction site electrophylicity. This is the reason why a symmetric 1,2-squaraine out of a dimethylindolenine anhydrobase could not be prepared. **4.36** is not reactive enough to directly react with **4.37**. The formation of small amounts of **4.38** is the consequence of the slow hydrolysis of **4.37** in ethanol solution (Scheme 4–13).

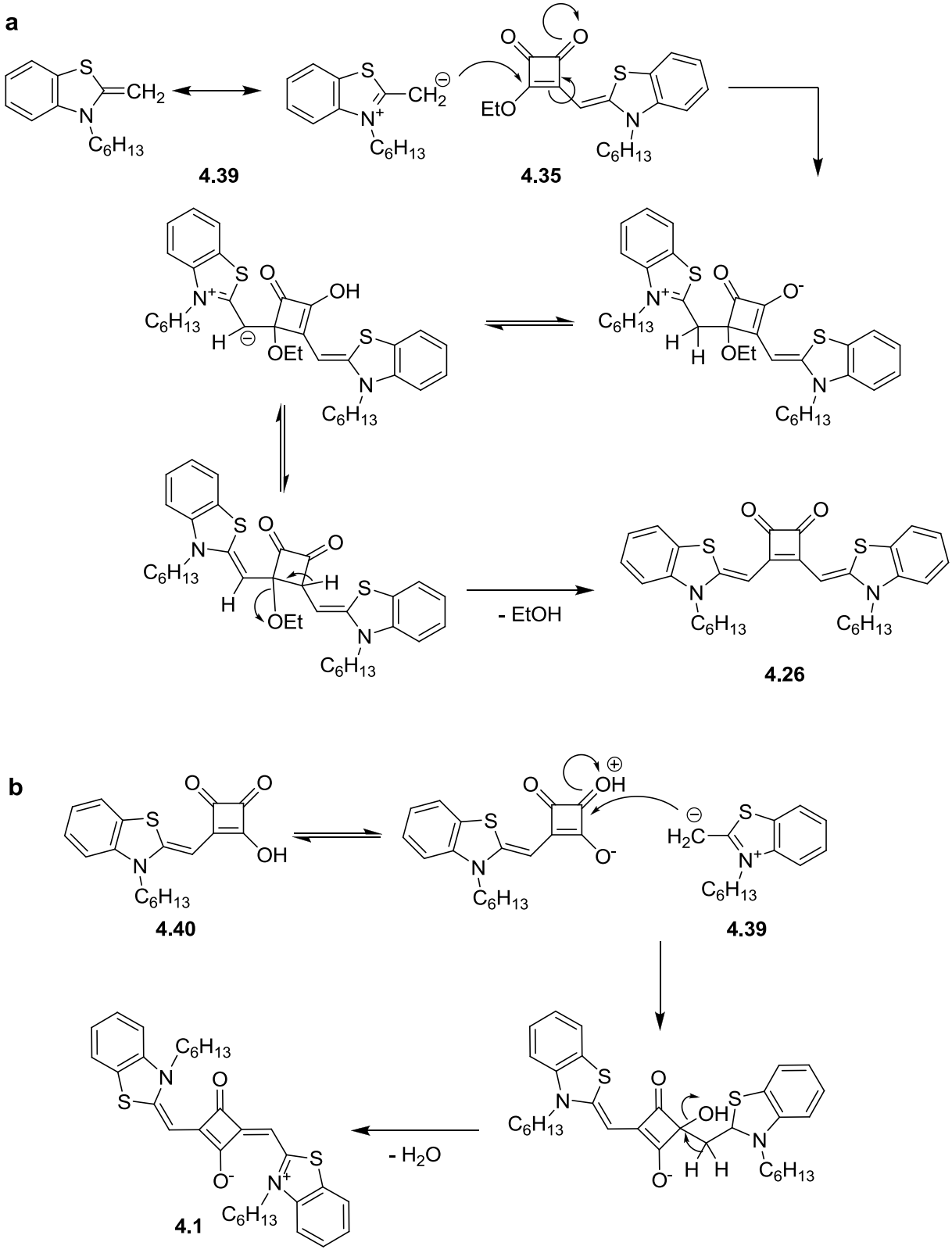

Scheme 4–15

One important consequence of the proposed mechanism is that the nonsymmetric 1,2-squaraine **4.41** bearing an indolenine and a benzothiazole as side groups could only be prepared by the reaction of **4.25** with **4.37**. The reaction of **4.36** with **4.35** only gave the starting materials (Scheme 4–16).

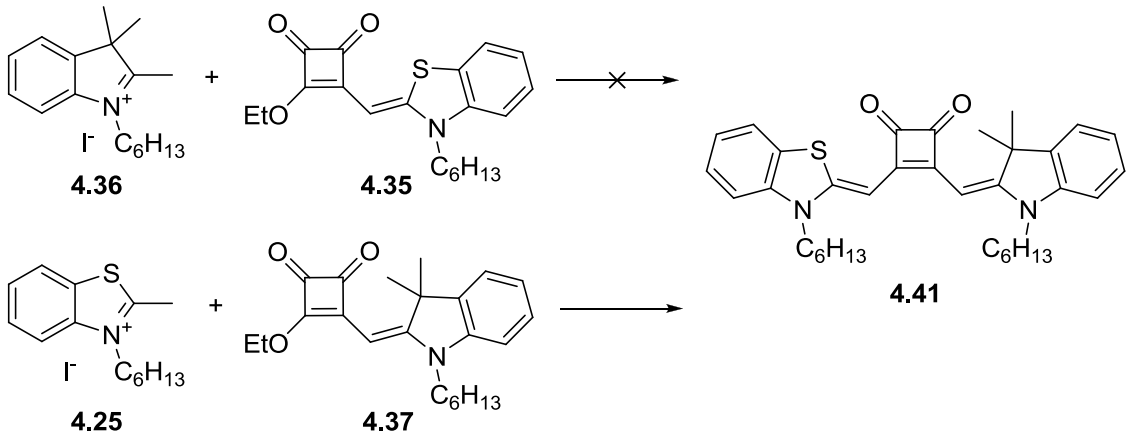

Scheme 4–16

In short, the amount of the 1,2-regioisomer in a 1,3-squaraine synthesis depends both on reaction conditions and nature of the reactants. First, only very reactive species are able to efficiently react with the emisquarate to give the 1,2-squaraine. On the other hand, the amount of emisquarate present in solution depends both on the nature of the alcohol employed (primary, secondary ...) and on the reaction time and temperature. Thus, in the case of poorly reactive arenes and anhydrobases, the amount of 1,2-regioisomer will be low in any case whilst in the case of highly reactive electron rich molecules the condensation regioselectivity can only be controlled by reducing the parasite esterification of the emisquaraine intermediate.

The electrochemical properties were tested for both the symmetric derivative **4.26** (Figure 4–5) and the unsymmetrical one **4.41** (Figure 4–6). The cyclic voltammetries have been performed in a 0.1 M solution of tetrabutylammonium hexafluorophosphate in dichloromethane. The plots show two completely reversible oxidations associated with the oxidation of the two electron rich side groups. The data obtained place the HOMO level for **4.41** at -5.3 eV, significantly below that of the 1,3-squaraines so far employed in our group in organic photovoltaic devices.[28] This is considered beneficial for the increase of the open circuit voltage.

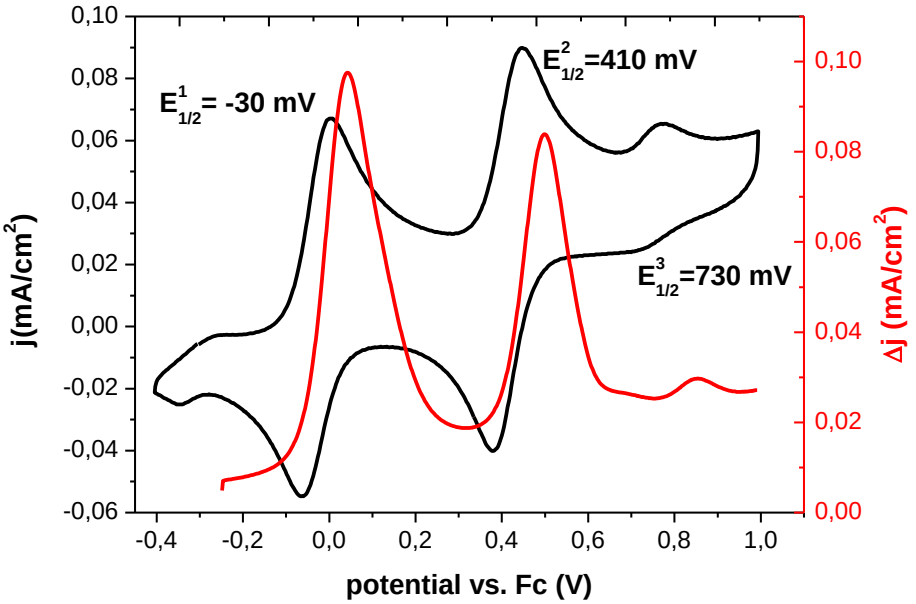

Figure 4–5 Cyclic voltammetry (black) and differential pulse voltammetry (red) for derivative 4.26 in 0.1 M $TBAMPF_6$ in DCM with respect to the Fc/Fc^+ redox couple. The working, counter and pseudoreference electrodes were a Glassy Carbon (GC) disk, a Pt flag, and an Ag/AgCl wire, respectively.

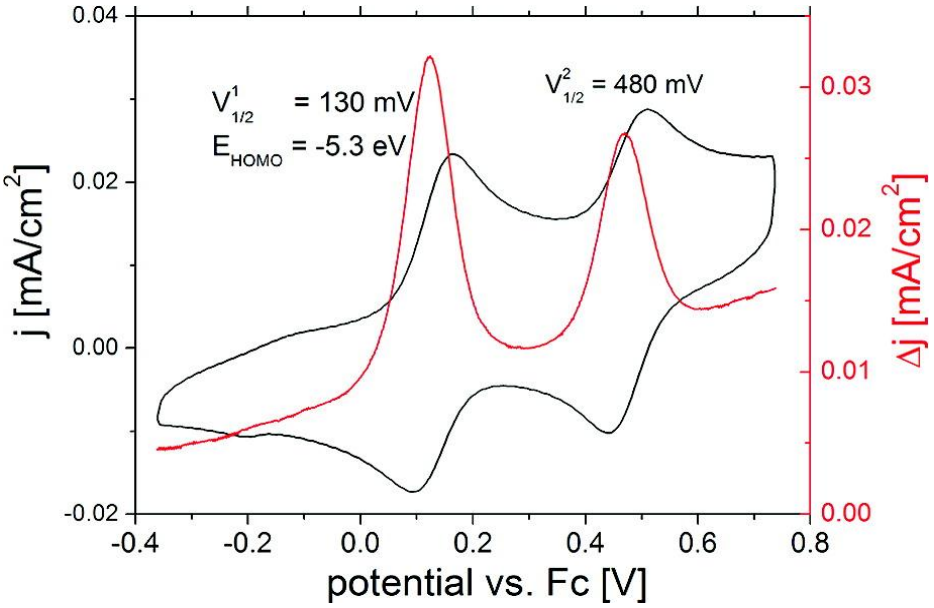

Figure 4–6 Cyclic voltammetry (black) and differential pulse voltammetry (red) for derivative 4.41 in 0.1 M $TBAMPF_6$ in DCM with respect to the Fc/Fc^+ redox couple. The working, counter and pseudoreference electrodes were a Glassy Carbon (GC) disk, a Pt flag, and an Ag/AgCl wire, respectively.

4.2.1 Photophysical characterization of 1,2-squaraines

From the standpoint of the photophysical properties, 1,3-squaraines are reminiscent of cyanines. In the case of 1,2-squaraines, the allowed canonic representations show a

delocalization of the nitrogen lone pair over the carbonyl of the squarate core, thus giving a merocyanine structure.

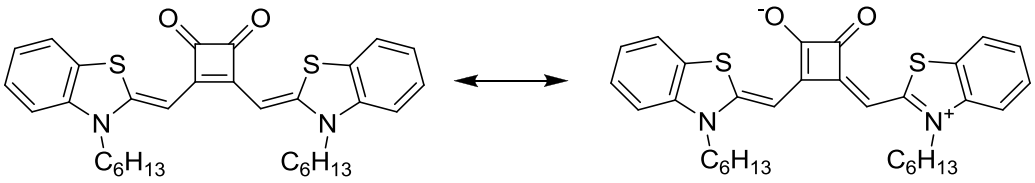

4.26

Scheme 4–17

This is confirmed by the linear correlation between the transition energies and in different solvents and the corresponding Brooker's χ_R values[29] for both the symmetric derivative **4.26** and the unsymmetrical one **4.41** (Figure 4–7).

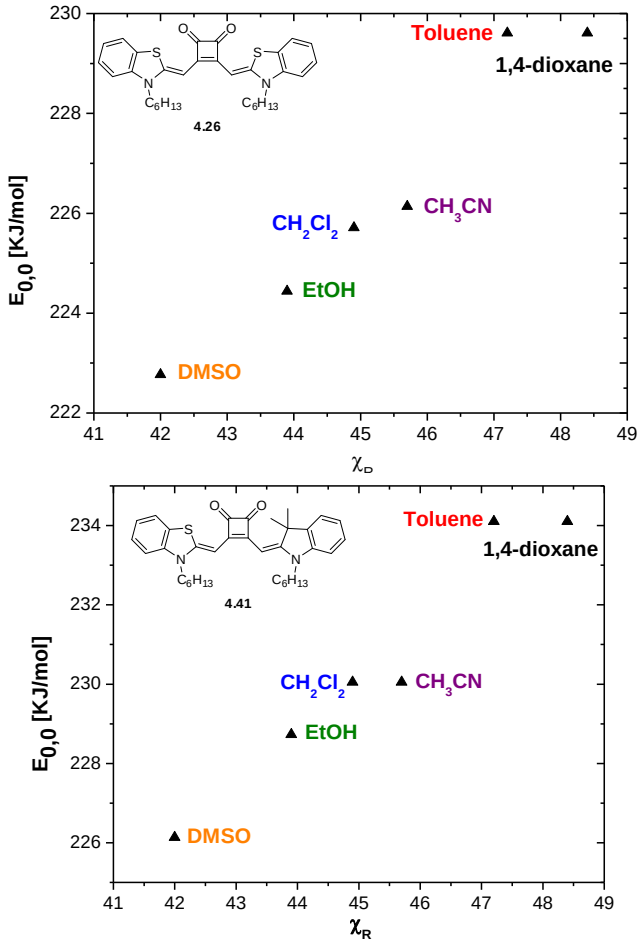

Figure 4–7 Transition energies of 4.26 (left) and 4.41 (right) in six solvents plotted against Brooker's χ_R values in the same solvents.

The absorption, excitation and emission spectra for **4.26** and **4.41** in DCM are shown in Figure 4–8. The bands are sharp and intense and the Stokes shift is small for both derivatives.

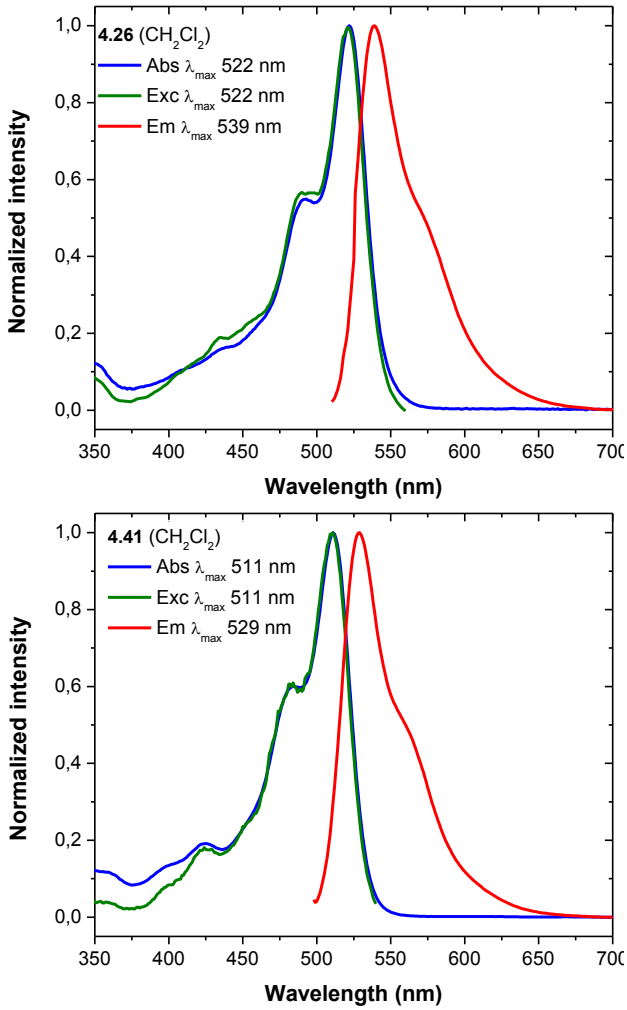

Figure 4–8 Normalized absorption, excitation and emission spectra of 4.26 and 4.41 in DCM.

The absorption and emission spectra in different solvents are shown in Figure 4–9 (squaraine **4.26**) and Figure 4–10 (squaraine **4.41**). A red shift is observed in the absorption and emission spectra with increasing solvent polarity. The molar extinction coefficients ε maintain the same order of magnitude. The fluorescence quantum yields Φ_F are much lower with respect to 1,3-squaraines, and they increase with increasing solvent polarity.

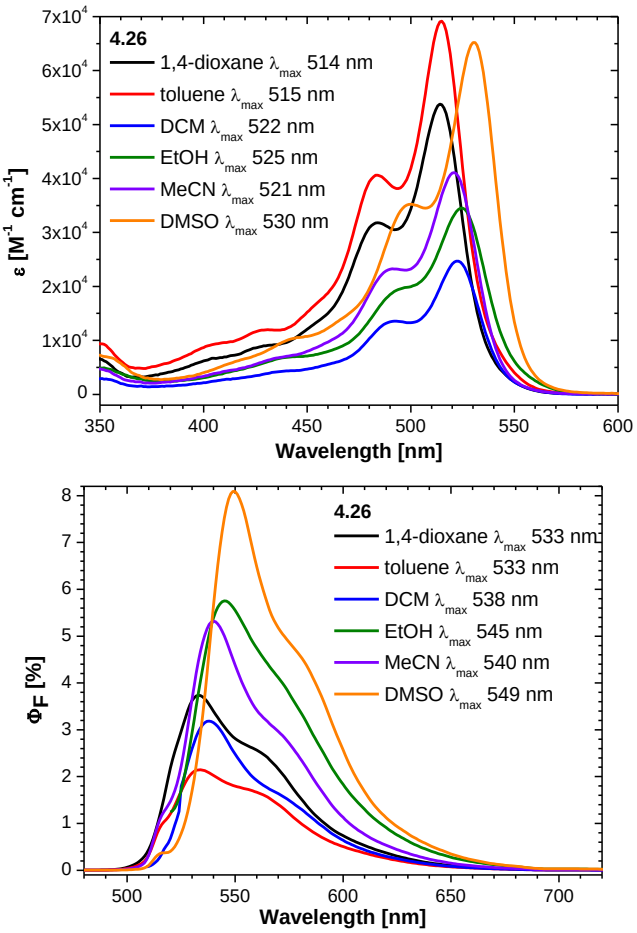

Figure 4–9 Absorption (left) and emission (right) spectra of 4.26 in different solvents.

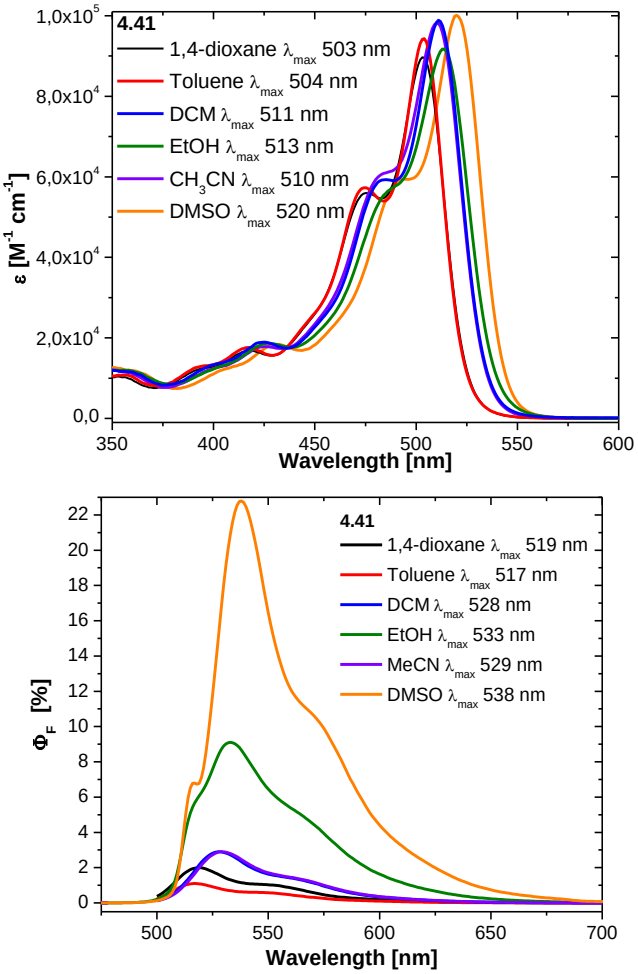

Figure 4–10 Absorption (left) and emission (right) spectra of 4.41 in different solvents.

In order to investigate the reasons of the reduced Φ_F with respect to 1,3-substituted squaraines, the emission and excitation spectra for **4.26** and **4.41** were also recorded in a rigid environment such as 2-methyl-tetrahydrofuran glass at 77 K[13] (Figure 4–11). The bands are narrower (FWHM 10-15 nm vs. 45-50 nm in DCM) and the vibronic replica is more defined.

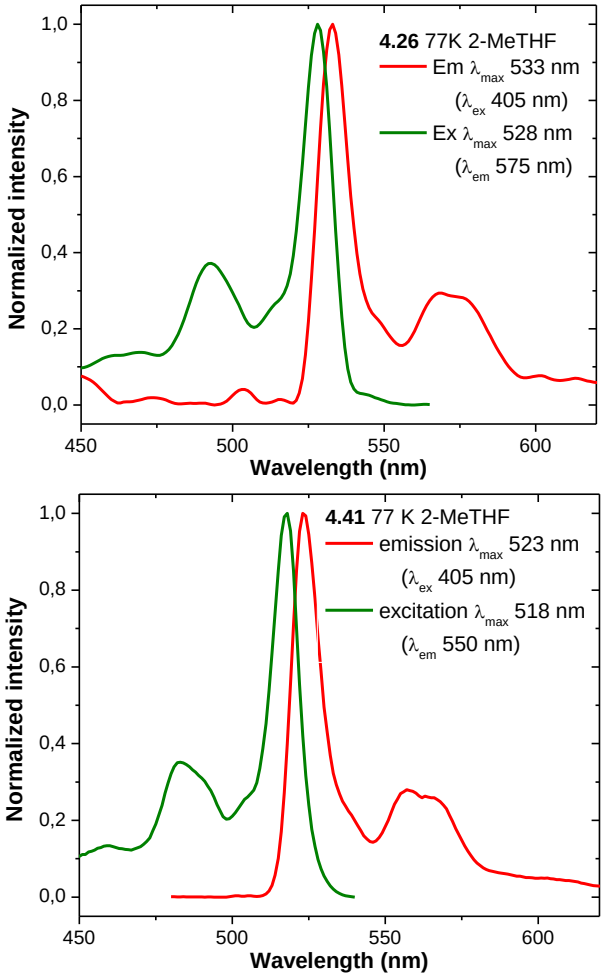

Figure 4–11 Normalized excitation and emission spectra of 4.26 (left) and 4.41 (right) in 2-methyl tetrahydrofuran glass at 77 K.

The fluorescence lifetimes were measured by irradiating the solutions at 405 nm, since this was the available laser with the closest wavelength to the absorption band of the compounds. The logarithmic scale decays are shown in Figure 4–12.

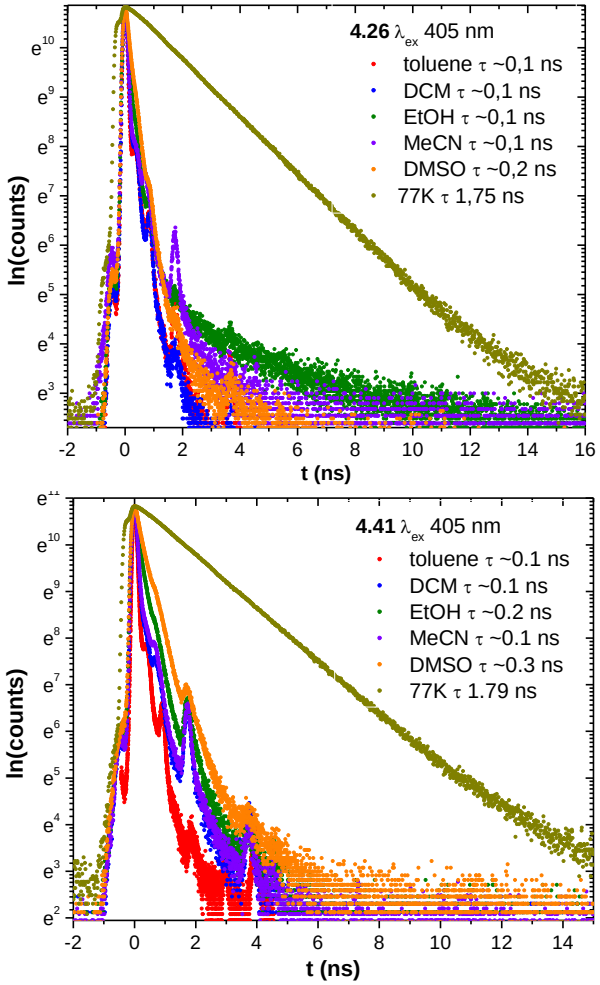

Figure 4–12 Logarithmic scale time-resolved decay of the fluorescence emission intensity of 4.26 (left) and 4.41 (right) recorded at the maximum emission wavelength.

As expected from the Φ_F values, the lifetimes at room temperature are shorter than the ones for the corresponding 1,3-substituted regioisomers.[14] Since the lifetimes are in the same range of the instrument response function (IRF) (Figure 4–13), only the order of magnitude of τ could be estimated from the deconvolution of the emission decay. The IRF was recorded at the same emission wavelength of the laser employed for the fluorescence lifetimes measurements, employing colloidal silica dispersion in water as scattering medium.

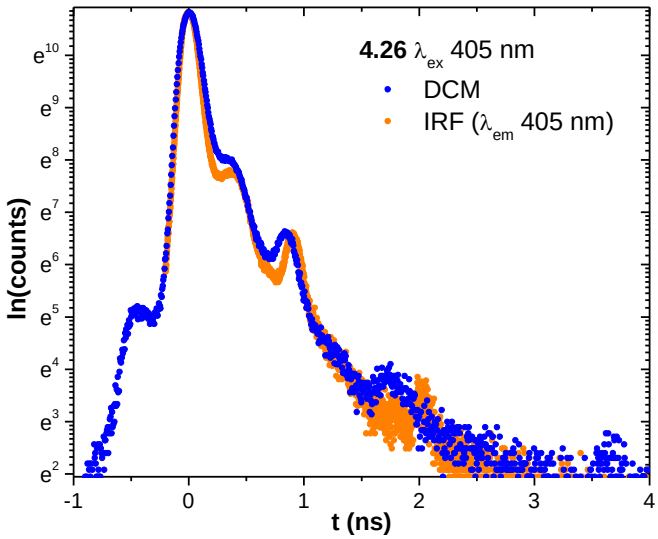

Figure 4–13 Logarithmic scale time-resolved decay of the fluorescence emission intensity recorded at the maximum emission wavelength of 4.26 in dichloromethane and IRF.

The fluorescence lifetimes recorded in a rigid environment such as 2-methyl-tetrahydrofuran glass at 77 K increase of an order of magnitude, a similar increase is expected for the fluorescence quantum yield. The effect is more evident with respect to 1,3-squaraines. The increase in fluorescence lifetime can be associated to the fact that at room temperature the non-radiative decay of excited state of 1,2-squaraines due to vibrations is predominant. Since such vibrations are highly reduced in a rigid environment such as a frozen solvent, the fluorescence lifetime and quantum yield increase.

The spectroscopic data for **4.26** and **4.41** are summarized in Table 4–3 and Table 4–4.

4.26	$\lambda_{abs,max}$[a] /nm (ε[b])	$\lambda_{exc,max}$[c] /nm	$\lambda_{em,max}$[d]/nm (FWHM/nm)	Stokes shift[e] /nm (/cm^{-1})	τ_F/ns	Φ_F[f]
1,4-dioxane	514 (5.38)		529	15 (551)		0.038 ± 0.002
Toluene	515 (6.91)	514	529	14 (514)	~0.1	0.020 ± 0. 001
CH_2Cl_2	522 (2.47)	521	539 (47)	17 (604)	~0.1	0.044 ± 0.001
Ethanol	525 (3.45)	524	543	18 (631)	~0.1	0.044 ± 0.004
MeCN	521 (4.11)	520	538	17 (606)	~0.1	0.033 ± 0.004
DMSO	530 (6.52)		545	15 (519)	~0.2	0.102 ± 0.003
2-MeTHF glass		528	533 (12)		1.75	

[a] Wavelength of absorption band maximum. Error of ±0.5 nm. [b] Molar extinction coefficient, × 10^4 L mol^{-1} cm^{-1}, estimated error ±10%. [c] Wavelength of excitation band maximum. Error of ±0.5 nm. [d] Wavelength of emission band maximum. Error of ±0.5 nm. [e] Stokes shift in both nm and cm^{-1}. Fluorescence quantum yield in air-equilibrated solvent, measured with relative method using Rhodamine B as a standard (Φ_F 0.31 in water), irradiation at 514 nm.[30]

Table 4–3 Spectroscopic data for 4.26.

4.41	$\lambda_{abs,max}$[a] /nm (ε[b])	$\lambda_{exc,max}$[c] /nm	$\lambda_{em,max}$[d]/nm (FWHM/nm)	Stokes shift[e] /nm (/cm^{-1})	τ_F/ns	Φ_F[f]
1,4-dioxane	514 (5.38)		529	15 (551)		0.038 ± 0.002
Toluene	515 (6.91)	514	529	14 (514)	~0.1	0.020 ± 0. 001
CH_2Cl_2	522 (2.47)	521	539 (47)	17 (604)	~0.1	0.044 ± 0.001
Ethanol	525 (3.45)	524	543	18 (631)	~0.1	0.044 ± 0.004
MeCN	521 (4.11)	520	538	17 (606)	~0.1	0.033 ± 0.004
DMSO	530 (6.52)		545	15 (519)	~0.2	0.102 ± 0.003
2-MeTHF glass		528	533 (12)		1.75	

[a] Wavelength of absorption band maximum. Error of ±0.5 nm. [b] Molar extinction coefficient, × 10^4 L mol^{-1} cm^{-1}, estimated error ±10%. [c] Wavelength of excitation band maximum. Error of ±0.5 nm. [d] Wavelength of emission band maximum. Error of ±0.5 nm. [e] Stokes shift in both nm and cm^{-1}. Fluorescence quantum yield in air-equilibrated solvent, measured with relative method using Rhodamine B as a standard (Φ_F 0.31 in water), irradiation at 514 nm.[30]

Table 4–4 Spectroscopic data for 4.41.

The enhanced fluorescence of 1,2-squaraines in a rigid environment has been studied further with the preparation and the photophysical characterization of spin-coated films of the dyes at different concentrations in a poly(methyl methacrylate) (PMMA) matrix.

A solution of PMMA (average MW: 35000) at the concentration of 25mg/mL in DCM and a solution of the squaraine **4.26** or **4.41** at the concentration of 5 mg/mL in the same solvent have been mixed together in order to obtain the %wt. concentrations of squaraine in the film of 0.25%, 2.5%, 25%, 50% and 75%. The films have been prepared by spin-coating the mixed solutions on glass at 2000 rpm for 40 seconds. Neat films of the squaraines (100% wt.) have also been prepared with the same procedure.

The absorption spectra of the films prepared with the symmetric 1,2-squaraine **4.26** (Figure 4–14) show the presence of aggregates at high concentrations, thus the films prepared with PMMA are not the optimal object of study to determine the behavior of this dye in a rigid environment.

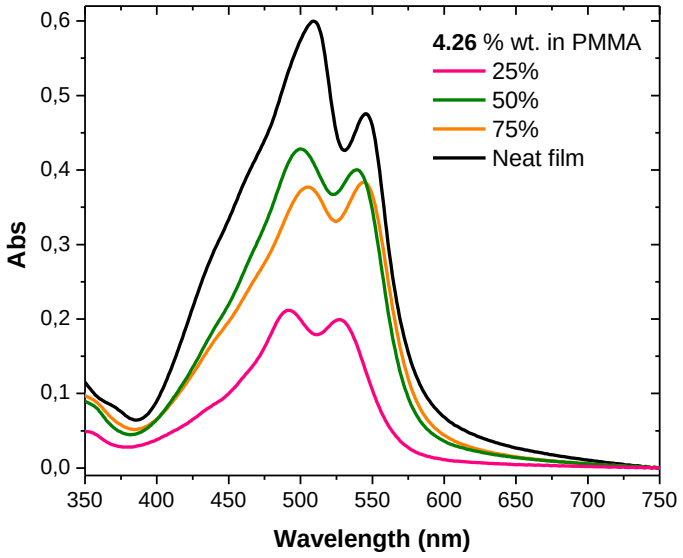

Figure 4–14 Absorption spectra of spin-coated 4.26 films at different concentrations in PMMA.

The absorption spectra of the unsymmetrical 1,2-squaraine **4.41** films show a red shift of the absorption maxima with increasing dye concentration due to the different polarity of the local environment (Figure 4–15). Unlike the symmetric derivative **4.26**, the band shape doesn't change, indicating that no aggregates are formed.

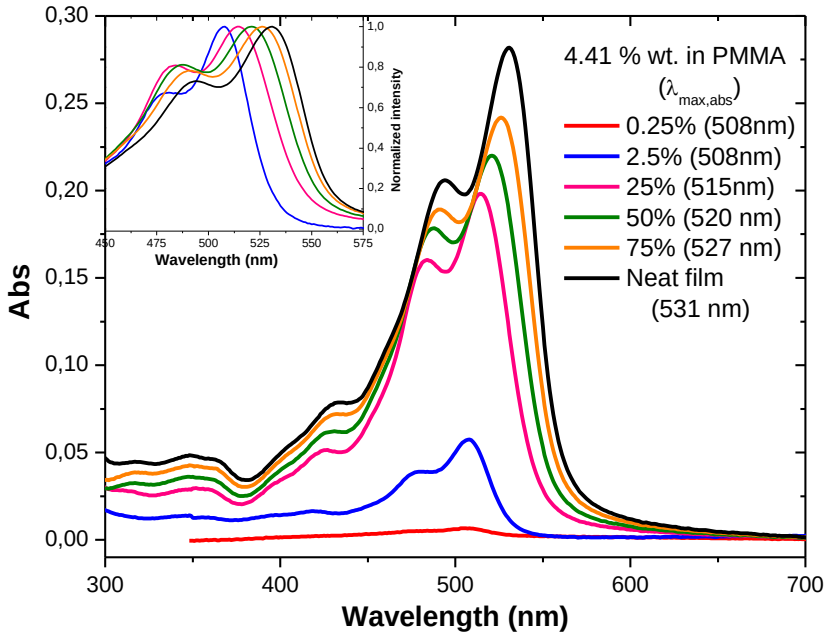

Figure 4–15 Absorption spectra of spin-coated 4.41 films at different concentrations in PMMA. The inset graph shows the normalized spectra.

Interestingly, the emission spectra of the unsymmetrical 1,2-squaraine **4.41** films at high concentrations show a new emission band at lower energy and at lower intensity

(Figure 4–16). Since the absorption spectra show that the dye is in the monomeric form at all concentrations, it is assumed that the new band is the excimer emission.

A preliminary confirmation of the excimer formation comes from the excitation spectra for the same film at different emission wavelengths, which are superimposable (Figure 4–17).

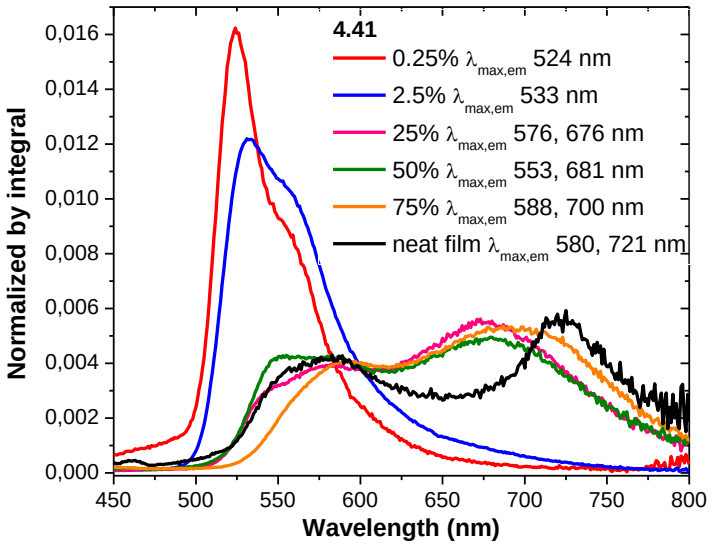

Figure 4–16 Emission spectra of spin-coated 4.41 films at different concentrations in PMMA. The intensity is normalized by the emission band integral.

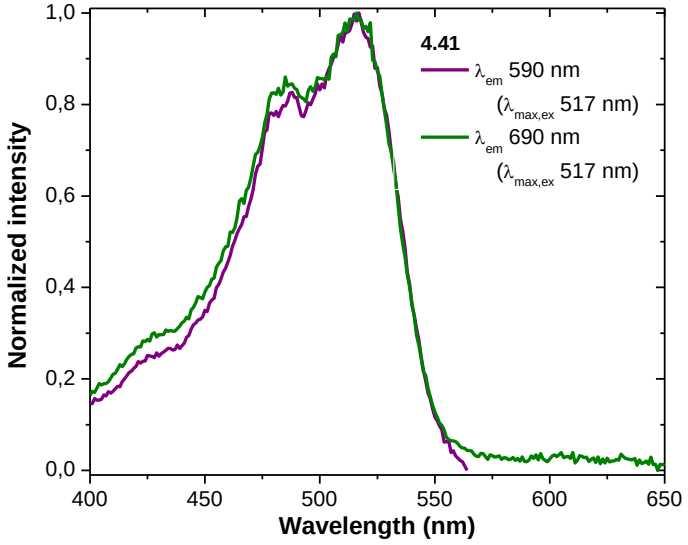

Figure 4–17 Normalized excitation spectra of the spin-coated 4.41 50% wt. in PMMA film at different emission wavelengths.

A time-resolved spectroscopic study has been planned to study the excimer of **4.41** both in concentrate solution and in the solid state (single crystal and film in PMMA).

4.3 Functionalized squaraines for active targeting

Although widely used to treat some cancers and age-related macular degeneration, the drugs used in photodynamic therapy (PDT) display poor chemical selectivity toward the intended targets, and uptake by cells most likely arises from passive, diffusional processes. Instead, the specific irradiation of the target tissues and the formation of the toxic species *in situ* are the primary factors that modulate the selectivity in the present mode of PDT.

As previously mentioned, targeting strategies have been shown to increase the selective uptake and/or binding of the photosensitizer to several cancer cell types.[31] There have also been reports of selective targeting subcellular compartments, including the mitochondria.[32] The biochemical usage of conjugated photosensitizers with appropriate targeting approaches have led to third-generation photosensitizers and some of the most promising results to date.

Conjugation in this sense may be defined as the covalent attachment of the principal molecular backbone to a second molecular moiety which confers beneficial property on the molecular ensemble. Some examples comprise the pegylation of *m*-THPC by the attachment of polyethylene glycol residues to the four phenolic functions to improve water solubility and targeting ability,[33] the functionalization of chlorins with estradiol to improve selectivity against breast carcinoma cells over expressing the estrogen receptors,[34] and the functionalization of chlorins with oligonucleotides which form specific complexes with suitable single-stranded and double-stranded polynucleotides, and site-direct photodamage to nucleic acid.[35]

The wide flexibility of the squaraine structure allows the insertion of several reactive groups (see Section 4.1) for the conjugation of targeting agents through ether bond formation, carboxylic acid derivatization to esters and amides, click chemistry with the formation of a triazole, alkylation to give quaternary ammonium salts.

During this Thesis work the attention was focused on the insertion of a vitamin (choline) and a sugar (galactose) as active agents for their pronounced targeting abilities and easiness of functionalization.

4.3.1 Choline functionalization

Abnormal choline metabolism is emerging as a metabolic hallmark that is associated with oncogenesis and tumor progression. In particular, high levels of phosphocholine (PCho) and total choline (tCho) have been found in a variety of cancers[36, 37] and cancer cell lines.[38, 39]

Choline metabolism occurs through a cascade of three enzymes in the Kennedy pathway resulting in the biosynthesis of phosphatidylcholine. The control of subcellular distribution of compartments involved in choline metabolism has been shown to be implicated in the regulation of metabolism itself.[40] Several enzymes in choline metabolism, such as choline transporter-like protein 1 (CTL1), choline kinase-α (CHKα), CTP:phosphocholine cytidylyltransferase (CCT), phosphatidylcholine-specific phospholipase D (PC-PLD) and PC-PLC, are overexpressed and/or activated in cancer and can potentially be used as prognostic markers.[41] the main steps of phospholipid biosynthesis pathway take place in the endoplasmic reticulum (ER) and in the mitochondrial membranes at contact regions with ER, known as mitochondria-associated membranes (MAM)[42].

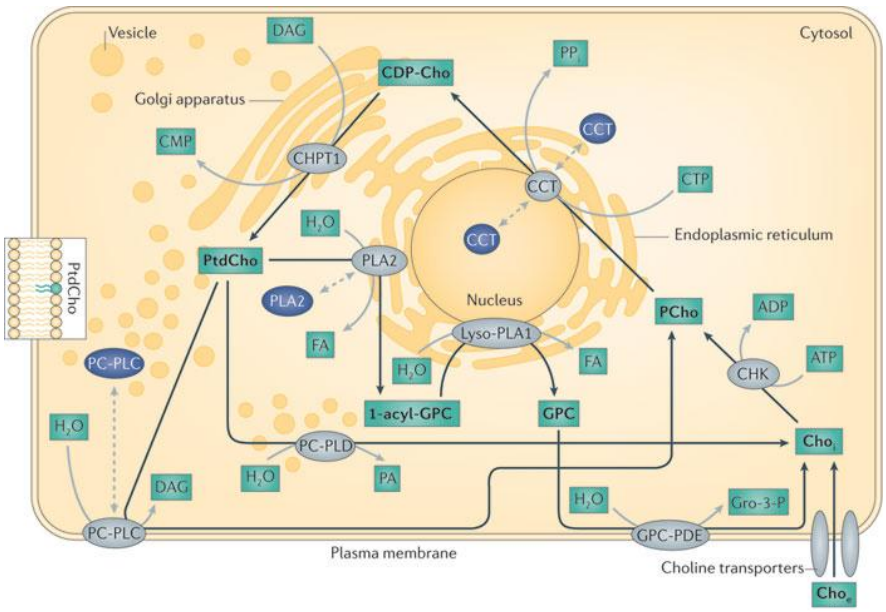

Figure 4–18 The major enzymes involved in choline phospholipid metabolism in the cell. Black arrows represent the choline metabolism pathway. CCT, CTP: phospho-choline cytidylyltransferase; CDP-Cho, cytidine diphosphate-choline; Cho_e, extracellular free choline; Cho_i, intracellular free choline; CHPT1, diacylglycerol cholinephosphotransferase 1; CMP, cytidine monophosphate; CTP, cytidine triphosphate; FA, fatty acid; GPC, glycerophosphocholine; GPC-PDE, glycerophosphocholine phosphodiesterase; Gro-3-P, glycerol-3-phosphate; Lyso-PLA1, lyso-phospholipase A1; PCho, phosphocholine; PLA2, cytoplasmic phosphatidylcholine-specific phospholipase A2; PPi, diphosphate.

Choline-containing compounds can be detected by non-invasive magnetic resonance spectroscopy (MRS), or positron emission tomography (PET) by means of suitable radiotracers such as [^{11}C]-choline,[43] ENREF 39 thus increased levels of these compounds provide a non-invasive biomarker of transformation, staging and response to therapy. For example, the increased expression and activity of CHKα make it an attractive molecular target for anticancer therapy,[44] and CHKα inhibition has exhibited significant antiproliferative activity of cancer cells.[45]

An alternative strategy consists in taking advantage of the increased choline metabolism in cancer cells so that choline-containing compounds are preferentially taken up with respect to normal cells. The fluorescent probe **4.42** has been employed in the study of the subcellular localization of choline in cancer cells (Figure 4–19).[46]

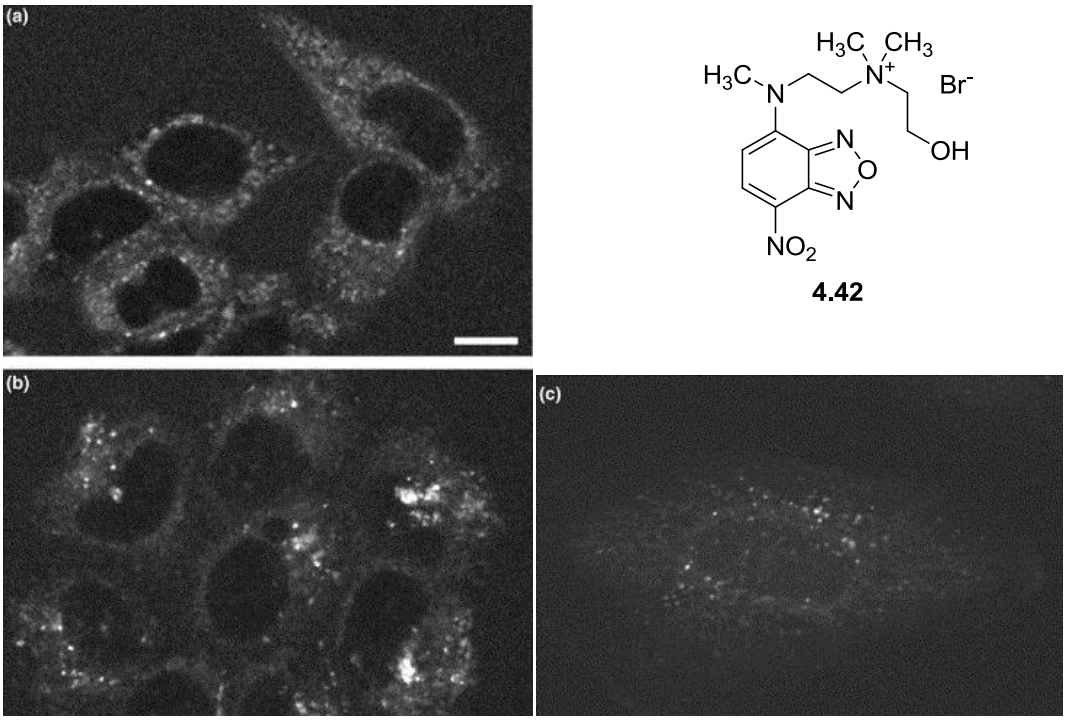

4.42

Figure 4–19 Confocal fluorescence image of 4.42 in carcinoma and normal breast epithelial cells. (a) sensitive carcinoma MCF-7 cells; (b) multidrug resistant carcinoma MCF-7/DX cells; (c) normal immortalized MCF10A cells (x3 intensity). Scale bar: 10 μm.

In particular, **4.42** was found to predominantly localize in the endoplasmic reticulum of drug-sensitive MCF-7 cells and in the Golgi apparatus of multidrug resistant MCF-7/DX cells. This difference in distribution suggests that multidrug resistant cells have changed choline metabolic pathways. Moreover, **4.42** entered almost exclusively into cancer cells and not in normal cells, a result that confirms *in vivo* imaging by [^{11}C]-choline of several human tumors.

The same strategy of functionalization for **4.42** has been employed for the synthesis of a choline-functionalized squaraine starting from the post-functionalizable derivative **4.14**. The cationic choline functionality should also impart water solubility to the final sensitizer, which can thus be delivered in the free form without the common vehiculating organic solvents (DMSO, EtOH).

The first synthesis strategy consisted in the preparation of a choline-functionalized squaraine with general structure **4.3** starting from the post-functionalizable derivative **4.21** (Scheme 4–18). The squaraine **4.44** has not been obtained due to the poor solubility

of the reagent in the reaction solvent (methyl ethyl ketone, MEK); the steric hindrance of the bulky quaternary salt on the side chain should also be taken into account.

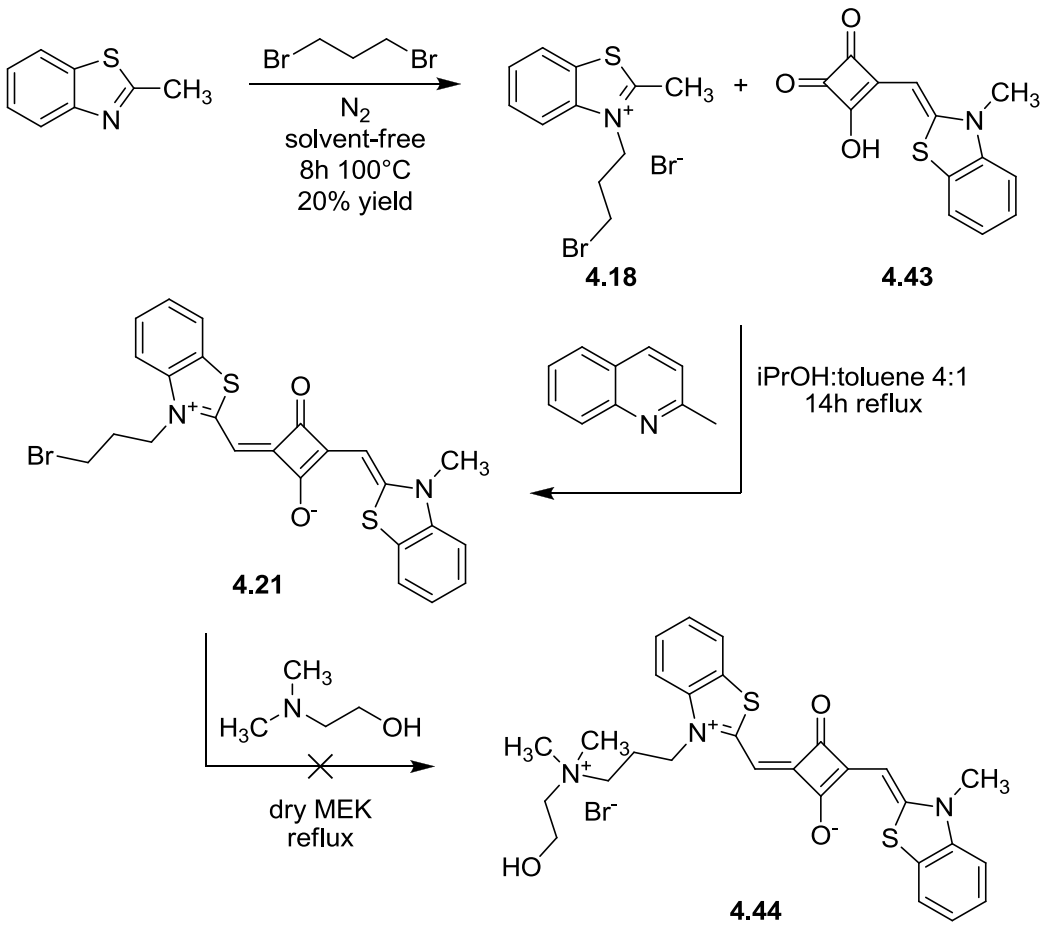

Scheme 4–18

A new synthesis strategy has been developed in order to prepare a choline-functionalized squaraine with general structure **4.2** starting from the post-functionalizable derivative **4.14** (Scheme 4–19). The side group containing choline is an indolenine derivative instead of benzothiazole so that the squaraine obtained is unsymmetrical. The indolenine derivative has been chosen over benzothiazole due to synthetic availability and for a higher solubility of the final product. The squaraine condensation has been performed in 2-propanol:toluene 4:1 mixture in azeotropic distillation conditions with a non-nucleophilic base such as quinaldine in order to avoid nucleophilic addition of the base on the alkyl bromide functionality. The choline-functionalized squaraine **4.46** has been obtained in good yield from the quaternarization of 2-(dimethylamino)ethanol on the alkyl bromide on squaraine **4.14**.

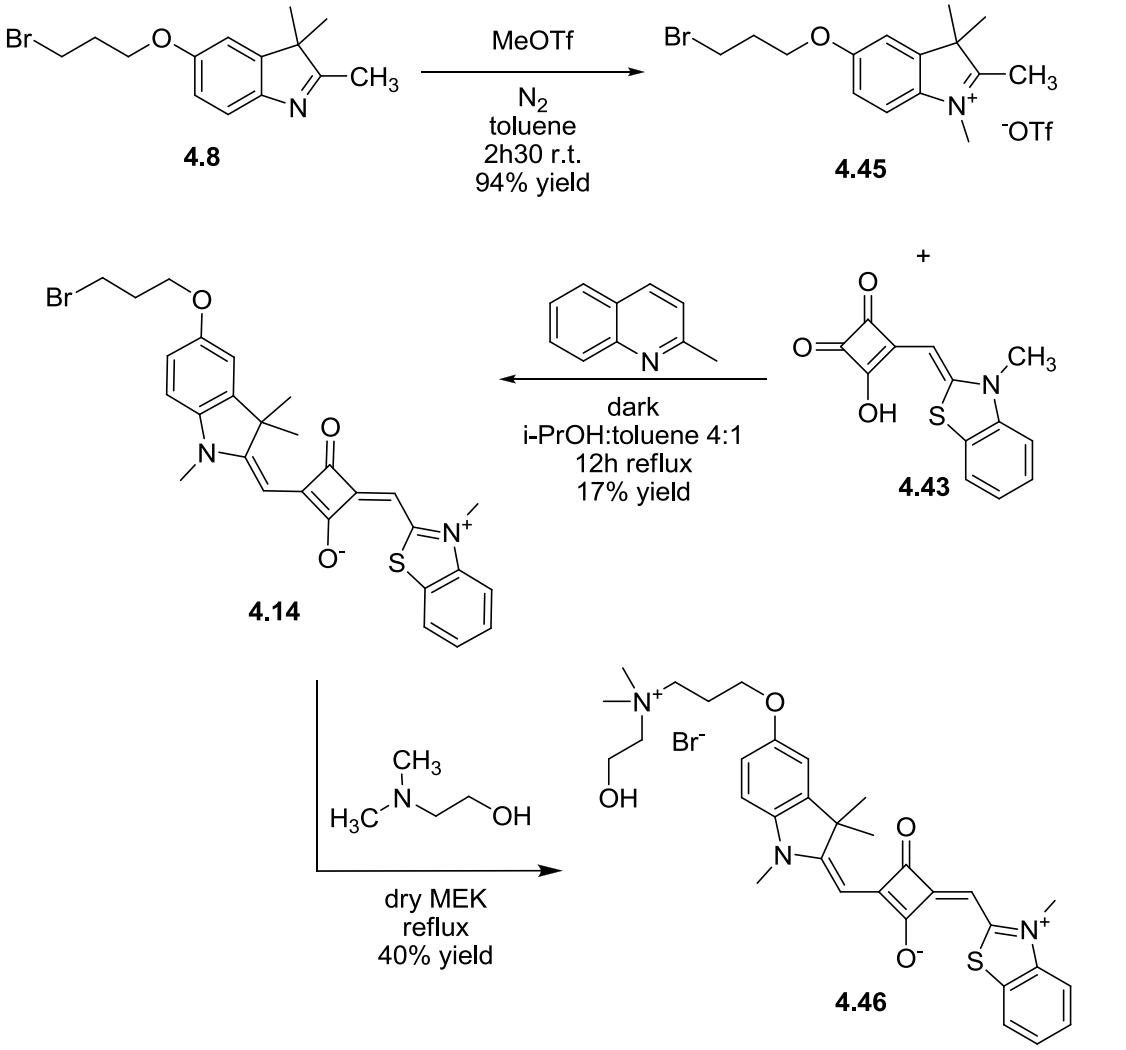

Scheme 4–19

The unsymmetrical squaraine **4.46** presents strong absorption and emission bands in the Vis-NIR region, as shown in Figure 4–20. The absorption, excitation and emission maxima are blue-shifted of about 15 nm with respect to the symmetric derivative **4.1**. This can be attributed to the presence of one less electron-rich fragment with respect to benzothiazole, such as indolenine. Also the other differences in the photophysical properties can be ascribed to the different molecular structure. In a more polar solvent such as acetonitrile the emission band is slightly blue-shifted and the fluorescence lifetime decreases, as well as the fluorescence quantum yield, while in 2-methyl-tetrahydrofuran glass at 77 K[13] the bands are narrower and the vibronic replica is more defined (Figure 4–21).

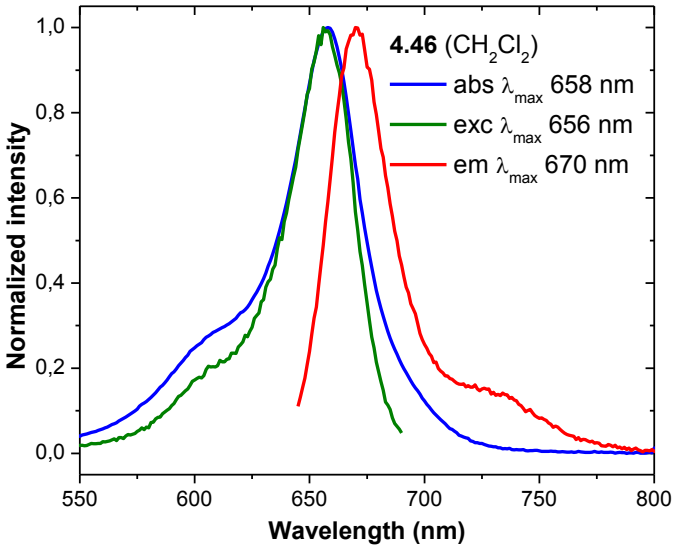

Figure 4–20 Normalized absorption, excitation and emission spectra of 4.46 in DCM.

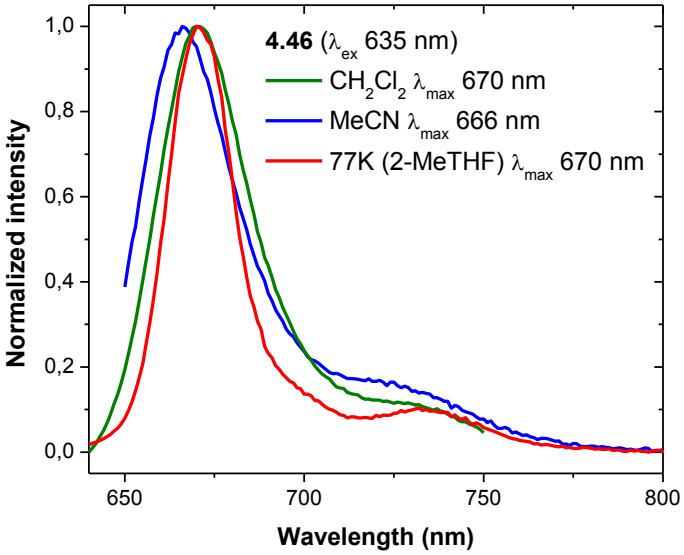

Figure 4–21 Normalized emission spectra of ER-121 in different solvents.

The fluorescence quantum yield and lifetime measured in absence of oxygen show a smaller increase with respect to **4.1**, showing that the excited state for this squaraine is less deactivated in the presence of oxygen (Figure 4–22).

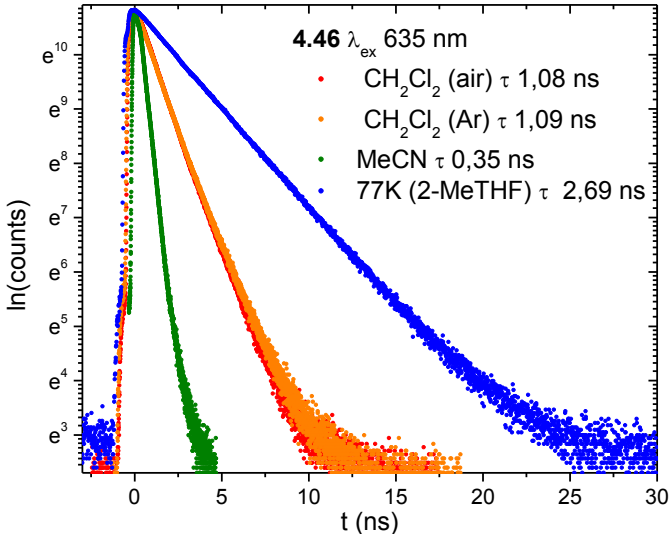

Figure 4–22 Logarithmic scale time-resolved decay of the fluorescence emission intensity of 4.46 recorded at the maximum emission wavelength.

The spectroscopic data for **4.46** are summarized in Table 4–5.

4.15	$\lambda_{abs,max}$[a] /nm (ε[b])	$\lambda_{exc,max}$[c] /nm	$\lambda_{em,max}$[d]/nm (FWHM/nm)	Stokes shift[e] /nm (/cm^{-1})	τ_F/ns	Φ_F[f]
CH_2Cl_2	658 (1.1)	656	670 (31)	12 (272)	1.08 (air) 1.09 (Ar)	0.73 (air) 0.79 (Ar)
MeCN	653	651	667 (32)	15 (345)	0.35 (air)	0.25 (air) 0.26 (Ar)
2-MeTHF glass			670 (22)		2.69	

[a] Wavelength of absorption band maximum. Error of ±0.5 nm. [b] Molar extinction coefficient, × 10^5 L mol^{-1} cm^{-1}, estimated error ±10%. [c] Wavelength of excitation band maximum. Error of ±0.5 nm. [d] Wavelength of emission band maximum. Error of ±0.5 nm. [e] Stokes shift in both nm and cm^{-1}. Fluorescence quantum yield in air-equilibrated solvent, measured with relative method using Zinc 2,9,16,23-tetra-tert-butyl-29*H*,31*H*-phthalocyanine in toluene as a standard (ΦF 0.30), irradiation at 630 nm.[15]

Table 4–5 Spectroscopic data for 4.46.

4.3.2 Galactose functionalization

Since the role of saccharides in cell recognition, metabolism, and cell labeling is well-established, the conjugation of saccharides to drugs is an active area of research. Thus, one goal in the use of saccharide-drug conjugates is to impart a greater specificity toward a given cell type or other targets.

Galactose-functionalized prodrugs derivatives **4.47** and **4.48** have shown enhanced cell permeation in pituitary GH_3 cells (Figure 4–23), and the level of the free drug released is significantly higher than following the administration of free arginine .[47]

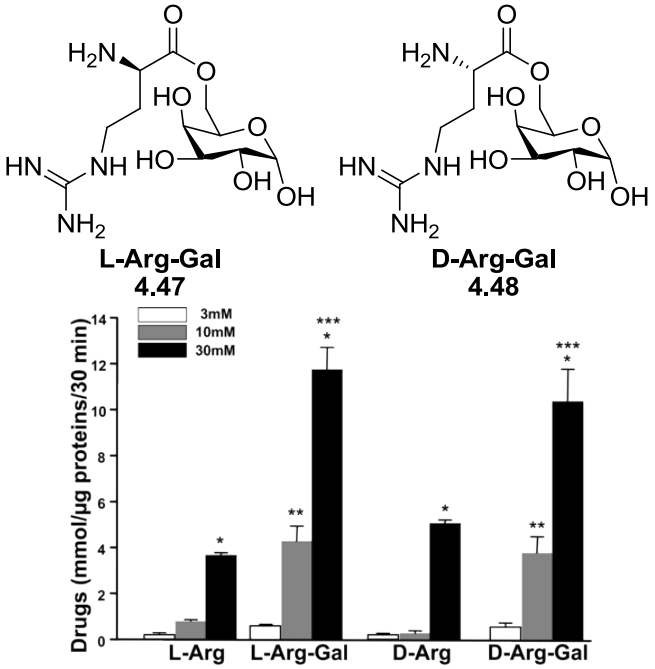

Figure 4–23 Detection of intracellular drug concentrations after incubation with L-arginine, 4.47, D-arginine, and 4.48 in pituitary GH_3 cells. The graph reports the amount of drugs measured in cell homogenates after 30 min incubation at 3, 10, and 30 mM.

Non-hydrolyzable saccharide–porphyrin conjugates have been prepared from tetra(pentafluorophenyl)porphyrin and the thio- derivative of the sugar. These photosensitizers have shown selective uptake to several cancer cells.[48] Different malignant cell types take up one type of saccharide–porphyrin conjugate preferentially over others, for example human breast cancer cells (MDA-MB-231) absorb the tetraglucose–porphyrin conjugate **4.49** over the corresponding galactose derivative **4.50** (Figure 4–24). The conjugates induce cell death by necrosis and apoptosis after irradiation.

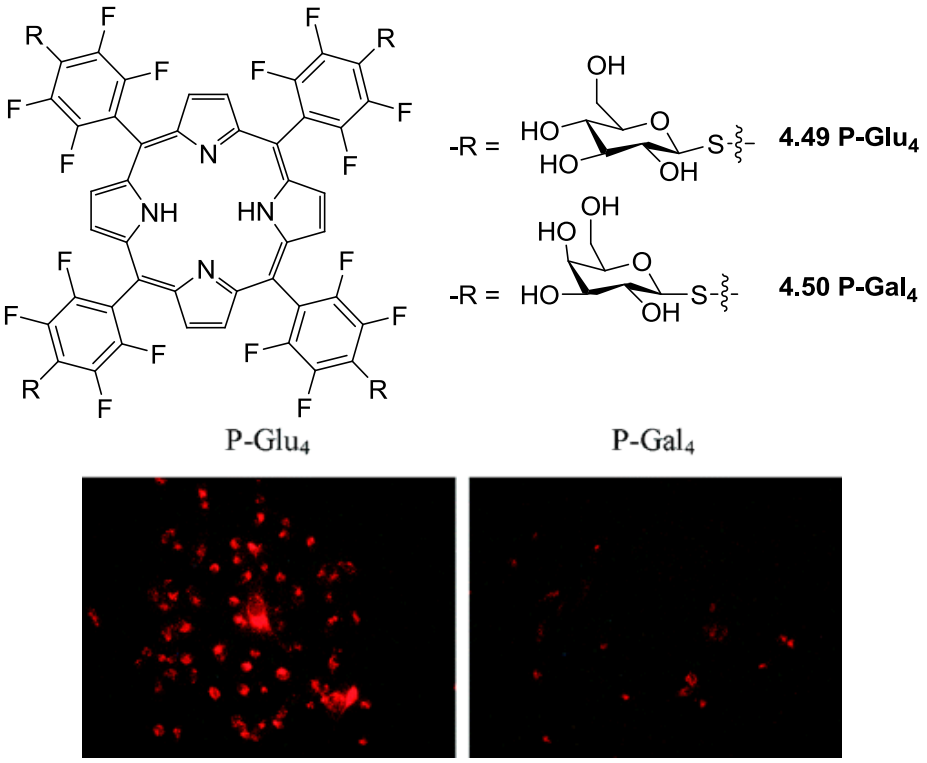

Figure 4–24 4.49 is preferentially taken up by human breast cancer MDA-MB-231 cells over 4.50. Cells were treated with 10 µM sensitizer for 24 h, rinsed, and fixed with a 4% paraformaldehyde solution. The extent of conjugate uptake by these cells is 2.3:1 for 4.49:4.50.

The commercially available diacetone-D-Galactose **4.51** has been chosen as the protected galactose functionality since the deprotection conditions are compatible with the squaraine substrate.

The first synthesis strategy consisted in the preparation of a galactose-functionalized squaraine with general structure **4.3** *via* Steglich esterification of the post-functionalizable squaraine **4.24** (Scheme 4–20). The squaraine **4.52** has not been obtained.

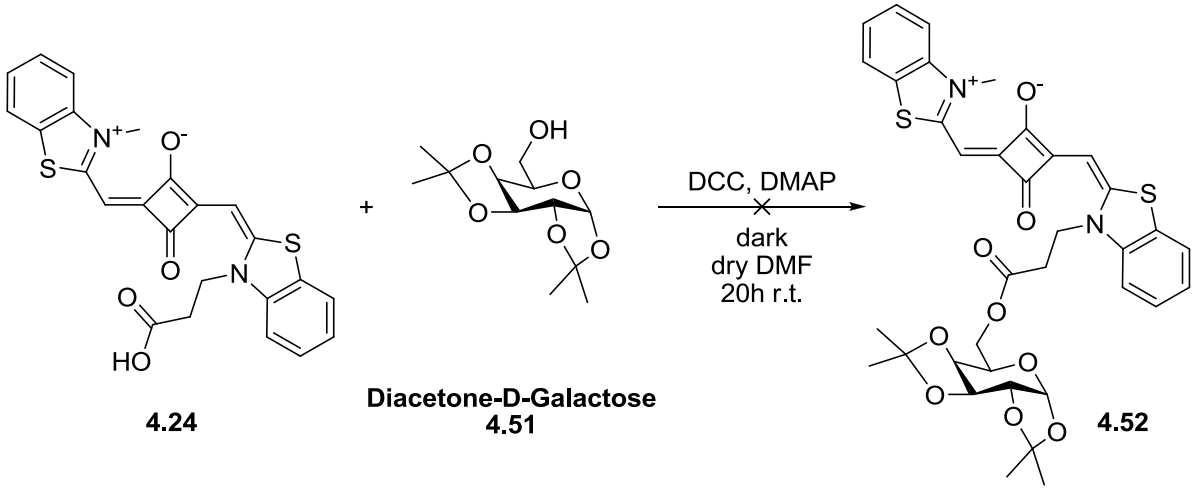

Scheme 4–20

A new synthesis strategy has been developed in order to prepare a galactose-functionalized squaraine with general structure **4.2**, with the insertion of the protected galactose on the indolenine derivative **4.5** for easiness of purification rather than on the post-functionalizable squaraine. The alkylation of the hydroxyl group with diacetone-D-Galactose tosilate **4.53** gave the product **4.54** in very low yield (Scheme 4–21).

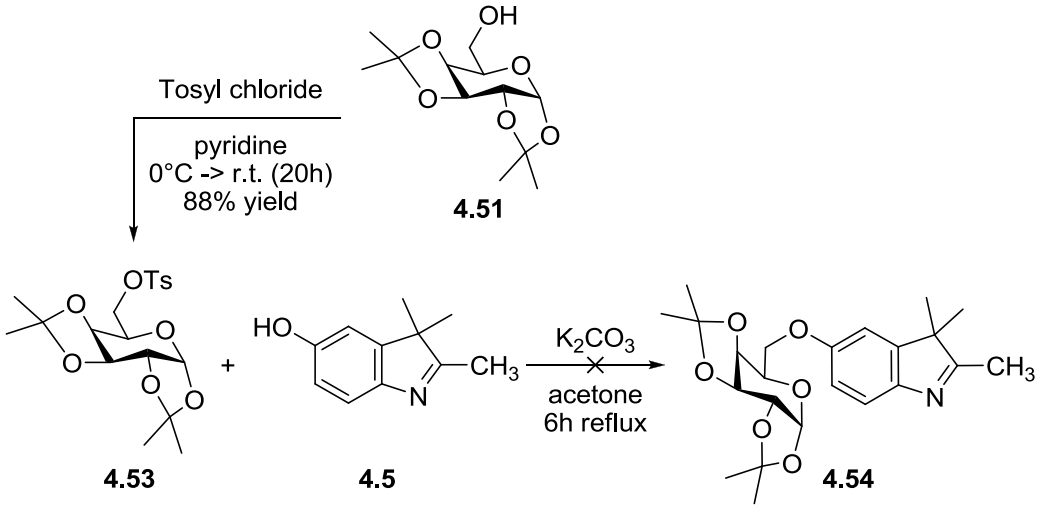

Scheme 4–21

On the contrary, the protected galactose has been successfully inserted on the indolenine derivative **4.5** *via* Mitsunobu reaction (Scheme 4–22). The galactose-indolenine conjugate **4.54** has been alkylated with iodomethane at room temperature, the indoleninium salt **4.55** obtained has been condensed with benzothiazole emisquaraine **4.43** in pyridine to give the protected galactose-functionalized squaraine

4.56. The deprotection of the galactose functionality has been performed by hydrolysis with trifluoroacetic acid.[47]

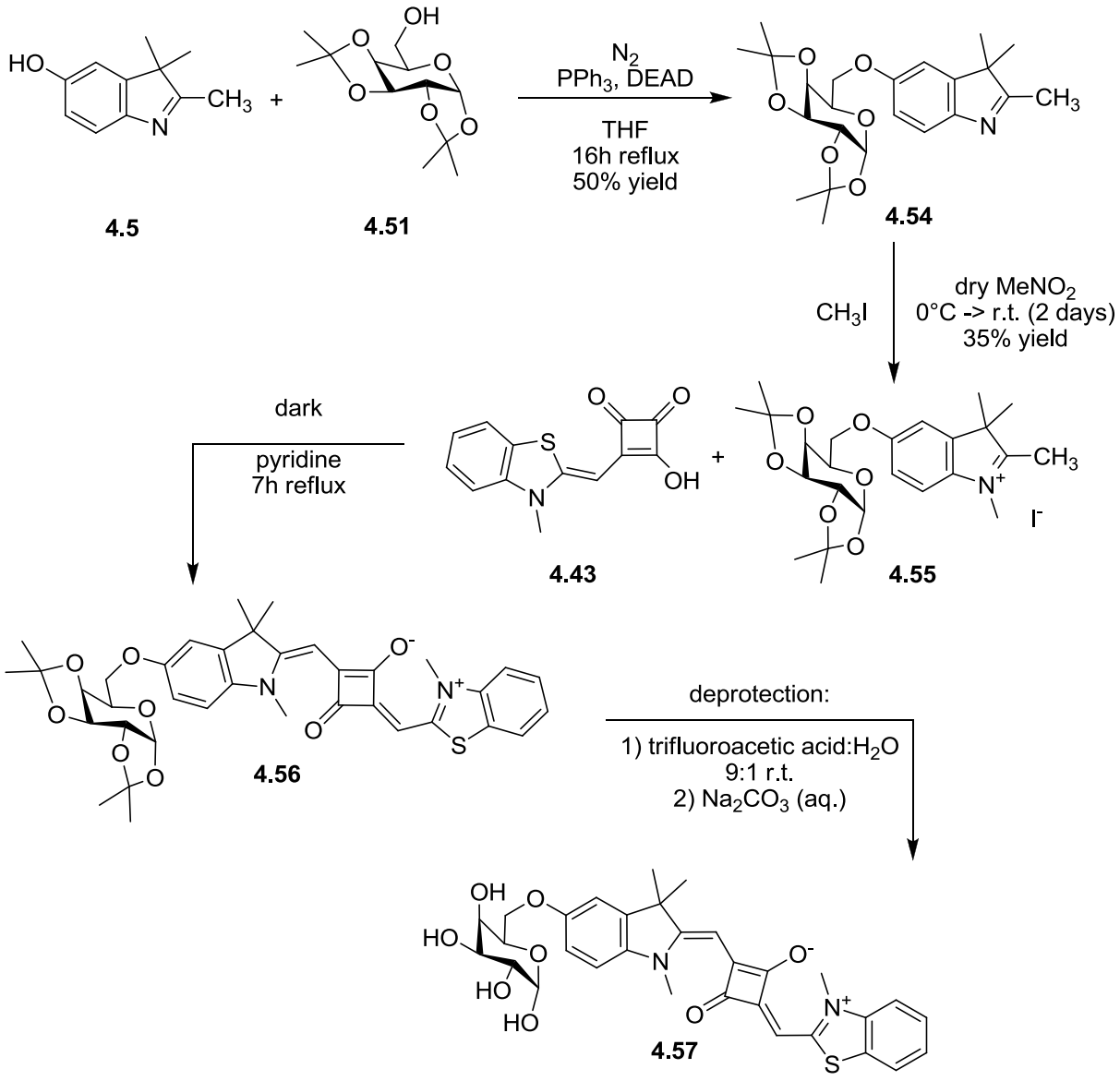

Scheme 4–22

4.4 Fullero-squaraine dyad

The potential applications of fullerenes and their derivatives have increased in recent years, particularly in the fields of biology and medicine, where they can be employed as DNA photocleaving agents, anti-HIV protease inhibitors, antibacterial agents.[49] Due to their extended π-conjugation they absorb in the UV-Vis region, have a high triplet yield and can generate reactive oxygen species upon illumination, suggesting a possible role of fullerenes in photodynamic therapy.[50]

The type II mechanism, that is the energy transfer to the excited triplet state of C_{60} to ground state oxygen is predominant in a non-polar environment.[51] In a polar environment, especially in the presence of physiological concentration of reducing agents such as NADH, the type I mechanism is also possible, with the photogeneration of superoxide anion radical $O_2^{-\bullet}$.[52]

Fullerenes and their derivatives have also been successfully employed in anticancer PDT. Since fullerenes are non-fluorescent, the intracellular uptake and subcellular localization has been evaluated with radiolabeled derivatives.[53] The first demonstration of photodynamic action in cancer cells was in 1993 when Tokuyama used carboxylic acid functionalized fullerenes at 6 μM and white light to produce growth inhibition in human HeLa cells.[54]

To facilitate their medicinal and therapeutic applications in biological systems, solubilization of fullerenes has been the primary research target of many investigators. The disaggregation and solubilization in water or polar environment has been increased by either introducing water-soluble substituents or mixing the fullerenes with solubilizing agents. As a result of these investigations, water-soluble fullerenes (C_x: x = 60 or 70) have attracted attention recently as potential photosensitizers for PDT.

The most common water-soluble derivatives obtained from functionalization are carboxylic acid derivatives, glicoconjugates, quaternary pyrrolidinium cations (Figure 4–25)[55]. Mono-substituted C_{60} derivatives show in general higher photocytotoxicity.

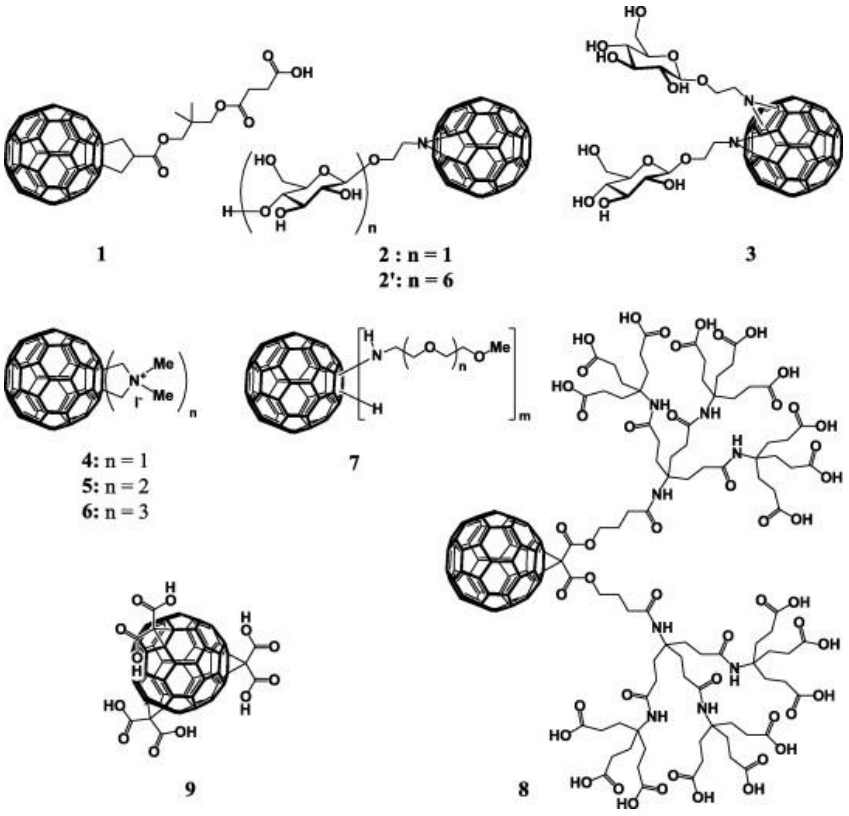

Figure 4–25 Examples of water-soluble fullerene derivatives.

The water solubility may also be achieved by addition of solubilizing agents such as the encapsulation in cyclodextrins[56] and calixarenes,[57] block copolymer micelles[58] and liposomes.[59]

The insertion of light-harvesting chromophores in the visible region both directly linked to C_{60} and in the solubilizing agent improve the photodynamic activity for irradiations in this spectral region, opening the way to deep theranostic applications. Some examples include fullerene-bis-pyropheophorbide *a* derivatives,[60] and porphyrin–C_{60} dyads.[61, 62]

Following this approach, a fullero-squaraine dyad has been designed in order to conjugate the light-harvesting ability of the squaraine in the NIR region with the high photodynamic activity of fullerene.

Moreover, such compound would also find application in optical limiting, in bulk-heterojunction solar cells to improve the interface between donor and acceptor, and in organic photodetectors as preferential exciton splitting site.

The most suitable functionalization strategy for the fullero-squaraine dyad formation is the fulleropyrrolydine *via* the decarboxylation route (Scheme 4–23).[63] A mixture of *N*-methylglycine, or sarcosine, **4.58** and an aldehyde **4.59** are refluxed in dichlorobenzene in the presence of C_{60}, affording the mono-*N*-methylpyrrolidine derivative **4.60** in high yield.

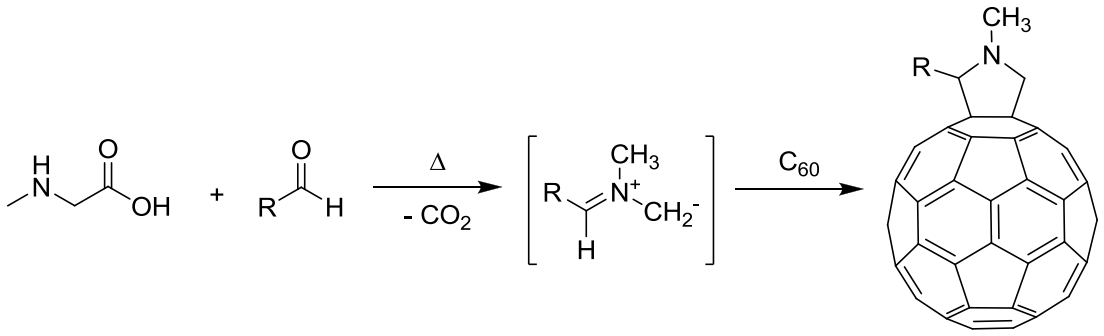

4.58 **4.59** **4.60**

Scheme 4–23

The strategy has been chosen since an aldehyde functionality can be readily inserted in the squaraine structure without affecting the electronic properties. The post-functionalization has been performed through palladium-catalyzed coupling on the arylic halogen derivative **4.13**.

A Sonogashira coupling reaction with 4-ethynylbenzaldehyde **4.61** was attempted (Scheme 4–24), by analogy with the phthalocyanine-C_{60} dyad by Torres,[64] but the strategy was not successful. The coupling reaction was also attempted on the indolenine derivative **4.6**, but the product could not be isolated from the reaction mixture due to the low yield.

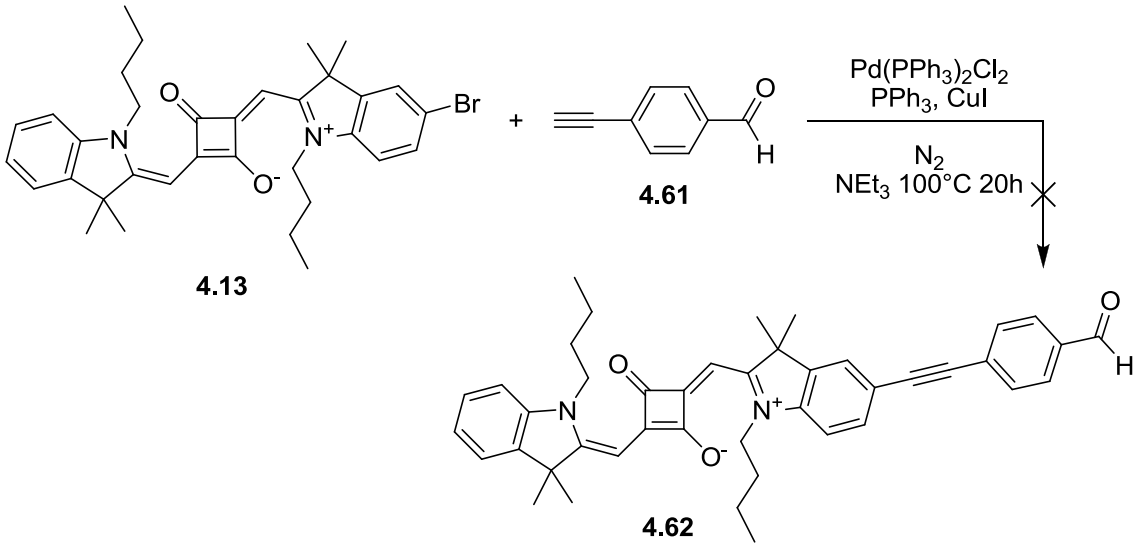

Scheme 4–24

The Suzuki coupling of the same post-functionalizable squaraine **4.13** with 5-formylthiophen-2-ylboronic acid **4.63** by analogy with Marder[65] has been successful and the aldehyde-functionalized squaraine **4.64** has been obtained in good yield. The

fulleropyrrolydine **4.65** has been thus synthesized *via* the decarboxylation route (Scheme 4–25).

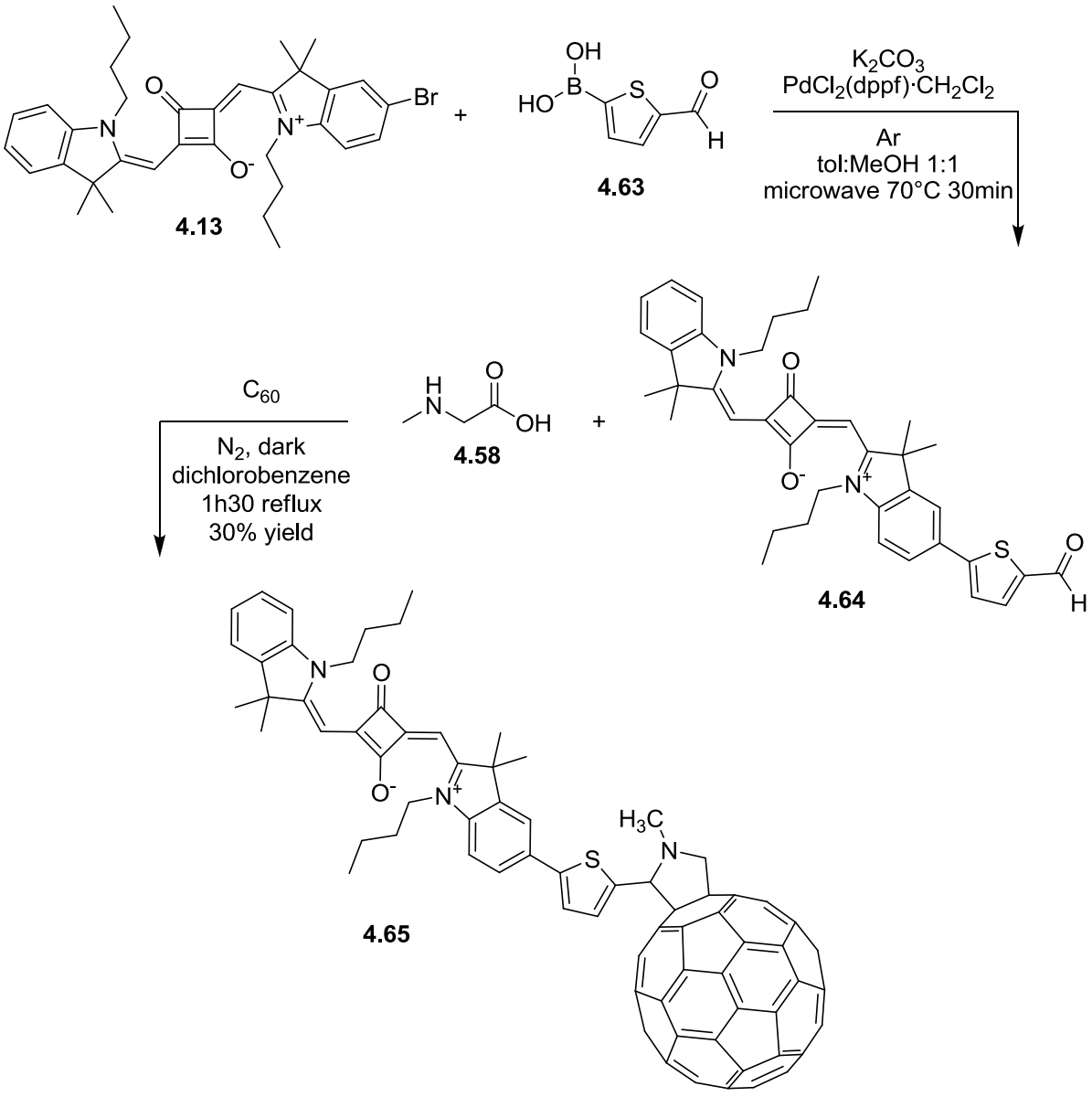

Scheme 4–25

The fuller-squaraine dyad is characterized by a strong absorption band in the NIR region due to the squaraine portion. Moreover, the spectrum also shows the diagnostic peak at 430 nm which is characteristic of fulleropyrrolydines (Figure 4–26).

Preliminary fluorescence emission and lifetime experiments have shown that the emission is strongly quenched. This is an indication that the excitation could be

transferred to the fullerene portion *via* intra-molecular energy transfer. The fullerene portion could thus effectively generate singlet oxygen (Figure 4–27).

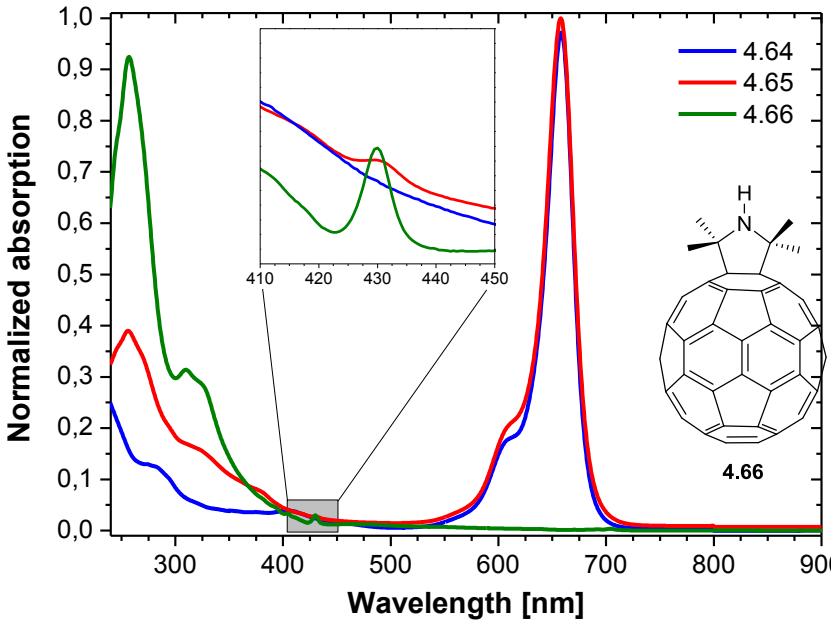

Figure 4–26 UV-vis spectra of compounds 4.64, 4.65 and the fulleropyrrolydine reference 4.66 in air-equilibrated chloroform.

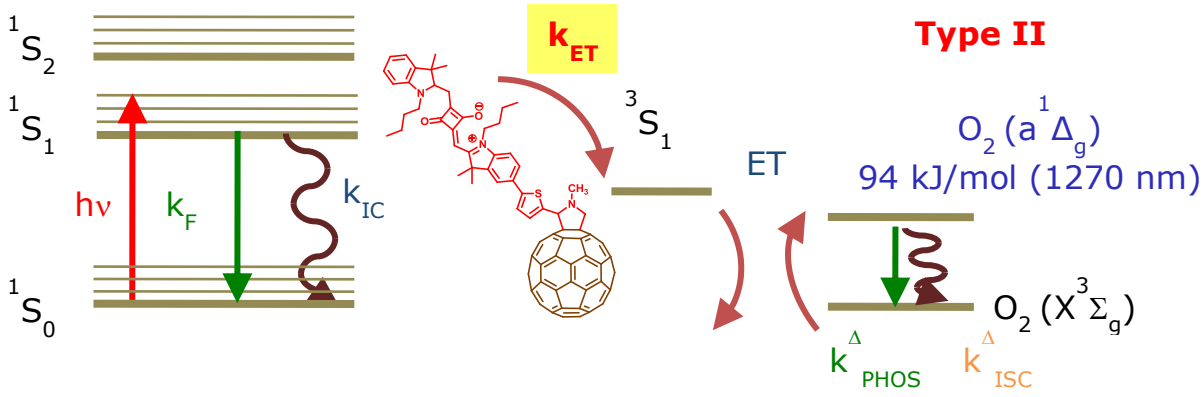

Figure 4–27 Modified Jablonski diagram to show energy transfer and singlet oxygen generation in the fullero-squaraine dyad.

It should be taken into account, however, that squaraine dyes are effective singlet oxygen quenchers.[14] Since it has been ascertained that the fullero-squaraine dyad generates singlet oxygen (see section 4.6), time-resolved singlet oxygen emission will be performed in order to evaluate the singlet oxygen quenching due to the squaraine portion.

4.5 Nanoformulation: squaraine-functionalized nanocarriers

As already mentioned in the background section, a critical advantage in treating cancer with advanced, non-solution based therapies is the inherent leaky vasculature present serving cancerous tissues. The defective vascular architecture, created due to the rapid vascularization necessary to serve fast-growing cancers, coupled with poor lymphatic drainage allows an enhanced permeation and retention effect (EPR effect)[66].

The nanoformulation of photosensitizers with nanoparticles of suitable material, size and shape could thus enhance the drug accumulation in the cancer tissue.

4.5.1 Zeolite L as nanocarrier

Among the well-known silica based nanocontainers, natural or artificially synthesized zeolites represent a promising choice as nanocarriers.[67]

Natural zeolites are minerals that are the result of a very low grade metamorphism, typically formed in the cavities or vesicles of volcanic rocks. They are framework silicates consisting of interlocking tetrahedrons of SiO_4 and AlO_4, where each oxygen of a given tetrahedron is shared between this tetrahedron and one of the four others, so that the ratio (Si+Al):O is 1:2. The presence of trivalent aluminum in the zeolite makes it negatively charged, thus cations such as Na^+, Ca^{2+} and NH_4^+, are present in the vacant spaces in the structure for charge compensation. In many zeolites the vacant spaces are interconnected and form a characteristic channels system of varying sizes, depending on the zeolite type.

The history of zeolites starts in 1756, when Stilbite was discovered by A.F. Cronstedt. This mineral seemed to boil under fast heating conditions. The boiling phenomenon is the result of reversible adsorption/expulsion of water from the porous internal void space and internal surface of zeolite crystals. Therefore, he named this mineral compound zeolite, stemming from the Greek for “boiling stone” (ζειν = zein = to boil; λιθος = lithos = stone).

Nowadays synthetic zeolites have main advantages over natural ones, such as the easy control of their size and morphology along with their highly selective functionalization properties.[68] Zeolites are currently employed in the purification of gaseous and liquid mixtures and solutions by sorption, in reversible sorption capacity for water, in removal of odors and pollutants, for ion exchange, as softeners of water for washing (substituted polyphosphates), for the removal of heavy metal ions in mine wastewater and radioactive fission products, and for catalysis in petrochemical industries.

The modern definition of zeolite is “a three-dimensional framework of tetrahedrally coordinated T-atoms with cavities or channels with the smallest opening larger than six T-

atoms"[67], where T-atoms are Si, Al, P, As, Ga, Ge, B, Be. Figure 4–28 shows the framework and SEM images of three common zeolites.

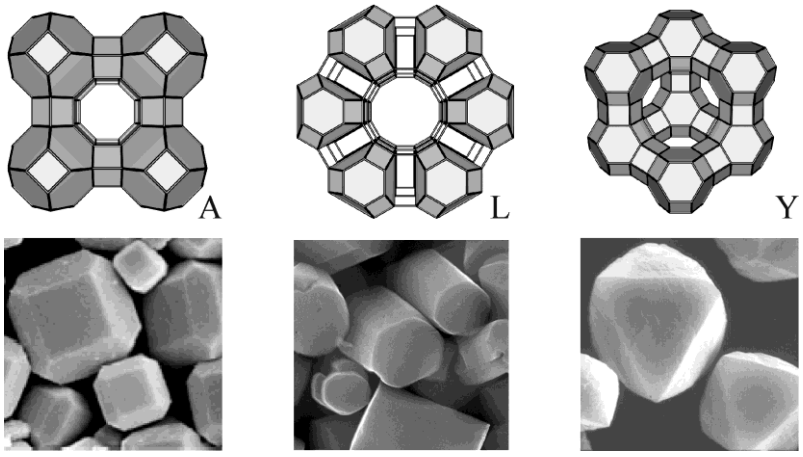

Figure 4–28 Framework for zeolite A (left) zeolite L (middle) and zeolite Y (right) and corresponding SEM images.

Zeolite L is a synthetic zeolite with hexagonal symmetry.[69] The primary building unit of the framework consists of TO_4 tetrahedrons where T represents either Al or Si. The secondary building unit, the *cancrinite*- or ε-cage, is made up by 18 corner-sharing tetrahedrons. These units are stacked into columns along the *c* axis and are connected through oxygen bridges in the *a*,*b* plane to form a one dimensional channel system running parallel to the *c* axis with hexagonal symmetry, as shown in Figure 4–29. The center-to-center distance between two main channels is 1.84 nm. The framework of zeolite L illustrates that the shape of the crystals can be well described by assuming cylinder morphology. The number of channels lying parallel to the *c* axis is equal to $0.265(d_c)^2$, where d_c is the diameter of the cylinder in nanometers.

Four different sites have been reported for the charge-compensating cations. The water molecules in the large cavities of zeolite L have been reported to behave as an intercrystalline liquid, whereas they seem to build clusters around the cations in the smaller pores. The stoichiometry of zeolite L with monovalent cations is $(M)_9[Al_9Si_{27}O_{72}]\cdot nH_2O$, where *n* equals 21 in fully hydrated materials, and 16 at about 22 % relative humidity.

An important feature of zeolite L is that it is possible to control size and aspect ratio during the condensation, allowing the preparation of uniform distributions of crystals with different morphologies and sizes ranging from 30 nm to about 10000 nm (Figure 4–30)[70].

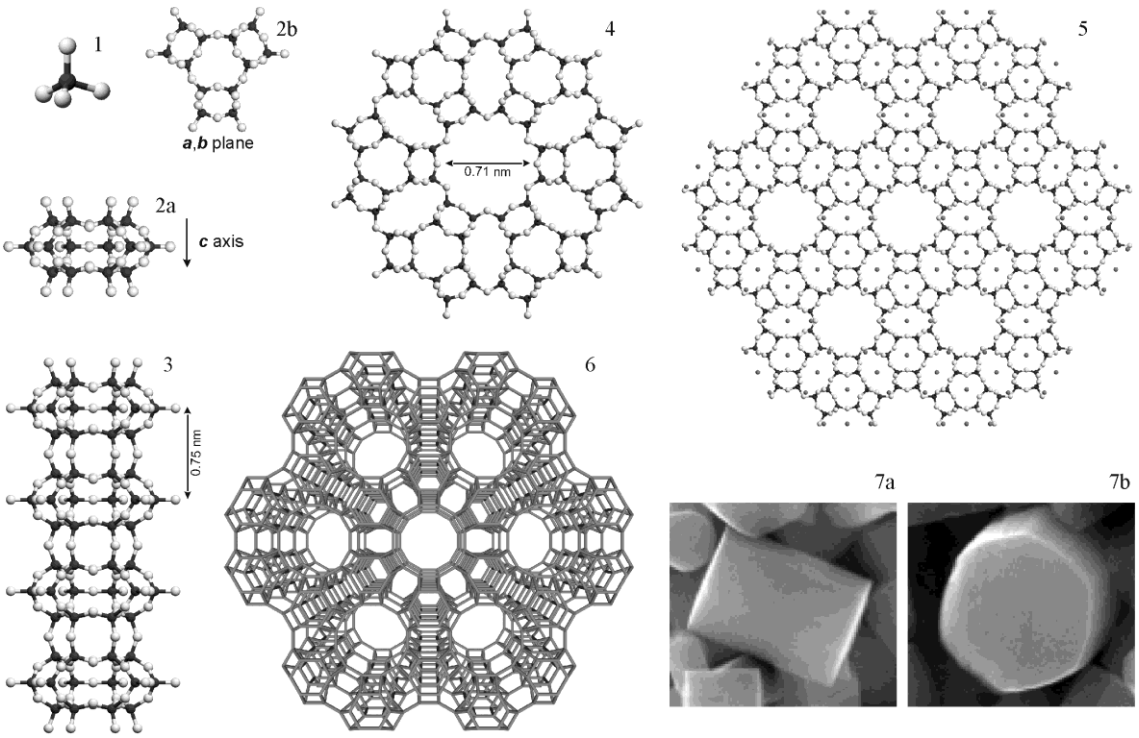

Figure 4–29 1) SiO_4/AlO_4 tetrahedron 2) cancrinite- or ε-cage, a) side view (*c* axis), b) front view (*a*,*b* plane) 3) connection of the ε-cages along the *c* axis, 4), 5) connection of the ε-cage in the *a*,*b* plane with cations represented as dark balls, 6) framework of zeolite L 7) SEM images of zeolite L a) side surface, b) hexagonal base of a crystal.

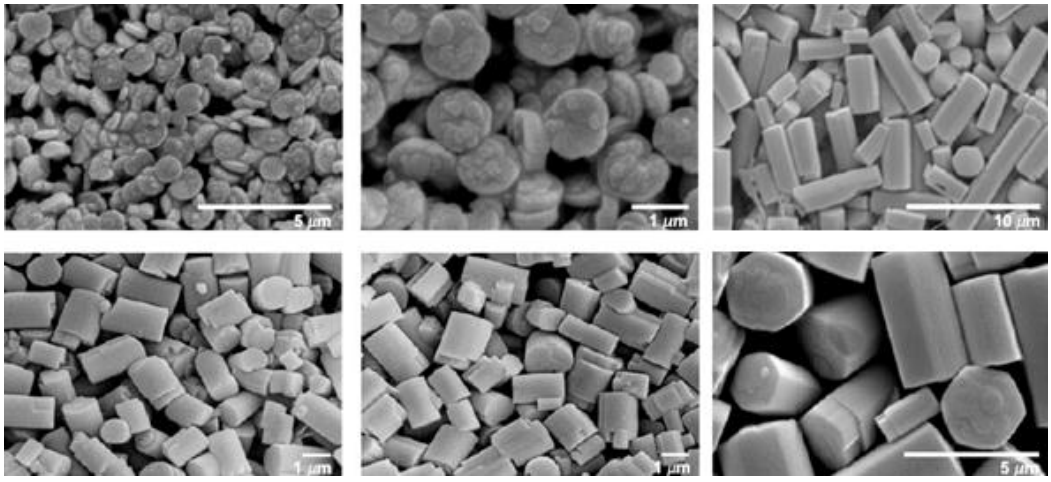

Figure 4–30 SEM images of zeolite L crystals of different size and morphology.

The one-dimensional channel system of zeolite L makes this material a suitable host for the spatial organization of a large variety of guest molecules.[71]

On this regard, a wide spectrum of guests in zeolites has been studied. Once incorporated into the host, molecules or clusters undergo changes in properties and

reactivity. Such nanocomposites have found application in gas separation,[72] selective catalysis,[73] removal of pollutants and ion exchangers,[74] data storage,[75] energy conversion[76] and drug delivery.[77]

There are four strategies for the encapsulation of molecules in the zeolite channels:

Adsorption from liquid phase[78] or from the gas phase[79] for neutral guests;
Ion exchange[80] for cationic guests;
Crystallization inclusion;[81]
In situ synthesis of the guest (ship-in-a-bottle strategy).[82]

The last two methods are suitable for guest molecules that exceed the free pore diameter of the zeolite. Adsorption from liquid or gas phase and ion exchange are both reversible methods. Some typical dyes which have been inserted into zeolite L channels are shown in Figure 4–31.

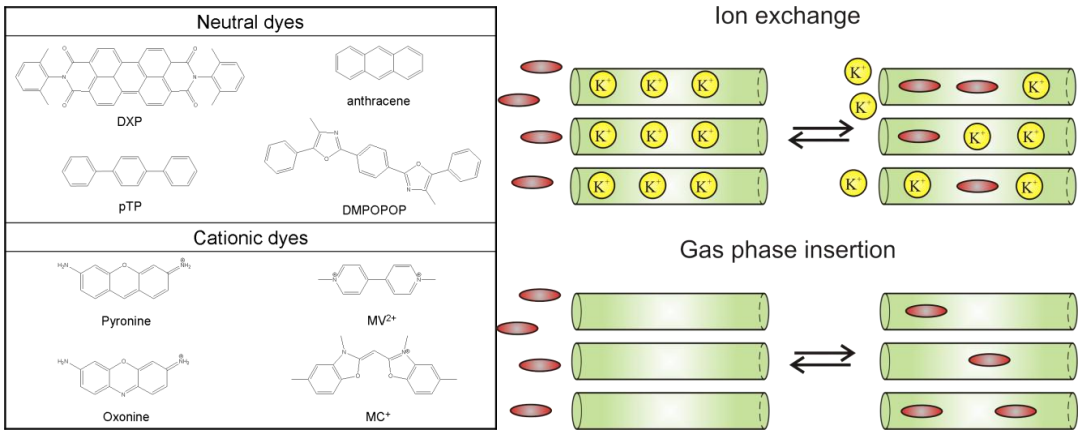

Figure 4–31 Left: selection of dyes (and abbreviations) which have been inserted in Zeolite L. Right: schematic representation of the ion exchange and gas phase loading equilibriums.

The pore openings are the second functionalization site of zeolites. The pore openings play an essential role in view of further functionalizations. They are responsible for the entry or release of guest species and control over their structure is required for many applications, such as drug delivery.[83]

An interesting concept developed for zeolite L are the so-called stopcock molecules.[84, 85] Due to size restrictions only a part of the molecule (tail) can enter the channel, while the head remains outside the pore (Figure 4–32). The stopcocks can be bound either by physisorption, by electrostatic interaction or by covalent bonding. Since these molecules are located at the interface between the interior of a zeolite L crystal and the surrounding, they can be considered as mediators for communication between dye molecules inside the nanochannels and the outer environment. Stopper molecules can

also be used to prevent penetration of small molecules such as oxygen and water or to hinder encapsulated dye molecules from leaving the channels.[86]

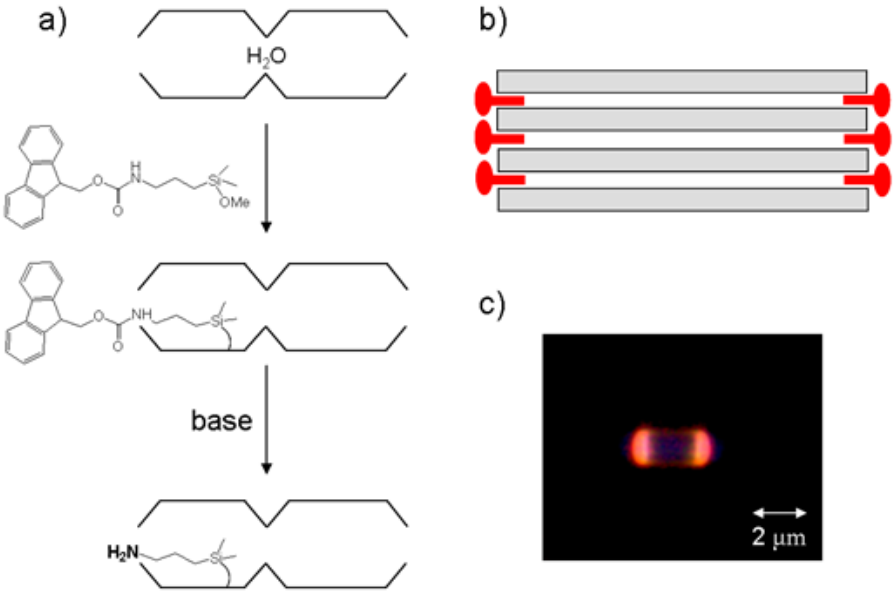

Figure 4–32 a) Procedure for the selective amino-functionalization of the zeolite pores; b) the stopcock concept; c) fluorescence microscopy picture of a zeolite crystal bearing an amino-reactive dye at the pore openings.

The external surface of zeolite crystals can also be covalently functionalized in order to tune the interaction with the environment. Most of these modifications are aimed at improving the dispersion and the biocompatibility of the material.[86-88] The functionalization of the external surface can also be envisaged to enable targeting of bio-molecules, bacteria or cells,[89] to add chemical, luminescent, magnetic or radioactive labels,[90] or even to promote self-assembly of host-guest objects into well-defined macroscopic structures on various supports.[91]

The covalent functionalization of the external surface of zeolite L crystals is carried out with silane chemistry. The most common procedure involves the condensation of the hydroxyl groups on the outer surface with an alkoxy silane. Some of the functionalities introduced are primary amines,[89] epoxides,[92] carboxylic acids[93] aldehydes,[94] polymers and DNA bases.[95]

The covalent binding of complex molecules such as fluorescent dyes or biological markers is usually achieved in two steps. First the external surface of zeolite L is functionalized with an alkoxy silane bearing a reactive moiety, which then reacts with the desired complex molecule. The most common linkers are amides[96] and triazoles *via* click chemistry.[97]

4.5.2 *Squaraine-functionalized zeolite L nanocrystals*

Zeolite L nanocrystals have been chosen as suitable nanocarriers for squaraine dyes because it is possible to obtain nanoparticles with uniform size and aspect ratio and since the functionalization is compatible with the post-functionalized dyes already prepared.

The functionalization method chosen is the external surface covalent modification. The channel inclusion, indeed, can only be performed *via* ship-in-a-bottle strategy due to the size of squaraine dyes. Moreover the additional diffusion of molecular oxygen to the channels and the subsequent diffusion of ROS and singlet oxygen from the channels should be taken into account

The covalent binding has been performed in a two-step process *via* amide bond. Two carboxylic acid-functionalized squaraines with different substitution patterns have been prepared, **4.17** (generic structure **4.2**, Scheme 4–26) and **4.21** (generic structure **4.3**, Scheme 4–27).

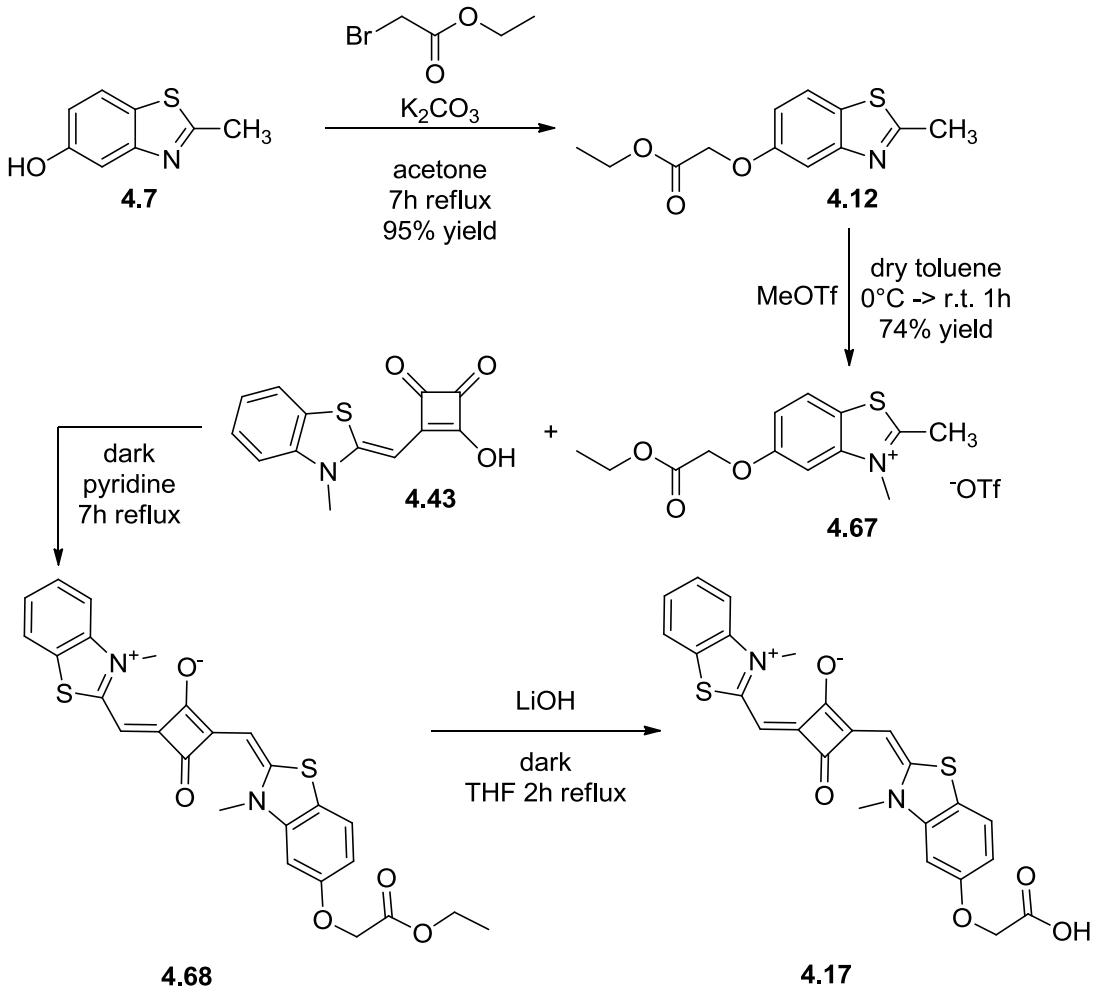

Scheme 4–26

Squaraine **4.17** has been prepared by deprotection in basic condition of the corresponding ester derivative **4.68** since the reaction conditions for the formation of the benzothiazole derivative **4.12** were not compatible with a free carboxylic acid functionality.

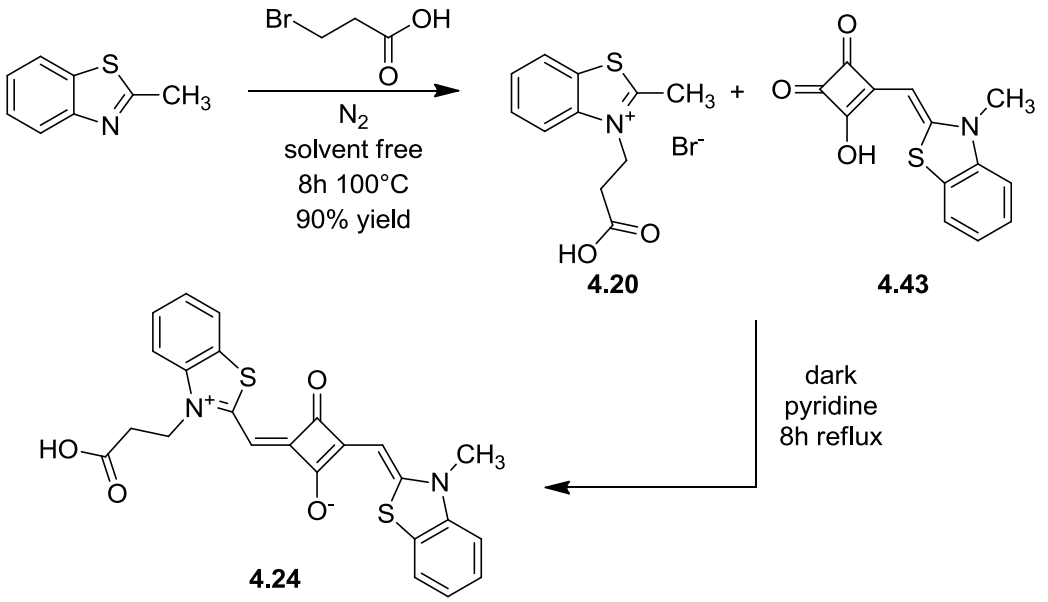

Scheme 4–27

In order to take advantage of the EPR effect for the preferential accumulation of the nanocomposites in tumor cells, the zeolite L sample chosen **4.69** is composed by disc-shaped crystal with a medium diameter of 180 nm and medium height of 30 nm.

Prior to the functionalization, the mixed cations (Na^+, K^+, H^+) inside the zeolite channels have been exchanged in order to have a starting material with homogeneous properties **4.70** (

Scheme 4–28).

The first functionalization step involves the condensation of the hydroxyl groups on the outer surface with (3-aminopropyl)trimethoxysilane (APTES, **4.71**).

The squaraines **4.17** and **4.21** have been linked to the zeolite via amide bond formation with N-(3-dimethylaminopropyl)-N-ethyl carbodiimide hydrochloride (EDC) and N-hydroxy-succinimide (NHS) in DMSO at room temperature in the dark in the presence of N-ethylmorpholine (NEM) as a base. The nanocomposites are washed several times in order to remove the non-covalently linked dye which might be physisorbed on the surface.

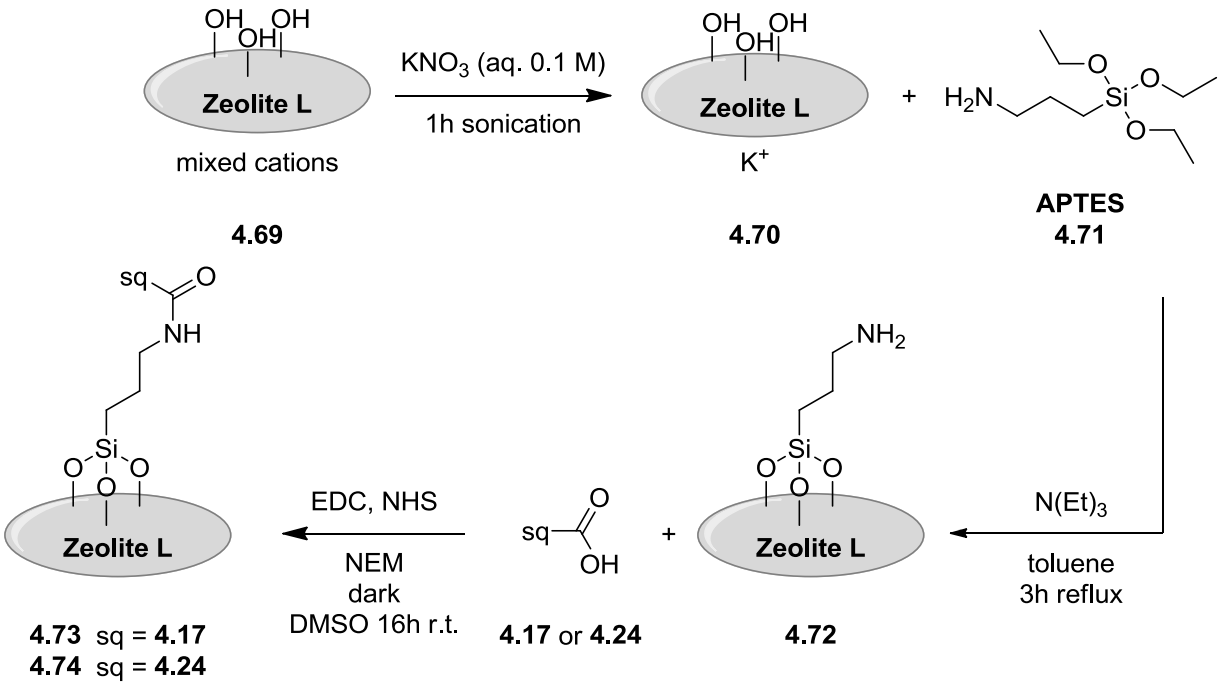

Scheme 4–28

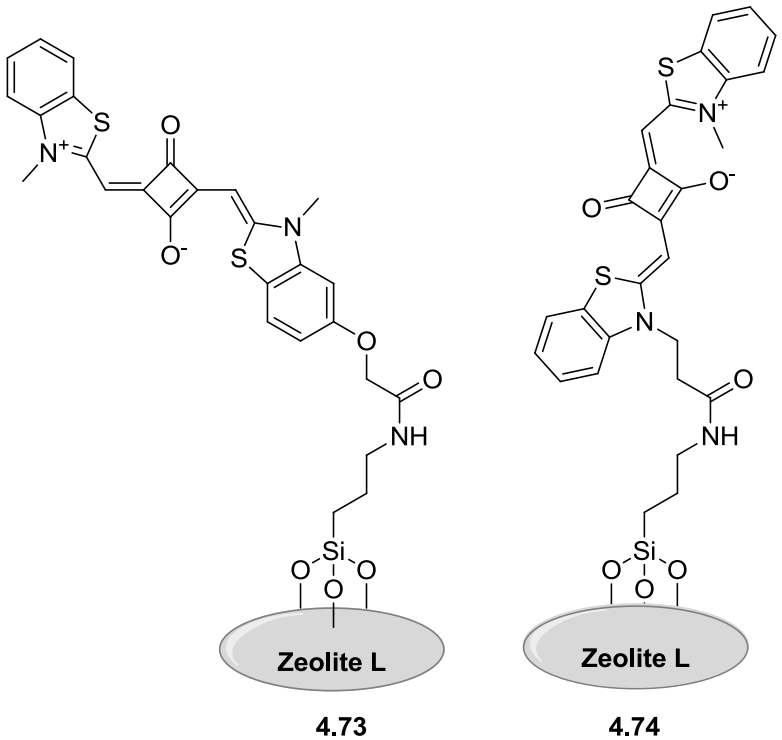

Scheme 4–29

The ζ potential values reported in Table 4–6 confirm the successful two-step functionalization.

	ζ potential (mV)	Medium diameter
4.70	-36±5 (PBS)	173
4.72	-10±3 (PBS); 20±8 (pH 5)	228
4.73	-20±5 (PBS)	
4.74	-22±6 (PBS)	

Table 4–6 Zeta potential in PBS and acetate buffer (pH 5) and medium diameter from DLS measurements in PBS (from number distribution) for the functionalized zeolites.

The absorption, excitation and emission spectra for dispersions of **4.73** and **4.74** in DMSO (1mg/mL) are shown in Figure 4–33. The solvent has been chosen in order to obtain a homogeneous dispersion and to match the refractive index of zeolite. The absorption spectrum shows the scattering at lower wavelengths due to the presence of nanoparticles in suspension and the squaraine absorption peak in the NIR region. After the deconvolution of the scattering curve, the loading for both nanocomposites has been estimated in the order of 10^{-7} mol squaraine/mg zeolite.

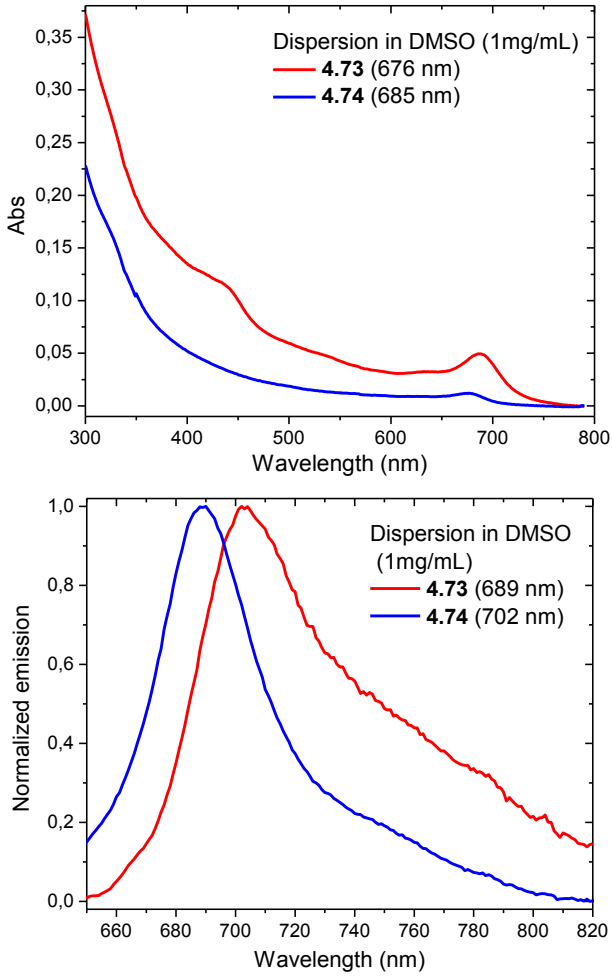

Figure 4–33 Absorption (left) and normalized emission (right) of dispersion in DMSO (1mg/mL) of 4.73 and 4.74.

4.6 Photooxidation ability of squaraine dyes

When **4.1** is dissolved in air-equilibrated acetonitrile and irradiated with a laser or a halogen lamp, it undergoes extensive degradation (Figure 4–34).[98] This behavior does not occur when acetonitrile is saturated with nitrogen, and it slowly occurs in air-equilibrated low polar solvents such as toluene.

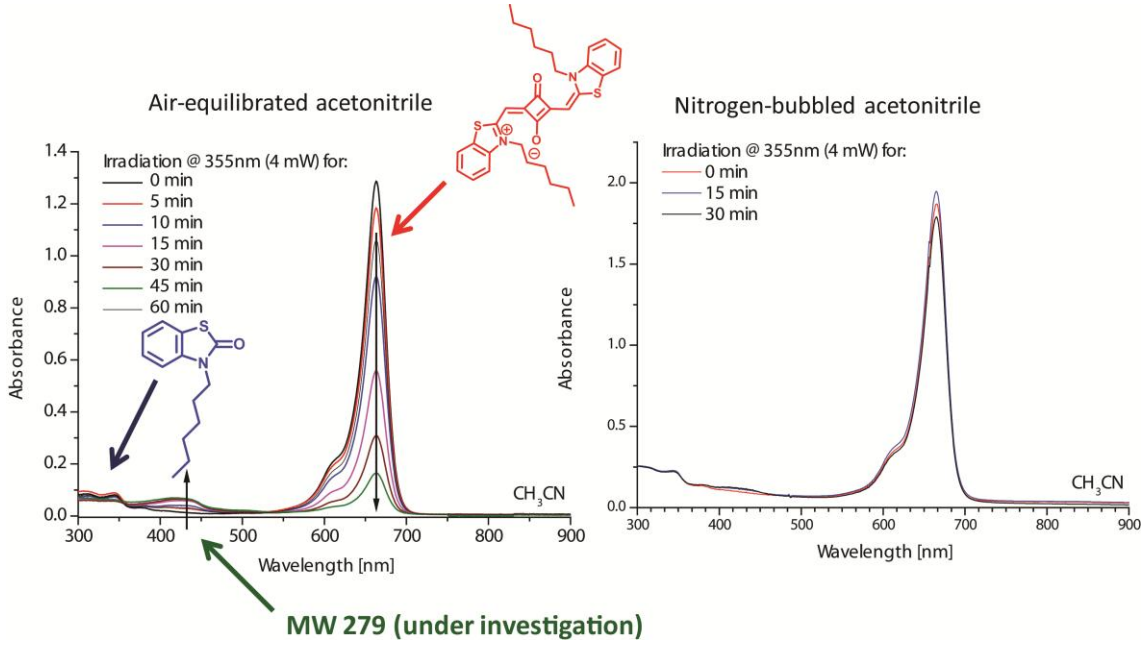

Figure 4–34 Change in the absorption spectra of 4.1 in air-equilibrated and nitrogen-bubbled acetonitrile upon irradiation with a laser source at 355 nm.

This behavior has been rationalized in terms of the formation of a charge-transfer encounter complex between the squaraine and the molecular oxygen, eventually evolving in the formation of different chemical species. To unveil the photochemical mechanism involved, a completely sun-bleached solution of **4.1** in air-equilibrated acetonitrile has been previously analyzed by GC-MS. Among other species, the formation of 3-hexylbenzo[*d*]thiazol-2(3*H*)-one (3-HBT) has been reported, in agreement with the chemistry of photooxygenation of enaminones and other electron-rich double bonds.[99, 100]

Scheme 4–30 illustrates the proposed mechanism for the degradation of **4.1**. The first steps involved a non-concerted 1,2-cycloaddition to give a dioxetane intermediate which cleaves to two carbonyl derivatives, one of the two in its triplet state. The excited carbonyl compound formed can then react according to both Norrish Type I and Type II reactions: α-cleavage of the excited carbonyl compound leading to an acyl-alkyl radical pair (from an acyclic carbonyl compound) or an acyl-alkyl diradical (from a cyclic carbonyl compound) as the primary photoproduct and intramolecular abstraction of a γ-hydrogen

to produce a 1,4-diradical as the primary photoproduct, respectively. The radicals formed can establish a radical reaction chain is responsible for the phototoxicity behavior observed in benzothiaziolium based squaraines.[98]

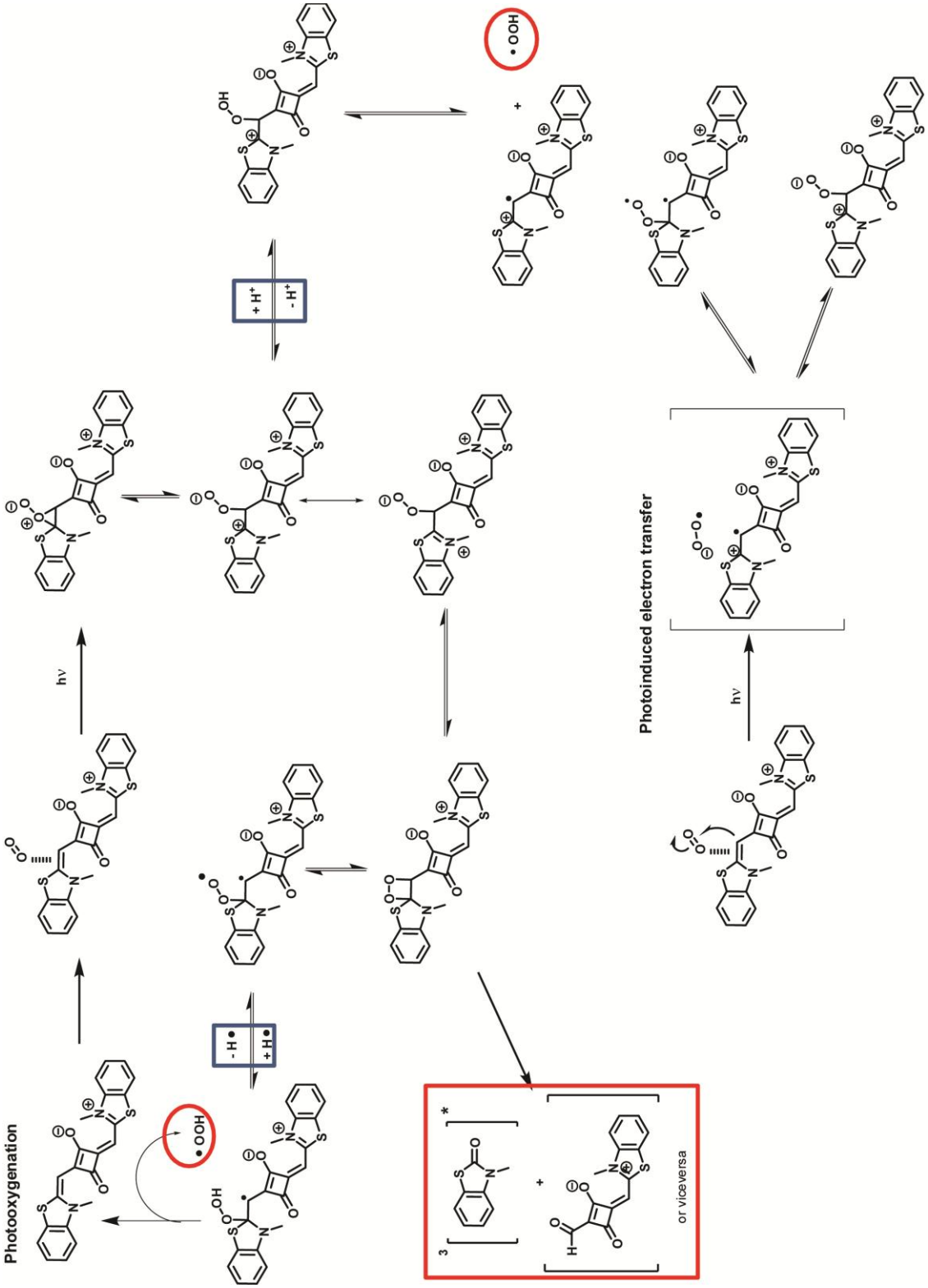

Scheme 4–30

To further elucidate the nature and role of the photogenerated species, the product distribution of the reaction between light, squaraines and oxidizable substrates (i.e., limonene, cholesterol, and methyl linoleate) has been studied in order to investigate all the mechanisms leading to photooxidative damage. The photosensitized oxygenations were carried out by irradiating a solution of squaraine dye filtered below 500 nm (white halogen lamp, 300 W) for 30 minutes and subsequent analysis of the product peroxides reduced with $NaBH_4$ by GC-MS analysis (Figure 4–35).[101] The oxidation products were identified by comparison with literature data, using the NIST 05 database[102] (Table 4–7).

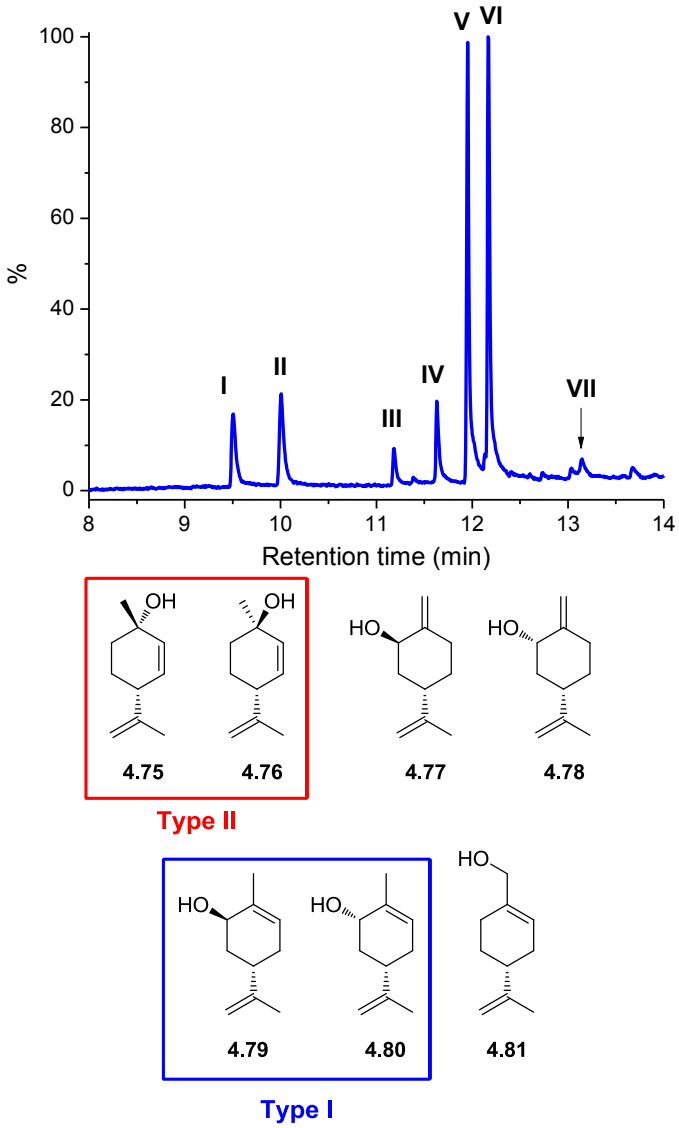

Figure 4–35 GC-MS chromatogram of a (*R*)-(+)-limonene solution (CH_3CN) photosensitized by 4.1.

Peak	Product	Characteristic ions	Retention time

		(*m/z*)	(min)
I	**4.75** or **4.76**	91 119 79 134	9.55
II	**4.75** or **4.76**	91 119 134 79	10.05
III	**4.77** or **4.78**	91 109 134 119	11.19
IV	**4.77** or **4.78**	91 119 134 109	11.63
V	**4.79**	109 91 84 119	11.95
VI	**4.80**	84 91 134 119	12.17
VII	**4.81**	79 91 67 55	13.09

Table 4–7 Peak identification of chromatogram in Figure 4–35.

The oxygenation of (*R*)-(+)-limonene provides a particularly sensitive fingerprint for the reactive intermediate. This substrate contains two double bonds, one disubstituted and one trisubstituted. Photooxygenation yields all six possible products of singlet oxygen attack at the trisubstituted double bond; no products with unshifted double bond are formed, and the disubstituted double bond is inert. The predominant products have exocyclic double bond, and the formation of endocyclic products is unfavorable. Byproducts which involve the shift of the tertiary hydrogen atom from an isopropyl group to oxygen are formed only in minor amounts, probably because the most favorable conformation for the isopropyl hydrogen is in the plane of the double bond.

Product (%)	4.75	4.76	4.77	4.78	4.79	4.80	4.81
Singlet oxygen sensitization	10	34	19	23	9	4	0
4.1 sensitization	6 + 8		4 + 7		36	37	2

Table 4–8 Product distributions in photosensitized oxygenation of *(R)*-(+)-limonene.

Table 4–8 shows the photooxidation products distribution in the photosensitized oxygenation of (*R*)-(+)-limonene. Row 1 shows the percentage distribution of oxidized products expected for singlet oxygen reaction.[99] Row 2 shows the observed product distribution for squaraine **4.1** photosensitization. The fact that the preponderance products are the two carveol derivatives **4.79** and **4.80** and the appearance of **4.81** brought to the conclusion that the most likely mechanism involves the ablation of the allylic hydrogen by a radical species (either a ROS or a triplet carbonyl compound) and the reaction of the allyl radical with molecular oxygen to yield a peroxy radical. The latter can ablate the hydrogen of another limonene molecule to yield a hydroperoxide and an allyl radical according to a type I radical chain process. The photochemical data were in agreement with the photophysical ones.[14]

The encounter complex between squaraine and molecular oxygen can evolve by either photooxygenation of the enaminic bond in the squaraine backbone or ROS production. In both cases, the photogenerated products can then establish radical chain events (lipid peroxidation) that lead to type I cytotoxicity in cells. Interestingly, the same mechanism seems to describe the photooxygenation behavior of a number of cyanine-based photosensitizers (e.g., merocyanine 540,[103] indocyanine green, and MKT-077).[104]

Photobleachings of (*R*)-(+)-limonene have been carried out in the presence of representative squaraines prepared during this thesis work, in order to further evaluate how the substituents affect the photooxidation ability with respect to the benchmark sensitizer **4.1**. The photooxidation experiments have been performed in ethanol rather than acetonitrile in order to reduce the steps involved.

Choline-functionalized squaraine **4.46** has been chosen as representative compound for post-functionalizable and functionalized dyes for active targeting. The oxidation product distribution (Figure 4–36) indicates that indeed the choline functionality does not affect the photosensitization mechanism (Table 4–10).

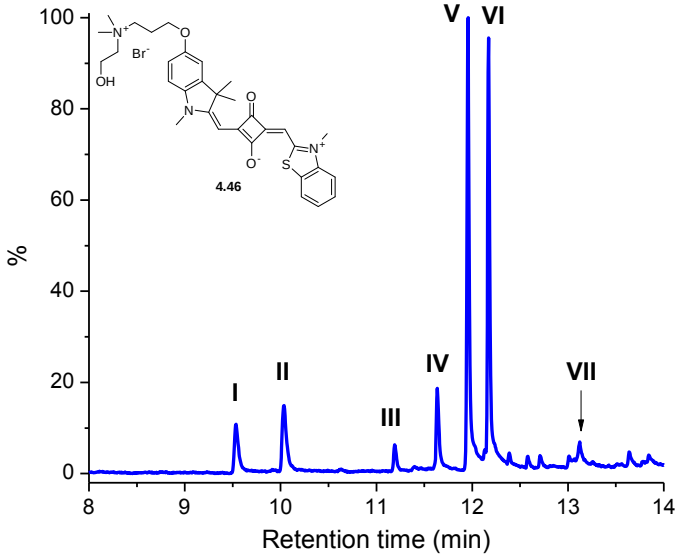

Figure 4–36 GC-MS chromatogram of a (*R*)-(+)-limonene solution (EtOH) photosensitized by 4.46.

The same oxidation products distribution has also been found for squaraine-functionalized zeolite **4.74** (Figure 4–37). The covalent conjugation of a benzothiazole squaraine to a nanocarrier has thus led to an efficient photoactive drug with passive targeting ability.

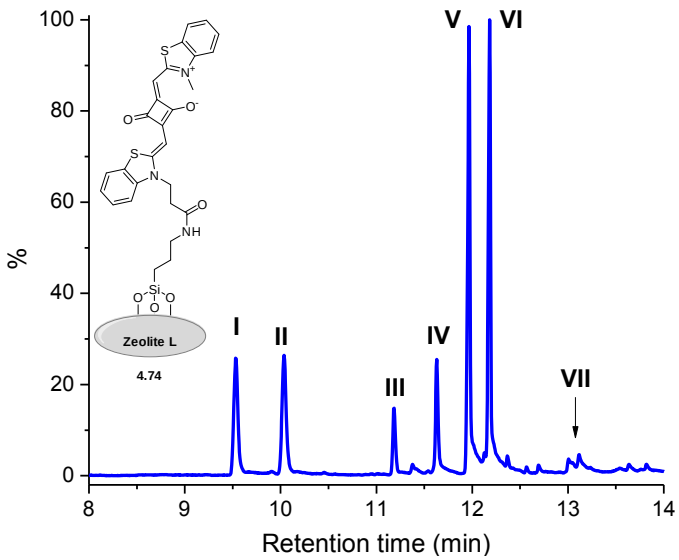

Figure 4–37 GC-MS chromatogram of a (*R*)-(+)-limonene solution (EtOH) photosensitized by 4.74.

The singlet oxygen phosphorescence emission spectra of the choline-functionalized squaraine **4.46** and the squaraine **4.68** employed for zeolite functionalization, along with the benchmark squaraine **4.1**, are shown in Figure 4–38. The spectra are normalized to the sensitizer concentration, since the Zinc phthalocyanine solution used as reference was ten times more diluted than the squaraine ones (10^{-7} M vs. 10^{-6} M).

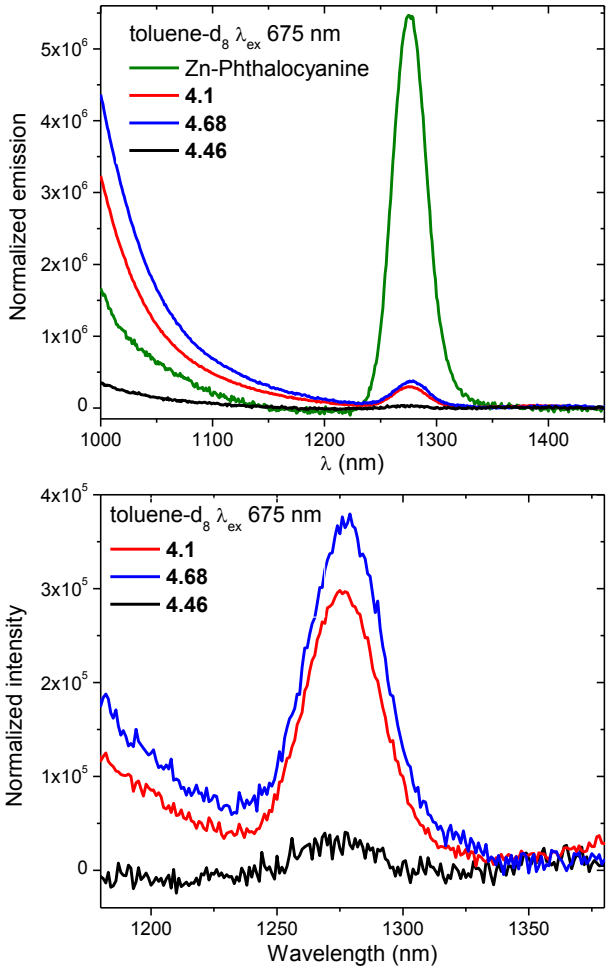

Figure 4–38 Left: emission spectrum recorded in the IR region for the 1,3-substituted squaraines and the reference compound (Zinc 2,9,16,23-tetra-*tert*-butyl-29*H*,31*H*-phthalocyanine in toluene-d_8 normalized on the concentration. Right: enlargement of the phosphorescence emission of singlet oxygen.

The excitation spectra for the singlet oxygen phosphorescence are shown in Figure 4–39, the characteristic bands are easily identified, confirming that the emission at 1277 nm is due to squaraine sensitization. It should be noted that the spectrum for **4.46** has been smoothed because very noisy, because of the lower intensity of the emission band.

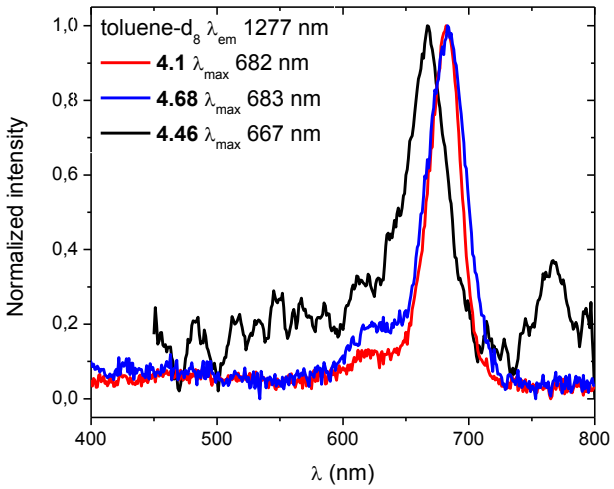

Figure 4–39 Singlet oxygen excitation spectra for the 1,3-substituted squaraines

The calculated sensitized singlet oxygen quantum yields Φ_Δ for the different squaraine dyes are shown below in Table 4–9. The values found are in accordance with literature. The quantum yield for **4.68** is comparable to the one for the symmetric derivative **4.1**, while the quantum yield for **4.46** is lower, probably due to the presence of only one heavy atom (sulfur) which favors intersystem crossing to triplet state.

Compound	Φ_Δ
Reference	0.61[105]
4.1	1,8±0,5 (lit[14]: 1,2±0,4)
4.68	2,7±0,5
4.46	0,31±0,05

Table 4–9. Sensitized Singlet Oxygen Quantum Yield, Φ_Δ in toluene-d_8 solutions upon irradiation at 675 nm.
Reference compound: Zinc 2,9,16,23-tetra-*tert*-butyl-29*H*,31*H*-phthalocyanine.

The photobleaching of (*R*)-(+)-limonene performed with 1,2-squaraine **4.26** shows a products distribution analogue to the experiment performed with the 1,3-regioisomer **4.1** (Figure 4–40). The chromatogram also shows the peak relative to 3-HBT. This is in agreement with the chemistry of photooxygenation of enaminones and other electron-rich double bonds previously illustrated (Scheme 4–30).

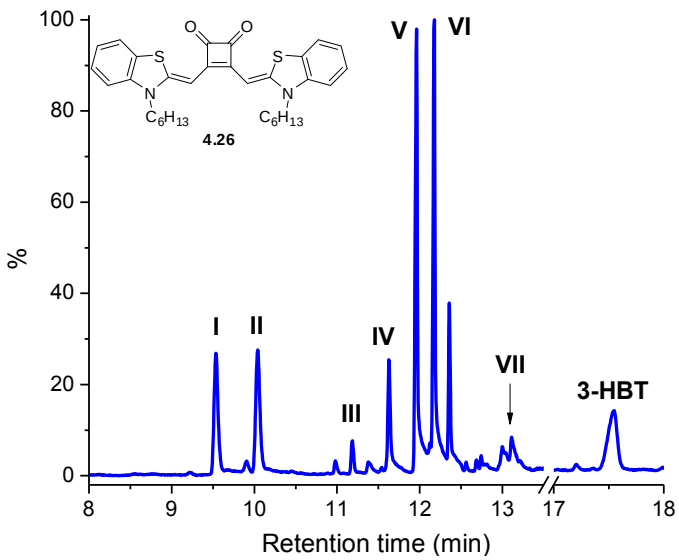

Figure 4–40 GC-MS chromatogram of a (*R*)-(+)-limonene solution (EtOH) photosensitized by 4.26.

A photobleaching experiment of (*R*)-(+)-limonene has also been performed with the irradiation of the fullero-squaraine **4.65** for λ > 550 nm, i.e. through the excitation of the squaraine portion only.

Interestingly, the oxidation products distribution (Figure 4–41) shows a different relative intensity with respect to the other squaraines studies (Table 4–10). This is in accordance with the design of this dyad, in which the energy transfer from the squaraine portion to the fullerene portion could lead to an increased singlet oxygen photogeneration. Indeed, the relative intensity of peaks I and II is higher with respect to peaks V and VI. The result also indicates that the singlet oxygen generated by the fullerene portion is not completely quenched by the squaraine. As previously mentioned in section 4.4, time-resolved singlet oxygen emission will be performed in order to evaluate the degree of singlet oxygen quenching.

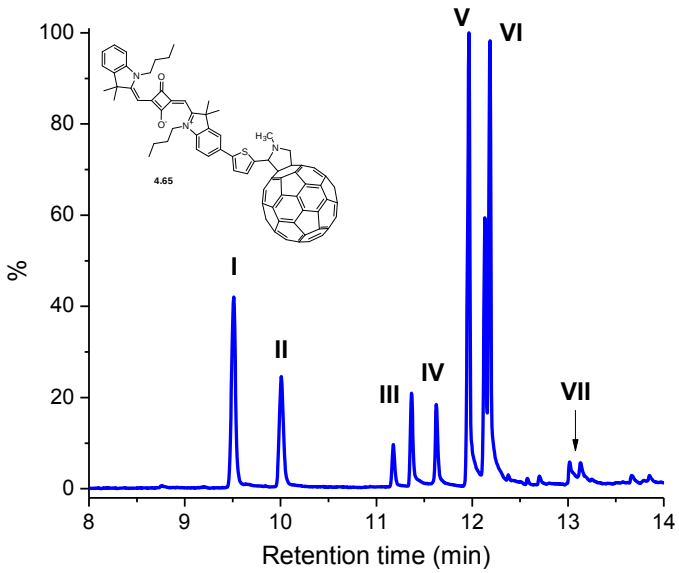

Figure 4–41 GC-MS chromatogram of a (*R*)-(+)-limonene solution (EtOH) photosensitized by 4.65.

Product (%)	4.75	4.76	4.77	4.78	4.79	4.80	4.81
4.46 sensitization	4 + 6		3 + 7		39	38	3
4.74 sensitization	5 + 7		4 + 8		37	35	2
4.65 sensitization	14 + 8		7 + 6		32	31	1
4.26 sensitization	8 + 8		3 + 7		36	35	3

Table 4–10 Product distributions in photosensitized oxygenation of *(R)*-(+)-limonene.

4.7 References

1. Treibs, A.; Jacob, K., Cyclotrimethine Dyes Derived from Squaric Acid. *Angewandte Chemie International Edition in English* **1965,** 4, (8), 694-694.
2. Sprenger, H. E.; Ziegenbein, W., Cyclobutenediylium Dyes. *Angewandte Chemie International Edition in English* **1968,** 7, (7), 530-535.
3. Schmidt, A. H., Reaktionen von Quadratsäure und Quadratsäure-Derivaten. *Synthesis* **1980,** 1980, (12), 961-994.
4. Beverina, L.; Salice, P., Squaraine Compounds: Tailored Design and Synthesis towards a Variety of Material Science Applications. *European Journal of Organic Chemistry* **2010,** 2010, (7), 1207-1225.
5. Seitz, G.; Imming, P., Oxocarbons and pseudooxocarbons. *Chemical Reviews* **1992,** 92, (6), 1227-1260.
6. Law, K. Y.; Bailey, F. C., Squaraine chemistry. Synthesis, characterization, and optical properties of a class of novel unsymmetrical squaraines: [4-(dimethylamino)phenyl](4'-methoxyphenyl)squaraine and its derivatives. *The Journal of Organic Chemistry* **1992,** 57, (12), 3278-3286.
7. Chen, C.-T.; Marder, S. R.; Cheng, L.-T., Syntheses and Linear and Nonlinear Optical Properties of Unsymmetrical Squaraines with Extended Conjugation. *Journal of the American Chemical Society* **1994,** 116, (7), 3117-3118.
8. Cohen, S.; Cohen, S. G., Preparation and Reactions of Derivatives of Squaric Acid. Alkoxy-, Hydroxy-, and Aminocyclobutenediones. *Journal of the American Chemical Society* **1966,** 88, (7), 1533-1536.
9. Law, K.-Y.; Bailey, F. C., Squaraine chemistry. Synthesis of bis(4-dimethylaminophenyl)squaraine from dialkyl squarates. Mechanism and scope of the synthesis. *Canadian Journal of Chemistry* **1986,** 64, (12), 2267-2273.
10. De Selms, R. C.; Fox, C. J.; Riordan, R. C., Reactions of squaric acid and some derivatives with thionyl chloride/N,N-dimethylformamide. *Tetrahedron Letters* **1970,** 11, (10), 781-782.
11. Beverina, L.; Ruffo, R.; Patriarca, G.; De Angelis, F.; Roberto, D.; Righetto, S.; Ugo, R.; Pagani, G. A., Second harmonic generation in nonsymmetrical squaraines: tuning of the directional charge transfer character in highly delocalized dyes. *Journal of Materials Chemistry* **2009,** 19, (43), 8190-8197.
12. Potisek, S. L.; Davis, D. A.; Sottos, N. R.; White, S. R.; Moore, J. S., Mechanophore-Linked Addition Polymers. *Journal of the American Chemical Society* **2007,** 129, (45), 13808-13809.
13. Marco Montalti, A. C., Luca Prodi, M. Teresa Gandolfi, *Handbook of Photochemistry, Third Edition*. CRC Press Taylor & Francis Group: Boca Raton, FL, 2006.
14. Salice, P.; Arnbjerg, J.; Pedersen, B. W.; Toftegaard, R.; Beverina, L.; Pagani, G. A.; Ogilby, P. R., Photophysics of Squaraine Dyes: Role of Charge-Transfer in Singlet Oxygen Production and Removal. *The Journal of Physical Chemistry A* **2010,** 114, (7), 2518-2525.
15. Fernández, D. A.; Awruch, J.; Dicelio, L. E., Photophysical and Aggregation Studies of t-Butyl-Substituted Zn Phthalocyanines. *Photochemistry and Photobiology* **1996,** 63, (6), 784-792.

16. Sreejith, S.; Carol, P.; Chithra, P.; Ajayaghosh, A., Squaraine dyes: a mine of molecular materials. *Journal of Materials Chemistry* **2008,** 18, (3), 264-274.
17. Santos, P. F.; Reis, L. V.; Almeida, P.; Serrano, J. P.; Oliveira, A. S.; Vieira Ferreira, L. F., Efficiency of singlet oxygen generation of aminosquarylium cyanines. *Journal of Photochemistry and Photobiology A: Chemistry* **2004,** 163, (1-2), 267-269.
18. Blomquist, A. T.; LaLancette, E. A., Diphenylcyclobutadienoquinone. Synthesis and Structure. *Journal of the American Chemical Society* **1961,** 83, (6), 1387-1391.
19. Ried, W.; Vogl, M., Reaktionen von Cyclobutendionen, XLV. Reaktion von Cyclobutendionen mit Fluoren. *Justus Liebigs Annalen der Chemie* **1977,** 1977, (1), 101-105.
20. Aguilar-Aguilar, A.; Peña-Cabrera, E., Selective Cross-Couplings. Sequential Stille−Liebeskind/Srogl Reactions of 3-Chloro-4-arylthiocyclobutene-1,2-dione. *Organic Letters* **2007,** 9, (21), 4163-4166.
21. Treibs, A.; Jacob, K., Über Tetracyclotrimethin-Farbstoffe. Cyclobutenderivate der Pyrrolreihe. *Justus Liebigs Annalen der Chemie* **1966,** 699, (1), 153-167.
22. Eldo, J.; Ajayaghosh, A., New Low Band Gap Polymers: Control of Optical and Electronic Properties in near Infrared Absorbing π-Conjugated Polysquaraines. *Chemistry of Materials* **2001,** 14, (1), 410-418.
23. Chenthamarakshan, C. R.; Eldo, J.; Ajayaghosh, A., Synthesis and Properties of Alternating Acceptor−Donor Copolymers of Squaric Acid with 1-Dodecyl- and 3-Dodecylpyrroles. *Macromolecules* **1998,** 32, (2), 251-257.
24. Sprenger, H. E.; Ziegenbein, W., The Cyclobutenediylium Cation, a Novel Chromophore from Squaric Acid. *Angewandte Chemie International Edition in English* **1967,** 6, (6), 553-554.
25. Binda, M.; Agostinelli, T.; Caironi, M.; Natali, D.; Sampietro, M.; Beverina, L.; Ruffo, R.; Silvestri, F., Fast and air stable near-infrared organic detector based on squaraine dyes. *Organic Electronics* **2009,** 10, (7), 1314-1319.
26. Binda, M.; Natali, D.; Sampietro, M.; Agostinelli, T.; Beverina, L., Organic based photodetectors: Suitability for X- and Γ-rays sensing application. *Nuclear Instruments and Methods in Physics Research Section A: Accelerators, Spectrometers, Detectors and Associated Equipment* **2010,** 624, (2), 443-448.
27. West, R.; Powell, D. L., New Aromatic Anions. III. Molecular Orbital Calculations on Oxygenated Anions. *Journal of the American Chemical Society* **1963,** 85, (17), 2577-2579.
28. Bagnis, D.; Beverina, L.; Huang, H.; Silvestri, F.; Yao, Y.; Yan, H.; Pagani, G. A.; Marks, T. J.; Facchetti, A., Marked Alkyl- vs Alkenyl-Substitutent Effects on Squaraine Dye Solid-State Structure, Carrier Mobility, and Bulk-Heterojunction Solar Cell Efficiency. *Journal of the American Chemical Society* **2010,** 132, (12), 4074-4075.
29. Brooker, L. G. S.; Craig, A. C.; Heseltine, D. W.; Jenkins, P. W.; Lincoln, L. L., Color and Constitution. XIII.1 Merocyanines as Solvent Property Indicators. *Journal of the American Chemical Society* **1965,** 87, (11), 2443-2450.
30. Snare, M. J.; Treloar, F. E.; Ghiggino, K. P.; Thistlethwaite, P. J., The photophysics of rhodamine B. *Journal of Photochemistry* **1982,** 18, (4), 335-346.
31. Hudson, R.; Carcenac, M.; Smith, K.; Madden, L.; Clarke, O. J.; Pelegrin, A.; Greenman, J.; Boyle, R. W., The development and characterisation of porphyrin

isothiocyanate-monoclonal antibody conjugates for photoimmunotherapy. *Br J Cancer* **2005,** 92, (8), 1442-1449.

32. Dummin, H.; Cernay, T.; Zimmermann, H. W., Selective photosensitization of mitochondria in HeLa cells by cationic Zn(II)phthalocyanines with lipophilic side-chains. *Journal of Photochemistry and Photobiology B: Biology* **1997,** 37, (3), 219-229.

33. Hornung, R.; Fehr, M. K.; Monti-Frayne, J.; Krasieva, T. B.; Tromberg, B. J.; Berns, M. W.; Tadir, Y., Highly Selective Targeting of Ovarian Cancer with the Photosensitizer PEG-m-THPC in a Rat Model. *Photochemistry and Photobiology* **1999,** 70, (4), 624-629.

34. Montforts, F.-P.; Meier, A.; Scheurich, G.; Haake, G.; Bats, J. W., Chlorins Designed for Photodynamic Tumor Therapy and as Model Systems for Photosynthesis. *Angewandte Chemie International Edition in English* **1992,** 31, (12), 1592-1594.

35. Boutorine, A. S.; Brault, D.; Takasugi, M.; Delgado, O.; Hélène, C., Chlorin-Oligonucleotide Conjugates: Synthesis, Properties, and Red Light-Induced Photochemical Sequence-Specific DNA Cleavage in Duplexes and Triplexes. *Journal of the American Chemical Society* **1996,** 118, (40), 9469-9476.

36. Roebuck, J. R.; Cecil, K. M.; Schnall, M. D.; Lenkinski, R. E., Human breast lesions: characterization with proton MR spectroscopy. *Radiology* **1998,** 209, (1), 269-275.

37. Podo, F., Tumour phospholipid metabolism. *NMR in Biomedicine* **1999,** 12, (7), 413-439.

38. Aboagye, E. O.; Bhujwalla, Z. M., Malignant Transformation Alters Membrane Choline Phospholipid Metabolism of Human Mammary Epithelial Cells. *Cancer Research* **1999,** 59, (1), 80-84.

39. Katz-Brull, R.; Margalit, R.; Bendel, P.; Degani, H., Choline metabolism in breast cancer; 2H-, 13C- and 31P-NMR studies of cells and tumors. *Magnetic Resonance Materials in Physics, Biology and Medicine* **1998,** 6, (1), 44-52.

40. Tronchère, H.; Record, M.; Tercé, F.; Chap, H., Phosphatidylcholine cycle and regulation of phosphatidylcholine biosynthesis by enzyme translocation. *Biochimica et Biophysica Acta (BBA) - Lipids and Lipid Metabolism* **1994,** 1212, (2), 137-151.

41. Glunde, K.; Bhujwalla, Z. M.; Ronen, S. M., Choline metabolism in malignant transformation. *Nat Rev Cancer* **2011,** 11, (12), 835-848.

42. Stone, S. J.; Vance, J. E., Phosphatidylserine Synthase-1 and -2 Are Localized to Mitochondria-associated Membranes. *Journal of Biological Chemistry* **2000,** 275, (44), 34534-34540.

43. Hara, T.; Kosaka, N.; Kishi, H., PET imaging of prostate cancer using carbon-11-choline. *Journal of nuclear medicine : official publication, Society of Nuclear Medicine* **1998,** 39, (6), 990-5.

44. Glunde, K.; Raman, V.; Mori, N.; Bhujwalla, Z. M., RNA Interference–Mediated Choline Kinase Suppression in Breast Cancer Cells Induces Differentiation and Reduces Proliferation. *Cancer Research* **2005,** 65, (23), 11034-11043.

45. Hernandez-Alcoceba, R.; Saniger, L.; Campos, J.; Nunez, M. C.; Khaless, F.; Gallo, M. A.; Espinosa, A.; Lacal, J. C., Choline kinase inhibitors as a novel approach for antiproliferative drug design. *Oncogene* **1997,** 15, (19), 2289-301.

46. Villa, A. M.; Caporizzo, E.; Papagni, A.; Miozzo, L.; Buttero, P. D.; Grilli, M. D.; Amboldi, N.; Fazio, F.; Doglia, S. M.; Giglioni, B., Choline and phosphatidylcholine

fluorescent derivatives localization in carcinoma cells studied by laser scanning confocal fluorescence microscopy. *European Journal of Cancer* **2005,** 41, (10), 1453-1459.
47. Melisi, D.; Secondo, A.; Montoro, P.; Piacente, S.; Rimoli, M. G.; Minale, M.; de Caprariis, P.; Annunziato, L., Galactosyl Derivatives of L-Arginine and D-Arginine: Synthesis, Stability, Cell Permeation, and Nitric Oxide Production in Pituitary GH3 Cells. *Journal of Medicinal Chemistry* **2006,** 49, (16), 4826-4833.
48. Chen, X.; Hui, L.; Foster, D. A.; Drain, C. M., Efficient Synthesis and Photodynamic Activity of Porphyrin-Saccharide Conjugates: Targeting and Incapacitating Cancer Cells. *Biochemistry* **2004,** 43, (34), 10918-10929.
49. Bosi, S.; Da Ros, T.; Spalluto, G.; Prato, M., Fullerene derivatives: an attractive tool for biological applications. *European Journal of Medicinal Chemistry* **2003,** 38, (11-12), 913-923.
50. Mroz, P.; Tegos, G. P.; Gali, H.; Wharton, T.; Sarna, T.; Hamblin, M. R., Photodynamic therapy with fullerenes. *Photochemical & Photobiological Sciences* **2007,** 6, (11), 1139-1149.
51. Arbogast, J. W.; Darmanyan, A. P.; Foote, C. S.; Diederich, F. N.; Whetten, R. L.; Rubin, Y.; Alvarez, M. M.; Anz, S. J., Photophysical properties of sixty atom carbon molecule (C60). *The Journal of Physical Chemistry* **1991,** 95, (1), 11-12.
52. Yamakoshi, Y.; Umezawa, N.; Ryu, A.; Arakane, K.; Miyata, N.; Goda, Y.; Masumizu, T.; Nagano, T., Active Oxygen Species Generated from Photoexcited Fullerene (C60) as Potential Medicines: O2-• versus 1O2. *Journal of the American Chemical Society* **2003,** 125, (42), 12803-12809.
53. Scrivens, W. A.; Tour, J. M.; Creek, K. E.; Pirisi, L., Synthesis of 14C-Labeled C60, Its Suspension in Water, and Its Uptake by Human Keratinocytes. *Journal of the American Chemical Society* **1994,** 116, (10), 4517-4518.
54. Tokuyama, H.; Yamago, S.; Nakamura, E.; Shiraki, T.; Sugiura, Y., Photoinduced biochemical activity of fullerene carboxylic acid. *Journal of the American Chemical Society* **1993,** 115, (17), 7918-7919.
55. Yano, S.; Hirohara, S.; Obata, M.; Hagiya, Y.; Ogura, S.-i.; Ikeda, A.; Kataoka, H.; Tanaka, M.; Joh, T., Current states and future views in photodynamic therapy. *Journal of Photochemistry and Photobiology C: Photochemistry Reviews* **2011,** 12, (1), 46-67.
56. Liu, Y.; Zhao, Y.-L.; Chen, Y.; Liang, P.; Li, L., A water-soluble β-cyclodextrin derivative possessing a fullerene tether as an efficient photodriven DNA-cleavage reagent. *Tetrahedron Letters* **2005,** 46, (14), 2507-2511.
57. Ikeda, A.; Suzuki, Y.; Yoshimura, M.; Shinkai, S., On the prerequisites for the formation of solution complexes from [60]fullerene and calix[n]arenes: A novel allosteric effect between [60]fullerene and metal cations in calix[n]aryl ester complexes. *Tetrahedron* **1998,** 54, (11), 2497-2508.
58. Akiyama, M.; Ikeda, A.; Shintani, T.; Doi, Y.; Kikuchi, J.-i.; Ogawa, T.; Yogo, K.; Takeya, T.; Yamamoto, N., Solubilisation of [60]fullerenes using block copolymers and evaluation of their photodynamic activities. *Organic & Biomolecular Chemistry* **2008,** 6, (6), 1015-1019.
59. Ikeda, A.; Sato, T.; Kitamura, K.; Nishiguchi, K.; Sasaki, Y.; Kikuchi, J.-i.; Ogawa, T.; Yogo, K.; Takeya, T., Efficient photocleavage of DNA utilising water-soluble lipid

membrane-incorporated [60]fullerenes prepared using a [60]fullerene exchange method. *Organic & Biomolecular Chemistry* **2005,** 3, (16), 2907-2909.
60. Rancan, F.; Helmreich, M.; Mölich, A.; Jux, N.; Hirsch, A.; Röder, B.; Witt, C.; Böhm, F., Fullerene-pyropheophorbide a complexes as sensitizer for photodynamic therapy: Uptake and photo-induced cytotoxicity on Jurkat cells. *Journal of Photochemistry and Photobiology B: Biology* **2005,** 80, (1), 1-7.
61. Milanesio, M. E.; Alvarez, M. G.; Rivarola, V.; Silber, J. J.; Durantini, E. N., Porphyrin-fullerene C60 Dyads with High Ability to Form Photoinduced Charge-separated State as Novel Sensitizers for Photodynamic Therapy. *Photochemistry and Photobiology* **2005,** 81, (4), 891-897.
62. Cheng, P.; R. Wilson, S.; I. Schuster, D., A novel parachute-shaped C60-porphyrin dyad. *Chemical Communications* **1999**, (1), 89-90.
63. Maggini, M.; Scorrano, G.; Prato, M., Addition of azomethine ylides to C60: synthesis, characterization, and functionalization of fullerene pyrrolidines. *Journal of the American Chemical Society* **1993,** 115, (21), 9798-9799.
64. Bottari, G.; Olea, D.; Gómez-Navarro, C.; Zamora, F.; Gómez-Herrero, J.; Torres, T., Highly Conductive Supramolecular Nanostructures of a Covalently Linked Phthalocyanine–C60 Fullerene Conjugate. *Angewandte Chemie* **2008,** 120, (11), 2056-2061.
65. Hashimoto, S., Optical Spectroscopy and Microscopy Studies on the Spatial Distribution and Reaction Dynamics in Zeolites. *The Journal of Physical Chemistry Letters* **2011**, 509-519.
66. Sledge Jr, G. W.; Miller, K. D., Exploiting the hallmarks of cancer: the future conquest of breast cancer. *European Journal of Cancer* **2003,** 39, (12), 1668-1675.
67. S. M. Auerbach, K. A. C., P. K. Dutta, *Handbook of Zeolite Science and Technology*. CRC Press: 2003.
68. Sherman, J. D., *Proc. Natl. Acad. Sci. U. S. A.* **1999,** 96, 3471.ì.
69. Ohsuna, T.; Slater, B.; Gao, F.; Yu, J.; Sakamoto, Y.; Zhu, G.; Terasaki, O.; Vaughan, D. E. W.; Qiu, S.; Catlow, C. R. A., Fine Structures of Zeolite-Linde-L (LTL): Surface Structures, Growth Unit and Defects. *Chemistry – A European Journal* **2004,** 10, (20), 5031-5040.
70. Megelski, S.; Calzaferri, G., Tuning the Size and Shape of Zeolite L-Based Inorganic–Organic Host–Guest Composites for Optical Antenna Systems. *Advanced Functional Materials* **2001,** 11, (4), 277-286.
71. Calzaferri, G.; Huber, S.; Maas, H.; Minkowski, C., Host—Guest Antenna Materials. *ChemInform* **2003,** 34, (50), no-no.
72. Ackley, M. W.; Rege, S. U.; Saxena, H., Application of natural zeolites in the purification and separation of gases. *Microporous and Mesoporous Materials* **2003,** 61, (1–3), 25-42.
73. Robert J, D., New perspectives on basic zeolites as catalysts and catalyst supports. *Journal of Catalysis* **2003,** 216, (1–2), 396-405.
74. Okamoto, M.; Sakamoto, E., 31-P-15-Application of natural zeolites to purify polluted river water. In *Studies in Surface Science and Catalysis*, A. Galarneau, F. F. F. D. R.; Vedrine, J., Eds. Elsevier: 2001; Vol. Volume 135, p 372.

75. Schulz-Ekloff, G., Zeolite-Hosted Metals and Semiconductors as Advanced Materials. In *Studies in Surface Science and Catalysis*, P.A. Jacobs, N. I. J. L. K.; Wichterlov´, B., Eds. Elsevier: 1991; Vol. Volume 69, pp 65-78.
76. Gfeller, N.; Megelski, S.; Calzaferri, G., Transfer of Electronic Excitation Energy between Dye Molecules in the Channels of Zeolite L. *The Journal of Physical Chemistry B* **1998,** 102, (14), 2433-2436.
77. Uglea, C. V.; Albu, I.; Vatajanu, A.; Croitoru, M.; Antoniu, S.; Panaitescu, L.; Ottenbrite, R. M., Drug delivery systems based on inorganic materials: I. Synthesis and characterization of a zeolite-cyclophosphamide system. *Journal of Biomaterials Science, Polymer Edition* **1995,** 6, (7), 633-637.
78. Liu, X.; Thomas, J. K., Photophysical Properties of Pyrene in Zeolites: Adsorption and Distribution of Pyrene Molecules on the Surfaces of Zeolite L and Mordenite. *Chemistry of Materials* **1994,** 6, (12), 2303-2308.
79. Ramachandra, S.; Popovic', Z. D.; Schuermann, K. C.; Cucinotta, F.; Calzaferri, G.; De Cola, L., Förster Resonance Energy Transfer in Quantum Dot–Dye-Loaded Zeolite L Nanoassemblies. *Small* **2011,** 7, (10), 1488-1494.
80. Calzaferri, G.; Gfeller, N., Thionine in the cage of zeolite L. *The Journal of Physical Chemistry* **1992,** 96, (8), 3428-3435.
81. Ganschow, M.; Schulz-Ekloff, G.; Wark, M.; Wendschuh-Josties, M.; Wohrle, D., Microwave-assisted preparation of uniform pure and dye-loaded AlPO-5 crystals with different morphologies for use as microlaser systems. *Journal of Materials Chemistry* **2001,** 11, (7), 1823-1827.
82. Ros-Lis, J. V.; Martinez-Manez, R.; Soto, J.; Villaescusa, L. A.; Rurack, K., Squaraine "ships" in the Y zeolite "bottle": a chromogenic sensing material for the detection of volatile amines and thiols. *Journal of Materials Chemistry* **2011**.
83. Fisher, K. A.; Huddersman, K. D.; Taylor, M. J., Comparison of Micro- and Mesoporous Inorganic Materials in the Uptake and Release of the Drug Model Fluorescein and Its Analogues. *Chemistry – A European Journal* **2003,** 9, (23), 5873-5878.
84. Calzaferri, G.; Maas, H.; Pauchard, M.; Pfenniger, M.; Megelski, S.; Devaux, A., Supramolecularly Organized Luminescent Dye Molecules in the Channels of Zeolite L. In *Advances in Photochemistry*, John Wiley & Sons, Inc.: 2003; pp 1-50.
85. Dieu, L.-Q.; Devaux, A.; Lopez-Duarte, I.; Victoria Martinez-Diaz, M.; Bruhwiler, D.; Calzaferri, G.; Torres, T., Novel phthalocyanine-based stopcock for zeolite L. *Chemical Communications* **2008**, (10), 1187-1189.
86. Tsotsalas, M. M.; Kopka, K.; Luppi, G.; Wagner, S.; Law, M. P.; Schäfers, M.; De Cola, L., Encapsulating 111In in Nanocontainers for Scintigraphic Imaging: Synthesis, Characterization, and In Vivo Biodistribution. *ACS Nano* **2009,** 4, (1), 342-348.
87. Suárez, S.; Devaux, A.; Bañuelos, J.; Bossart, O.; Kunzmann, A.; Calzaferri, G., Transparent Zeolite–Polymer Hybrid Materials with Adaptable Properties. *Advanced Functional Materials* **2007,** 17, (14), 2298-2306.
88. Devaux, A.; Popović, Z.; Bossart, O.; De Cola, L.; Kunzmann, A.; Calzaferri, G., Solubilisation of dye-loaded zeolite L nanocrystals. *Microporous and Mesoporous Materials* **2006,** 90, (1–3), 69-72.

89. Strassert, C. A.; Otter, M.; Albuquerque, R. Q.; Höne, A.; Vida, Y.; Maier, B.; De Cola, L., Photoactive Hybrid Nanomaterial for Targeting, Labeling, and Killing Antibiotic-Resistant Bacteria. *Angewandte Chemie International Edition* **2009,** 48, (42), 7928-7931.
90. Tsotsalas, M.; Busby, M.; Gianolio, E.; Aime, S.; De Cola, L., Functionalized Nanocontainers as Dual Magnetic and Optical Probes for Molecular Imaging Applications. *Chemistry of Materials* **2008,** 20, (18), 5888-5893.
91. Choi, S. Y.; Lee, Y.-J.; Park, Y. S.; Ha, K.; Yoon, K. B., Monolayer Assembly of Zeolite Crystals on Glass with Fullerene as the Covalent Linker. *Journal of the American Chemical Society* **2000,** 122, (21), 5201-5209.
92. Kulak, A.; Lee, Y.-J.; Park, Y. S.; Yoon, K. B., Orientation-Controlled Monolayer Assembly of Zeolite Crystals on Glass and Mica by Covalent Linkage of Surface-Bound Epoxide and Amine Groups. *Angewandte Chemie International Edition* **2000,** 39, (5), 950-953.
93. Li, Z.; Luppi, G.; Geiger, A.; Josel, H.-P.; De Cola, L., Bioconjugated Fluorescent Zeolite L Nanocrystals as Labels in Protein Microarrays. *Small* **2011,** 7, (22), 3193-3201.
94. Lee, G. S.; Lee, Y.-J.; Ha, K.; Yoon, K. B., Orientation-Controlled Monolayer Assembly of Zeolite Crystals on Glass Using Terephthaldicarboxaldehyde as a Covalent Linker. *Tetrahedron* **2000,** 56, (36), 6965-6968.
95. Yoon, K. B., Organization of Zeolite Microcrystals for Production of Functional Materials. *Accounts of Chemical Research* **2006,** 40, (1), 29-40.
96. Kehr, N. S.; Riehemann, K.; El-Gindi, J.; Schäfer, A.; Fuchs, H.; Galla, H.-J.; De Cola, L., Cell Adhesion and Cellular Patterning on a Self-Assembled Monolayer of Zeolite L Crystals. *Advanced Functional Materials* **2010,** 20, (14), 2248-2254.
97. Kehr, N. S.; El-Gindi, J.; Galla, H.-J.; De Cola, L., Click chemistry on self-assembled monolayer of zeolite L crystals by microcontact printing – Applications in nanobiotechnology. *Microporous and Mesoporous Materials* **2011,** 144, (1–3), 9-14.
98. Rapozzi, V.; Beverina, L.; Salice, P.; Pagani, G. A.; Camerin, M.; Xodo, L. E., Photooxidation and Phototoxicity of π-Extended Squaraines. *Journal of Medicinal Chemistry* **2010,** 53, (5), 2188-2196.
99. Foote, C. S.; Lin, J. W.-P., Chemistry of singlet oxygen. VI. Photooxygenation of enamines: evidence for an intermediate. *Tetrahedron Letters* **1968,** 9, (29), 3267-3270.
100. Mazur, S.; Foote, C. S., Chemistry of singlet oxygen. IX. Stable dioxetane from photooxygenation of tetramethoxyethylene. *Journal of the American Chemical Society* **1970,** 92, (10), 3225-3226.
101. Marine, S. S.; Clemons, J., Determination of Limonene Oxidation Products Using SPME and GC?MS. *Journal of Chromatographic Science* **2003,** 41, (1), 31-35.
102. Mikaia, A. S., S. E.; Zaikin, V.; Zhu, D.; Milman, B.; Babishok, V.; Zenkevich, I.; Linstrom, P.; Mirokhin, Y.; Tchekhovskoi, D.; Mallard, W. G.; Sparkman, O. D.; Sparkman, J. A. *NIST/EPA/NIH Mass Spectral Library;Version 2.0d*, National Institute of Standards and Technology: Gaithersburg, MD, 2005.
103. Hoebeke, M.; Piette, J.; van de Vorst, A., Photosensitized production of singlet oxygen by merocyanine 540 bound to liposomes. *Journal of Photochemistry and Photobiology B: Biology* **1991,** 9, (3–4), 281-294.

104. Kawakami, M.; Suzuki, M.; Kawai, H.; Ogawa, K.; Shishido, T., A self-sensitized photoreaction of rhodacyanine dye, MKT 077. *Tetrahedron Letters* **1998,** 39, (13), 1763-1766.
105. Shinohara, H.; Tsaryova, O.; Schnurpfeil, G.; Wöhrle, D., Differently substituted phthalocyanines: Comparison of calculated energy levels, singlet oxygen quantum yields, photo-oxidative stabilities, photocatalytic and catalytic activities. *Journal of Photochemistry and Photobiology A: Chemistry* **2006,** 184, (1-2), 50-57.

5 Experimental part

5.1 Synthesis of the investigated compounds

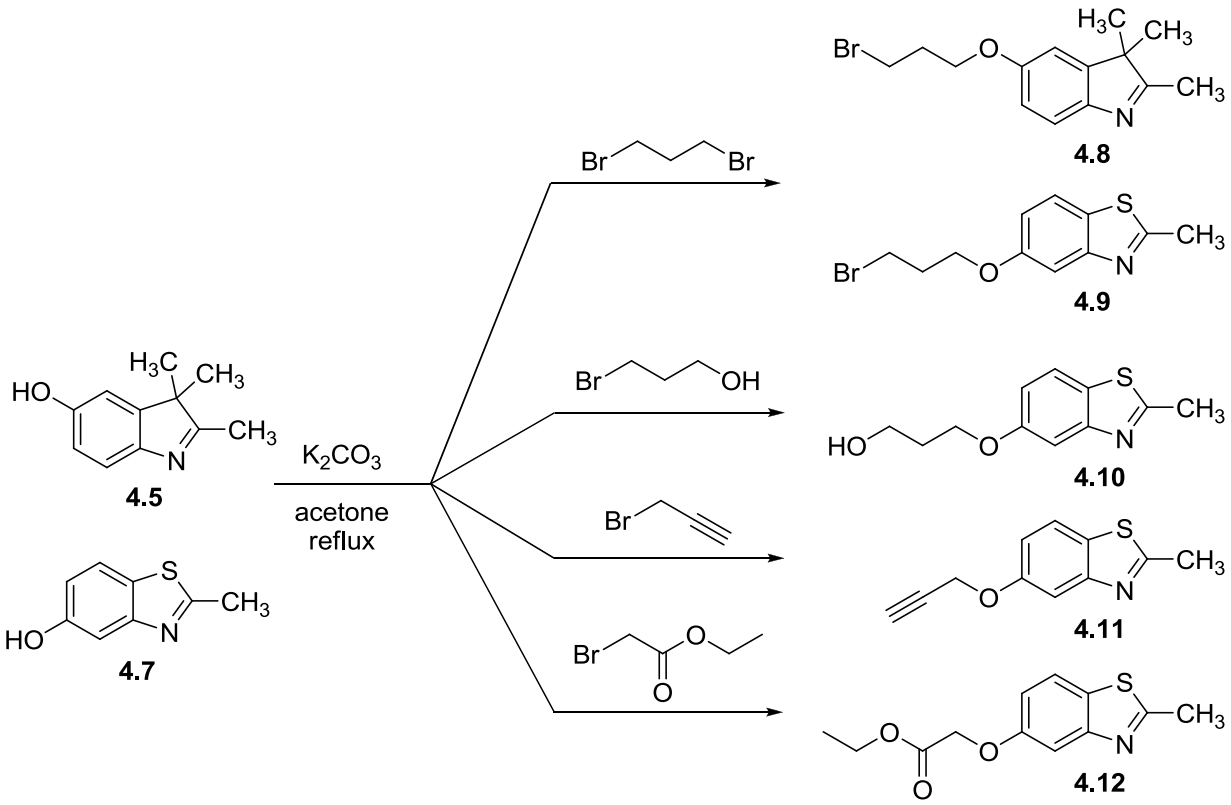

General procedure: **4.5** or **4.7** (1 mmol) and alkylating agent (3 mmol) were dissolved in 25 ml of acetone, K_2CO_3 (1 mmol) was added to give a dark suspension. The reaction mixture was refluxed for 15 hours. The reaction mixture was poured into deionised water (150 ml, pH 10) and extracted with AcOEt 3x30 ml. The organic phase was washed with brine 2x150 ml, then dried on Na_2SO_4. The product was purified with column chromatography on silica gel, elution with n-hexane to eliminate the excess of alkylating agent, then with AcOEt, to give the pure product as a yellow oil (0,863 g; 2,91 mmol).

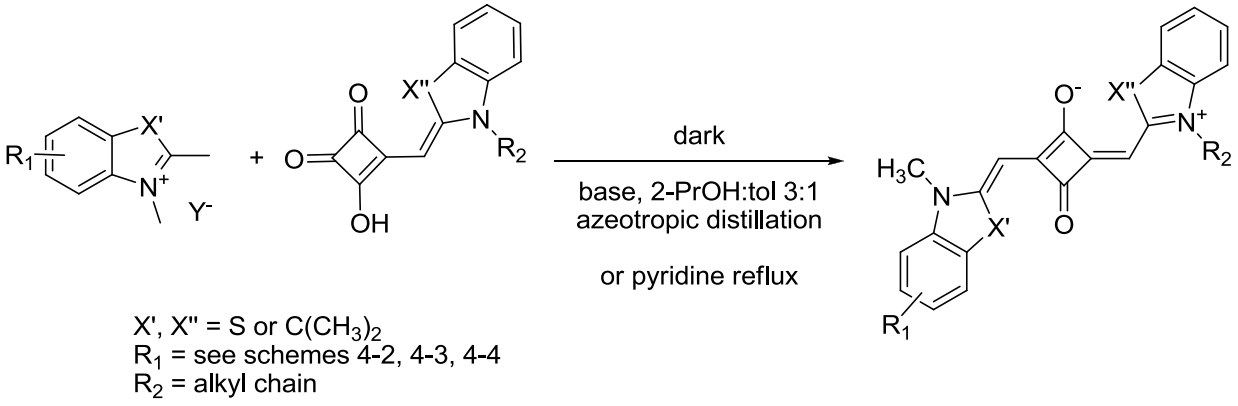

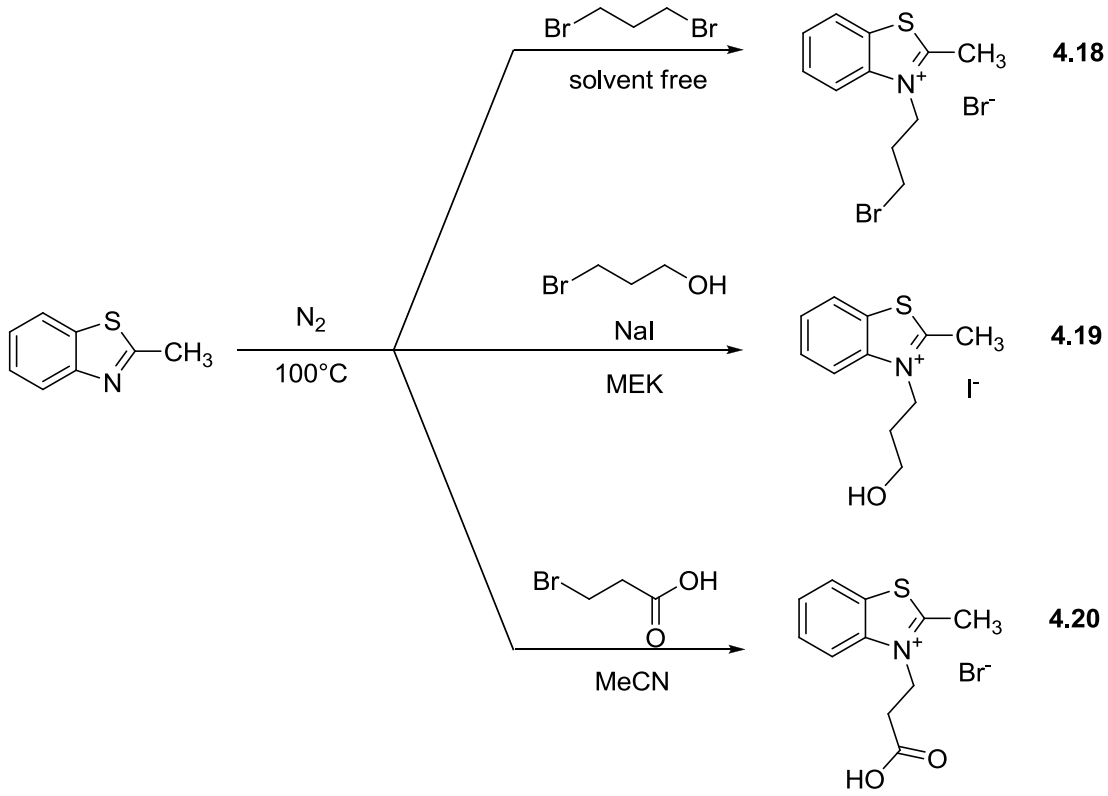

2-methylbenzo[d]thiazole (2.348 g; 15.74 mmol) and 1,3-dibromopropane (9.530 g; 47.21 mmol) were heated for 8 hours at 100 °C in anhydrous conditions under nitrogen atmosphere. The reaction mixture became light yellow and a white precipitate was formed. After stirring overnight at room temperature, the precipitate increased. n-hexane (10 mL) was added to the reaction mixture and the resulting suspension was filtered on a Hirsch funnel after 15 minutes stirring r.t. to give the product **4.18** as a white solid (1.048 g; 2.98 mmol) 20% yield.

2-methylbenzo[*d*]thiazole (1.174 g; 7.87 mmol), 3-bromopropan-1-ol (2.188 g; 15.74 mmol) and anhydrous sodium iodide (2.360 g; 15.74 mmol) were heated for 7½ hours at 100 °C in dry 2-butanone (2.11 mL; 23.61 mmol) in anhydrous conditions under nitrogen atmosphere. The reaction mixture became light yellow and thicker. Acetonitrile (15 mL) was added to the reaction mixture to give a yellow solution and a white precipitate was formed (NaBr). The inorganic salt was filtered off and washed with acetonitrile (5 mL). A yellow oil was obtained after evaporation of the solvent, which was taken up with ethyl acetate (15 mL) and acetonitrile (2 mL) and sonicated. A light yellow precipitate was formed, which was collected by filtration on a Hirsch funnel, washed with ethyl acetate (10 mL) and dried in vacuum at 50°C. **4.19** (0.9 g; 2.8 mmol). 36% yield.

2-methylbenzo[*d*]thiazole (2.348 g; 15.74 mmol) and 3-bromopropanoic acid (4.815 g; 31.48 mmol) were slowly heated to give a homogeneous solution, then heated for 5 hours at 100 °C in anhydrous conditions under nitrogen atmosphere. The reaction mixture became reddish, a white precipitate was formed. Since the reaction mixture could not be stirred due to the large amount of precipitate, anhydrous acetonitrile (5 mL) was added and the resulting suspension was refluxed for 2 hours. Diethyl ether (20 mL) was added to the reaction mixture, the white precipitate was collected by filtration on a Hirsch funnel and washed with diethyl ether (20 mL). TLC (silicagel, elution with MeOH:nitromethane:NH_4Cl (aq.,2M) 8:1:1) showed the presence of the reagents, so the precipitate was washed again with 2-butanone (30 mL). **4.20** (4.316 g; 14.28 mmol). 90% yield.

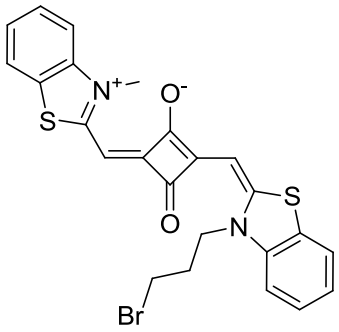

4.21

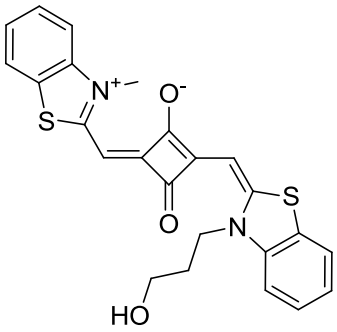

4.22

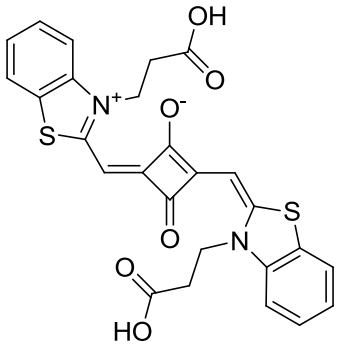

4.23

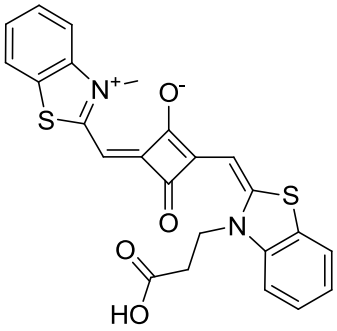

4.24

General procedure: The reaction was carried out in the dark under azeotropic conditions. A solution of the benzothiazolium salt (1 mmol), emisquaraine (1 mmol) and quinaldine (10 mmol) in 60 mL of 2-propanol:toluene 4:1 was refluxed for 14 hours in a dark flask, while it turned dark green. The reaction mixture was poured into HCl (aq. 1M, 100 mL) and $CHCl_3$ (40 mL) to eliminate the unreacted quinaldine. The phases were separated and the product was extracted $CHCl_3$ (2x40 mL). The organic phase was washed with NaOH (aq. 5%wt. 1x150 mL) and with NH_4Cl (aq. 1x150 mL) to eliminate the unreacted emisquaraine, then dried on Na_2SO_4 in the dark. The product was purified by column chromatography on silicagel, elution with $CHCl_3$:MeOH 10:1 to give a dark solid with a metallic-like surface.

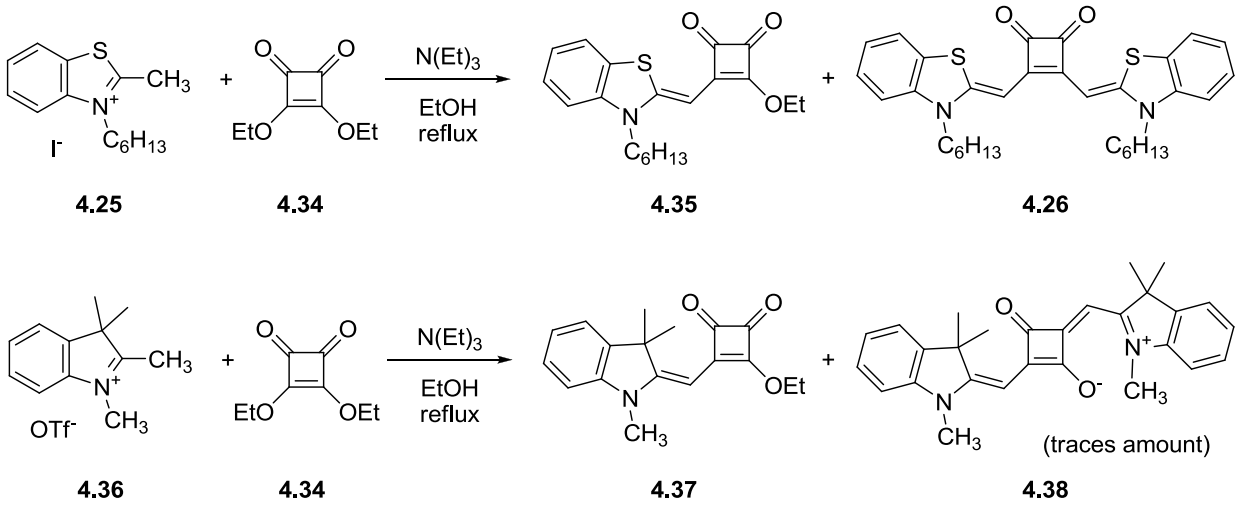

4.25 **4.34** **4.35** **4.26**

4.36 **4.34** **4.37** **4.38**

A mixture of 2-methylbenzo[*d*]thiazole (2.5 g, 16.8 mmol) in 1-iodohexane (7.1 g, 33.5 mmol) was heated at 110 °C for 14 h under a nitrogen atmosphere. Diethyl ether (25 mL) was then added, a white precipitate was formed which was isolated by suction filtration and washed directly on the filter with diethyl ether (20 mL) to give 3-hexyl-2-methylbenzo[*d*]thiazol-3-ium iodide (2.8 g, 7.8 mmol, 46% yield).

A solution of 3-hexyl-2-methylbenzo[*d*]thiazol-3-ium iodide (2.1 g, 5.9 mmol), triethylamine (0.6 g, 5.9 mmol) and ethyl squarate (0.5 g, 2.9 mmol) in ethanol (30 mL) was refluxed for 6 h. The red solid obtained after removing the solvent at reduced pressure was dissolved in tetrahydrofuran (20 mL), a solution of LiOH (0.3 g, 12.5 mmol) in water (10 mL) was added and the resulting red solution was refluxed for 4h. The red residue obtained after removing the organic solvent at reduced pressure was poured into warm water (250 mL, 40°C) a red precipitate was formed which was isolated by suction filtration and purified by filtration on silica gel (elution: from hexane:chloroform 1:1 to pure chloroform) to afford a dark red solid (1.1 g, 1.9 mmol) in 66% yield. Mp 228-230 °C. ^{1}H NMR (500 MHz, CD_2Cl_2, δ): 7.38 (dd, J_1 = 7.75 Hz, J_2 = 0.66 Hz, 2H), 7.30 (dt, J_1 = 8.31 Hz, J_2 = 1.07 Hz, 2H), 7.08-7-.04 (m, 4H), 5.41 (s, broad, 2H), 4.03 (t, J = 7.38 Hz, 4H), 1.84 (q, J = 7.62 Hz, 4H), 1.53-1.47 (m, 4H), 1.45-1.36 (m, 8H), 0.95(t, J = 7.07 Hz, 6H). ^{13}C NMR (125.7 MHz, CD_2Cl_2, δ): 191.1 (2C), 173.6 (2C), 157.2 (2C), 141.5 (2C), 127.1 (2C), 126.6 (2C), 122.8 (2C), 121.7 (2C), 110.6 (2C), 81.2 (2C), 45.8 (2C), 31.6 (2C), 26.9 (2C), 26.7 (2C), 22.7 (2C), 13.9 (2C). Anal. Calcd for $C_{32}H_{36}N_2O_2S_2$: C, 70.55; H, 6.66; N, 5.14. Found: C, 69.74; H, 6.59; N, 4.94.

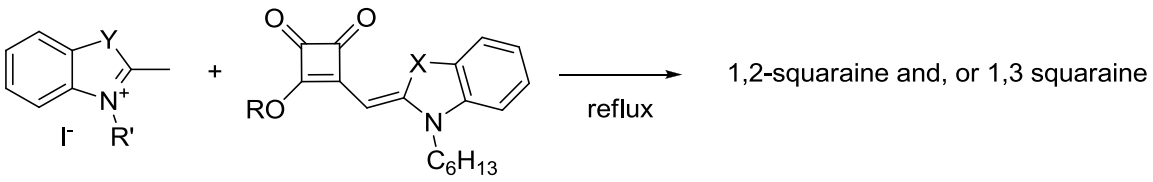

		Y	R'		R	X	Products
a	**4.25**	S	n-C_6H_{13}	**4.35**	Et	S	1,2-sq
b	**4.25**	S	n-C_6H_{13}	**4.40**	H	S	1,3-sq+ 1,2-sq (traces)
c	**4.25**	S	n-C_6H_{13}	**4.35**	Et	S	1,2-sq+ 1,3-sq[a]
d	**4.25**	S	n-C_6H_{13}	**4.37**	Et	$C(CH_3)_2$	1,2-sq
e	**4.36**	$C(CH_3)_2$	n-C_6H_{13}	**4.35**	Et	S	no reaction
f		$C(CH_3)_2$	CH_3	**4.37**	Et	$C(CH_3)_2$	1,3-sq[b]

[a]Refluxing pyridine as the solvent. [b]Microwave heating (100°c, 3 bar), the anhydrobase was generated *ex situ*.

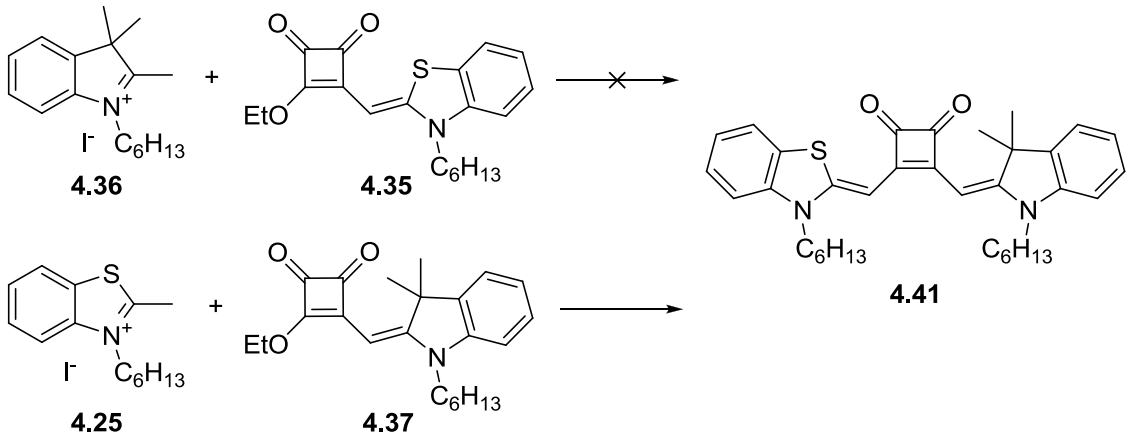

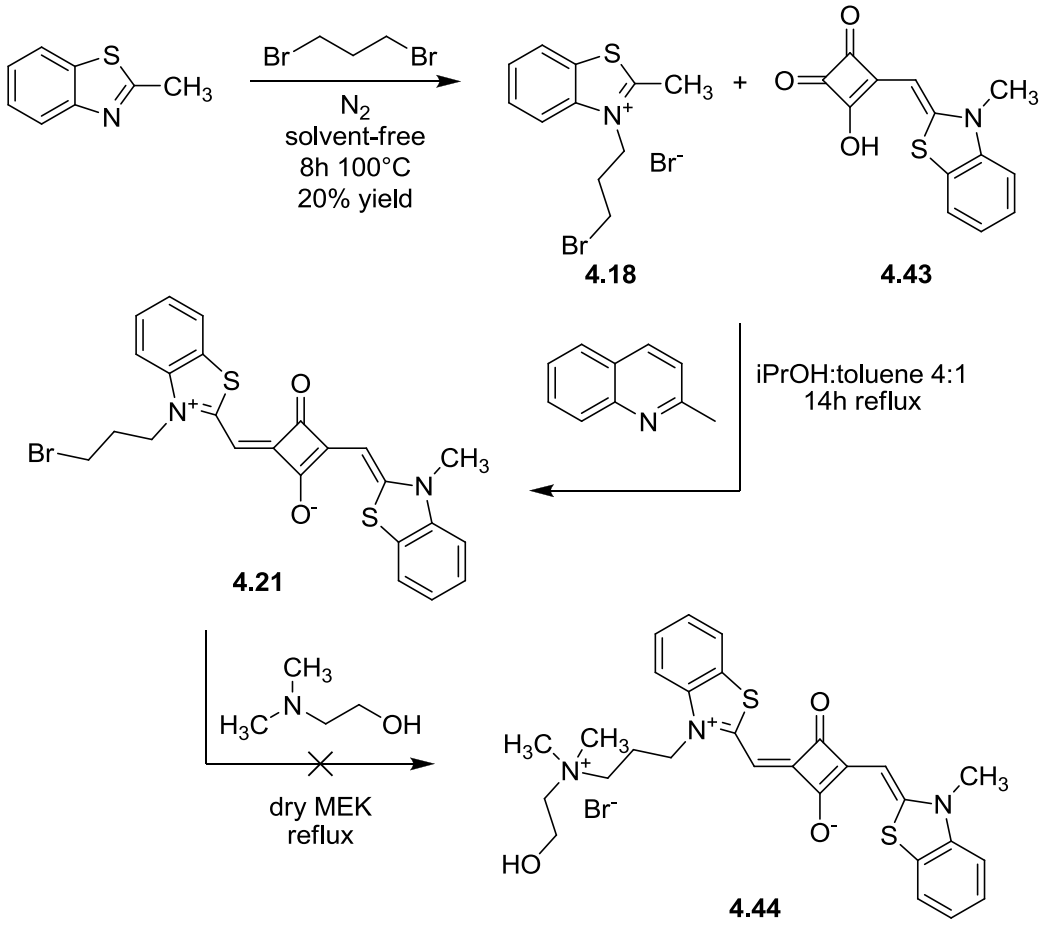

The reaction was carried out under azeotropic conditions. A solution of the benzothiazolium salt (**4.18**; 0,351 g, 1 mmol), emisquaraine (**4.43**; 0,259 g, 1 mmol) and quinaldine (1.35 mL; 10 mmol) in 60 mL of 2-propanol:toluene 4:1 was refluxed for 14 hours in a dark flask, while it turned dark green. The reaction mixture was poured into HCl (aq. 1M, 100 mL) and $CHCl_3$ (40 mL) to eliminate the unreacted quinaldine. The phases were separated and the product was extracted $CHCl_3$ (2x40 mL). The organic phase was washed with NaOH (aq. 5%wt. 1x150 mL) and with NH_4Cl (aq. 1x150 mL) to eliminate the unreacted emisquaraine, then dried on Na_2SO_4 in the dark. The product was purified by column chromatography on silicagel, elution with $CHCl_3$:MeOH 10:1 to give a dark solid with a metallic-like surface (~30 mg).

A solution of the squaraine (**4.21**; 30mg; 0,06 mmol) and 2-(dimethylamino)ethanol (0,105 g; 1,17 mmol, molar ratio 20:1) in 3 mL of dry butan-2-one was refluxed in a dark flask. After 7h reflux and stirring overnight at room temperature, a precipitate was formed which was collected by filtration on a Hirsch funnel to give a dark solid. TLC (silicagel, elution with MeOH:nitromethane:NH_4Cl (aq.,2M) 8:1:1) of the precipitate showed it to be mainly the reagent squaraine. 2-(dimethylamino)ethanol (0,1 g; 1,12

mmol) and dry butan-2-one (3 mL) were added to the reaction mixture, which was refluxed again for 7h, some more precipitate was formed and was collected by filtration on a Hirsch funnel (15 mg), but TLC showed it to be mainly the reagent squaraine.

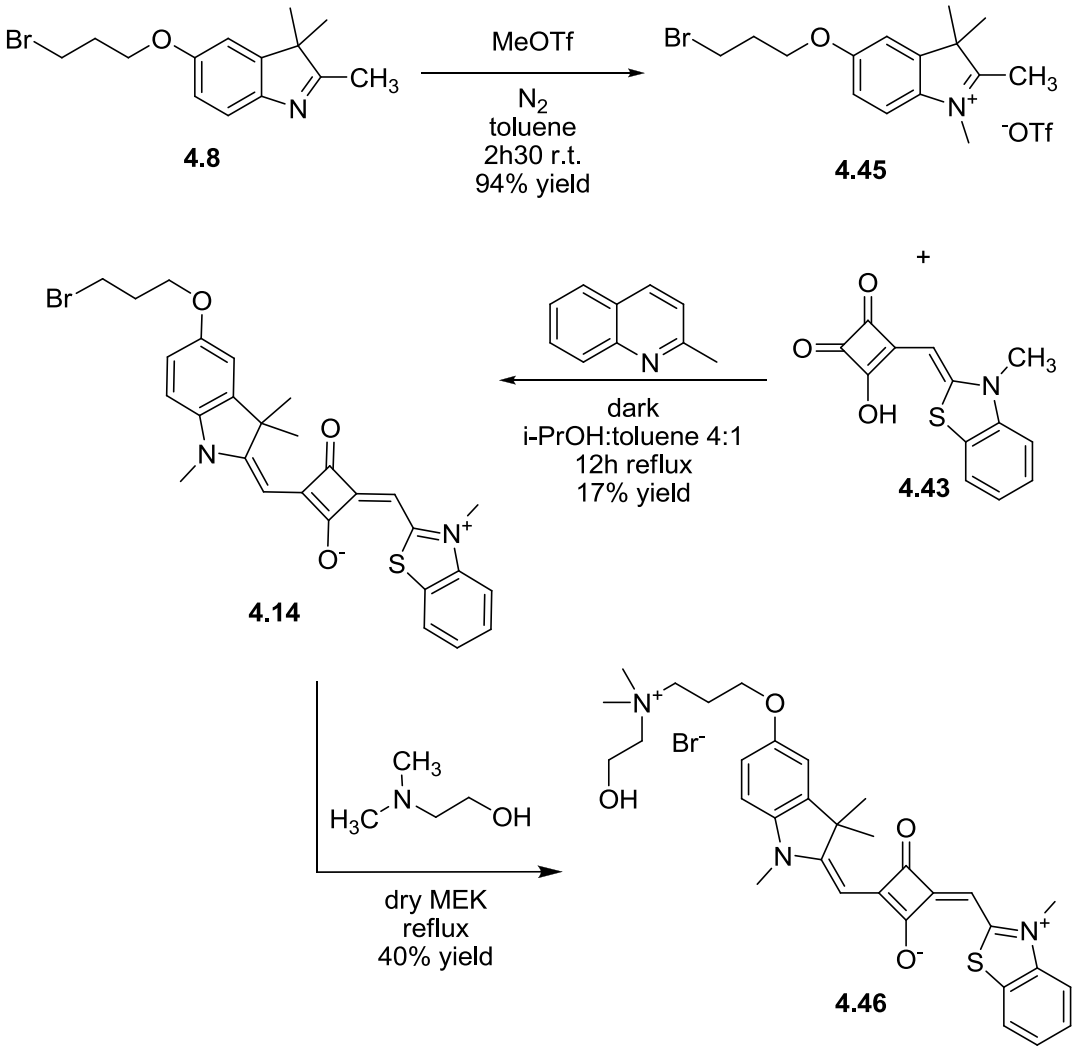

Ethyl squarate (1,04 g; 6,13 mmol) and triethylamine (0,71 ml; 5,11 mmol) were dissolved in ethanol (2 ml). A suspension of 2,3-dimethylbenzo[d]thiazol-3-ium triflate (1,6 g; 5,11 mmol) in ethanol (15 ml) was slowly added to the reaction mixture which immediately turned yellow and a precipitate was formed. TLC (silicagel. Elution with CH_2Cl_2:MeOH 9:1) showed almost no presence of the intense red byproduct. The reaction mixture was stirred at room temperature for 2 hours, while the precipitate increased, which was collected by filtration on a Hirsch funnel to give a dark yellow solid. The product was purified by filtration on silicagel, elution with CH_2Cl_2:MeOH 9:1 to give a powdery dark yellow solid, which was dried in vacuum at 40°C (emisquarate, 1,15 g; 4,0 mmol). 78% yield.

Benzothiazolium ethyl emisquarate (1,0 g; 3,48 mmol) was dissolved in tetrahydrofuran (40 ml) to give an intense yellow suspension. LiOH (aq, 2 M; 10,45 mmol) was added to the reaction mixture, which was then refluxed for 1 hour. The reaction mixture was poured in deionised water (150 ml, pH 9) and the resulting intense yellow solution was acidified to pH 5 with HCl (aq. 1M) and an intense yellow precipitate was formed, which was collected by filtration on a Hirsch funnel and dried in vacuum at 50°C (**4.43**; 0,717 g; 2,77 mmol). 79% yield.

The reaction was carried out under azeotropic conditions. A solution of the indoleninium salt (**4.45**; 1.494 g, 3.25 mmol), emisquaraine (**4.43**; 0,841 g, 3.25 mmol) and quinaldine (4.4 mL; 32.5 mmol) in 60 mL of 2-propanol:toluene 4:1 was refluxed for 14 hours in a dark flask, while it turned dark green. The reaction mixture was poured into HCl (aq. 1M, 250 mL) and $CHCl_3$ (50 mL) to eliminate the unreacted quinaldine. The phases were separated and the product was extracted $CHCl_3$ (2x40 mL). The organic phase was washed with NaOH (aq. 5%wt. 1x150 mL) and with NH_4Cl (aq. 1x150 mL) to eliminate the unreacted emisquaraine, then dried on Na_2SO_4 in the dark. The product was purified by column chromatography on silicagel, elution with $CHCl_3$:MeOH 10:1 to give a dark solid with a metallic-like surface (**4.14**; 0.310 g; 0.54 mmol). 17% yield.

A solution of the squaraine (**4.14**; 0.31 g; 0.54 mmol) and 2-(dimethylamino)ethanol (0.242 g; 2.72 mmol, molar ratio 5:1) in 18 mL of dry butan-2-one was refluxed in a dark flask. The reaction was monitored with TLC (silicagel, elution with MeOH:nitromethane:NH_4Cl (aq.,2M) 8:1:1). After 7h reflux and stirring overnight at room temperature, a precipitate was formed which was collected by filtration on a Hirsch funnel to give a dark solid with a metallic-like surface (**4.46**, 100 mg). Since TLC showed no degradation of the reagent in the filtered solution, 2-(dimethylamino)ethanol (0,3 mL; 2.98 mmol) was added to it to give the molar ratio 10:1 with respect to the squaraine. The solution was refluxed again for 7h, some more precipitate was formed and was collected by filtration on a Hirsch funnel (20 mg). TLC showed little degradation of the reagent in the filtered solution, 2-(dimethylamino)ethanol (0.3 mL; 2.98 mmol) was added to it to give the molar ratio 16:1 with respect to the squaraine. The solution was refluxed again, but no more precipitate was formed and TLC showed no more progression. **4.46** (0.13 g; 0.20 mmol). 37% yield. The product was stored in a drier in the dark at -18 °C.

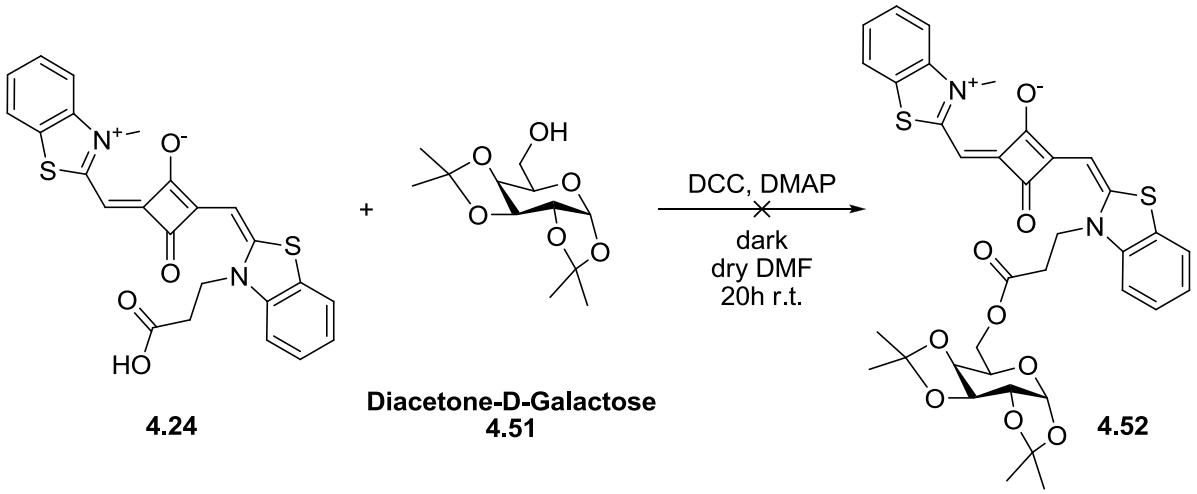

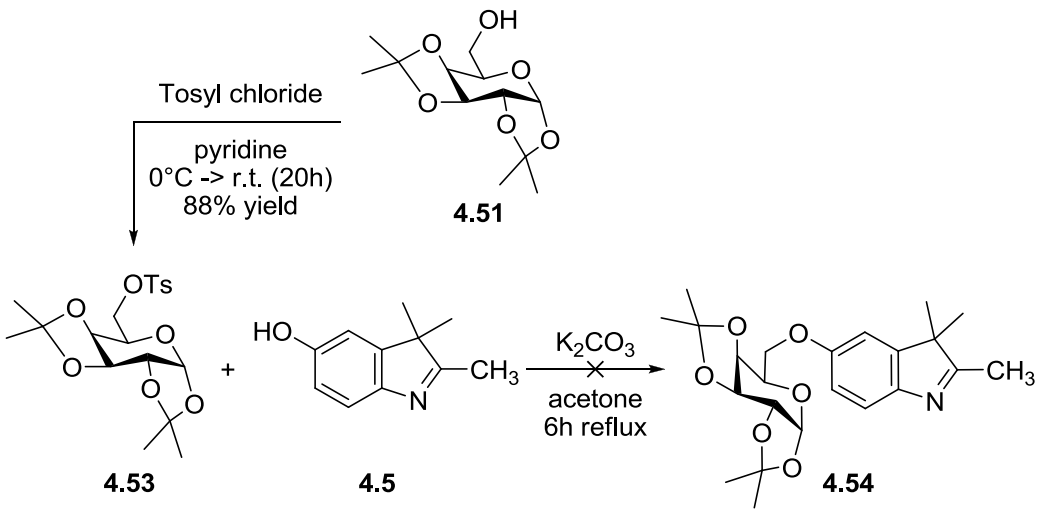

The reaction was carried out in dry conditions. Diacetone-D-galactose (1.00 g, 3.84 mmol) was dissolved in pyridine (5 mL). A solution of tosyl chloride (2.196 g, 11.52 mmol) in pyridine (2.5 mL) was added dropwise to the reaction mixture at 0°C. The reaction mixture was stirred at room temperature, a white precipitate was formed (pyridinium chloride). The reaction mixture was poured into water (15 mL) and Et_2O (15 mL). The phases were separated and the product was extracted with Et_2O (2x15 mL). The organic phase was dried on $MgSO_4$ in the dark. After solvent evaporation an oil was obtained, due to the presence of residual pyridine, which turned solid at low temperature (**4**; 1.4 g, 3.4 mmol). 88% yield. The product was stored at 4°C in a drier.

A solution of 2,3,3-trimethyl-3*H*-indol-5-ol (0.126 g, 0.72 mmol), **4.53** (0.450 g, 1.09 mmol) and K_2CO_3 (0.100 g, 0.72 mmol) in acetone (5 mL) was refluxed for 6 hours. TLC on

silicagel, elution with AcOEt:toluene 1:1 of the reaction mixture poured into water and extracted with Et_2O showed no reaction occurred.

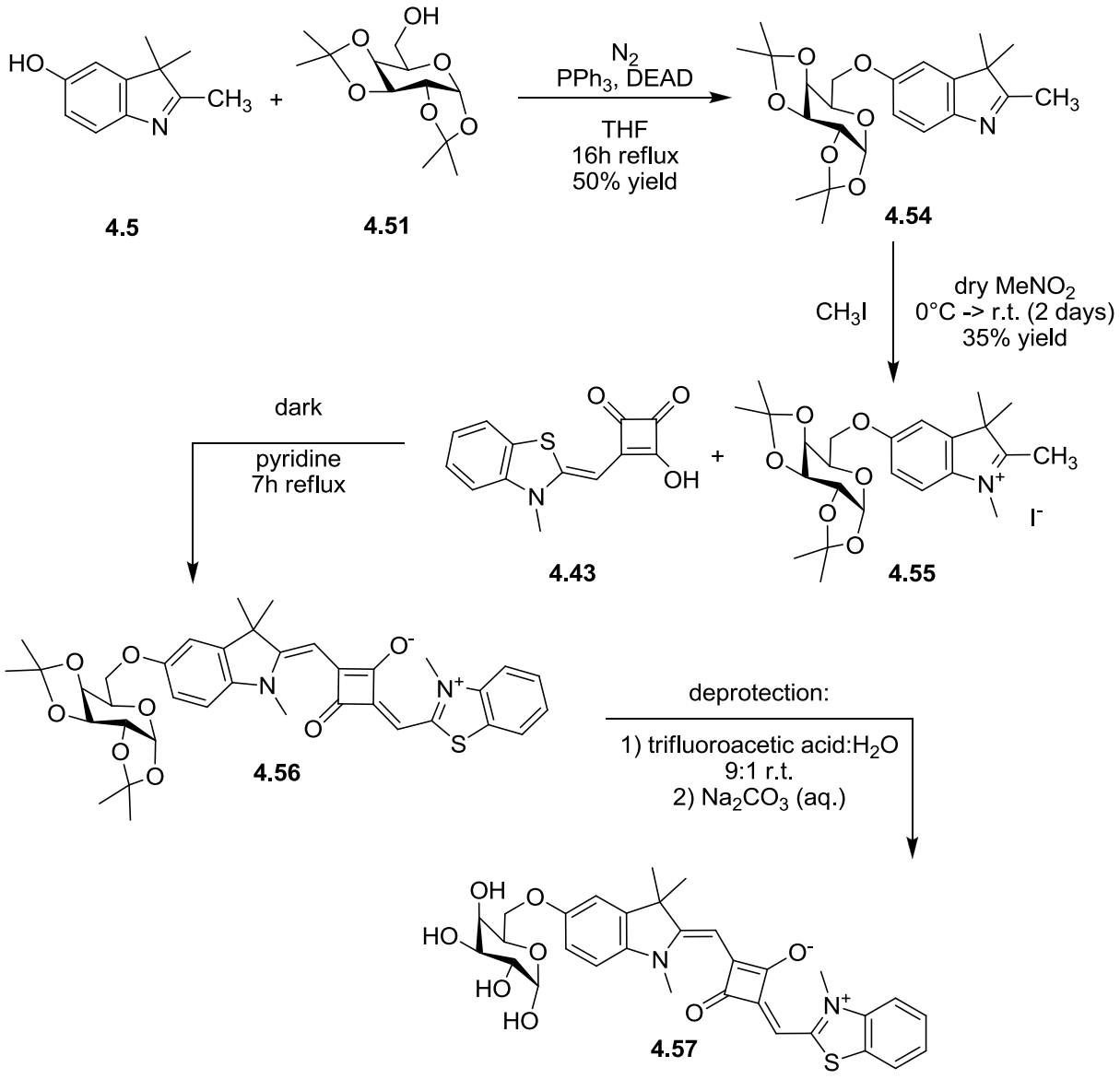

The reaction was carried out in anhydrous conditions under nitrogen atmosphere. A solution of DEAD (40%wt. in toluene, 0.96 mL; 2.11 mmol DEAD) was added dropwise at 0°C to a solution of triphenylphosphine (0.553 g, 2.11 mmol) in anhydrous THF (10 mL) The reaction mixture turned from orange to colorless. A solution of diacetone-D-galactose (0.5 g, 1.92 mmol) in anhydrous THF (5 mL) was added dropwise to the reaction mixture at 0°C. 2,3,3-trimethyl-3*H*-indol-5-ol (0.336 g, 1.92 mmol) was added portionwise at 0°C. The reaction was stirred at room temperature for 5 hours. Since TLC on silicagel, elution with AcOEt:toluene 3:2 of the reaction mixture poured into water and extracted with Et_2O

showed no variations, the reaction mixture was refluxed. TLC showed the presence of a new species at lower Rf than the reagent. After 16 hours reflux, the reaction mixture was poured into water (200 mL) and extracted with Et_2O (3x30 mL). The organic phase was dried on Na_2SO_4. The product was purified by column chromatography on silicagel, elution with AcOEt :toluene from 2:1 to 10:1 to give a yellow oil (0.405 g). ^{1}H-NMR (DMSO-d_6) showed the presence of the product **4.54**, little reagent and little triphenylphosphineoxide. ~50% yield.

The reaction was carried out in dry conditions. CH_3I (6 mL, 96.4 mmol) was added dropwise at 0°C to a solution of **5** (0.32 g, 0.77 mmol) in nitromethane (3.2 mL). The reaction mixture was stirred at room temperature for 2 days. The solvent was removed in vacuum pump at 40°C under stirring. Et_2O (15 mL) was added to the residue, a dark oil, and grey solid was formed which was collected by filtration on a Hirsch funnel. ^{1}H-NMR (DMSO-d_6) showed the presence of the pure product (**4.55**; 0.15 g, 0.27 mmol). 35% yield.

The reaction was carried in the dark. A solution of the indolenine salt (**4.55**; 0.1 g, 0.18 mmol) and emisquaraine (0.47 g, 0.18 mmol) was refluxed in pyridine (4 mL) for 7 hours, while it turned dark blue.The reaction mixture was poured into water and HCl (aq. ~7%aq.) was added till stable acid pH (~4). A dark solid was formed, which was collected by filtration on a Buchner funnel.

The reaction was carried out in dry conditions in the dark. Trifluoroacetic acid (0.2 mL, 2.6 mmol) was added dropwise to a solution of squaraine **4.56** (75 mg, 0,1 mmol) in dry CH_2Cl_2 (2.5 mL), the reaction mixture turned dark green. the reaction mixture was stirred at room temperature in the dark. After 1 day TLC (silicagel, elution with $CHCl_3$:MeOH 9:1) showed no reaction occurred, so trifluoroacetic acid (0.2 mL, 2.6 mmol) was added dropwise up to the molar ratio 50:1 with respect to the squaraine.

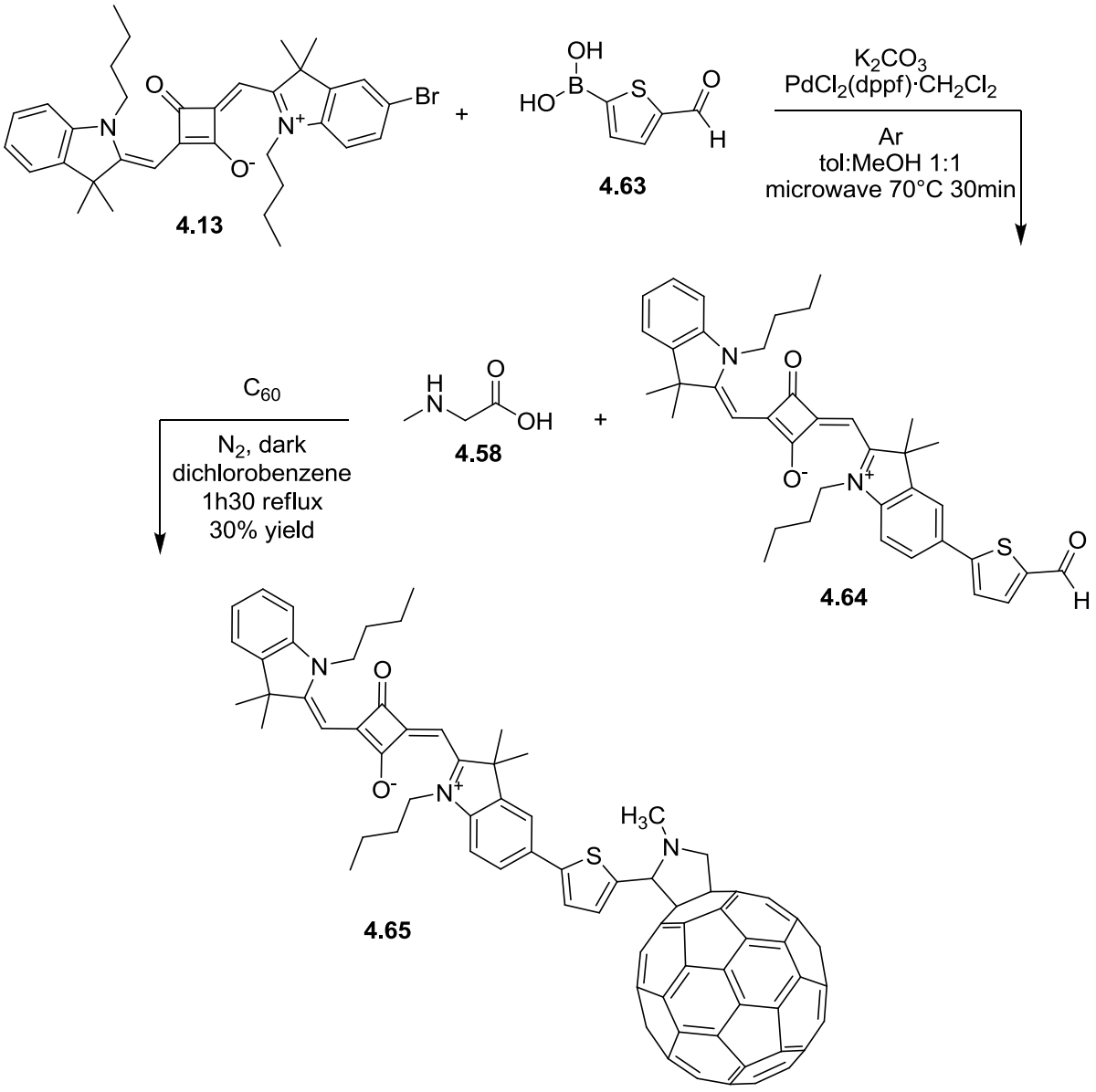

Squaraine **4.13** (100mg, 0.17 mmol) and finely ground anhydrous potassium carbonate (117.49 mg, 0.85 mmol) were added to a microwave tube. 5-formylthiophen-2-ylboronic acid (79.54 mg, 0.51 mmol) and $PdCl_2(dppf)\cdot CH_2Cl_2$ (13.88 mg, 0.017 mmol) were added to the tube in glove box with Argon atmosphere. Anhydrous toluene (2 mL) and anhydrous methanol (2 mL) were added to the reagents to give a blue suspension. The microwave tube was sealed under Ar. The reaction mixture was stirred in the dark at room temperature while setting up the microwave. The microwave reactor (CEM Discover) was set to: standard mode, T = 70°C, $Power_{max}$ = 60W, $pressure_{max}$ = 5 bar, stirring = high, cooling off, hold time = 30 min. The reaction mixture turned teal blue. Four batches were combined and the solvent was evaporated under reduced pressure to give a dark solid.

The product was purified by column chromatography (elution from $CHCl_3$:EtOAc: 1:1 to $CHCl_3$:MeOH 9:1). The first fraction collected (100 mg) was a 1:1 mixture of the product and the reagent ER-IV-09, which was purified by a second column chromatography with the same eluent. The second fraction collected gave the pure product as metallic green needles after solvent evaporation (**4.64**, 190 mg, 0.31mmol, 46% yield).

The reaction was performed under nitrogen in the dark. A solution of **4.64** (23 mg, 0.037 mmol) in 1,2-dichlorobenzene (2 ml) was added to a refluxing solution of C_{60} (27 mg, 0.037 mmol) in 1,2-dichlorobenzene (5 ml). Finely ground sarcosine (5 mg, 0.056 mmol) was then added portionwise. The reaction mixture was refluxed for 2 hours and then the solvent was removed under reduced pressure. The bluish residue was washed with methanol:toluene 9:1 (7 x 5 ml) to remove the non-fullerene byproducts and was purified by column chromatography on silica gel (elution gradient from chloroform to chloroform:methanol 96:4, $R_f(1)$ = 0.8, $R_f(2)$ = 0.74). The desired product **4.65** was obtained as a purple metallic solid (15 mg, 0.011 mmol, 29% yield).

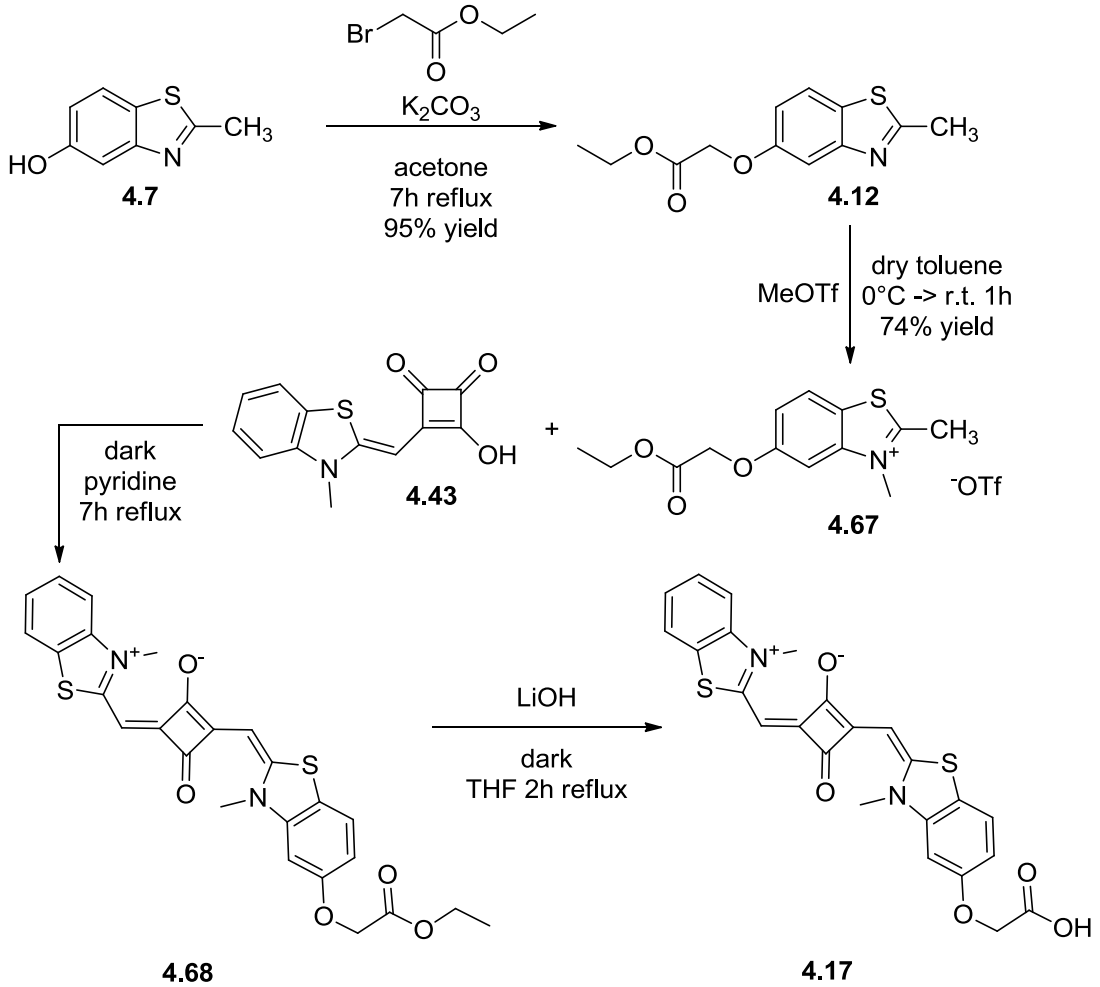

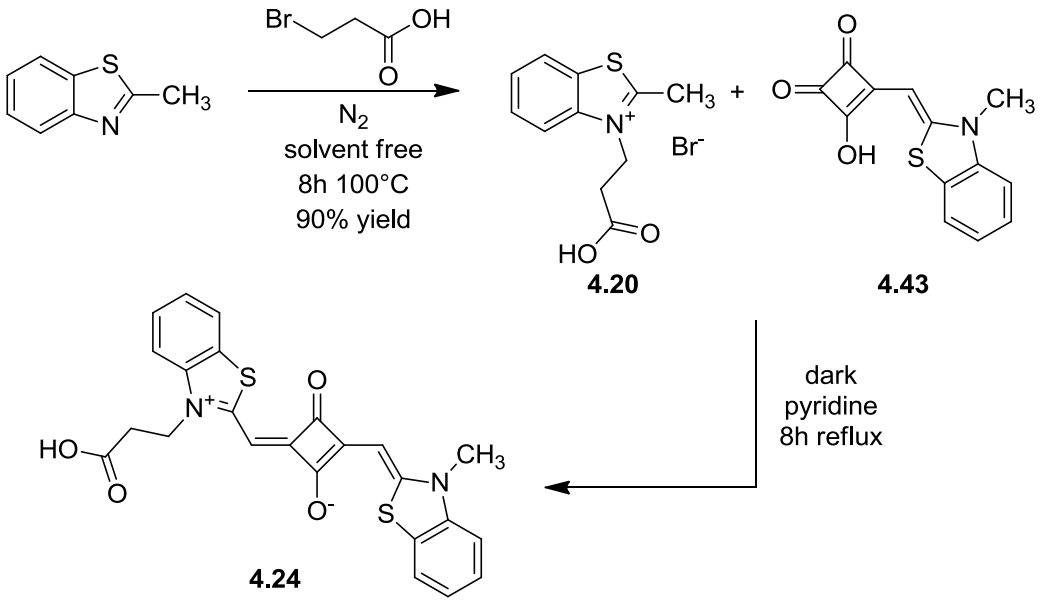
Br
OH
O
S
CH3
N
N2
solvent free
8h 100°C
90% yield
N+
Br-
HO
4.20
4.43
dark
pyridine
8h reflux
4.24

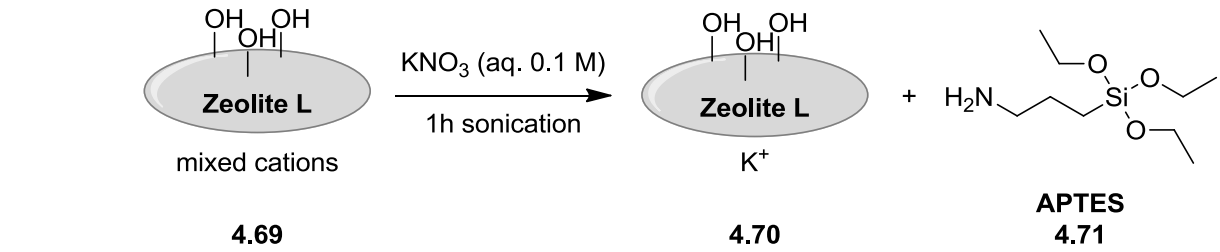
OH
Zeolite L
mixed cations
KNO3 (aq. 0.1 M)
1h sonication
K+
H2N
Si
APTES
4.69
4.70
4.71

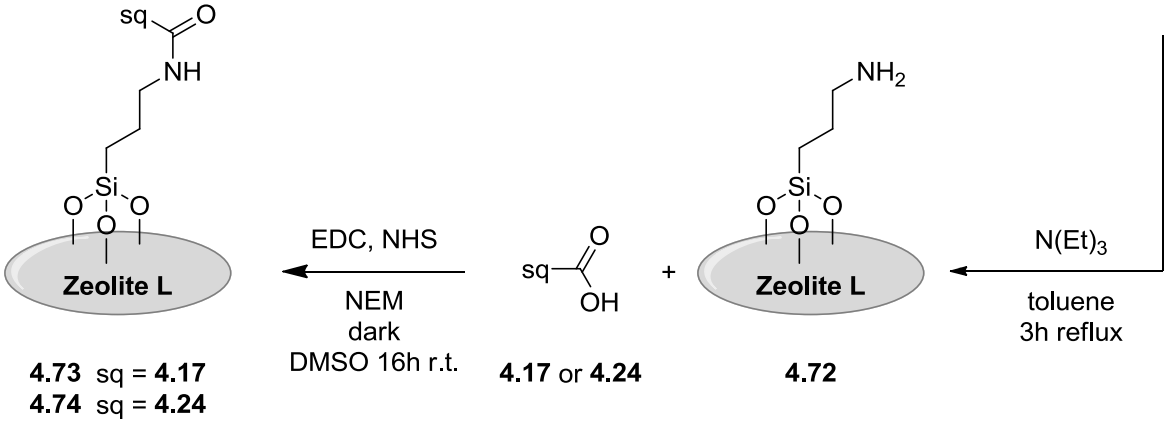
sq
NH
NH2
Zeolite L
EDC, NHS
NEM
dark
DMSO 16h r.t.
N(Et)3
toluene
3h reflux
4.73 sq = 4.17
4.74 sq = 4.24
4.17 or 4.24
4.72

5.2 Photophysical experimental setup

Steady-state UV/vis absorption spectra were recorded using UV/vis/NIR Jasco V570 or Varian Cary 5000 spectrometers. Steady state excitation and emission spectra were recorded using Jasco FP-6200 and Edinburgh LifeSpec II spectrometers. Time-resolved emissions were recorded using Edinburgh FS920 spectrometer. The phosphorescence spectrum of singlet oxygen was recorded by using a HORIBA Jobin-Yvon IBH FL-322 Fluorolog 3 spectrometer equipped with an air-cooled Hamamatsu H10330-75 (InP/InGaAs) PMT detector. Samples for measurements performed in the absence of oxygen were prepared by gently bubbling argon through the solution for approximately 20 min.

The fluorescence quantum yield Φ_F was estimated by comparison with a reference fluorophore of known quantum yield which absorbs and emits in the spectral region of the dyes investigated. The standard used for 1,3-squaraines was Zinc 2,9,16,23-tetra-*tert*-butyl-29*H*,31*H*-phthalocyanine ($\Phi_{F,R}$ 0.33 in toluene)[1] while the standard used for 1,2-squaraines was Rhodamine B ($\Phi_{F,R}$ 0.31 in water)[2].

Absorption and emission spectra of the dye and the standard were recorded with the same parameters (slits openings, excitation wavelength, filters, scan speed) for five different optical densities between 0.05 and 0.15 in order to avoid inner filter effect.

The emission maximum intensity was plotted as a function of absorption maximum optical density, and from the slopes m_S and m_R of the linear regressions for the sample and the reference respectively, the fluorescence quantum yield for the sample $\Phi_{F,S}$ was calculated with the following equation:

$$\Phi_{F,S} = \Phi_{F,R} \frac{m_S}{m_R} \frac{n_S^2}{n_R^2}$$

Equation 1

where n_S and n_R are the refractive indices of the sample and reference solutions, respectively.

5.3 Limonene photooxidation

The analysis of limonene photooxidized derivatives was carried out by GC-MS using a Clarus 500 instrument (PerkinElmer Instruments, Shelton, CT) equipped with a 30 m x 0.25 mm capillary column Elite-5MS (0.25 μm film thickness) (PerkinElmer). Helium was used as the carrier gas at a flow rate of 1 ml/min. The injector temperature was 250 °C and the samples were injected in a splitless mode of injection. Oven temperature was set at 80 °C for 5 min, raised to 100 °C at 5 °C/min, held for 1 min, raised to 200 °C at 20 °C/min and finally held for 3 min. The mass spectrometer was operated in the electron ionization mode (ionization energy of 70 eV). The source and transfer line temperatures were 160 and 180 °C, respectively. Detection was carried out in scan mode: m/z 50 to m/z 600.

Limonene photooxidation protocol:

50 mg of limonene and 2.5 mg of squaraine were dissolved in 4 ml of ethanol avoiding light exposure.

This mixture was illuminated for 30 minutes with a halogen lamp filtered below 500 nm.

The solution was cooled at 0°C. A solution of $NaBH_4$ (25 mg) in ethanol (1 ml) was added in order to reduce the peroxides to alcohols and the resulting mixture was stirred in the dark for 1 hour.

The mixture was poured in water (10 mL) and the ethanol was removed at reduced pressure. The suspension obtained was extracted with chloroform (7 mL) and dried over Na_2SO_4. The dried solution was filtered and loaded in the GC-MS apparatus.

5.4 References

1. Fernández, D. A.; Awruch, J.; Dicelio, L. E., Photophysical and Aggregation Studies of t-Butyl-Substituted Zn Phthalocyanines. *Photochemistry and Photobiology* **1996,** 63, (6), 784-792.

2. Snare, M. J.; Treloar, F. E.; Ghiggino, K. P.; Thistlethwaite, P. J., The photophysics of rhodamine B. *Journal of Photochemistry* **1982,** 18, (4), 335-346.

6 Conclusions

In this dissertation I have described the synthesis, the photophysical, photochemical and biological characterization of some organic aromatic heterocycle derivatives and their theranostical applications to cancer treatment.

I explored the synthetic accessibility of squaraine dyes and I reported the strategy aimed at the regioselectivity. I therefore prepared symmetric and unsymmetrical 1,3- and 1,2-substitued squaraines. Moreover, I inserted suitable groups in order to allow the post-functionalization of the dyes.

I reported two representative examples of post-functionalization, with choline and galactose, in order to improve squaraine bioavailability. Moreover, I conjugated the squaraine dyes to zeolite nanoparticles in order to obtain a new nanoformulate for PDT applications.

I also investigated the photophysical behavior of the 1,3- and 1,2-substitued squaraines prepared. In order to elucidate the photodamaging mechanism I also conducted simple photochemical experiments, studying the product distribution of the reaction between light, squaraines and limonene as a biologically relevant target, pointing out the presence of a radical chain of oxidative events.

The in-depth biological evaluation of functionalized squaraine dyes and of the nanoformulates are currently in progress.

Moreover, a fullero-squaraine dyad has been designed in order to combine the photophysical properties of the two portions, so that the conjugate unites the characteristic absorption of squaraine dyes and the high singlet oxygen generation of fullerene *via* intra-molecular energy transfer processes.

7 Publications

This thesis work has led to the following publications:

[1] Ronchi, E.; Beverina, L.; Pagani, G. A., Squaraine dyes as PDT sensitizers: Specific functionalization for biological targeting. *Photodiagnosis and Photodynamic Therapy* **2011,** 8, (2), 193-193.

[2] Ronchi, E.; Ruffo, R.; Rizzato, S.; Albinati, A.; Beverina, L.; Pagani, G. A., Regioselective Synthesis of 1,2- vs 1,3-Squaraines. *Organic Letters* **2011,** 13, (12), 3166-3169.

[3] Collini, E.; Carlotto, S.; Ferrante, C.; Bozio, R.; Polimeno, A.; Bloino, J.; Barone, V.; Ronchi, E.; Beverina, L.; Pagani, G. A., Multipolar symmetric squaraines with large two-photon absorption cross-sections in the NIR region. *Physical Chemistry Chemical Physics* **2011,** 13, (25), 12087-12094.

[4] Beverina, L.; Ruffo, R.; Salamone, M.; Ronchi, E.; Binda, M.; Natali, D.; Sampietro, M., Panchromatic squaraine compounds for broad band light harvesting electronic devices. *Journal of Materials Chemistry*, accepted.

[5] Beverina, L.; Monguzzi, A.; Vaccaro, G.; Meinardi, F.; Ronchi, E.; Moret, M.; Cosentino, U.; Moro, G.; Simonutti, R.; Mauri, M.; Tubino, R., NIR emitting Ytterbium chelates for colourless luminescent solar concentrators. *Journal of the American Chemical Society*, submitted.

[6] Ronchi, E.; El-Gindi, J.; De Cola, L.; Beverina, L.; Pagani, G. A., Choline-functionalized squaraine dye as a water-soluble PDT sensitizers with specific targeting ability. In preparation.

[7] Ronchi, E.; Kehr, S. De Cola, L.; Beverina, L.; Pagani, G. A., Squaraine-functionalized zeolites as effective nanocarriers for PDT applications. In preparation.

[8] Ronchi, E.; Beverina, L.; Pagani, G. A. et al., Photophysics of 1,2-squaraines and applications for sensing. In preparation.

[9] Ronchi, E.; Salice, P.; Menna, E.; Maggini, M.; Beverina, L.; Pagani, G. A., Tunable citotoxicity: the fullero-squaraine dyad. In preparation.